



Invited Review

Uranium in natural waters and the environment: Distribution, speciation and impact

P.L. Smedley^{a,*}, D.G. Kinniburgh^b^a British Geological Survey, Keyworth, Nottinghamshire, NG12 5GG, UK^b Formerly British Geological Survey, Wallingford, Oxfordshire, OX10 8BB, UK

ARTICLE INFO

Editorial handling by Dr T J. Gallegos

Keywords:

Uranium
Uranyl
U isotopes
Drinking water
Redox
Mine water
NORM
Radionuclide

ABSTRACT

The concentrations of U in natural waters are usually low, being typically less than 4 µg/L in river water, around 3.3 µg/L in open seawater, and usually less than 5 µg/L in groundwater. Higher concentrations can occur in both surface water and groundwater and the range spans some six orders of magnitude, with extremes in the mg/L range. However, such extremes in surface water are rare and linked to localized mineralization or evaporation in alkaline lakes. High concentrations in groundwater, substantially above the WHO provisional guideline value for U in drinking water of 30 µg/L, are associated most strongly with (i) granitic and felsic volcanic aquifers, (ii) continental sandstone aquifers especially in alluvial plains and (iii) areas of U mineralization. High-U groundwater provinces are more common in arid and semi-arid terrains where evaporation is an additional factor involved in concentrating U and other solutes. Examples of granitic and felsic volcanic terrains with documented high U concentrations include several parts of peninsular India, eastern USA, Canada, South Korea, southern Finland, Norway, Switzerland and Burundi. Examples of continental sandstone aquifers include the alluvial plains of the Indo-Gangetic Basin of India and Pakistan, the Central Valley, High Plains, Carson Desert, Española Basin and Edwards-Trinity aquifers of the USA, Datong Basin, China, parts of Iraq and the loess of the Chaco-Pampean Plain, Argentina. Many of these plains host eroded deposits of granitic and felsic volcanic precursors which likely act as primary sources of U. Numerous examples exist of groundwater impacted by U mineralization, often accompanied by mining, including locations in USA, Australia, Brazil, Canada, Portugal, China, Egypt and Germany. These may host high to extreme concentrations of U but are typically of localized extent.

The overarching mechanisms of U mobilization in water are now well-established and depend broadly on redox conditions, pH and solute chemistry, which are shaped by the geological conditions outlined above. Uranium is recognized to be mobile in its oxidic, U(VI) state, at neutral to alkaline pH (7–9) and is aided by the formation of stable U–CO₃(±Ca, Mg) complexes. In such oxidic and alkaline conditions, U commonly covaries with other similarly controlled anions and oxyanions such as F, As, V and Mo. Uranium is also mobile at acidic pH (2–4), principally as the uranyl cation UO₂²⁺. Mobility in U mineralized areas may therefore occur in neutral to alkaline conditions or in conditions with acid drainage, depending on the local occurrence and capacity for pH buffering by carbonate minerals. In groundwater, mobilization has also been observed in mildly (Mn-) reducing conditions. Uranium is immobile in more strongly (Fe-, SO₄-) reducing conditions as it is reduced to U(IV) and is either precipitated as a crystalline or ‘non-crystalline’ form of UO₂ or is sorbed to mineral surfaces. A more detailed understanding of U chemistry in the natural environment is challenging because of the large number of complexes formed, the strong binding to oxides and humic substances and their interactions, including ternary oxide-humic-U interactions. Improved quantification of these interactions will require updating of the commonly-used speciation software and databases to include the most recent developments in surface complexation models. Also, given their important role in maintaining low U concentrations in many natural waters, the nature and solubility of the amorphous or non-crystalline forms of UO₂ that result from microbial reduction of U(VI) need improved quantification.

Even where high-U groundwater exists, percentage exceedances of the WHO guideline value are variable and often small. More rigorous testing programmes to establish usable sources are therefore warranted in such vulnerable aquifers. As drinking-water regulation for U is a relatively recent introduction in many countries (e.g. the European Union), testing is not yet routine or established and data are still relatively limited. Acquisition of

* Corresponding author.

E-mail address: pls@bgs.ac.uk (P.L. Smedley).

more data will establish whether analogous aquifers elsewhere in the world have similar patterns of aqueous U distribution. In the high-U groundwater regions that have been recognized so far, the general absence of evidence for clinical health symptoms is a positive finding and tempers the scale of public health concern, though it also highlights a need for continued investigation.

1. Introduction

Uranium is the 49th most abundant element in the earth's crust with a similar abundance to beryllium, tin and arsenic. It is relatively abundant in seawater: ranking 26th, similar to that of arsenic and vanadium. It is a very dense metal (19.1 kg/m³), similar to gold, and has the greatest atomic number (92) of all the naturally-occurring elements in the periodic table.

Uranium is lithophile, reflecting its tendency to remain close to the earth's surface and be strongly bound to oxygen. It occurs naturally in all soils, minerals, rocks and water. It can also be derived from a wide variety of anthropogenic sources including phosphate fertilizers, mine waste, fly ash from power plants, and military use. Uranium occurs in oxidation states III, IV, V and VI but the dominant forms in nature are IV and VI. Uranium is an actinide element with three naturally-occurring isotopes, all weakly radioactive. Isotopic mass is dominated by ²³⁸U (99.27%), with a smaller abundance of ²³⁵U (0.72%) and ²³⁴U (0.0057%); radioactivity contributions of ²³⁸U, ²³⁵U and ²³⁴U are 47.3%, 2.2% and 50.5% respectively. Uranium is one of the main contributors to the earth's natural radioactivity which supplies about half of the earth's heat. In refined forms, it has been used to make nuclear weapons and supply nuclear power plants.

Human exposure to environmental uranium has long been considered a radiological health risk, although there are few epidemiological studies that have been able to demonstrate resultant harm, even in occupational contexts (The Royal Society, 2001, 2002; van Gerwen et al., 2020). There has been increasing concern that the chemical effects of uranium also pose a health risk to exposed populations as with other trace metals. Drinking water is considered to account for about 70% of the U uptake in a standard human diet (Haneklaus et al., 2021). Impacts of chemical exposure include nephritis (kidney disease) and changes in bone structure (Arzuaga et al., 2010; Brugge and Buchner, 2011; Kurttio et al., 2002, 2005; Milvey and Cothorn, 1990; Weir, 2004). Ingested uranium is considered less toxic than inhaled uranium, in part due to a relatively low gastrointestinal absorption of uranium compounds (Keith et al., 2013); average uptake of ingested U is said to be only about 1% (Zamora et al., 1998). In blood plasma, uranyl forms a U-CO₃ complex in equilibrium with a non-diffusible uranyl albumin complex which is excreted under alkaline conditions. Complexes with other proteins such as transferrin, ferritin and metallothionein may also be of importance (Michon et al., 2010).

Toxic effects of U have been found in animal species, including death at high exposures. Limited evidence in animal studies suggests that aqueous speciation plays a role in toxicity, with U-Ca-CO₃ complexes inferred to have reduced toxicity or bioavailability relative to other Ca-free species (Ansoborlo et al., 2006). So far, evidence of chemical toxicity in humans is limited (Kurttio et al., 2006, 2002; Staines et al., 2004; WHO, 2017) and restricted to sub-clinical effects (Kurttio et al., 2005; Seldén et al., 2009; Zamora et al., 1998); evidence for the impact of U aqueous speciation on toxicity in humans is also lacking. There is no evidence that U is essential to humans.

Globally, a wide variation is seen in the limits and guidelines imposed for U in drinking water, from 2 µg/L in Japan to 1700 µg/L in Russia (Sahoo et al., 2020). The WHO (1993) guidelines for drinking-water quality recognized U as a potential chemical hazard but concluded that insufficient data were available at the time to derive a realistic guideline value. Subsequent editions of the guidelines produced provisional guideline values which have been revised following increasing toxicological evidence. The fourth edition, incorporating the

first addendum (WHO, 2017) has recommended a provisional guideline value of 30 µg/L. Both the EU Directive for U in water intended for human consumption and the US-EPA maximum contaminant level (MCL) for U in drinking water are also currently set at 30 µg/L, although the EU Directive has only been in place since 2021 (Council of the European Union, 2020) with two years for Member States to transpose to national legislation. The drinking-water standard for U in Canada is 20 µg/L; that set nationally in Germany is 10 µg/L (Banning and Benfer, 2017).

These guidelines/limits are based on the chemical toxicity rather than radiological hazard. The EU, US-EPA and WHO limits for U of 30 µg/L equate to an activity of approximately 0.78 Bq/L, assuming natural U abundance. Calculations of radiological dose from drinking water using dose conversion factors for U indicate that the 0.1 mSv/yr individual dose criterion of WHO (2017) would only be breached at a U concentration of 100 µg/L or more. The WHO (2017) guideline values for radioactivity from ²³⁴U and ²³⁸U in drinking water are 1 Bq/L and 10 Bq/L respectively. In addition, the EU limits on radioactivity in water intended for human consumption are set at 2.8 Bq/L and 3.0 Bq/L for ²³⁴U and ²³⁸U respectively (Council of the European Union, 2013). Assuming natural abundances, these latter equate to concentrations of approximately 212 µg/L for ²³⁴U and 243 µg/L for ²³⁸U, although it should be noted that for a concentration of 243 µg/L at natural abundance, the limit for ²³⁴U will already have been exceeded since ²³⁴U is much more radioactive than ²³⁸U. Also, since the limits are set for isotopes individually, the aggregate activity of a concentration at natural abundance will be approximately twice as high because of the combined contributions of the isotopes. The WHO, EU and US-EPA guidelines/limits are therefore more stringent for chemical toxicity than for radiological hazard.

Measurements of gross alpha activity in water give an indication of the presence of alpha emitters including ²³⁸U and ²³⁴U. The WHO (2017) radiological screening level for gross alpha activity in drinking water of 0.5 Bq/L would be equivalent to a U concentration of approximately 19 µg/L, assuming activity is due only to U and that ²³⁸U and ²³⁴U are in secular equilibrium, with an aggregate activity of 0.0261 Bq/µg of U. Gross alpha activity is a screening method to prompt further investigation.

In many countries the regulations and guidelines for U in drinking water are relatively new (e.g. EU Directive) and where this is the case, there has commonly not been a history of widespread U measurement or monitoring. This paper highlights locations with known high concentrations in water, and also reveals the large data gaps in many countries. We also review the principal processes controlling the fate of U in the natural environment, and how these can be quantified: a prerequisite for understanding risks to drinking water and establishing the safety case for the long-term safe storage of radioactive waste. A vast literature exists on the topic of U in water and the environment; this review does not claim to have been able to cover all of it. It does however, outline the spatial distributions of the documented high concentrations in water and attempts to capture and summarize their key controls and impacts.

2. Methods of chemical analysis

2.1. Natural waters

2.1.1. Analysis of aqueous uranium

A wide variety of techniques has been developed to measure the concentration of dissolved U in natural waters and laboratory solutions,

including inductively coupled plasma mass spectrometry (ICP-MS), fluorimetry, inductively coupled plasma optical emission spectrometry (ICP-OES), fission track, instrumental neutron activation, spectrophotometry, graphite furnace AAS, voltammetry, alpha spectrometry and Raman spectroscopy (Table 1).

ICP-MS is arguably the most commonly used method today though laser fluorimetry is also widely used. Quadrupole ICP-MS offers rapid throughput, high precision and accuracy and low detection limits with a technique that can routinely analyze multiple elements across the mass range from Li to U. Use of a collision or reaction cell has been introduced to reduce spectral interferences. Developments in magnetic sector ICP-MS have also allowed greater discrimination of the elements via their mass/charge ratio to eliminate interferences suffered by quadrupole ICP-MS and provide improved detection limits, e.g. better than 10^{-4} µg/L for U (Z. Cheng et al., 2004). Laser fluorimetry is also rapid, sensitive and well-established. This involves excitation of uranyl by electromagnetic energy of suitable wavelengths and measurement of the decay in U phosphorescence following the cessation of the electromagnetic radiation usually in the presence of a fluorescence-enhancing reagent (Balaram et al., 2022). Ganesh et al. (2012) used the method with sodium pyrophosphate as the fluorescence-enhancing reagent and determined U in solutions with a detection limit of 0.2 µg/L. Light emitting diode (LED) fluorimetry is a variant of the method that offers reduced interferences and is field-portable (Balaram et al., 2022). Reduction of interference from fluorescence of organic compounds and hence improved sensitivity can be achieved by use of time-resolved laser fluorescence spectroscopy (TRLFS), with complexation of U(VI) usually with phosphoric acid (Moulin et al., 1990).

ICP-OES is a rapid, multi-element technique but with a detection limit for U typically around 20 µg/L, is normally insufficiently sensitive for routine analysis in natural waters without preconcentration. However, Singhal et al. (2012) analyzed U in water samples using ICP-OES without preconcentration by minimizing spectral interferences through optimization of chosen emission lines, and reported concentrations down to 8 µg/L. Li et al. (2021) also optimized spectral lines to improve detection of U in minerals. Chandrasekaran et al. (2011) used a dispersive liquid-liquid microextraction method for analysis of aqueous samples by ICP-OES and reported a detection limit of 2 µg/L.

Stucker et al. (2011) devised a method for evaluating U flux in groundwater at a U contaminated site over a 3-week field experiment using anion-exchange resins to adsorb U. Uranium was extracted using 1% nitric acid and measured by ICP-MS. Calculated flux-averaged U concentrations compared well with measured aqueous concentrations.

Graphite furnace atomic absorption spectroscopy (GF-AAS) has also been used for U analysis. This offers greater sensitivity than flame AAS and sensitivity has been improved further by resin preconcentration (Gupta et al., 2014).

Raman spectroscopy is typically used as a rapid screening technique and is field-portable (Ruan et al., 2007).

Fission track analysis of water samples has been carried out by irradiation of sample and standard in contact with a fission track detector and comparing track densities (Akram et al., 2004).

An increasing effort has been focused on developing sensors and probes for U detection based on its optical (colorimetry, spectrophotometry, fluorimetry) and electrochemical (voltammetry, electrochemical impedance spectroscopy, potentiometry) properties as well as the use of DNAzymes (Liu et al., 2007; Sun et al., 2022; X. Wu et al., 2019; Zhou et al., 2022). A membrane optical sensor (optode) formed by incorporation of a chromophore (2-(2-benzothiazolylazo)phenol (BTAP)) and uranyl into a plasticized cellulose triacetate matrix was used by Hassan and Amin (2017) for preconcentration and colorimetric determination of U(VI) in aqueous samples. A detection limit of 0.8 µg/L was achieved by the method. Serenjeh et al. (2016) measured uranyl in aqueous samples through its complexation by the chemical immobilization of arsenazo III on a transparent agarose membrane and determination by spectrophotometry. Byerley et al. (1987) separated U(VI)

Table 1
Methods for the analysis of uranium in aqueous solution.

Method	Detection limit ^a	Comments	Reference
ICP-MS	0.4–2 ng/L	Sensitive, rapid and used widely. Can give isotope abundances and isotope ratios. Often preceded by solid-phase separation to increase sensitivity. Seawater diluted to reduce matrix effects. Can measure multiple solutes	Korkisch and Gödl (1974), Boulyga and Becker (2002), Avivar et al. (2012), Qiao et al. (2018), Qiao and Xu (2018), Metzger et al. (2019), Rován and Strok (2019)
Laser fluorimetry	0.2 µg/L (water), 0.01 ng/L (coprecipitate)	Rapid, but subject to matrix interferences, e.g. from organic matter. Extreme sensitivity if U is coprecipitated with CaCl ₂ and the coprecipitate calcined at 800 °C then measured	Perry et al. (1981), Rathore (2008), Ganesh et al. (2012), Baik et al. (2015)
LED fluorimetry	0.2 µg/L	Interferences from organic matter reduced, field portable	Balaram et al. (2022)
Time-resolved laser fluorescence spectroscopy (TRLFS)	4–5 ng/L	Pulsed laser eliminates interference from fluorescence of organic compounds, complexation of U (VI) with e.g. phosphoric acid	Moulin et al. (1990)
ICP-OES	8 µg/L, 2 µg/L with extraction	Optimized for U by choice of spectral lines	Chandrasekaran et al. (2011), Singhal et al. (2012), Li et al. (2021)
Graphite-furnace AAS	0.2 µg/L		Gupta et al. (2014)
Raman spectroscopy	0.2 mg/L	Rapid screening, field portable, prone to interference from organic matter	Ruan et al. (2007), Balaram et al. (2022)
Anion exchange resin (passive flux meter)		Used to measure the cumulative flux of U from a contaminated groundwater site	Stucker et al. (2011)
Spectrophotometry	16 µg/L		Hassan and Amin (2017)
Fibre optic/ion exchange/colorimetry	1.4 µg/L	Uses Nafion cation exchange membrane tubing to separate U(VI), followed by reaction with arsenazo III and remote fibre-optic detection	Collins et al. (2002)
Cation exchange/ion chromatography	90–120 µg/L	Ion exchange separation of U(VI), reaction with 4-(2-pyridylazo)resorcinol	Byerley et al. (1987)
Optical chemical sensor (optode)	0.8 µg/L 140 µg/L 44 µg/L	Spectrophotometry based on an immobilized dye material	Hassan and Amin (2017), Serenjeh et al. (2016),

(continued on next page)

Table 1 (continued)

Method	Detection limit ^a	Comments	Reference
Anodic stripping voltammetry	0.1 µg/L	Electrochemical	Elhefnawy (2017)
Fission track		Irradiation followed by etching and counting of fission tracks	Sahu et al. (2014)
Alpha spectrometry	0.22 mBq/L (²³⁸ U and ²³⁴ U)	Needs separation steps, concentrations and natural isotopic ratios	Akram et al. (2004)
Thermal ionization mass spectrometry (TIMS)		High-precision isotope ratios	Jia et al. (2002)
Magnetic sector ICP-MS + low-flow nebulizer	0.1 ng/L 0.2 pg/L ²³⁶ U (0.04 ng/kg soil)	High precision, sensitive, isotopes and concentrations	Suzuki et al. (2010), Richter et al. (2011), Peñkin et al. (2018), Quemet et al. (2019)
ICP-MS/MS		High precision, isotopic ratios e. g. ²³⁶ U/ ²³⁸ U	Z. Cheng et al. (2004), Boulyga and Becker (2002)
Gamma spectrometry		Non-destructive, isotopic ratios (and concentrations)	Balcaen et al. (2015), Diez-Fernández et al. (2020), Zsigrai et al. (2015)

^a Detection limits vary depending on factors including preparation, methods, instrument used

by ion exchange and reacted with 4-(2-pyridylazo)resorcinol with measurement by ion chromatography. Elhefnawy (2017) determined U (VI) in acid medium by complexation with midodrine hydrochloride and detection by spectrophotometry. The challenge is to achieve the required sensitivity, selectivity, ease of operation and cost. An azo ligand, selected on the basis of Density Functional Theory (DFT) calculations, and immobilized on a test strip shows promise in detecting U with nanomolar sensitivity and freedom from interference (Wu et al., 2020).

For the measurement of isotopic ratios, thermal ionization mass spectrometry (TIMS) has good precision and accuracy and is used widely for both geochemical and nuclear applications. Many adjustments to the classical measurement procedure have been made to reduce mass fractionation, and improve precision for small quantities and the minor ratios ²³⁶U/²³⁸U and ²³⁴U/²³⁸U (Quemet et al., 2019; Richter et al., 2011; Suzuki et al., 2010). Magnetic sector ICP-MS is also used widely for U isotopic analysis. Boulyga and Becker (2002) measured U isotopes in water (and soil following digestion and separation) and reported detection limits of 0.2 pg/L ²³⁶U in water (0.04 ng/kg in soil) when used with a low-flow micro-concentric nebulizer. ICP tandem mass spectrometry (ICP-MS/MS) is a relatively new technique that augments ICP-MS by addition of a further quadrupole mass filter before the collision/reaction cell, improving the discrimination of the mass/charge ratio and increasing abundance sensitivity (Balcaen et al., 2015; Tanimizu et al., 2013). The technique has been used to determine ²³⁶U/²³⁸U isotopic ratios in environmental samples (Diez-Fernández et al., 2020). Accelerator mass spectrometry (AMS) has also been used, principally for the investigation of the long-half-life radionuclides including ²³⁶U (Fahey et al., 2016; Hain et al., 2022; Hotchkis et al., 2002).

Gamma spectrometry has also been used for the measurement of U isotopic ratios in both environmental and industrial samples (Ebaid, 2010).

2.1.2. Analysis of individual chemical species

The behaviour of U in both the environment and the laboratory is linked closely to its chemical speciation. This is unusually complex given the propensity of U to hydrolyze and to form complexes and solids with common macro-ions, notably CO₃²⁻, Ca²⁺, Mg²⁺, Na⁺ and PO₄³⁻. Some of the established techniques for obtaining information on individual chemical species and molecular structures are listed in Table 2.

2.2. Analysis of rocks, sediments and soils

Sample digestion of geological materials precedes analysis by many of the methods described for aqueous samples, including ICP-MS, ICP-OES and laser fluorimetry (Ramdoss et al., 1997). A method for complete digestion of soil for U investigation was described and used by Regenspurg et al. (2010). Soil was microwave digested at 100 °C using HNO₃ and H₂O₂ followed by HF and H₃PO₃. Radhamani et al. (2010) used NaH₂PO₄ and Na₂HPO₄ salts in equal proportion to dissolve refractory non-silicate minerals prior to analysis by laser fluorimetry.

A sequential extraction approach to ascertain metal partitioning, optimized for investigation of the actinides, was described by Schultz

Table 2
Techniques for acquiring information on uranium speciation.

Technique	Comment	Reference
Anion exchange	Aqueous; batch (Schubert method) and chromatographic separation of species	Korkisch and Gödl (1974), Gu et al. (2004), Dong and Brooks (2008)
UV-Vis spectroscopy	Species; requires high concentrations	Meinrath (1997)
Potentiometric titration	U(VI), U(IV) species	Yakshin and Krokhin (2011), Sahoo et al. (2012)
Time-Resolved Laser-Induced Fluorescence Spectroscopy (TRLFS) and cryo-TRLFS	Can distinguish between aqueous, sorbed and solid U(VI) species	Wang et al. (2004), Kimura et al. (1995), Meinrath (1997), Geipel et al. (1997), Arnold et al. (2011), Richter et al. (2016), Višňák et al. (2018), Kirishima et al. (2003)
Density Functional Theory (DFT)	Calculations to estimate structural, electronic, elastic, thermodynamic properties	Brincat et al. (2015), Gezahegne et al. (2012)
Photoacoustic spectroscopy (PAS)	Various approaches and frequencies including Laser-induced (LIPAS), Fourier Transform (FT-PAS), and UV-VIS-IR. Sensitive to redox state and aqueous (mM to µM concentration range) and solid phase.	Kimura et al. (1992), Bernhard et al. (2001)
X-ray absorption spectroscopy (XAS)	Molecular structure: extended X-ray absorption fine structure (EXAFS) for atomic distances, X-ray absorption fine structure (XANES) for oxidation state	Jroundi et al. (2007), Catalano et al. (2004)
Column chromatography	Combined with modelling, provides a sensitive way of resolving possible aqueous and surface interactions in sediments and soils	Dangelmayr et al. (2017)
Raman and Infrared spectroscopy (including attenuated total-reflectance Fourier transform infrared spectroscopy, ATR FTIR)	Of value for U(VI) species (not U(IV) species) in solid, solution and adsorbed phases but spectral overlap and matrix effects can complicate	Richter et al. (2016), Lu et al. (2018), Müller et al. (2008)

et al. (1998). The extraction comprised six operationally defined fractions (MgCl₂ water-soluble, NH₄Ac-HAc carbonate, NH₂OH.HCl-HAc metal oxides, H₂O₂-HNO₃ organic matter, HNO₃ acid-soluble, NaOH fusion or HNO₃/HCl/HF/HClO₄ residual). This broadly follows the method devised earlier for trace-metal extraction by Tessier et al. (1979). Extraction of U by bicarbonate (pH 8.7–9) under anoxic conditions is a useful addition (Cerrato et al., 2013; Zhou and Gu, 2005).

Tarafder et al. (2015) designed a field-laboratory method for U in solids using fluorimetry preceded by solvent extraction to remove Fe which strongly quenches the fluorescence. The detection limit for this method was 0.2 mg/kg and precision 2–3% RSD.

Fedotov et al. (2019) pre-concentrated and separated U and Th from Pb in Roman lead shields for measurement of ultra-trace U using counter-current (liquid-liquid) chromatography coupled with quadrupole ICP-MS. The detection limit for U was 3 ng/kg (Table 3).

Laser-ablation (LA) ICP-MS is a long-established method for characterization of solid surfaces such as minerals. Spatial resolution is typically 20–200 μm (Eggins et al., 1998; Gäbler, 2002). Magnetic sector LA-ICP-MS provides greater sensitivity and isotopic ratio capability (Table 3).

Spectrophotometry with organic dyes has been used widely for U measurement in environmental samples. Spectrophotometry was used with arsenazo-III as a chromogenic reagent and perchloric acid as medium of measurement in geological standard reference materials (Khan et al., 2006). Uranium contents of 0.05 mg/kg and more were detected (Table 3).

Instrumental Neutron Activation Analysis (INAA) is a quantitative or semi-quantitative technique in which samples are irradiated with a neutron flux in a reactor. No sample pretreatment is required and the method is simple, cost-effective and non-destructive. Landsberger and Kapsimalis (2013) analyzed NIST standard reference materials and found interferences (e.g. ²⁴Na, ³⁸Cl, ⁵⁶Mn), could be reduced by Compton suppression. Detection limits were as low as 0.015 mg/kg, performing best with the use of epithermal as opposed to thermal neutrons. Haddad et al. (2021) compared INAA with alpha and gamma spectrometry methods for analysis of U in soils. They concluded that INAA was the preferred method; alpha and gamma spectrometry tended to overestimate U contents relative to INAA (Table 3).

X-ray fluorescence spectrometry (XRF) can be used in wavelength-dispersive (Pandey et al., 2020) or energy-dispersive (Kumar and Dhara, 2022) mode, involves minimal sample preparation (typically pelletization) and has detection limits in the mg/kg range. Sample handling requirements in ore fields and contaminated sites have popularized field-portable XRF which is a rapid screening and non-destructive method, albeit of reduced sensitivity.

Electron probe microanalysis (EPMA) is a long-established method for determining elemental concentrations at point locations in minerals with a spatial resolution of typically a few μm. Secondary-ion mass

spectrometry (SIMS) is more sensitive and determines either concentrations or isotopic ratios in minerals with a spatial resolution of typically ca. 1 μm (Luo et al., 2015) (Table 3).

3. Uranium in minerals, rocks, sediments and soils

3.1. Minerals

Uranium can form more than 250 primary and secondary minerals (the more common shown in Table 4) with the redox state of the surrounding environment being a primary factor controlling formation.

Table 4
Principal uranium minerals.

Mineral	Formula	Occurrence
Uranium(IV) minerals		
Uraninite	UO ₂	Magmatic, hydrothermal, sedimentary
Pitchblende	U ₃ O ₈	Hydrothermal, sedimentary
Coffinite	U(SiO ₄) _{1-x} (OH) _{4x}	Magmatic, hydrothermal, sedimentary
Brannerite	UTi ₂ O ₆	Hydrothermal
Davidite	(La,Ce)(Y,U,Fe)(Ti,Fe) ₂₀ (O,OH) ₃₈	Magmatic, hydrothermal
Betafite	(Ca,U) ₂ (Nb,Ti) ₂ O ₆ OH	Magmatic, hydrothermal
Uranothorite	(U,Th)SiO ₄	Hydrothermal
Thucholite	Uraninite with hydrocarbons	Diagenetic
Uranium(VI) minerals		
Autunite	Ca(UO ₂) ₂ (PO ₄) ₂ ·10–12H ₂ O	Pegmatite, schist
Metaautunite	KCa (H ₃ O) ₃ (UO ₂) ₇ (PO ₄) ₄ O ₄ ·6–8H ₂ O	Associated with autunite, evaporation
Saléeite	Mg(UO ₂) ₂ (PO ₄) ₂ ·10H ₂ O	Sedimentary, weathering
Torbernite	Cu(UO ₂) ₂ (PO ₄) ₂ ·12H ₂ O	Weathering
Uranocircite	Ba(UO ₂) ₂ (PO ₄) ₂ ·8–10H ₂ O	Weathering
Renardite	Pb(UO ₂) ₂ (PO ₄) ₂ (OH) ₄ ·7H ₂ O	Weathering
Metaankoleite	KUO ₂ PO ₄ ·4H ₂ O	Weathering, hydrothermal
Coconinoite	Fe ₂ Al ₂ (UO ₂) ₂ (PO ₄) ₄ (SO ₄) (OH) ₂ ·20H ₂ O	Weathering
Uranophane	Ca(UO ₂) ₂ (SiO ₃ (OH) ₂ ·5H ₂ O	Weathering
Boltwoodite	HK(UO ₂) ₂ SiO ₄ ·1.5H ₂ O	Weathering
Slodowskrite	Mg(UO ₂) ₂ (HSiO ₄) ₂ ·5H ₂ O	Weathering
Soddyite	(UO ₂) ₂ SiO ₄ ·2H ₂ O	Weathering
Schoepite	(UO ₂) ₈ O ₂ (OH) ₁₂ ·12H ₂ O	Weathering
Metaschoepite	(UO ₂) ₈ O ₂ (OH) ₁₂ ·10H ₂ O	Synthetic or UO ₃ (H ₂ O) ₂
Bequerelite	Ca[(UO ₂) ₃ O ₂ (OH) ₃] ₂ ·8H ₂ O	Weathering
Carnotite	K ₂ (UO ₂) ₂ (VO ₄) ₂ ·1–3H ₂ O	Weathering
Tyuyamunite	Ca(UO ₂) ₂ V ₂ O ₈ ·5–8H ₂ O	Weathered uraninite
Zeunerite	Cu(UO ₂) ₂ (AsO ₄) ₂ ·8–10H ₂ O	Weathering, hydrothermal
Umohoite	(UO ₂)MoO ₄ ·2H ₂ O	Weathering
Liebigite	Ca ₂ UO ₂ (CO ₃) ₃ ·10H ₂ O	Weathering
Rutherfordine	UO ₂ CO ₃	Weathering

Table 3
Analytical methods for analysis of geological and other solid materials.

Technique	Detection limit	Comment	Reference
Extraction/digestion + e.g. ICP-MS, fluorimetry	Various		Regenspurg et al. (2010), Radhamani et al. (2010)
Counter-current chromatography + ICP-MS	3 ng/L	Used to determine U in Roman Pb by liquid-liquid chromatography using 1 M HNO ₃ /0.01 M tetraphenylmethylenediphosphine dioxide in chloroform followed by ICP-MS	Fedotov et al. (2019)
Laser ablation-ICP-MS	not given	Surface characterization, measurement of individual spots: 20–200 μm typical	Eggins et al. (1998), Gäbler (2002)
Spectrophotometry	<0.05 mg/kg	Preconcentration and complexation with arsenazo-III	Khan et al. (2006)
INAA	0.015 mg/kg	Minimal sample preparation, non-destructive	Landsberger and Kapsimalis (2013)
XRF Portable XRF	5 mg/kg 10 mg/kg portable	Portable versions for field use, reduced sensitivity; rapid screening, non-destructive, simple	Pandey et al. (2020), Proctor et al. (2020)
EPMA	100 mg/kg	Surface characterization, spatial resolution a few μm	Luo et al. (2015)
Secondary-ion MS	μg/kg–ng/kg	Elemental and isotopic, surface characterization, sensitive, spatial resolution a few μm	Tamborini et al. (1998)
Gamma spectrometry	10 mg/kg	Semi-quantitative; suitable for large U contents	Landsberger and Kapsimalis (2013)

Many of the uranium minerals are yellow or greenish in colour. U(VI) minerals are more numerous than U(IV) minerals and just one U(V) mineral, wyartite, has been identified so far (Burns and Finch, 1999). The U(IV) minerals are typically primary oxides or silicates (Bowell et al., 2011). The oxygen and silicate moieties form covalent bonds with U(IV) and the minerals are typically sparingly soluble (Cumberland et al., 2016). The main ores are uraninite (UO_2), coffinite ($\text{U}(\text{SiO}_4)_{1-x}(\text{OH})_{4x}$) and brannerite (UTi_2O_6) (Table 4). Uraninite can also occur in its oxidized or partly oxidized massive form, pitchblende (U_3O_8). Uranium ore grade material typically contains more than 0.1% U_3O_8 . Uraninite forms under high-temperature conditions and is present in igneous rocks and hydrothermal assemblages. It can also form at low temperature under reducing conditions in sediments, often in replacement of fossil material and intimately associated with organic carbon and pyrite (Cumberland et al., 2016). Coffinite can also occur as a secondary alteration mineral, often replacing uraninite in Si-rich, anoxic groundwater conditions (Warner et al., 2011).

Other rarer U(IV) ore minerals include davidite ((La,Ce)(Y,U,Fe)(Ti,Fe)₂₀(O,OH)₃₈), which forms under high-temperature high-pressure conditions and was reported at the Radium Hill complex in South Australia, and betafite ((Ca,U)₂(Nb,Ti)₂O₆OH), found in Rössing, Namibia (Table 4). The U-REE-Ti oxides all form solid solutions (Bowell et al., 2011). Thucholite is a rare amorphous bitumen-bearing U(IV) mineral observed in association with uraninite in palaeoplacers and in sediments including black shales (Luo et al., 2014).

Uranium(VI) minerals are most commonly replacements of primary U(IV) minerals and are notable by the number of hydrated minerals formed. The U(VI) minerals include hydrated uranyl phosphates, silicates, vanadates, carbonates, arsenates and molybdates (Table 4). The most common U(VI) minerals are autunite ($\text{Ca}(\text{UO}_2)_2(\text{PO}_4)_2 \cdot 10\text{--}12\text{H}_2\text{O}$) and uranophane ($\text{Ca}(\text{UO}_2)_2\text{SiO}_3(\text{OH})_2 \cdot 5\text{H}_2\text{O}$). The U(VI) minerals commonly occur in the alteration zones of primary U ore deposits as a result of hydrothermal alteration or weathering, including oxidation (Jerden and Sinha, 2006; Murakami et al., 1997; Pérez et al., 2000; Porcelli and Swarzenski, 2003). Carnotite has been commonly associated with calcrete and gypsum deposits in arid areas (Fujii and Swain, 1995). A variety of exotic metal hydrates are also found as efflorescences on mine walls in U-rich environments. Uranophane has also been found in association with corrosion of cement waste in nuclear installations (Kienzler et al., 2010).

The U oxide hydrate mineral, schoepite, occurs naturally through weathering. The synthetic uranium mineral metaschoepite (Table 4), is readily produced by alteration of schoepite under pressure at low temperature and by precipitation from uranyl-bearing solutions (Cot-Auriol et al., 2021; Weller et al., 2000). Metaschoepite formation is significant in the context of corrosion of U-based nuclear fuel and in laboratory experiments where a Na-rich background electrolyte is used.

Of the rock-forming minerals, U(VI) partitions strongly with phosphate, iron oxides and clay minerals. Concentrations of U in the range 20–300 mg/kg have been reported for phosphate ores from the USA (EPA, 1991). Smith et al. (1996) reported concentrations of 75–200 mg/kg in phosphate ores from Jordan. Weathered saprolite overlying the Coles Hill uranium deposit in Virginia, USA contains barium meta-autunite, a U(VI)-bearing phosphate mineral formed by alteration of primary coffinite and minor uraninite (Jerden et al., 2003). Uranium contents up to 1300 mg/kg were found in the lower part of the weathering profile, indicating enrichment relative to the unaltered primary ore. Similar associations between U and phosphate have also been found in the Southern Karoo province of South Africa and the Northwestern province of Zambia (Sanding and Bruno, 1992). Uranium also has a strong affinity for hydroxyapatite (Arey et al., 1999; Jerden and Sinha, 2003, 2006).

Uranium is found in association with goethite, hematite, ferrihydrite, magnetite and ilmenite (Bargar et al., 1999; Duff et al., 2002; Lahrouch et al., 2021; Missana et al., 2003; Payne et al., 1994; Schindler et al., 2010; Wazne et al., 2003; Zhao et al., 2012). These associations are

commonly attributed to sorption of the uranyl ion ($\text{U}(\text{VI})\text{O}_2^{2+}$) to surfaces (Bargar et al., 2000), although U(VI) can also be incorporated within the mineral structures (Duff et al., 2002). The uranium content of secondary iron oxides was in the range 773–4540 mg/kg (up to 8 wt % UO_3) (Sato et al., 1997) downgradient of a U deposit in Australia. Similarly, contents up to 2000 mg/kg were found in iron veins from Israel (Ilani et al., 1987). The largest contents were found in hematite.

Both U(VI) and U(IV) have been found in pyrite, where contents have been reported up to 1000 mg/kg (Qafoku et al., 2009) (Table 5).

Both U(IV) and U(VI) have been found to substitute for Ca^{2+} in structural sites of calcite. Sturchio et al. (1998) reported contents of 5–35 mg/kg, principally as U(IV), in calcite from Zn ore deposits. Kelly et al. (2003) reported a U range of around 80–500 mg/kg U(VI) in a stable structural position in a natural calcite speleothem. U(VI) can also sorb to calcite surfaces (Ma et al., 2014). A very small U content (0.023 mg/kg) was found in marine foraminiferal tests cleaned to remove clay and oxides (Delaney and Boyle, 1983) (Table 5).

Small amounts of U (<1 mg/kg) are also typical in quartz from magmatic and metamorphic rocks (Table 5). However, larger contents have been found in macrocrystalline quartz and chalcedony in agates associated with late-stage or post-volcanic alteration or weathering (Götze et al., 2015). The U occurrence in agates was inferred as surface-bound uranyl and U contained within radiation-induced structural defects. Large contents of U have also been found in opal, e.g. 207 mg/kg (Neymark and Paces, 2000) or up to 20,000 mg/kg (Schindler et al., 2010). Opal forms as a low-temperature silica precipitate in freshwater environments (Neymark and Paces, 2000), as a wood replacement (Castor and Henry, 2000), from remains of diatoms and radiolaria in a marine environment (Bradt Miller et al., 2010) or as a product of low-temperature alteration of volcanic rocks (Schindler et al., 2010). Bright green fluorescence of uraniferous opal is well-recognised (Othmane et al., 2016; Schindler et al., 2010).

Uranium is also concentrated in primary magmatic silicates, oxides and phosphates, especially zircon, titanite, monazite and allanite (Table 5). These occur in granitic rocks as accessory late-stage minerals (Porcelli and Swarzenski, 2003) and sedimentary rocks derived from them. Filippidis et al. (1997) reported a content of 157 mg/kg U in zircon from black heavy-mineral-bearing sands; Chentsov (1961) reported much larger contents of 1600–1860 mg/kg for zircon in granite and Moncur et al. (2011) up to 4000 mg/kg in detrital till. Amphiboles and micas in igneous rocks can also contain relatively large U contents (Table 5).

3.2. Occurrence of uranium ores

Uranium ore deposits consist most commonly of uraninite (UO_2), pitchblende (U_3O_8) and/or coffinite ($\text{U}(\text{SiO}_4)_{1-x}(\text{OH})_{4x}$) and their alteration products. Gangue minerals are typically quartz or carbonates (Dahlkamp, 2009). The ores may be nonmetallic or may occur combined with other amorphous trace metals (Co, Ni, Cu, Pb, Zn and Mo, V) as sulphides or arsenides. Pyrite and Fe oxides are ubiquitous (Dahlkamp, 2009).

The largest deposits of economic U ore occur in Australia, Kazakhstan and Canada (NEA and OECD, 2020) (Fig. 1). Primary uranium minerals rarely occur in sufficient quantity in igneous rocks to reach economic grades; for that to occur, redistribution via hydrothermal or low-temperature fluids is necessary (Pownceby and Johnson, 2014). Uranium ores can be categorized broadly into igneous-type, hydrothermal-type or sandstone-type deposits (Andersen et al., 2017). Within these categories, a number of discrete geological settings have been described. The three most significant in terms of ore tonnage are unconformity-related, Fe ore-Cu-Au deposits and sandstone-hosted deposits (Cuney, 2008; Dahlkamp, 1993; NEA and OECD, 2020).

Among the highest-grade and largest deposits in the world are the unconformity-related U ores. These occur at the unconformity between sandstones and underlying older metamorphic rocks. The two largest U

Table 5
Uranium content of some naturally-occurring primary and secondary minerals.

Mineral	U content (mg/kg)	Environment	Method	Reference
Calcite	0.023	Cleaned foram tests		Delaney and Boyle (1983)
Calcite	0.1–10	Reducing		Sturchio et al. (1998)
Calcite	5–35	Zn ore, USA		Sturchio et al. (1998)
Calcite	10–20	Speleothem	PIXE	Ortega et al. (2003)
Calcite	80–500	Speleothem	XRF	Kelly et al. (2003)
Aragonite	60–350	Speleothem	PIXE	Ortega et al. (2003)
Dolomite	1–11	Salt pan, Utah, USA		Bell (1963)
Quartz	<1	Igneous, metamorphic rocks		Götze et al. (2015)
Quartz	2.8–4.2	Agate, felsic igneous rocks	ICP-MS	Götze et al. (2015)
Quartz	2.1–3.0	Granite		Chentsov (1961)
Chalcedony, agate	<0.01–72	Agate, felsic igneous rocks	LA-ICP-MS	Götze et al. (2015)
Opal	2.03–207	Secondary, cavities in felsic tuffs, Yucca Mountain, USA	TIMS	Neymark and Paces (2000)
Opal	63–137	Tuffaceous sedimentary rocks, Nevada; unknown, Montana	ICP-MS	Pan et al. (2021)
Opal	to 20,000	Nopal U deposit, Peña Blanca, Mexico	EPMA	Schindler et al. (2010)
Agate	27–35.1	Sedimentary agate, Montana; agate in tuffs and ignimbrite, Saxony	ICP-MS	Pan et al. (2021)
Volcanic glass	2.56–5.69	Cordoba ash, Argentina		Nicolli et al. (1989)
Microcline	3.1–3.8	Granite		Chentsov (1961)
Plagioclase	3.8–4.4	Granite		Chentsov (1961)
Biotite	26–40	Granite		Chentsov (1961)
Muscovite	18–20	Granite		Chentsov (1961)
Amphibole	28–35	Granite		Chentsov (1961)
Apatite	25–32	Granite		Chentsov (1961)
Allanite	450–600	Granite		Chentsov (1961)
Monazite	1000–1300	Granite		Chentsov (1961)
Zircon	1600–1860	Granite		Chentsov (1961)
Ilmenite	30–40	Granite		Chentsov (1961)
Titanite	30–40	Granite		Chentsov (1961)
Chlorite	15–20	Granite		Chentsov (1961)
Zircon	157	Mineral sands	INAA	Filippidis et al. (1997)
Zircon	79–4000	Till deposits		Moncur et al. (2011)
Tourmaline	<0.002–4.13	Singhbhum Shear Zone, India, hydrothermal	LA-ICP-MS	Patel et al. (2021)
Apatite	10–100	Igneous rocks		Altschuler et al. (1957)
Apatite	50–200	Sedimentary rocks		Altschuler et al. (1957)
Fluorapatite	<10–790	Crystalline rocks		Altschuler et al. (1957)
Fluorapatite	45–240	Marine phosphorite		Altschuler et al. (1957)
Fluorapatite	41–125	Seafloor nodules		Altschuler et al. (1957)
Fluor-hydroxyapatite	60–8300	Fossil bone		Altschuler et al. (1957)
Hydroxyapatite	<10–10	Guano-derived phosphorite		Altschuler et al. (1957)
Phosphate	50–110	Sedimentary phosphorite	Fluorimetry	Shlewit and Alibrahim (2008)
Phosphate	20–300	Ore deposit, USA		EPA (1991)
Phosphate	75–200	Ore deposit, Jordan		Smith et al. (1996)
Iron oxide	773–4540	U deposit, Koongarra, Australia		Sato et al. (1997)
Amorphous iron oxide	485	Ore deposit, Pinhal do Souto, Portugal	ICP-OES	Neiva et al. (2014)
Hematite	2000	Israel		Ilani et al. (1987)
Hematite	to 14,000	Nopal U deposit, Peña Blanca, Mexico	EPMA	Schindler et al. (2010)
Fe precipitate	1500	Jordan		Smith (2000)
Pyrite	<100–1000	Sediment, Rifle, USA	EPMA	Qafoku et al. (2009)

deposits in the world occur in the McArthur River mine, Athabasca Basin, Saskatchewan, Canada (Chi et al., 2018; Cuney, 2005) and the Ranger deposit, McArthur Basin, Northern Territory, Australia (Fig. 1). The Athabasca Basin hosts the only known high-grade U ore (>1% and up to 20% as U₃O₈) (Chi et al., 2018; Dahlkamp, 2009). Operations at both mines have been suspended (Cameco, 2021).

In the Athabasca Basin, redox processes have played a large role in determining U distributions. Organic-rich Palaeoproterozoic metasedimentary basement rocks underlie the unconformity, with relatively undeformed continental Palaeo-Mesoproterozoic sediments above (Bruce et al., 2020). Hot (160–220 °C), acidic, oxic, basinal brines (about 1540–1590 Ma age, Alexandre et al., 2007; Chi et al., 2018) are inferred to have migrated to the underlying reduced basement rocks, setting up a redox gradient with reductive immobilization of U ore at the unconformity and associated with reactivated basement faults (Cuney, 2005). Ore deposits may straddle the unconformity but are typically within the crystalline basement below, potentially extending some hundreds of metres below (Bruce et al., 2020).

Other large unconformity-related deposits in Australia include Jabiluka, Naberlek and Koongarra in Northern Territory and Kintyre in Western Australia (Dahlkamp, 2009; Pownceby and Johnson, 2014). Here too, U ore is emplaced through oxidizing hydrothermal fluids

permeating the unconformity (Li et al., 2016). In these high-grade unconformity-related ores, mineral assemblages are typically dominated by uraninite, pitchblende, coffinite and brannerite (Bowell et al., 2011).

Iron ore-Cu-Au assemblages in granite breccia are also a major locus of U mineralization. The Olympic Dam complex in South Australia is the best-known example and the largest resource of low-grade U in the world (Fig. 1). The deposit (around 0.05% U₃O₈) hosts around 66% of Australia's U resources (Mudd, 2014), typically as brannerite. Hydrothermal fluids remobilized granite-hosted U and deposited it in greater concentration in quartz-hematite breccia. Olympic Dam is also the fourth largest copper deposit in the world and the majority of the revenue from the mine is generated from copper. Today, Olympic Dam is the only operational U mine in Australia.

Uranium ores can also be hosted by sandstones, often arkosic, of continental or marginal marine origin. Examples of mined resources include Inkai, Kazakhstan and Smith Ranch-Highland, Wyoming, USA. Sandstone-hosted ore deposits are typically of low to medium grade (0.05–0.4% U₃O₈). Uranium from proximal or parent U-bearing rocks (e. g. granite, pegmatite or black shale) or from intercalated volcanic beds (Abzalov, 2012), can be mobilized in oxic conditions as U(VI) until encountering anoxic conditions downgradient, at which point U is

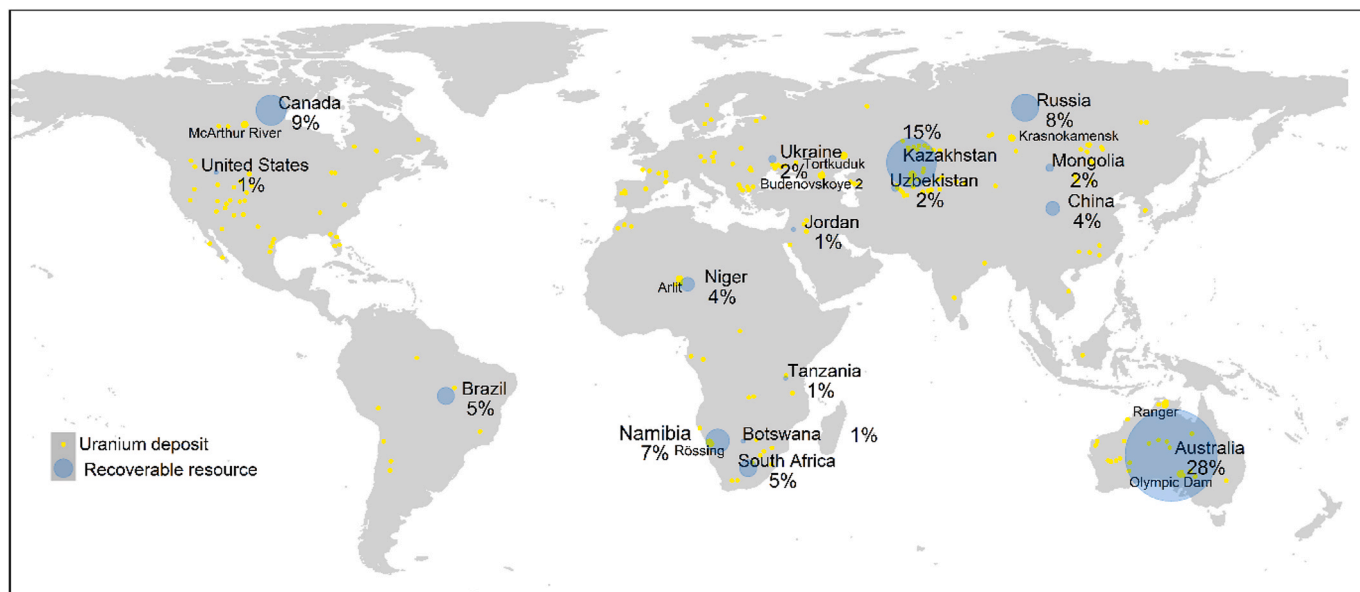


Fig. 1. Global distribution of known recoverable uranium resources (2019) belonging to major uranium producers (after NEA and OECD, 2020) and principal recognized uranium deposits, eight largest named (after Fairclough et al., 2018).

reduced and immobilized as U(IV). The U minerals commonly occur as roll-front deposits, the term reflecting the potential for reoxidation and mobilization in a dynamic system (Langmuir, 1978). The deposits are typically arcuate in cross section, and sinuous or irregular in plan view. Forms reflect the interactions of groundwater flow paths with the surrounding rock and may cut across bedding planes. Intermontane basins are a common environment for roll-front deposits and the occurrences can be laterally extensive. The Inkai deposit of Kazakhstan extends for some 100 km (Cuney, 2008). Uranium minerals in roll fronts have been identified typically as uraninite, pitchblende and coffinite, although U(IV) adsorbed to amorphous metal oxides or organic matter also occur (Bhattacharyya et al., 2017). Sandstone-deposited U ore may also be in tabular form, in basal channels where U may be immobilized in the presence of organic matter such as lignite (e.g. Monument Valley, Colorado Plateau, USA), or as deposits in fault zones, e.g. Arlit deposit, Niger, (Fig. 1) (Abzalov, 2012). The U mineralization in sandstone-hosted deposits can be accompanied by other redox-controlled trace elements including Se, Mo and V (Bullock and Parnell, 2017; Reynolds and Goldhaber, 1983). Most of the world's sandstone-hosted deposits date to around 850–540 Ma (Jaireth et al., 2016).

Uranium deposits may also occur in quartz-pebble conglomerates. These are deposits from alluvial fans or braided streams where detrital uraninite was deposited as placers, concentrated by gravity. These are the oldest U deposits, identified in eight locations globally, including the Huronian Supergroup, Ontario, Canada and the Witwatersrand Supergroup in South Africa. These types of U deposit predate the Great Oxidation Event (GOE) at around 2.4 Ga and were transported at a time when atmospheric oxygen was inferred to be absent. They are restricted to Archaean and Palaeoproterozoic ages. The GOE marked the appearance of atmospheric oxygen and therefore a shift in the redox status and hence mobilization mechanisms of U (Cumberland et al., 2016; Holland, 2005). The subsequent increase in U(VI) mobilization was linked with oxidative weathering.

In granitic rocks or around their margins, U can occur in veins and stockworks and grades are low to medium, ranging up to a few percent (Dahlkamp, 2009). The deposits derive from late-stage magmatic fluids circulating in fractures and joints. This type is responsible for much of the U mineralization occurring in Europe (e.g. France, Germany, Czech Republic) where U minerals are hosted by Variscan peraluminous

leucogranites (Dahlkamp, 2016), emplaced during extensional tectonism in the late Carboniferous/early Permian. Uranium mineralization has much less association with granitic rocks of the Caledonian and Alpine orogens in Europe (Dahlkamp, 2016). Uranium deposition is believed to be due to the mixing of oxic fluids leaching uraninite from granites with reducing groundwater from nearby sedimentary basins (Cuney, 2008). The mineralogy is typically dominated by uraninite. The largest resources across Europe occur in veins in the Massif Central, Armorican Massif and Vosges of France, the Iberian Meseta of Spain and the Bohemian Massif and Erzgebirge of Central Europe (Dahlkamp, 2016).

3.3. Rocks, sediments and soils

As U is a lithophile element, its content in the crust is higher than in the mantle (2.8 mg/kg and up to 0.022 mg/kg respectively, Table 6). Uranium contents of rocks are typically around 1–4 mg/kg (Drever, 1997; Hess et al., 1985; Taylor and McLennan, 1985) although as detailed in Section 3.2, larger contents can occur in granitic rocks, pegmatites, organic-rich-rocks, argillaceous sediments (clays, shales) and Fe- and PO₄-rich rocks (Table 6).

In igneous rocks, U is an incompatible element as it does not fit readily into the crystal structure of many rock-forming silicates. Contents increase in acidic rocks through fractional crystallization. Relatively large U contents can be found in granites, especially peralkaline types. In peralkaline rhyolites, U can be present in glass, from which the U is readily released on devitrification (Cuney, 2008). Peralkaline nepheline syenites can also have large contents. These are the products of extreme fractional crystallization of highly evolved magmas and can accumulate incompatible elements and volatiles under closed-system conditions. Similar accumulations can also occur in late-stage pegmatites, commonly as uraninite.

Popit et al. (2004) noted ranges for felsic igneous rocks of 3–4 mg/kg compared to intermediate igneous rocks (around 1.5 mg/kg), basic igneous rocks (around 0.6 mg/kg) and ultrabasic rocks (around 0.03 mg/kg). Langmuir (1978) reported contents in granite of 2.2–15 mg/kg. Simpson et al. (1979) found a range of <1–67 mg/kg for granites of various ages across the British Isles; of these, largest contents are present in the Variscan granites of south-west England. The U in British granites is concentrated in zircon, monazite and uraninite as primary magmatic

Table 6

Uranium contents of selected rocks, sediments and soils.

ROCK/SEDIMENT	LOCATION	RANGE (MG/KG)	SOURCE
Primitive mantle		0.008–0.022	Palme and O'Neill (2007)
Average upper crust		2.8	Taylor and McLennan (1985)
<i>Igneous/metamorphic rocks</i>			
Granite	British Isles	2.2–15	Langmuir (1978)
Granite	British Isles	<1–67	Poole (2001), Hussain (1997); Ball and Miles (1993); Hennessy (1981), Simpson et al. (1979)
Granite	Stripa, Sweden	20–54	Andrews et al. (1989)
Kaolinised Variscan granite	South-west England	5.4–8	Simpson et al. (1979)
Granite	Leinster, Ireland	1.8–7.0	O'Connor et al. (1982)
Granite	Yilgarn, Western Australia	5–10	Butt et al. (1977)
Granite	Telangana, India	10.2–116	Shrivastava et al. (1992)
Granite	Manitoba, Canada	6.5	Gascoyne (1989)
Fresh granite	Coffee Au deposit, Yukon, Canada	1.9–29	Skierszkan et al. (2020b)
Fresh gneiss	Coffee Au deposit, Yukon, Canada	0.27–20	Skierszkan et al. (2020b)
Fresh schist	Coffee Au deposit, Yukon, Canada	0.34–6.2	Skierszkan et al. (2020b)
Rhyolitic volcanic ash	Argentina	1.25–8.0	Nicolli et al. (1989)
Rhyolite	Nevada/Oregon, USA	9–20	Castor and Henry (2000)
Felsic volcanic rocks		1.04–6.88	Morales-Arredondo et al. (2018)
Felsic igneous rocks		3–4	Popit et al. (2004)
Intermediate igneous rocks		1.5	Popit et al. (2004)
Basic igneous rocks		0.6	Popit et al. (2004)
Ultrabasic igneous rocks		0.03	Popit et al. (2004)
Basalt		1	Alloway (2013)
Peralkaline nepheline syenite	Ilímaussaq, Greenland	32–338	Sørensen (1992)
<i>Sedimentary rocks</i>			
Chalk	Southern England	0.05–6.3	Murphy (1998); Ivanovich and Alexander (1985)
Limestone		1.3	Eisenbud and Gesell (1997)
Fluvial/marine sandstone	Great Artesian Basin, Australia	1.0–4.3	Priestley et al. (2018)
Triassic red-bed sandstone	England	0.5–11	Andrews and Lee (1979); Haslam and Sandon (1991); Cuttell et al. (1988); Ball and Miles (1993)
Devonian red-bed sandstone	Broubster, Scotland	20–114	Read et al. (1993)
Palaeoproterozoic red-bed sandstone	Francheville Basin, Gabon	0.43–75.6	Bankole et al. (2016)
Siwalik sand/siltstone	Himachal Pradesh, India	1.65–24.7	Singh et al. (2001)
Palaeozoic shales	Britain	3.2–14	Bowie et al. (1979)
Continental margin sediments	Off California, USA	2–8	McManus et al. (2005)
Continental shelf sediments	Off California, USA	1.29–5.77	Klinkhammer and Palmer (1991)
Distal turbidites		1–10	

Table 6 (continued)

ROCK/SEDIMENT	LOCATION	RANGE (MG/KG)	SOURCE
	Madeira abyssal plain		Colley and Thomson (1985)
Loess silts	Argentina	0.9–5.1	Smedley et al. (2005)
Loess silts	Salí River Basin, Argentina	3.34–16	Nicolli et al. (2012a)
Quaternary alluvial sediments	Datong Basin, China	1.9–8.8	Wu et al. (2019)
Tidal flat, Fe-oxide-rich alluvial fans	Baja California	2.0–4.3	Zielinski et al. (1983)
Alluvial sediments	San Joaquin Valley, California, USA	1.22–4.20	Jurgens et al. (2008)
Reduced marine sediment	Black Sea	20–40	Degens et al. (1977)
Black shales	Britain	5–60	Ball et al. (1992); Ball and Miles (1993); Bottrell (1993)
Black shales	Okchun, South Korea	250	Lee et al. (2001)
Devonian black shale	Appalachian Basin, USA	56	Leventhal et al. (1986)
Cretaceous oil shale	Israel	10–56	Ilani et al. (2006, 1987)
Coal		up to 200	Bowen (1979)
Coal	Paraná, Brazil	66–211	Galhardi and Bonotto (2017)
Coal	Guiding Coalfield, China	67.9–288	Dai et al. (2015)
Phosphatic horizons in Devonian Old Red Sandstone	Scotland	100–1300	Michie (1970); Gallagher et al. (1971)
Phosphatic sedimentary rocks	Eastern England	30–119	Sutherland (1991)
Phosphatic rocks	USA	up to 120	Roessler et al. (1979); Eisenbud and Gesell (1997)
Phosphate-rich sediments	Jordan	75–200	Smith et al. (1996)
Phosphorite	Middle East	120–130	Dahlkamp (2009)
Phosphorite	Bakouma, Central African Republic	1660–5600	Gony (1971)
<i>Ore deposits</i>			
Breccia pipes	Grand Canyon, Arizona, USA	24–12,100	Wenrich and Sutphin (1989)
Lignite-hosted palaeochannel U deposit	Gunbarrel Basin, W Australia	1–5870	Douglas et al. (2011)
Athabasca metasediment	Canada	120,000	Leventhal et al. (1986)
Roll-front sandstone, oxidized	Erlian Basin, NE China	1.4–14.8	Bonnetti et al. (2020)
Roll-front sandstone, reduced	Erlian Basin, NE China	2.4–70.3	Bonnetti et al. (2020)
Roll-front sandstone, mineralized	Erlian Basin, NE China	79.6–1058	Bonnetti et al. (2020)
U roll-front sandstone	Wyoming, Colorado, USA	1–25,000	WoldeGabriel et al. (2014), Bullock and Parnell (2017)
U phosphate mineral deposit	Coles Hill, Virginia, USA	1300	Jerden et al. (2003)
Lake sediment, mining-affected	Ontario, Canada	100–800	Novotnik et al. (2018)
Calcrete	Yilgarn Craton, Western Australia	10–10,000	Butt et al. (1977)
<i>Soils</i>			
Soils over schist/gneiss	Himachal Pradesh, India	1.62–19.8	Singh et al. (2001)

(continued on next page)

Table 6 (continued)

ROCK/SEDIMENT	LOCATION	RANGE (MG/KG)	SOURCE
Unfertilized/ fertilized soil	Illinois, USA	4.2–4.9	Hamamo et al. (1995)
Unfertilized soil	Florida, USA	0.3–0.9	Zielinski et al. (2006)
Phosphate-fertilized soil	Florida, USA	1.0–1.4	Zielinski et al. (2006)
Peat	Florida, USA	0.2–9	Zielinski et al. (2000)
Peat	Broubster, Scotland	1–1000	Read et al. (1993)
Organic-rich wetland soil	Switzerland	500–4000	Regenspurg et al. (2010)
Peat, lacustrine clay	Laramie River Valley, Colorado, USA	2–3280	Owen and Otton (1995)
Soils over quartz-veined granite, U mine	Pinhal do Souto, Portugal	<25–337	Neiva et al. (2014)
Soils over granite/sandstone	Erlian Basin, north-east China	1.56–35.6	Zhang et al. (2020)
Paddy soils	Jiangxi Province, China	0.09–5.22	Ma et al. (2020)
Soils, U mine	South China	1.44–416	Shi et al. (2021)
Contaminated wetland soil/sediment	Tims Branch wetlands (Savannah River), South Carolina, USA	3.78–281	Kaplan et al. (2017)
Soils, control area around U mine	South China	2.1–3.1	Shi et al. (2021)
Soils, U mine	South Terras, England	111–1690	Corkhill et al. (2017)
Soils, phosphorite deposit	Jordan	<48–1068	Xoubi (2015)

minerals, but also redistributed in hydrothermal veins and secondary minerals such as kaolinite and Fe oxide (Poole, 2001; Simpson et al., 1979). Contents of 20–54 mg/kg were reported from the Stripa granite, Sweden (Andrews et al., 1989) (Table 6), where uraninite was found to be the main U mineral. Peralkaline nepheline syenites from the Ilímaussaq intrusion of southern Greenland have reported contents of 32–338 mg/kg (Sørensen, 1992). Associated hydrothermal veins contain pitchblende while skarns produced by contact metasomatism contain uranopyrochlore and betafite.

In sedimentary rocks, the largest U contents are typically found in organic-rich deposits, including black shale, peat and coal, and in phosphorites. Accumulations of U can exceed those in parent igneous or metamorphic rocks. The organic matter can produce reducing conditions favouring the precipitation of U(IV) minerals such as coffinite, U(SiO₄)_{1-x}(OH)_{4x} (Xu et al., 2015) and a ²³⁸U-heavy form of biogenic uraninite containing ‘non-crystalline’ U(IV) (Stylo et al., 2015). However, not all analyses support this reductive mechanism (Cumberland et al., 2018). Uranium can also bind strongly to organic matter as both U(IV) and U(VI). A U content of 56 mg/kg was reported for a black shale from the Appalachian Basin, USA (Leventhal et al., 1986) and 10–56 mg/kg were found in Cretaceous oil shales from northern Negev, Israel (Ilani et al., 1987). Bottrell (1993) found U contents in the range 5–10 mg/kg in UK Carboniferous shales, while values of 10–60 mg/kg were reported by Ball et al. (1992) (Table 6). Carboniferous black shales in south-west England have contents of 5–21 mg/kg (Ball and Miles, 1993).

Contents of U in the range 0.2–9 mg/kg were found in peats variably impacted by inputs from agricultural drainage in Florida, USA (Zielinski et al., 2000). The U was considered dominantly partitioned with organic carbon. Holocene peat deposits from Scotland have contents in excess of 200 mg/kg (Read et al., 1993). Contents up to 4000 mg/kg were found in Swiss peats (Regenspurg et al., 2010).

Eocene lignite deposits formed in palaeochannels in Gunbarrel Basin, Western Australia have U contents up to 5870 mg/kg (Table 6). Original

U sources were taken to be nearby lamproite and carbonatite intrusive rocks with redistribution following weathering (Douglas et al., 2011). The U is principally associated with organic matter in the deposits, though minor coffinite and uraninite are present. Large contents are also found in coal, e.g. 66–288 mg/kg (Bowen, 1979; Dai et al., 2015; Galhardi and Bonotto, 2017).

Elevated U contents can be found in argillaceous deposits but these tend to be lower than organic-rich types. Argillaceous marine deposits in the range 2–14 mg/kg are typical (Bowie et al., 1979; McManus et al., 2005) (Table 6).

Uranium is present in large concentrations in phosphorites. These P-rich deposits form in shallow continental shelves with restricted circulation (Cuney, 2008). One of the best-known examples is the Late Cretaceous uraniferous phosphorite belt of the Middle East which extends from Turkey to Morocco via Syria, Iraq, Jordan, Israel and Egypt. These deposits contain typically 120–130 mg/kg U (Dahlkamp, 2009). Sedimentary phosphorites consist in large part of francolite, a carbonate-rich fluorapatite (Ca₁₀(PO₄)_{6-x}(CO₃)_x(F,OH)_{2+x}).

Uranium contents of continental red-bed sandstones can also be relatively large in places, likely dependent on associations with Fe oxides and/or phosphate minerals. In the oldest red beds known, Palaeoproterozoic deposits of the Francheville Basin, Gabon, have contents in the range 0.43–75.6 mg/kg with higher values in the finer fraction (Bankole et al., 2016). In the continental red-bed Devonian sandstone of Scotland, contents up to 1300 mg/kg have been found in phosphate-rich horizons (Michie, 1970). In the red-bed Triassic Sandstone of England, a range of 0.5–11 mg/kg has been reported (Table 6), again with highest values in finer-grained horizons (Cuttell et al., 1988). Weibel and Friis (2004) observed phosphatic coffinite in the mineralized cores of reduction spots in the Triassic (Bunter) Sandstone of Germany.

Limestones typically contain relatively small amounts of U unless associated with mineralization. An average U content of 1.3 mg/kg was quoted for limestones by Eisenbud and Gesell (1997) (Table 6). Ivanovich and Alexander (1985) determined average values of 2.03 mg/kg for the English Chalk. Contents of 0.05–6.3 mg/kg were given for the Chalk by Murphy (1998), but pure carbonate samples were usually found to have <1 mg/kg with higher values in marls and hardgrounds. These may have contained U-bearing phosphate.

By contrast, contents can be extremely large in calcrete deposits from U mineralized areas. Ranges in valley-fill and playa calcretes of the Archaean Yilgarn Craton of Western Australia have in the range of 10–10,000 mg/kg U and associated large contents of V. The U occurs almost invariably as carnotite (Table 4) and is present as void and fracture coatings and finely disseminated grains in playas. The calcretes, formed by evaporation, include calcite and dolomite with lesser amounts of aragonite, clays including sepiolite and occasional gypsum and halite. Oxidic evaporitic conditions favoured the precipitation of uranyl vanadate (Butt et al., 1977).

Red-bed tidal-flat and alluvial-fan deposits from Baja California were found to have U contents of 1.8–4.3 mg/kg (Zielinski et al., 1983). The U was concentrated either in the rare refractory minerals or adsorbed to more widely disseminated detrital magnetite grains or authigenic mineral surface coatings. The quartz and feldspar minerals forming the bulk of the rock had small U contents (Zielinski et al., 1983).

Average contents of U in soil are around 2 mg/kg (Dissanayake and Chandrajith, 2009). The median content of U in 5700 surface soils from England and Wales was 2.2 mg/kg (Rawlins et al., 2012). Unfertilized soils from Florida, USA, were reported to contain 0.3–0.9 mg/kg U (Zielinski et al., 2006) (Table 6). Soils from control areas not affected by U mining activity in southern China had contents of 2.1–3.1 mg/kg (Shi et al., 2021). Contents of 1.62–19.8 mg/kg were found in soils over metamorphic rocks (schist/gneiss) from Himachal Pradesh, India (Singh et al., 2001) reflecting increased U content of bedrock sources. Small increases have been recorded in phosphate-fertilized soils: Zielinski et al. (2006) reported a range of 1.0–1.4 mg/kg in fertilized soils from Florida, USA, slightly above the 0.3–0.9 mg/kg baseline range.

Table 7
Uranium concentration ranges in precipitation, surface water and seawater.

Water type	Location	Range ($\mu\text{g/L}$)	n	Source
<i>Precipitation (rain/snow)</i>				
Snow	San Luis Valley, Colorado, USA	0.001–0.007	11	Lanzoni (2019)
Rain	San Luis Valley, Colorado, USA	0.001–0.10	64	Lanzoni (2019)
Rain	Kirundo Province, Burundi	0.031	2	Post et al. (2017)
<i>Surface water</i>				
Average rivers	World	0.3		Mangini et al. (1979)
Rivers	Germany	0.23–3.5	14	Mangini et al. (1979)
River	Dischmar River, Switzerland	2.4		Regenspurg et al. (2010)
Rural rivers	River Clyde catchment, Scotland	0.0118–0.299	60	Smedley et al. (2017)
Urban river	River Clyde catchment, Scotland	<0.02–1.24	122	Smedley et al. (2017)
River water	Various cities in India	0.92–5.37	7	Singh et al. (1996)
River	Yellow River, China	3.85–7.57		Juanjuan et al. (2014)
Stream	Strengbach stream, Vosges, France	0.08–0.35	16	Riotte and Chabaux (1999)
Streams	Germany	0.007–43.7	944	Birke et al. (2009)
Streams	Europe	<0.002–21.4	808	Salminen et al. (2005)
Streams	River Clyde catchment, Scotland	<0.003–10.8	1702	Smedley et al. (2017)
Surface water	India	≤ 0.2 –22	936	Sahoo et al. (2021)
Surface water	Ohio, USA	0.3–3.9	35	Lyons et al. (2020)
Streams over Siwalik Group sediments	Himachal Pradesh, India	0.29–1.79	7	Singh et al. (1999)
Rivers/lakes/tanks	Karnataka, India	0.1–23	37	Lapworth et al. (2021)
Surface water	Datong Basin, China	1.2–16	5	Wu et al. (2014)
Lake	Lake Tshohoha, Burundi	0.1–6.3	7	Post et al. (2017)
Alkaline lakes	Rift Valley, Ethiopia	0.2–73.5	6	Rango et al. (2010)
Alkaline lake	Ulaanbaatar, Mongolia	0.01–57	129	Nriagu et al. (2012)
Alkaline lake	Mono Lake, California, USA	554	5	Simpson et al. (1982)
Hyperalkaline (soda) lake	E Mongolian steppe	57–1490		Linhoff et al. (2011)
<i>Runoff</i>				
Surface runoff, unfertilized soils,	Florida	<0.001–0.022	4	Zielinski et al. (2006)
Surface runoff, phosphate-fertilized soils	Florida	0.065–0.091	4	Skierszkan et al. (2020a)
Agricultural drainage from peat, fertilized	Everglades, Florida	0.09–2.4	31	Zielinski et al. (2000)
Unfertilized drainage from peat	Everglades, Florida	<0.01–0.1	17	Zielinski et al. (2000)
Streams over unfertilized peatland	Switzerland	29–93		Regenspurg et al. (2010)
<i>Surface water in mineralized areas</i>				
Retention pond water	Ranger U mine, Northern Territory, Australia	1200		Brown et al. (1998)
Tailings dam	San Marcos Dam, Chihuahua valley, Mexico	620	1	Rentería Villalobos et al. (2007)
Surface water, with Au mineralization	Dawson Range, Yukon, Canada	<1–340	2539	Skierszkan et al. (2020a)
Surface water, U mineralized	Sinai, Egypt	600–1130	2	Ramadan et al. (2022)
Acid mine drainage in river water	Tinto River, Spain	0.26–18.6	12	Hierro et al. (2013)
Acid mine drainage	Hejiacun U mine, Hunan, China	0.014–1370	15	Peng et al. (2009)
Acid mine lake	Osamu Utsumi pit lake, Brazil	100–4200	4	Ferrari et al. (2015)
Acid drainage in river	Ribeira da Pantanha, Portugal	7.7–48.6	4	Carvalho et al. (2015)
Acid mine drainage	Curilo, Bulgaria	100–2750		Groudev et al. (2007)
River in coal mine area	Figueira, Paraná, Brazil	8.1–24.3	8	Gallhardi and Bonotto (2017)
Acid mine drainage	Poços de Caldas U Mine, Brazil	6000–14,000		Ladeira and Gonçalves (2007)
<i>Seawater</i>				
Open seawater		3.3		Mangini et al. (1979); Colley et al. (1989)
Anoxic seawater	Black Sea	1.31–2.13	36	Anderson et al. (1989)
Hydrothermal fluids	Mid-Ocean Ridge, East Pacific Rise, Gulf of California	0.06–0.18		Chen et al. (1986)
Continental shelf	Off California, USA	0.63–4.3	35	Klinkhammer and Palmer (1991)
Estuarine/seawater	Tampa Bay, Florida	2.07–3.05	33	Swarzenski and Baskaran (2006)
River/estuary transect	Alafia River/Tampa estuary, Florida, USA	0.86–3.97	11	Swarzenski and Baskaran (2006)
Estuarine water	Delaware estuary, USA	0.013–2.57	37	Sarin and Church (1994)
Estuarine water	River Amazon	0.056–3.22		Swarzenski et al. (2004)
Estuarine water	Off New South Wales, Australia	0.9–5.95		Sanders et al. (2017)
Estuarine water	Yellow River, China	3.85–7.57		Juanjuan et al. (2014)
Estuarine water	River Clyde catchment, Scotland	<0.1–1.2	8	Smedley et al. (2017)
Estuarine water	Huelva Estuary, Spain	0.22–4.02	15	Hierro et al. (2013)
Estuarine/bay water	Waquoit Bay, Cape Cod, Massachusetts, USA	2.31–2.95	27	Charette and Sholkovitz (2006)

Strong binding of U to soil organic matter means that significant enrichments can be observed in organic-rich soils, in both natural and contaminated settings. Uranium contents of 25–4000 mg/kg were found in Swiss natural organic-rich wetland soils, U correlating well with soil organic carbon content (Regenspurg et al., 2010). Contents of 3.78–281 mg/kg were found in industrially contaminated organic-rich wetland soils of South Carolina, USA (Kaplan et al., 2017). Contents in the range 2–3280 mg/kg were also reported in peat from Colorado, USA in areas close to old mine workings (Owen and Otton, 1995). These studies typically show U(VI) dominance, despite often reducing conditions, and a strong association of the uranyl with the humic fraction.

Large U contents can be seen more generally in soils proximal to U mining or mineralized areas. For example, in areas close to abandoned U

mines, contents of 1.44–416 mg/kg have been reported in China (Shi et al., 2021), <25–337 mg/kg in Portugal (Neiva et al., 2014) and 111–1690 mg/kg in England (Corkhill et al., 2017).

4. Uranium in natural waters

4.1. Rainwater

Lanzoni (2019) reported concentrations of dissolved U up to 0.007 $\mu\text{g/L}$ in snowfall and up to 0.10 $\mu\text{g/L}$ in rainfall from the San Luis Valley, Colorado, USA (Table 7). Post et al. (2017) found 0.031 $\mu\text{g/L}$ U in rainwater from Burundi. Specific events can lead to anomalous concentrations of U in rainfall. For example, the breakup of the

nuclear-powered Soviet satellite Kosmos-954 over Canada on January 24, 1978 led to rainfall enriched in ^{234}U and ^{235}U relative to ^{238}U at Fayetteville, Arkansas in April–May 1980. Also the concentration of ^{238}U in rainfall increased markedly after the eruption of Mount St. Helens in 1980 (Sakuragi et al., 1983).

4.2. Surface water

Uranium concentrations of typically less than around 4 $\mu\text{g/L}$ have been reported in river water. A worldwide average of 0.3 $\mu\text{g/L}$ has been reported (Mangini et al., 1979). A range of 0.23–3.5 $\mu\text{g/L}$ was found in rivers of Germany (Mangini et al., 1979), while Regenspurg et al. (2010) found 2.4 $\mu\text{g/L}$ in the Dischmar River of Switzerland. Indian rivers have a typical range of 0.92–5.37 $\mu\text{g/L}$ (Singh et al., 1996). Concentrations in the River Clyde of Scotland were <0.02–1.24 $\mu\text{g/L}$ (Smedley et al., 2017). The Yellow River, China, provides about 1% of the global dissolved flux of U to the sea, probably its single largest source, with monthly samples taken in 2010 at Lijn close to the estuary ranging from 3.85 to 7.57 $\mu\text{g/L}$ (Juanjuan et al., 2014).

Concentrations can be higher in small-order streams, depending on local geology and land use. For European first-order streams, the FOREGS (Forum of European Geological Surveys) geochemical database provides a range for U of <0.002–21.4 $\mu\text{g/L}$ (Salminen et al., 2005). Distributions are strongly controlled by geology and by streamwater pH, higher concentrations occurring in relatively alkaline streams. Highest values are observed in: (i) the Baltic countries, with dominant rock types including marl, limestone, dolomite and phosphorite; (ii) northern Poland on superficial deposits; (iii) Hungary on Alpine rocks; (iv) the southern Iberian Peninsula on Variscan granites; (v) southern Italy on alkaline volcanic rocks, and (vi) southern Germany on Mesozoic rocks (Fig. 2). Isolated high concentrations are also seen in areas of known U mineralization, e.g. Essone river valley, France; southern Polish border; Badajoz, south-west Spain. Low concentrations occur over much of Scandinavia, which is characterized by Precambrian Shield and Caledonide bedrocks, as well as the UK, which also includes Caledonides, and Denmark which has superficial deposits over Precambrian Shield formations. Low concentrations are also seen over Variscan formations of the north-west and central Iberian Peninsula, Massif Central and northern France, and south-west England.

In the Clyde catchment around Glasgow, Scotland, mapping of U in streamwaters (<0.003–10.8 $\mu\text{g/L}$) also showed a strong geological control, with pH having an influence. Lowest U concentrations occurred in upland areas in the north-west of the catchment (Fig. 3). These overlie basaltic rocks of the Clyde Plateau Volcanic Formation and the upland soils are commonly peaty; streams in this area are the most acidic of the catchment (pH 4–7) and carbonate poor. Streams overlying Ordovician and Silurian rocks at the southern end of the catchment also had low U concentrations. Highest concentrations were in streams over Devonian red-bed sandstone and Carboniferous Scottish Coal Measures Group. The former contains iron oxides and some phosphate minerals; the latter is an organic-rich deposit. Concentrations in the Clyde river waters generally reflected diluted forms of the contributing streams (Smedley et al., 2017).

In streams from Germany, Birke et al. (2009) found a range of 0.007–43.7 $\mu\text{g/L}$ (Table 7). Highest concentrations were in mining areas and relative highs were also associated with streams over Triassic red-bed Bunter and Keuper sediments. In France, slightly high U concentrations (2.4–5.7 $\mu\text{g/L}$) were found in streams passing through a peat bog (water pH ca. 6) downgradient of former U mines. However, in these the dominant U fraction was found to be in the particulate and colloidal rather than dissolved fraction (Phrommavanh et al., 2013).

In the Yukon, Canada, streamwater U concentrations are reported in the range <1–340 $\mu\text{g/L}$, the concentrations influenced by the presence of mineralized bodies, including the Coffee Au-sulphide deposit and Casino Cu–Au–Mo porphyry deposit. Both these areas had U concentrations in surface water usually above 15 $\mu\text{g/L}$ (Skierszkan et al.,

2020a). Two samples of surface water in a U mineralized area, El Allouga mine, Sinai, Egypt had concentrations of 600–1130 $\mu\text{g/L}$ (Ramadan et al., 2022).

Application of phosphate fertilizer has often been cited as a contributory source of U in surface waters (e.g. Schnug and Lottermoser, 2013) (Section 5.3). Concentrations greater than 2 $\mu\text{g/L}$ in the Birke et al. (2009) study were prevalent in agricultural areas. Drainage from phosphate-fertilized peats in the northern Everglades, USA, showed increased concentrations (0.3–2.4 $\mu\text{g/L}$) compared to unfertilized peat (<0.1 $\mu\text{g/L}$) (Zielinski et al., 2000), again suggesting an additional phosphate fertilizer source. Concentrations of U in runoff from agricultural pastureland elsewhere in central Florida were lower than for the peat study (Table 7) but still higher than for natural grassland sites. The low overall dissolved concentrations were considered to be due to sorption of U to organic carbon in the soils (Zielinski et al., 2006).

Uranium concentrations in alkaline and saline lakes from the central Rift Valley of Ethiopia have concentrations in the range 0.2–73.5 $\mu\text{g/L}$ (Rango et al., 2010). Values were <10 $\mu\text{g/L}$ in all but one sample. This had a pH of 10 and alkalinity as HCO_3^- of 38,600 mg/L. Mono Lake, California, USA, had concentrations of around 554 $\mu\text{g/L}$ (Simpson et al., 1982). Hyperalkaline groundwater-fed soda lakes from eastern Mongolia also had a range of 57–1490 $\mu\text{g/L}$ with a typical pH of 10 (Linhoff et al., 2011). High U concentrations were attributed to evaporation; the original U source was inferred to be alkaline rhyolites.

High concentrations of U have also been found in some acid mine drainage. Hejiacun U mine in Hunan Province, China, produces acid mine drainage with U concentrations in the range 0.014–1370 $\mu\text{g/L}$ and associated high concentrations of Fe, Mn, Cd, Cu, As, Ni and Zn. Black shales of the region host pyrite along with autunite, cuprouranite and uraninite. Concentrations of U were observed decreasing along a 1.2 km stretch of stream flowing downgradient from the mine adit discharge point, with pH rising from 2.76 to 7.77 along the stretch (Peng et al., 2009).

Uranium concentrations in the range 6000–14000 $\mu\text{g/L}$ were also found in surface drainage from Poços de Caldas U Mine in Minas Gerais State, Brazil. The water had a pH of 2.7 with high concentrations of SO_4 , F and Fe. Dissolved U was mainly in the form $\text{UO}_2(\text{SO}_4)_3^{4-}$ (Ladeira and Gonçalves, 2007). Similarly, drainage from Curilo U mine, Bulgaria, had a pH of 2.5–4.0 with high concentrations of U (100–2750 $\mu\text{g/L}$) and other dissolved metals (Groudev et al., 2007). Lower but still elevated concentrations (0.26–18.5 $\mu\text{g/L}$) were found in the Tinto River, Spain in water affected by acid mine drainage from the Iberian Pyrite Belt (Hierro et al., 2013).

Seasonal variability in U concentrations of surface waters has been observed in response to cyclical changes in physico-chemical conditions (pH, redox) caused for example by varying inputs of rainfall and temperature-dependent biological activity (Ma et al., 2011; Mochizuki et al., 2016).

4.3. Seawater

Supply of U to seawater derives from river inputs as well as potentially from groundwater. In open seawater, U behaves conservatively and occurs as uranyl (U(VI)), mainly complexed with carbonate and Ca/Mg. Under these conditions, uranyl has a long residence time of some hundreds of thousands of years (Barnes and Cochran, 1990; Henderson and Anderson, 2003). In open seawater, U is present in concentrations of around 3.3 $\mu\text{g/L}$ (Table 7). Its removal from solution occurs via reduction to U(IV) and sequestration in reducing organic-rich sediments or carbonates (Andersen et al., 2017; Klinkhammer and Palmer, 1991; Mangini et al., 1979; Russell et al., 1994). Uranium is also removed from solution as U(IV) in high-temperature hydrothermal zones at mid-ocean ridges (Chen et al., 1986).

Reducing organic-rich, U-rich sediments occur in anoxic basins and pelagic and estuarine environments. Nonetheless, the reduction from U(VI) to U(IV) can be slow and not necessarily within the anoxic water

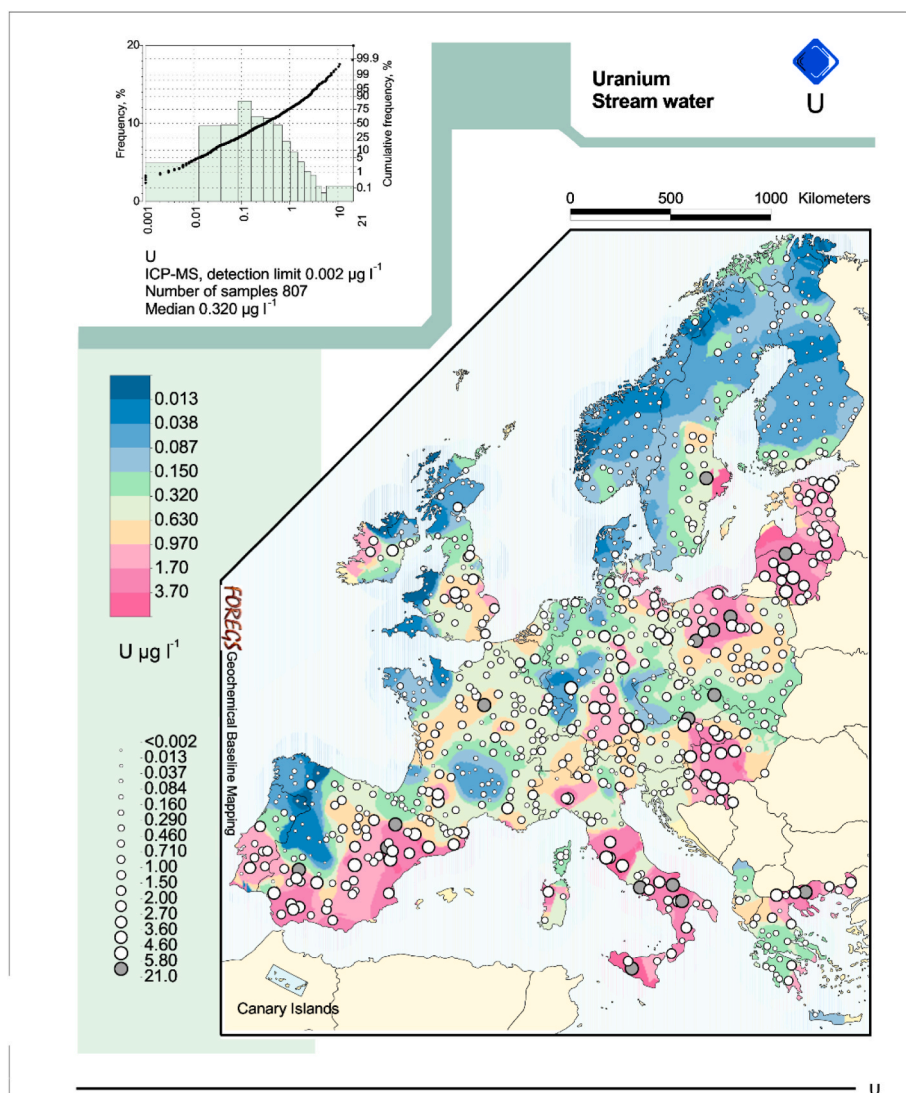


Fig. 2. Uranium concentrations in European streamwaters (FOREGS) (Salminen et al., 2005). Geochemical Atlas of Europe; copyright © 2005 the Association of the Geological Surveys of The European Union (EuroGeoSurveys)/the Geological Survey of Finland.

column. Anderson et al. (1989) noted U concentrations in a Black Sea profile of 1.31–2.13 $\mu\text{g/L}$, varying with salinity, but with the lowest values in the deepest part at 2000 m depth. No inflection in concentrations was visible at the $\text{O}_2/\text{H}_2\text{S}$ interface, and U was maintained as U(VI) throughout the profile. Similar observations were made for the Cariaco Basin (Anderson, 1987). Estimated U residence times in the anoxic, sulphidic bottom waters in both areas were inferred as a thousand years or more, much longer than would be anticipated for reduction of U(VI) to U(IV) in the water column (Anderson, 1987; Anderson et al., 1989). Accumulation of U(IV) in the sulphidic bottom sediments (Degens et al., 1977) was attributed to slow kinetics of U(VI) reduction to U(IV), the process taking place within the sediments rather than the overlying water column (Anderson et al., 1989). Diffusion of U across the sediment-water interface has also been shown by enrichments in marine porewaters from organic-rich sediments (Klinkhammer and Palmer, 1991). Reduction of U(VI) to U(IV) was inferred as coincident with SO_4 reduction, resulting ultimately in the formation of uraninite, possibly via a U(V) metastable phase.

Sanders et al. (2017) noted a U range of 0.90–5.95 $\mu\text{g/L}$ (salinity-corrected) in estuarine waters off New South Wales, Australia. The U correlated positively with dissolved Fe, suggesting that reductive dissolution of Fe oxides released U, causing increased concentrations in solution relative to seawater. Concentrations in a transect across the

Alafia River/estuarine mixing zone of Tampa, Florida, USA were in the range 0.86–3.97 $\mu\text{g/L}$, also indicative of non-conservative mixing, with U possibly contributed from dissolution of carbonate rocks, discharge of groundwater and/or from local phosphate mining (Swarzenski and Baskaran, 2006). Relatively high concentrations (3.85–7.57 $\mu\text{g/L}$) were also recorded in the Yellow River estuary, China, and attributed to desorption of U from loess river-bed sediments (Juanjuan et al., 2014). Swarzenski et al. (2004) noted a U range of 0.056–3.22 $\mu\text{g/L}$ across the Amazon estuary with net loss of U, attributed to sorption to metal oxides. Sarin and Church (1994) also noted losses of U due to sorption to Fe oxides or reduction to U(IV) in the Delaware estuary, USA. Charette and Sholkovitz (2006) reported slight net U loss from estuarine water from Cape Cod, USA. Similarly, Hierro et al. (2013) concluded that U in acidic mine-affected river water adsorbed to Fe oxides in estuarine waters on mixing with seawater. Estuaries have been inferred as either net sources or net sinks of U depending on redox conditions, pH and seasonal variability (Hierro et al., 2013; Juanjuan et al., 2014; Sanders et al., 2017), the dominant processes being site-specific (Swarzenski and Baskaran, 2006).

4.4. Groundwater

Groundwaters can contain substantially higher U concentrations

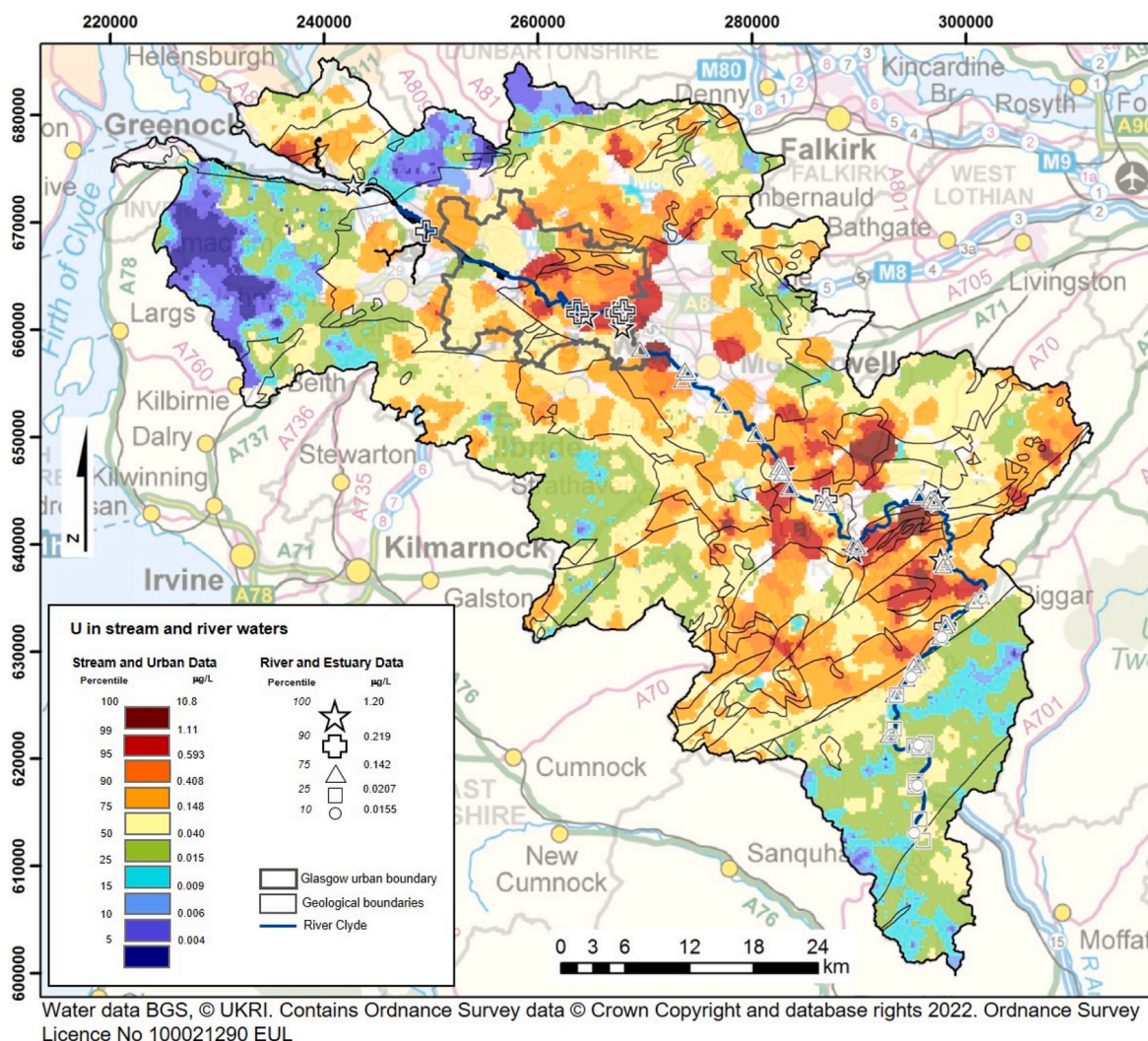


Fig. 3. Dissolved uranium in stream and river water from the River Clyde catchment, Scotland (from Smedley et al., 2017).

than adjacent surface waters (Table 8). Concentrations in groundwater significantly above the provisional WHO (2017) guideline value (30 µg/L) have been reported in numerous countries, including India, Australia, Canada, USA, as well as locations in South Korea, Burundi, China, Cyprus, Iraq, Portugal, southern Finland and South Africa (Fig. 4). In many other countries, concentrations in groundwater close to the WHO guideline value have also been found. Reporting has been sporadic: in many countries, U in water has not been measured routinely because of a lack of regulation until recently.

Distributions in India are among the best-documented, with numerous groundwater studies having been carried out over several decades. A recent national compilation of 54,618 analyses of groundwater in India has given a range of U concentrations of ≤ 0.2 –4918 µg/L (median 1.9 µg/L) (Sahoo et al., 2021). Concentrations substantially above 30 µg/L have been reported in Uttar Pradesh, Andhra Pradesh, Madhya Pradesh, Telangana, Tamil Nadu, Rajasthan, Haryana, Karnataka, Punjab, Himachal Pradesh and West Bengal. Large areas of peninsular India have high concentrations in groundwater from areas of Archaean granitic and Proterozoic granitic gneiss basement.

In northern Rajasthan concentrations of 2.54–133 µg/L were reported by Rani et al. (2013a), almost all being greater than 30 µg/L. A range of 11–63 µg/L was found in Uttar Pradesh (Kumar et al., 2015) and 0.8–72 µg/L were found in Tamil Nadu (Adithya et al., 2019). Uranium concentrations in the range 0.2–68 µg/L (Brindha et al., 2011)

and 7–370 µg/L (Keesari et al., 2014) have been reported in groundwater from granitic rocks in Nalgonda district of Telangana; 22% and 68% respectively were above 30 µg/L (Brindha et al., 2011; Keesari et al., 2014). The granites of the district are also relatively enriched in U (Table 6).

In Karnataka, a range of 0.3–1443 µg/L was reported by Babu et al. (2008) and of 1–5995 µg/L by Srinivasan et al. (2021). Here, 78% were >30 µg/L. Higher values were observed in the dry season than during the monsoon. High concentrations are associated with granite bedrock, in Archaean rocks of the Dharwar craton (Srinivasan et al., 2021). Concentrations of 0.2–589 µg/L were also reported for groundwater from granitic areas in Karnataka; 30% were greater than 30 µg/L and most were less than 130 µg/L (Lapworth et al., 2021).

Coyte et al. (2018) found high concentrations in groundwater from granite and metamorphic basement rocks from Rajasthan and Gujarat. In Rajasthan, 33% of groundwater samples exceeded 30 µg/L and in Gujarat, the exceedance was 5%. The high concentrations were associated with high alkalinity under oxic conditions. A statistically significant decrease in U concentration with depth was observed in Gujarat samples. The groundwaters also had high F, salinity and nitrate concentrations.

High concentrations also occur in large regions of Punjab, either in association with granitic basement aquifers or the Quaternary alluvial Indo-Gangetic plains. Kochhar et al. (2007) found high concentrations

Table 8
Uranium concentration ranges in groundwater, including porewater.

Aquifer type	Location	Range (µg/L)	n	Source
Sedimentary				
J aquifer fluvial/marine sandstone	Great Artesian Basin, Australia	0.02–19.1	25	Priestley et al. (2018)
Alluvial	High Plains, USA	<0.5–2670	26255	Nolan and Weber (2015)
Alluvial	Central Valley, California, USA	<0.5–5400	4916	Nolan and Weber (2015)
Alluvial	Central Valley, California, USA	<1–455	558	Belitz et al. (2003), Lopez et al. (2020)
Alluvial	San Joaquin Valley, California, USA	0.04–2500	350	Jurgens et al. (2010)
Alluvial, lacustrine	Tulare Basin, Central Valley, California	1.1–5400	110	Fujii and Swain (1995)
Aeolian, alluvial and lacustrine	Carson Desert, Nevada, USA	3.4–550	14	Welch and Lico (1998)
Cretaceous marine limestone and alluvial sand	Edwards-Trinity, Texas, USA	<1–154	108	Hudak (2018)
Miocene alluvial/lacustrine, Tesuque Formation	Española Basin, New Mexico, USA	<0.2–1820	688	Linhoff et al. (2016)
Sivalik Group sandstone/siltstone	Himachal Pradesh, India	0.26–2.56	15	Singh et al. (2001)
Mixed alluvium, older sedimentary, basement	Himachal Pradesh, India	0.56–10.1	30	Rani et al. (2013b)
Conglomerate, sand, gritstone	Upper Siwaliks, India	1.08–19.7	34	J. Singh et al. (2009)
Quaternary alluvium	Ganga basin, Hisar city, Haryana, India	5.3–114	38	Garg et al. (2014)
Quaternary alluvium	Indo-Ganga basin, Punjab, India	1.24–45.4	15	Rani et al. (2013b)
Quaternary alluvium	Ganga basin, Malwa, Punjab, India	5.41–43.4	34	Mehra et al. (2007)
Quaternary alluvium	Ganga basin, south-west Punjab, India	0.5–579	498	Bajwa et al. (2017)
Quaternary alluvium	Ganga basin, Punjab, India	3.19–45.6	28	Singh et al. (2003)
Quaternary alluvium	Ganga basin, Amritsar-Bathinda, Punjab, India	0.9–63		H. Singh et al. (2009)
Quaternary alluvium	Indo-Ganga basin, south-west Punjab, India	0.02–476	2062	Sahoo et al. (2022)
Quaternary alluvium	Indo-Ganga basin, Punjab, India	5–316	18	Kochhar et al. (2007)
Quaternary alluvium	Indo-Ganga basin, Punjab, India	2–644	102	Kumar et al. (2014)
Quaternary alluvium	Ganga basin, Bihar	0.1–238	456	Kumar et al. (2018)
Quaternary alluvium	Gujarat and Rajasthan, India	0.2–294	135	Coyte et al. (2018)
Quaternary alluvium	Indus basin, Punjab, Pakistan	0.1–556	110	Ali et al. (2019)
Quaternary alluvium	Indus basin, Sindh, Pakistan	0.8–59	38	Ali et al. (2019)
Sedimentary indurated	Rajasthan, India	0.02–31.3	50	Coyte et al. (2018)
Sedimentary	Kudankulam, Tamil Nadu, India	<0.2–6.6	36	Selvi et al. (2016)
Sedimentary	Hyderabad and Secunderabad cities, Andhra Pradesh, India	0.6–82		Balbudhe et al. (2012)
Springs, Sivalik Group sandstone and clay rocks	Himachal Pradesh, India	0.07–4.65	19	Singh et al. (1999)
Quaternary alluvium	Datong Basin, China	0.02–288	161	Wu et al. (2014)
Quaternary alluvium	Huhhot Basin, China	<0.01–53	73	Smedley et al. (2003)
Alluvium	Dornogobi Aimag Province, Mongolia	<0.24–429	202	Nriagu et al. (2013)
Alluvial fan	Al Batin, Iraq	0.1–98	43	Alkinani et al. (2016)
Limestone, marl	northern Greece	0.01–10.0	21	Katsoyiannis et al. (2007)
Quaternary alluvium	La Rioja, Argentina	up to 362		Martinez and Carillo-Rivera (2006)
Quaternary loess	Sali River Basin, Argentina	0.03–125		Nicollini et al. (2012b)
Quaternary loess silt	La Pampa, Argentina	6.2–250	108	Smedley et al. (2002)
Quaternary loess silt	Córdoba, Argentina	1.45–365	60	Nicollini et al. (1989)
Quaternary loess	Córdoba, Argentina	8.8–97	39	Matteoda et al. (2019)
Mixed lithologies				
Mixed sedimentary, granitic, metamorphic	Chhattisgarh, India	0.21–10.04	53	Singh et al. (2021)
Metamorphic (khondalite, charnockite)	Vishakhapatnam, Andhra Pradesh, India	0.6–12.3	12	Bhangare et al. (2013)
Ophiolite, sedimentary	Cyprus	0.15–39.1	41	Charalambous et al. (2013)
Quaternary alluvium, Cenozoic basalt, Mesozoic sandstone	New South Wales, Australia	0.001–2.77	91	Atkins et al. (2016)
Metamorphic/sedimentary	Kumaun, Uttar Pradesh; Sivalik, Himachal Pradesh, India	1.08–35.8		Ramola et al. (1988)
Various	India	<0.2–4918	54618	Sahoo et al. (2021)
Quaternary alluvium, Karoo mudrock, Proterozoic gneiss	Namakwaland, South Africa	1.3–5100	86	Makubalo and Diamond (2020)
Mixed bedrock: granite, gneiss, pelite	Connecticut, USA	<1–3170	2191	Gross and Brown (2020)
Mixed bedrock, sedimentary	USA	<0.006–550	3541	Ayotte et al. (2011)
Alluvium, felsic igneous	Platte River Valley, Nebraska, USA	0.3–99.3	151	Snow and Spalding (1994)
Mixed, sandstone, limestone, igneous, metamorphic	Great Britain	<0.002–67.2	2174	BGS (unpublished)
Porphyry Cu–Mo deposit	Spence deposit, Chile	0.1–18.9	50	Leybourne and Cameron (2008)
Granitic basement				
Granitic basement	Bhatinda district, Punjab	5–316	18	Kochhar et al. (2007)
Granite and alluvium	Bhiwani Dist, Haryana, India	6.37–43.3	23	Kansal et al. (2011)
Granite	Uttar Pradesh, India	11–63		Kumar et al. (2015)
Granite	northern Rajasthan, India	2.54–133		Rani et al. (2013a)
Granite	Nalgonda district, Telangana, India	0.2–68	44	Brindha et al. (2011)
Granite	Nalgonda district, Telangana, India	7–370	31	Keesari et al. (2014)
Granite	Nalgonda district, Telangana	0.6–521		Raghavendra et al. (2014)
Granite	Tamil Nadu, India	0.79–72	54	Adithya et al. (2019)
Granite-gneiss	Tamil Nadu, India	0.2–113		Thivya et al. (2014)
Granite-gneiss	Kolar district, Karnataka, India	0.3–1443	52	Babu et al. (2008)
Granite	Karnataka, India	1–5995	142	Srinivasan et al. (2021)
Granite, metamorphic	Gujarat, India	0.6–26.8	22	Coyte et al. (2018)
Granite-metamorphic	Rajasthan, India	5.1–320	41	Coyte et al. (2018)
Granite-metamorphic	Karnataka, India	0.2–589	92	Lapworth et al. (2021)
Proterozoic metasediment	Tummalapalle, Andhra Pradesh	0.38–79.7	106	Rana et al. (2016)

(continued on next page)

Table 8 (continued)

Aquifer type	Location	Range ($\mu\text{g/L}$)	n	Source
Basalt	Gujarat, India	0.1–2.1	10	Coyte et al. (2018)
Layered alluvial	Gujarat, India	<0.2–85.8	66	Coyte et al. (2018)
Icheon granite	South Korea	0.02–1640	74	Jo et al. (2011)
Granite and gneiss and hydrothermal veins	South Korea	<0.01–3610	4140	Shin et al. (2016)
Okchun area granite, black shale	South Korea	0.54–263	33	Lee et al. (2001)
Granite	Rio de Janeiro, Brazil	1–390	30	Godoy et al. (2019)
Granite, gneiss, and mixed sedimentary	Switzerland	0.05–92.0	5548	Stalder et al. (2012)
Mixed sedimentary, metamorphic	Kosovo	0.012–166	951	Berisha and Goessler (2013)
Granite	Southern Finland	0.001–1920	325	Kurttio et al. (2002)
Granite	Southern Finland	6–3400		Prat et al. (2009)
Metamorphic, granite	Trondheim–Oslofjord, Norway	0.32–170	30	Banks et al. (1995)
Mixed metamorphic	Norway	<2.5–750	476	Frengstad et al. (2000)
Gneiss	Arjäng, Sweden	<0.2–470	153	Seldén et al. (2009)
Granite	Stripa, Sweden	0.02–90.2	100	Andrews et al. (1989)
Granite	Leinster granite, Ireland	0.002–309	126	Papageorgiou et al. (2022)
Metasediment	Kitigan Zibi, Québec, Canada	<1–845	113	Zamora et al. (2009)
Granite and metasediment	north-east Washington, USA	1–8860	2327	Kahle et al. (2018)
Granite-gneiss	Greenville County, South Carolina, USA	1.8–7780	35	Orloff et al. (2004)
Granite	Greenville/Simpsonville, South Carolina, USA	0.1–5570		Warner et al. (2011)
Granite	Lac Du Bonnet, Manitoba, Canada	<0.5–837	74	Gascoyne (1989)
Granite	Kirundo, Burundi	0.238–734	215	Post et al. (2017)
Igimbrite, rhyolite	Rift Valley, Ethiopia	0.1–49.9	23	Rango et al. (2010)
Hot springs, ignimbrite, rhyolite	Rift Valley, Ethiopia	<0.1–0.9	12	Rango et al. (2010)
Alluvium	Kazakhstan	0.54–64	19	Kawabata et al. (2008)
<i>U mineralized areas</i>				
Alluvial aquifer with local U mineralization	Punjab, India	11.7–114	16	Singh et al. (1995)
Unconfined alluvial aquifer, U processing plant	Rifle, Colorado, USA	95–333		Anderson et al. (2003)
Unmined U deposit	Coles Hill, Virginia, USA	5–13.9	3	Jerden and Sinha (2003)
Groundwater close to Permian breccia U deposit	Grand Canyon, USA	<1–293	573	Tillman et al. (2021)
Groundwater with weathered phosphate	Florida, USA	<1–460	22	Missimer et al. (2019)
Sandstone-hosted groundwater across a roll front	Smith Ranch-Highland, Wyoming, USA	5–40,000	20	Brown et al. (2016)
Quaternary alluvium above sandstone-hosted U deposit	Grants, New Mexico, USA	18.8–8390		Ulrich et al. (2019)
U deposit	Okélobondo, Gabon	0.32–332		Salas and Ayora (2004)
Unmined schist-hosted U ore groundwater	Koongarra, Australia	0.12–440	42	Payne (1991); Yanase et al. (1995)
Channel and playa deposits	Yilgarn Craton, Western Australia	0.5–696	1220	Noble et al. (2011)
Channel and playa deposits	Yilgarn Craton, Western Australia	100–500		Butt et al. (1977)
Quartz-veined granite U deposit	Pinhal do Souto, Portugal	29.6–104	32	Neiva et al. (2014)
Granite-hosted U mine	El Atshan, Egypt	519	1	Dabous et al. (2002)
Carboniferous sediment U deposit	El Allouga, Sinai, Egypt	90–500	10	Ramadan et al. (2022)
Granite/sandstone-U deposits	Erlian Basin, north-east China	0.18–453	329	B. Zhang et al. (2020)
Shallow groundwater, U mine	south China	550–3360	8	Shi et al. (2021)
U mine tailings area	Jiangxi Province, China	550–3360	7	Ma et al. (2020)
Palmetto U deposit	Southern Finland	2.2–765		Ahonen et al. (2004)
U deposit	Helsinki, Southern Finland	<1–14,870	308	Asikainen and Kahlos (1979)
U deposits, metamorphic, granite	Dawson Range, Yukon, Canada	<1–535	384	Skierszman et al. (2020a)
Unconformity-type sandstone U deposit	Cigar Lake, Saskatchewan, Canada	<0.1–11.9	15	Cramer (1986)
Acidic groundwater, coal mine	Figueira, Paraná, Brazil	16.1–2370	8	Galhardi and Bonotto (2017)
Acid drainage in U mine	Königstein, Germany	7140–69000		Arnold et al. (2011)
<i>Porewater</i>				
Peat soil porewater	Switzerland	2.4–71		Regenspurg et al. (2010)
Soil porewater	Savannah River, South Carolina, USA	0.47–59.5	137	Kaplan et al. (2017)
Soil porewater	Broubster, Scotland	0.55–14.3	6	Read et al. (1993)
Loess sediment porewater	La Pampa, Argentina	0.8–119	105	Smedley et al. (2002)
Estuarine porewater	Long Island Sound, USA	0.63–5.35	20	Barnes and Cochran (1993)
Estuarine porewater	Amazon, Brazil	0.67–33.7	34	Barnes and Cochran (1993)
Estuarine porewater	Waquoit Bay, Cape Cod, Massachusetts, USA	<0.02–6.43	137	Charette and Sholkovitz (2006)
Mining-contaminated lake porewater	Bentley, Bow lakes, Bancroft, Canada	10–1300	39	Novotnik et al. (2018)

up to 316 $\mu\text{g/L}$ in Bhatinda district, Punjab, in association with granite within the Aravalli-Delhi Supergroup and the Malani igneous suite of the basement. Singh et al. (1995) also found concentrations up to 114 $\mu\text{g/L}$ in groundwaters from Bathinda, Punjab, taken to be due to local U mineralization. Bajwa et al. (2017) found concentrations in the range 0.5–579 $\mu\text{g/L}$ in south-west Punjab (68% of samples >30 $\mu\text{g/L}$) in groundwater from Indo-Gangetic Quaternary alluvium but located on the crest of the Aravali-Delhi ridge. Uranium was inferred by the authors to be leaching from granite.

Associated with the Quaternary Indo-Gangetic alluvial aquifer of India, H. Singh et al. (2009) found U concentrations up to 63 $\mu\text{g/L}$ in Bathinda district, Punjab. Singh et al. (2003) found a range of 3.19–45.6 $\mu\text{g/L}$ in the Amritsar area of Punjab (pH range 7.0–8.7). Sahoo et al. (2022) reported a range in alluvial groundwaters from Punjab of

0.02–476 $\mu\text{g/L}$. They concluded that shallow groundwater <60 m depth had higher concentrations overall (0.15–476 $\mu\text{g/L}$) than those from 61 to 518 m depth (0.02–275 $\mu\text{g/L}$), though both had representatives well above the WHO guideline value. Groundwater in the affected area is oxic, pH neutral to alkaline and with higher TDS (up to 3200 mg/L) in the shallow aquifer. The high As groundwaters of Bangladesh generally contained very low U concentrations, samples with As >100 $\mu\text{g/L}$ having <10 $\mu\text{g/L}$ U and only 4 samples out of 271 exceeding 30 $\mu\text{g/L}$ U (BGS and DPHE, 2001). Many of these groundwaters are strongly reducing.

High U concentrations (0.1–556 $\mu\text{g/L}$) were noted in groundwater from the Indus basin of Punjab, Pakistan. Concentrations were highest in Lahore district. Relative highs were also seen in Sindh, Pakistan (range 0.8–59 $\mu\text{g/L}$). Groundwater was pH-neutral to alkaline (7.1–9.0), and appeared to be oxic (low Mn concentrations) where U concentrations



Fig. 4. Global occurrence of high-uranium groundwaters (with representatives above 30 $\mu\text{g/L}$) (for data sources, see Table 8).

were highest (Ali et al., 2019). Concentrations tend to be lower ($<30 \mu\text{g/L}$) in groundwater from the Miocene-Pleistocene sedimentary aquifers of the Siwalik Group of Himachal Pradesh, northern India (Rani et al., 2013b; Singh et al., 2001).

In South Korea, the Icheon granite has associated groundwater U concentrations of 0.02–1640 $\mu\text{g/L}$, 11% of samples exceeding 30 $\mu\text{g/L}$ (Jo et al., 2011). Groundwater is mostly slightly acidic although the pH range is 5.38–8.15; groundwater is oxic (NO_3 -bearing). A similarly large range of concentrations (<0.01 –3610 $\mu\text{g/L}$) was also reported by Shin et al. (2016) for a wider area of granitic rocks of South Korea; some 4% exceeded 30 $\mu\text{g/L}$. Concentrations of 0.54–263 $\mu\text{g/L}$ were found in groundwater from the Okchun area of South Korea where black shales and granite occur; higher concentrations were found in hot springs than cold springs in the area (Lee et al., 2001).

In the Datong Basin, China, groundwater U concentrations of <0.02 –288 $\mu\text{g/L}$, 24% above 30 $\mu\text{g/L}$, were reported by Wu et al. (2014). Groundwater is from a Quaternary alluvial aquifer and is alkaline (pH 7.36–9.58, HCO_3 up to 1500 mg/L) and oxic. In the Quaternary alluvial aquifer of the Huhhot Basin of China, a much lower range of <0.01 –53 $\mu\text{g/L}$ was reported (Smedley et al., 2003). These are also alkaline, but are predominantly strongly (SO_4 -) reducing. In north-east China, concentrations in the range 0.18–453 $\mu\text{g/L}$ have been found above sandstone-hosted and granitic U mineralized areas of the Erlian Basin (B. Zhang et al., 2020).

In Mongolia, groundwaters from Dornogobi Aimag Province alluvium have U in the range <0.24 –429 $\mu\text{g/L}$, 36% of analyzed samples being above 30 $\mu\text{g/L}$. Higher concentrations were present in shallow ($<10 \text{ m}$) than deeper ($>50 \text{ m}$) groundwater sources. Groundwater pH was 6.4–9.7. Uranium covaried with Mo and As as well as Mn (Nriagu et al., 2013).

In Western Australia, the Yilgarn Craton has high recorded U groundwater concentrations close to palaeochannel-related U mineralization where the dominant mineral is carnotite hosted by calcrete. Uranium concentrations up to 696 $\mu\text{g/L}$ occur in and around the U mineralized areas. The main source of U is granite (Butt et al., 1977; Noble et al., 2011). Around the Koongarra uranium deposit, concentrations up to 440 $\mu\text{g/L}$ occur in groundwater above the deposit although they are lower ($<30 \mu\text{g/L}$) both upstream and downstream of it (Payne, 1991; Payne and Airey, 2006; Yanase et al., 1995) (Section 8.2).

In the USA, high U concentrations have been documented in a number of areas, including the High Plains aquifer, Central Valley of

California, Carson Desert of Nevada, New Mexico, New England and Florida, as well as localized occurrences in areas of known U mineralization. The USGS National Water Quality Assessment (NAWQA) survey of groundwater showed a range up to 550 $\mu\text{g/L}$, concentrations were found to be significantly higher ($P < 0.0001$) in dry areas (range <0.21 –550 $\mu\text{g/L}$) than humid areas (range <0.006 –440 $\mu\text{g/L}$) (Ayotte et al., 2011) (see also Fig. 18, Section 8.5).

In the Central Valley, concentrations of <0.5 –5400 $\mu\text{g/L}$ have been found (Nolan and Weber, 2015); concentrations up to 5400 $\mu\text{g/L}$ were also reported for the area by Fujii and Swain (1995). Complexation with CO_3 and PO_4 were suggested as mechanisms for U mobility in these groundwaters. Concentrations up to 550 $\mu\text{g/L}$ have also been reported for groundwater from Quaternary aeolian, lacustrine and alluvial deposits of the Carson Desert of Nevada, USA (Welch and Lico, 1998). High values were taken to be due to evaporation although additional release from metal oxides under mildly reducing conditions (likely Mn-reducing, with dissolved oxygen concentrations $<1 \text{ mg/L}$) was also proposed. The sediments were derived ultimately from granitic and tuffaceous rocks and these might be the original sources of U. The similarities in geological setting with sandstone-type U deposits were noted by Welch and Lico (1998).

The major Plio-Pleistocene High Plains aquifer encompasses eight states across central USA from South Dakota to Texas. Sediments comprise mainly alluvial deposits. Groundwater U concentrations in the range <0.5 –2670 $\mu\text{g/L}$ were reported by Nolan and Weber (2015). High concentrations of NO_3 were also reported.

Linhoff et al. (2016) found a U range of <0.2 –1820 $\mu\text{g/L}$ in groundwater from Miocene alluvial, lacustrine and tuff fan deposits of the Española Basin, New Mexico. pH was in the range 5.8–9.6 and HCO_3 18.3–2380 mg/L . High concentrations of U were associated with highs of F (<1 –6.5 mg/L), Mo (<1 –136 $\mu\text{g/L}$), V (<1 –373 $\mu\text{g/L}$) and As (<0.2 –89.5 $\mu\text{g/L}$). TDS was typically high (7–11,350 mg/L). Aquifer sediments are weathered from volcanic precursors and U roll-front deposits occur in the vicinity; both were considered likely origins of the aqueous U (Linhoff et al., 2016).

In Texas, mixed Cretaceous sediments of the Edwards-Trinity aquifer, largely comprising sand but including limestone and evaporite, have oxic groundwater with pH in the range 6.07–7.6 and U concentrations of <1 –154 $\mu\text{g/L}$ (Hudak, 2018). Some 29% of sampled wells had U concentrations greater than 30 $\mu\text{g/L}$. The aquifer is hydraulically connected to the Mio-Pliocene High Plains aquifer in its northern

margins (Barker et al., 1994).

In Connecticut, Gross and Brown (2020) found over 100 private water-supply wells with U concentrations greater than 30 µg/L (range <1–3170 µg/L, median <1 µg/L). High concentrations were in groundwater from bedrock including granite, gneiss and pelite, but also included mafic rocks, e.g. norite.

In and around Greenville County, South Carolina, high U concentrations (up to 7780 µg/L) have been found in groundwater from granitic and granite-gneiss basement rocks (Orloff et al., 2004; Warner et al., 2011). Sources were inferred to be primary uraninite and secondary coffinite in the granite matrix and fractures. Secondary calcite and Ca zeolite were also present. Uranium concentrations correlated with groundwater pH and alkalinity and were highest where pH was in the range 7.25–8.25 and HCO₃ greater than 55 mg/L (Warner et al., 2011).

In Florida, NAWQA data indicate occurrence of groundwater with concentrations greater than 30 µg/L (Figs. 4 and 18). Concentrations are elevated in superficial deposits compared to underlying limestone and pumping-induced drawdown to the main Florida limestone aquifer may be responsible (Ayotte et al., 2011). Shallow groundwater from Florida in superficial deposits containing weathered phosphate minerals is also reported to contain U at concentrations in the range <1–460 µg/L (Missimer et al., 2019).

Jerden and Sinha (2003) reported three analyses for groundwater, each with U < 15 µg/L, in the Coles Hill U deposit of Virginia, USA. The site contained a reduced primary ore zone of uraninite and coffinite with a shallow oxic weathered zone with U phosphate mineralization. The low solubility of Ba meta-autunite was inferred as the cause of the low concentrations. In contrast, high U concentrations (95–333 µg/L) were reported in shallow groundwater from an unconfined alluvial aquifer contaminated from a former uranium ore processing plant at Rifle, Colorado, USA (Anderson et al., 2003).

In Canada, the Lac du Bonnet granite of Manitoba hosts groundwater with U concentrations of <0.5–837 µg/L. Wells are shallow and many have been used for drinking water. Groundwater is oxic and alkaline (HCO₃ up to 1000 mg/L) and with pH of mostly 8.0–8.5; groundwater is calcite-saturated (Gascoyne, 1989). Uranyl carbonates are taken to be the dominant species with U derived from the granitic rocks (U typically 6.5 mg/kg) (Gascoyne, 1989). In the Yukon of Canada, U in groundwater was found to be higher in rocks dominated by gneiss and schists than granite bedrocks. The former contained carbonate minerals (calcite, dolomite, ankerite, siderite) and these were considered instrumental in increasing U mobility by facilitating the formation of dissolved Ca–U-carbonate species. Granitic bedrock had <1 wt% carbonate, with lower groundwater Ca concentrations, alkalinity and undersaturation with calcite (Skierszkan et al., 2020a). The area is also mineralized, hosting the Coffee Au-sulphide deposit and the Casino Cu–Au–Mo porphyry deposit.

In contrast, Cramer (1986) reported U concentrations only up to 11.9 µg/L in groundwater from the unconformity-type U deposit of Cigar Lake, Saskatchewan, Canada. Groundwater was mostly pH-neutral with low alkalinity (HCO₃ 4–125 mg/L); the groundwater sampled in this study was anoxic due to flow restrictions caused by clays overlying the U deposit.

In Argentina, concentrations in the range 1.45–365 µg/L were found in Córdoba Province (Nicolli et al., 1989), 8.8–97 µg/L in Valle de la Cruz, Córdoba (Matteoda et al., 2019) and 6.2–250 µg/L in La Pampa Province (Smedley et al., 2002). Groundwaters in these areas are from Quaternary loess deposits with interbedded rhyolitic or dacitic volcanic ash and occur under oxic and alkaline conditions (Section 8.4).

In Namakwaland, South Africa, Makubalo and Diamond (2020) reported U concentrations in the range 1.3–5100 µg/L in groundwater from mixed Quaternary alluvium and metamorphic aquifers (most were <400 µg/L). High values were attributed to evaporation and release from secondary U mineralization; groundwater had salinity values up to seawater concentrations. In northern Burundi, groundwater has been

found with U up to 734 µg/L. Of 66 groundwater samples analysed, 29% were >30 µg/L (Post et al., 2017). The aquifers were granitic and metamorphic bedrock and weathered granitic sand. Groundwaters had a range of redox conditions, demonstrated by variations in Fe, Mn, NO₃ and NH₄ but the highest U concentrations were present where these were oxic (Post et al., 2017).

In southern Finland, concentrations up to 3400 µg/L have been found in groundwater from granite (Prat et al., 2009). High concentrations are also found in proximity to the Palmottu U deposit where deposits of uraninite with alteration rims of coffinite occur within micaceous gneiss and granite. Groundwater concentrations in the range 2.2–765 µg/L were found, highest values in oxic groundwater above the ore body, with low values at depths greater than 150 m under reducing conditions (Ahonen et al., 2004). In a deposit from the Helsinki area, concentrations up to 14,870 µg/L were recorded (4.5% of groundwater samples were greater than 1000 µg/L) (Asikainen and Kahlos, 1979). Bedrock hosts were granites, amphibolites and migmatites.

In Norway, concentrations up to 170 µg/L were found in a few samples of groundwater from granite in the Iddefjord, Oslofjord area (Banks et al., 1995). In Switzerland too, highest concentrations (up to 92 µg/L) were found in groundwater associated with granite and gneiss bedrocks (cantons of Valais, Graubünden, Fribourg and Ticino), though here 99.7% of analyses were below 30 µg/L (Stalder et al., 2012).

In Cyprus, groundwater samples have been found with U concentrations of 0.15–39.1 µg/L in groundwater from ophiolite and from sedimentary rocks (Charalambous et al., 2013). In Britain, concentrations of U are usually low but with a small number of occurrences above 30 µg/L (<0.002–67.2 µg/L; Fig. 5). Highest concentrations are found in oxic zones of red-bed sandstone aquifers of Triassic and Devonian age as well as some Precambrian bedrocks. Relatively low concentrations are found in groundwater from the Variscan granites of south-west England (Shand et al., 2007).

In Iraq, 0.1–98 µg/L U were found in groundwater from an unconfined Quaternary gypsiferous alluvial fan deposit. U concentrations were lower in deeper groundwaters from an underlying confined aquifer (greater than around 150 m deep). Mobilization of U was linked to carbonate and phosphate complexation under oxic conditions (Alkinani et al., 2016).

In Egypt, occurrences of a limited extent occur in places linked to U mineralization. Examples with near-neutral pH include El Atshan (U concentration 519 µg/L) and El Allouga mines (U concentration 90–500 µg/L) (Dabous et al., 2002; Ramadan et al., 2022).

Acid mine drainage with high concentrations of U has also been found to affect some groundwaters. Arnold et al. (2011) reported concentrations up to 69,000 µg/L in mine dripstone waters with pH ca. 2.5 in Königstein, Saxony, Germany. Galhardi and Bonotto (2017) found concentrations of 16.1–2370 µg/L in groundwater in the approximate pH range 3–6 in a coal-mining area of southern Brazil.

4.5. Porewater

Soil and sediment porewaters commonly have close associations with organic matter, either through complexation in solution or the solid phase (Haas and Northup, 2004; Regenspurg et al., 2010). Porewaters to 20 cm depth in lake sediments from the U-mining-contaminated Bentley and Bow Lakes of Bancroft area, Ontario, Canada, had U concentrations of 10–1300 µg/L and 10–460 µg/L respectively. Porewaters were reducing in both profiles but the U peaks were attributed to complexation with dissolved organic matter (Novotnik et al., 2018). Uranium(VI) in oxic soil porewater (range 0.55–14.3 µg/L) from Broubster, Scotland, was also inferred to be complexed with fulvic acid at pH 5.75–6.48 (Read et al., 1993).

Soil porewater with U concentrations of 2.4–71 µg/L was reported in Swiss organic-rich wetland soils having U contents up to 4000 mg/kg. The porewater was anoxic; U was present dominantly in the solid phase, partitioned with the solid organic matter (Regenspurg et al., 2010).

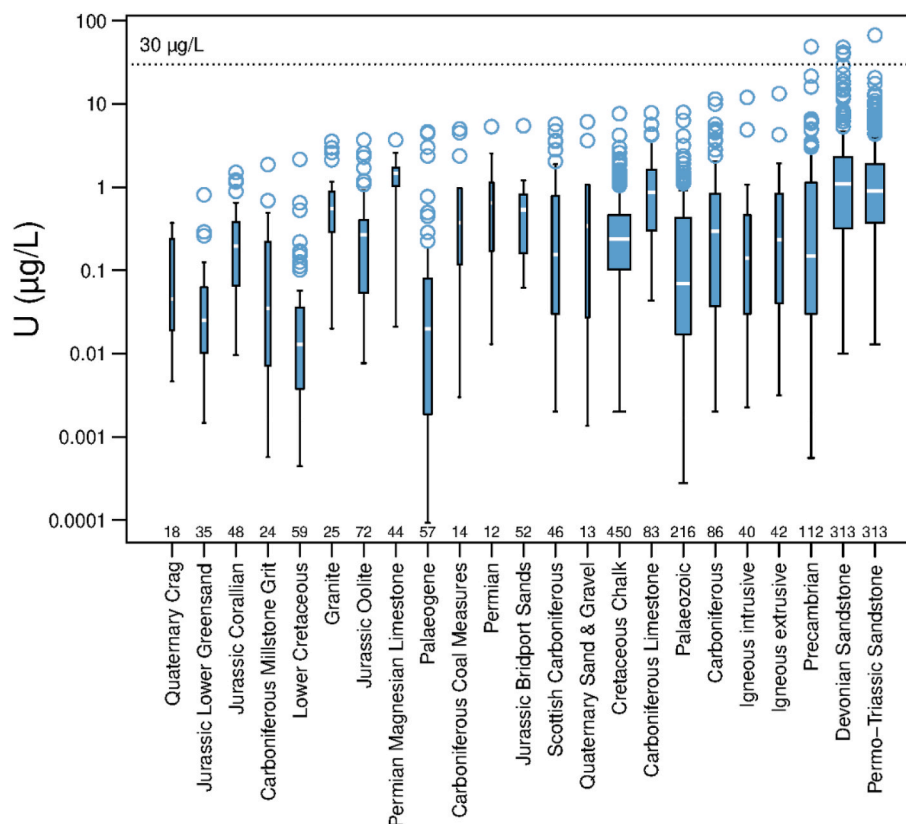


Fig. 5. Box plots showing concentration ranges of dissolved uranium in groundwater from different rock types/ages in Great Britain in relation to the EU drinking-water Directive 2020/2184 parametric value and WHO guideline value for uranium (30 µg/L); data source: BGS unpublished; outliers are shown as circles; non-detects are modelled by regression-on-order statistics; numbers along x indicate numbers of analyses (n); width of boxes is proportional of the square root of n.

Similarly, Kaplan et al. (2017) found U concentrations of 0.47–59.5 µg/L in soil porewaters from wetlands of Savannah River site, South Carolina, USA. Porewater was mildly acidic (pH 5.2–6.9) and U concentrations were highest in more oxic conditions ($E_h > 400$ mV). Nonetheless, U as U(VI) partitioned dominantly with the sediment fraction (K_d values were 2100–6900 L/kg), mainly bound to organic matter.

Estuarine porewaters have been found with up to 33.7 µg/L U (Barnes and Cochran, 1993). In the reducing sediment profile of the Amazon Estuary, Brazil, dissolved concentrations increased in response to release from Fe and Mn oxides undergoing reductive dissolution, below which concentrations diminished as a result of microbially-mediated SO_4 reduction (Barnes and Cochran, 1993). Several other studies have shown depletion of dissolved U in estuarine sediments under Fe- and Mn- reducing conditions, suggesting loss to sediments by reduction of U(VI) to U(IV) and sorption to Fe, Mn oxides and organic matter (Charette and Sholkovitz, 2006; Swarzenski et al., 2004; Windom and Niencheski, 2003).

In oxic, alkaline conditions (pH 7.2–8.8, HCO_3^- 49–1010 mg/L), porewaters extracted from loess silty aquifer sediment from La Pampa, Argentina, had U concentrations in the range 0.8–119 µg/L (Smedley et al., 2002). Aqueous U speciation was inferred to be dominated by U-carbonate complexes.

5. Anthropogenic contamination

5.1. Mining

Uranium mines occur in some 20 countries but the five largest producers: Kazakhstan, Canada, Australia, Namibia and Uzbekistan, accounted for 83% of world production in 2018 (NEA and OECD, 2020). During the period 1945–1990, the three principal suppliers were USA,

Canada and GDR (East Germany). Demand from the former GDR was largely from the former Soviet Union (Kazakhstan) until GDR mines closed on German reunification and supplies localized to Soviet (Kazakhstan) sources (Wellmer and Scholz, 2017). Traditionally, U mining involved open pit or deep mines but some of the largest producers, especially in Kazakhstan, Uzbekistan and USA, now use in-situ leaching (ISL) (referred to as in-situ recovery, ISR, in the USA). More than 90% of USA U production and around half of global output derives from ISL (Brown et al., 2016; Mudd, 2014). Sandstone-type roll fronts, which typically have low-grade U (<0.1% U) and a suitable U mineralogy and permeable rock type, are the only ore deposits suitable for U extraction by ISL (Abzalov, 2012). Roll fronts also tend to be contained by confining layers of low hydraulic conductivity, thereby facilitating ISL. A typical ISL site operates for one to three years and recovers about 60–80% of the U. The circulating fluid may be amended with acid (H_2SO_4), alkali (Na_2CO_3) or oxidants (H_2O_2) to enhance leaching. Heap leaching is a variant that may be suitable for smaller sites.

In principle, ISL can also have the lowest environmental impact (Fig. 6) as U is extracted in aqueous form and so does not involve excavations, tailings piles, ponds or the dispersal of radioactive dust. Nonetheless, it usually involves the injection of substantial quantities of lixiviants, for example sulphuric acid, to mobilize the U (and other trace metals) and uncertainty remains about the effectiveness of post-extraction remediation (Schneider et al., 2001).

Small amounts of U are also produced as a by-product of Cu, Au and P mining (e.g. Durand, 2012) (Section 9.3). As a result of the requirement for production of ^{235}U exclusively from mined uranium, large quantities of waste ^{238}U (depleted) are stored worldwide. In this respect, uranium is an unusual waste product.



Fig. 6. (left) Aerial view of the Ranger open-pit mine, Pit 3, Northern Territory, Australia, viewed as it was in 2013 before rehabilitation, © Energy Resources of Australia (ERA), 2013, with permission; (right) In-situ leaching, Honeymoon uranium Mine, South Australia (attribution: Geomartin under Creative Commons Attribution-Share Alike 3.0 Unported licence, unedited).

5.2. Industrial

The two main uses of U are as a fuel for electricity generation in nuclear power plants and in the production of nuclear weapons. Uranium was also exploited as a colouring agent until the 1940s (Campbell et al., 2015). For the production of U fuel rods, the proportion of ^{235}U is enriched to around 3–5% to improve the fission process (Mudd, 2014). Depleted U (DU) is a by-product of the nuclear enrichment and nuclear reprocessing industries and is used in armour-piercing munitions and as armoured vehicle cladding. DU munitions have been used in both Gulf Wars and in Serbia, Kosovo and Syria. Experiments on soil columns with buried DU munitions identified corrosion and after 3 years, leaching of up to 0.6% of the corroded DU mass (identified by the $^{235}\text{U}/^{238}\text{U}$ ratio); leaching rates of up to 1 mg/week U to the soil were inferred by the third year (Schimmack et al., 2007). Recently-deposited DU metal has been found to sorb weakly to soil surfaces compared to the natural U and may therefore be relatively mobile (Harguindeguy et al., 2014).

Uranium is also enriched in fly ash. Dai et al. (2015) reported a range of 135–1890 mg/kg U in Chinese coal ash samples. This can be mobilized in the atmosphere via coal combustion or in some areas may be incorporated into construction materials (Jambhulkar et al., 2018; Papastefanou, 2010). Fallout of fly ash from coal-fired power stations has been detected in shallow soils locally (Papp et al., 2002).

5.3. Fertilizers

Animal manure has been found to contain up to around 2.6 mg/kg U (Kratz and Schnug, 2006). In contrast, rock phosphate used in fertilizer production contains up to 245 mg U/kg (Table 9). China is by far the largest phosphate rock processing country in the world, mining more than 48% of global rock phosphate in 2018 (Shang et al., 2021). It is looking to increase domestic U production by using this unconventional resource even though many of the local rock phosphate deposits do not contain large U contents (<30 mg/kg U). Mines in Sichuan and Yunnan provinces are the most promising with up to 480 mg/kg U found in the Leibo deposit in Sichuan (Ye et al., 2019). Morocco is currently the country exporting the largest amount of rock phosphate and also has the largest reserves estimated at 75% of global reserves (Shang et al., 2021). Natural rock phosphate (e.g. Ca fluorapatite) has a low solubility in water and so is processed with strong acids to make a more soluble fertilizer (Hamamo et al., 1995). There are about 400 phosphoric acid plants in operation worldwide producing about 90 million tonnes/yr of which about 85% is used for fertilizers. Processed phosphate fertilizers can contain around 20–500 mg U/kg (average 100 mg/kg) (Taha et al.,

Table 9

Uranium content of rock phosphate and of some rock-phosphate-derived fertilizers.

Country	Average or range (mg/kg)	Source	Reference
Algeria	63; 25–100	rock	Tulsidas et al. (2019); Sun et al. (2020)
Brazil	30–67.5	rock	Sun et al. (2020)
China	20; 11–54	rock	Ye et al. (2019)
Egypt	90; 40–130	rock	Tulsidas et al. (2019); Sun et al. (2020)
India	4–65	rock	Sun et al. (2020)
Israel	120; 60–153	rock	Tulsidas et al. (2019); Sun et al. (2020)
Jordan	84; 46–135	rock	Tulsidas et al. (2019); Sun et al. (2020)
Morocco	97; 70–245	rock	Tulsidas et al. (2019); Sun et al. (2020)
RSA	23; 11.2	rock	Tulsidas et al. (2019); Sun et al. (2020)
Russia	28; 17–88.5	rock	Tulsidas et al. (2019); Sun et al. (2020)
Senegal	67; 64–154	rock	Tulsidas et al. (2019); Sun et al. (2020)
Syria	75; 36–138	rock	Tulsidas et al. (2019); Sun et al. (2020)
Tunisia	44; 12–88	rock	Tulsidas et al. (2019); Sun et al. (2020)
USA	21–200	rock	Sun et al. (2020)
Brazil	5–54	fertilizer	Yamazaki and Geraldo (2003)
Croatia	66–127	fertilizer	Dissanayake and Chandrajith (2009)
Germany	3–185	fertilizer	Dissanayake and Chandrajith (2009)
India	16–36	fertilizer	Dissanayake and Chandrajith (2009)
USA	9–300	fertilizer	Zielinski et al. (2006); Dissanayake and Chandrajith (2009); Zielinski et al. (2000)
Uzbekistan	11–70	fertilizer	Dissanayake and Chandrajith (2009)
Yugoslavia (former)	59–162	fertilizer	Dissanayake and Chandrajith (2009)

2018). A survey of P-fertilizers in Germany found an average of U content of 58 mg/kg (n = 303) (Schnug and Haneklaus, 2015). P-fertilizers can also contain appreciable amounts of other contaminants such as Cd (Kratz et al., 2016), F and Ra.

The production of fertilizers from phosphate ore also produces phosphogypsum as a waste by-product. This may be composed of gypsum ($\text{CaSO}_4 \cdot 2\text{H}_2\text{O}$) or calcium sulphate hemihydrate ($\text{CaSO}_4 \cdot 0.5\text{H}_2\text{O}$) with admixed sulphuric or phosphoric acid, depending on the raw material and processing method (Rutherford et al., 1994; Saenko et al., 2021). The U content of phosphogypsum also depends on the production process: gypsum production has been shown to result in a U content of some 5–25 mg/kg while the hemihydrate process produces a product with some 5–100 mg/kg (Rutherford et al., 1994). Some countries (e.g. USA) have recovered U from phosphogypsum, and could again, depending on the prevailing economic conditions (Haneklaus et al., 2017; Steiner et al., 2020).

Although phosphate fertilizers and their by-products provide a measurable input of anthropogenic U to the environment, the magnitude of their overall impact is unclear. The degree of fertilizer U retention in soils depends on the texture, mineralogy, and especially on the organic matter and clay content (Rothbaum et al., 1979) but, in general, it can be expected to be high. However, some studies have found U not to accumulate significantly in fertilized agricultural soils. Hamamo et al. (1995) found little difference between long-term fertilized soils and unfertilized soils in Illinois, USA (range 4.2–4.9 mg/kg). Others have demonstrated a difference. Unfertilized soils in the UK showed slightly smaller U contents than fertilized soils, with ranges of 2.33–2.52 mg/kg (mean 2.44 mg/kg) and 2.25–3.11 mg/kg (mean 2.88 mg/kg), respectively (Rothbaum et al., 1979).

Zielinski et al. (2006) studied phosphate-fertilized pastureland in Florida, USA and found slightly higher U contents in soils in the top 15 cm than in deeper soils, and also compared with local native pasture (Table 6). In addition, $^{234}\text{U}/^{238}\text{U}$ activity ratios were distinct, being close to 1.0 ± 0.05 values in shallow soil extracts suggestive of a fertilizer signature (Zielinski et al., 2000), compared to higher activity ratios (mostly >1.1) in extracts from greater than 15 cm deep and in native soils. Soil U content also correlated well with P content. Nonetheless, all soil U contents were small at less than 1.4 mg/kg and a simple mass balance suggests that the increase in total soil U would in any case be undetectably small. A similar conclusion was reached by Liesch et al. (2015) but they nevertheless found a small increase in median U concentrations in groundwaters when comparing agricultural (0.9 $\mu\text{g/L}$) to non-agricultural (0.7 $\mu\text{g/L}$) areas in Germany, a finding that may or may not be related to the use of P fertilizers. Other studies have also demonstrated increased concentrations of U in surface water, agricultural drainage and shallow groundwater, and have implicated phosphate fertilizers (Barišić et al., 1992; Lyons et al., 2020; Schnug and Lottemoser, 2013). Changes in U concentrations in drainage waters are more sensitive to fertilizer inputs than changes in total soil contents.

Increases in U concentrations in surface waters downstream from P fertilizer factories have been observed in Sichuan, China (Wang et al., 2019) and southern Spain (Martinez-Aguirre et al., 1994) but the increases are also generally small in comparison with the natural variation and are not sufficient to lead to exceedances of the drinking-water guideline values.

5.4. Decontaminating contaminated sites

Numerous U contaminated sites have been the subject of extensive research and remediation over several decades (Dinis and Fiúza, 2021; Gavrilescu et al., 2009). Examples of well-documented sites include US Department of Energy (DOE) Hanford site, Washington; DOE Rifle site, Colorado; DOE Savannah River site, South Carolina; Monticello Superfund site, Utah; Oak Ridge processing facility, Tennessee and numerous former mine sites. Methods of remediation of U contaminated land have been reviewed extensively by Campbell et al. (2015). Traditional remediation methods include excavation and disposal and pump-and-treat, but potentially less expensive and less disruptive alternatives include in-situ barriers and in-situ treatments. These include physical barriers, reactive barriers, U mineral precipitation, sorption to

organic matter or metal oxides, co-precipitation with metal oxides, microbial remediation and substitution in silicates and carbonates (Duff et al., 2002). Physical covers designed to prevent water infiltration and release of Rn gas may be used. A barrier involving layers of earth, geotextile membrane and liner has been used at the Monticello site (Campbell et al., 2015). Permeable reactive barriers investigated for U remediation include zero-valent iron (ZVI) (Fiedor et al., 1998; Morrison et al., 2002), phosphate (Arey et al., 1999; Pan et al., 2016; Simon et al., 2008) and Fe(III) (Duff et al., 2002). These barrier methods typically have a high U removal efficiency, albeit concerns include reduced aquifer permeability following precipitation of Fe(III) oxides and the potential for subsequent U remobilization.

Reduction of U(VI) to U(IV) for incorporation into a low-solubility U(IV) mineral can involve either natural attenuation or amendments using abiotic reductants, e.g. sulphide compounds, or electron donors for biotic processes. Experiments at the Rifle field site, Colorado, involved addition of acetate and resulted in removal of U(VI) through initial Fe reduction involving *Geobacteraceae*, with subsequent SO_4 reduction achieved by *Desulfobacteraceae* (Williams et al., 2011). Simultaneous addition of acetate and Fe(III) was found to be a promising approach (Zhuang et al., 2012). Again, concerns include aquifer clogging by reaction products and biomass and the long-term stability of the reduced forms (Campbell et al., 2015). Laboratory experiments have investigated use of amorphous FeS (Hua and Deng, 2008) and H_2S (Hua et al., 2006) as abiotic reductants. Experiments at the DOE Hanford site have shown that phosphate addition is a promising remediation amendment (Knox et al., 2008; Wang et al., 2017). Natural attenuation has been tried at numerous sites, including Hanford and Rifle, though the results have commonly proven disappointing (Maher et al., 2013).

Constructed wetlands have also been employed in U remediation for sites with low to moderate contamination. These can alter the ambient pH and redox conditions with assistance from microbes and wetland plant species. The approach has been tried successfully in experimental studies with *Phragmites*, *Typha* and *Carex riparia* (Groza et al., 2010), and operationally at Ranger mine, Australia using *Eleocharis* (spike rush) and *Nymphaea* sp. (water lilies) (Ring et al., 2004) and with varying success, at the WISMUT Pöhla site, Germany using ‘Aquamats’ and reactive filters (Kunze et al., 2007). Physical and chemical treatment plants can be added inline to boost remediation effectiveness (Campbell et al., 2015) and to provide a backup in case of fluctuations outside of the regulatory tolerances (Kunze et al., 2007).

Uranium mining and waste site remediation depends on local aqueous and solid conditions and effective methods differ according to local site conditions. Remediation of U typically also requires remediation of associated radionuclides, e.g. ^{226}Ra , and non-radioactive solutes such as As, Ni, V, Mo, F, SO_4 and NO_3 , which often require differing remediation strategies. One approach being explored for old tailings sites as well as the Fukushima nuclear accident site is the use of geopolymers to solidify the toxic material and thereby reduce the leakage of radioactivity. Geopolymers are synthetic cement-like materials that can offer improved physical and chemical characteristics over ordinary Portland cement for the long-term immobilization of a wide range of radioactive elements including U. They also offer a low carbon footprint compared to conventional Portland cements. One such geopolymer is made from calcined kaolinite (‘metakaolin’) treated with phosphoric acid (T. Zhao et al., 2022).

The recent widespread use of horizontal drilling and high-volume hydraulic fracturing (‘fracking’) to exploit unconventional hydrocarbon reserves in U-rich marine black shales has led to concerns over the unintentional release of naturally-occurring radioactive materials (NORM) associated with the flowback and produced fluids. Radium has received the most attention but U has also been of potential concern. Fortunately the strongly-reducing nature of many of these reserves means that U mobility is severely restricted and that U does not reach detrimental concentrations (Nelson et al., 2015). Mining for U, REE and P can also lead to possibly high exposures of NORM.

6. Uranium isotopic compositions and applications

The three natural U isotopes, ^{238}U , ^{235}U and ^{234}U , have long half-lives of 4.47×10^9 years, 7.04×10^8 years and 2.46×10^5 years respectively. The ^{238}U and ^{235}U isotopes are each parents in two separate decay chains, and the ^{234}U isotope is a daughter in the ^{238}U series (Vengosh et al., 2022).

A $^{234}\text{U}/^{238}\text{U}$ activity ratio, AR, of 1.0 indicates a condition of secular equilibrium. This occurs in a closed system or where conditions are geochemically undisturbed for at least 1 Ma according to the nuclides' respective half-lives (Andrews et al., 1989). In secular equilibrium, the daughter ^{234}U decays at the same rate as the ^{238}U parent and the rate of production of ^{234}U will be equal to its rate of decay (i.e. the activity of ^{238}U is equal to the activity of ^{234}U). $^{234}\text{U}/^{238}\text{U}$ activity ratios other than 1 indicate conditions out of secular equilibrium.

The radioactive decay of the ^{238}U isotope to ^{234}U , via the short-lived ^{234}Th (half-life 24.1 days) and ^{234}Pa (6.74 hours), involves in turn the emission of one alpha particle and two beta particles. In minerals, this causes damage to the crystal structure. The ^{234}U atom recoils as a result of the energy produced by alpha decay and this may translocate the atom to a different position in the crystal structure or eject it completely from the mineral into solution. The distance translocated can be 30–40 nm in silicate minerals (Brown et al., 2016). The intermediate ^{234}Th atom can etch a track in the crystal and increase the leaching potential in the zone of the track (Fleischer, 1982; Fleischer et al., 1972). Daughter ^{234}U is thereby more easily leached. Moreover, the ionizing alpha particle released from ^{234}U can also attract two valence electrons from the parent to balance its 2+ charge (producing a helium atom), leaving the daughter ^{234}Th with two fewer valence electrons. As a result, the ^{234}U atom produced will be hexavalent rather than tetravalent, with consequent increased mobility (Andrews et al., 1989). The total activity of ^{234}U in the system will be composed of the component supported by secular equilibrium and the recoil-derived excess which will decay over time. Both ^{235}U and ^{238}U are bound strongly to the crystal structure relative to ^{234}U (Stirling et al., 2007).

Excesses of ^{234}U in water can therefore be attributed to alpha-recoil-related release and selective leaching (Andrews et al., 1989; Porcelli and Swarzenski, 2003). The variation in the $^{234}\text{U}/^{238}\text{U}$ ratio can be a useful indicator of hydrological and geochemical processes including as a tracer of groundwater provenance and an indicator of mixing, weathering, groundwater/surface-water interactions, redox processes and pollution (Brown et al., 2016; Riotte and Chabaux, 1999; Zielinski et al., 2000).

The $^{234}\text{U}/^{238}\text{U}$ activity ratio is constant in the open ocean at 1.14 (Anderson et al., 1989; Swarzenski et al., 2004). In more restricted marine conditions, ratios can vary according to river and groundwater inputs and redox transformations (Anderson et al., 1989). In surface water, $^{234}\text{U}/^{238}\text{U}$ is usually >1 : the average ratio of the riverine flux to the oceans is 1.25 (Henderson and Anderson, 2003).

The ratios in groundwater are also commonly >1 (Cewart and Osmond, 1980; Coyte et al., 2018; Porcelli and Swarzenski, 2003; Priestley et al., 2018). Groundwater ratios from deep aquifers may be much higher (Andrews et al., 1989). $^{234}\text{U}/^{238}\text{U}$ activity ratios vary as a function of redox conditions and groundwater residence time (Lee et al., 2001). In oxic conditions, relatively high dissolved U concentrations can potentially exist, with secular equilibrium values of $^{234}\text{U}/^{238}\text{U}$. Under reducing conditions, release of ^{234}U via alpha recoil is favoured, thereby increasing the $^{234}\text{U}/^{238}\text{U}$ ratio in the groundwater (Osmond et al., 1983). In addition, if groundwater residence time is extended, recoil-generated ^{234}U can increase, leaving an increased $^{234}\text{U}/^{238}\text{U}$ activity ratio. An activity ratio of <1 is uncommon in groundwater except near ore bodies (Yanase et al., 1995). This may result from ^{234}U losses from a weathered mineral, with subsequent mineral weathering reducing the ratio in solution (Porcelli and Swarzenski, 2003; Yanase et al., 1995) (Section 8.2).

Variations in the $^{238}\text{U}/^{235}\text{U}$ ratio can also be of help in understanding

geochemical processes in aqueous systems. The isotopic composition may be expressed in absolute ratios as $^{238}\text{U}/^{235}\text{U}$ or as a relative per mil deviation, $\delta^{238}\text{U}$. The different half-lives of ^{238}U and ^{235}U have resulted in the $^{238}\text{U}/^{235}\text{U}$ ratio changing over geological time from around 3 to around 138 over the 4.5×10^9 years of earth history (Andersen et al., 2017). Fractionation of the isotopes occurs via non-radioactive physico-chemical processes in low-temperature environments, principally associated with microbially-mediated reduction of U(VI) to U(IV), with overall preferential reduction of ^{238}U relative to ^{235}U (Stirling et al., 2015). Microbially-driven redox changes have been shown to fractionate the ratio by some 1‰ or more (Stylo et al., 2015). Wang et al. (2015) found U(IV) to be around 1.6‰ heavier than U(VI) from experiments with the species in aqueous form (in acidic conditions). Preferential removal of ^{238}U in the solid phase as U(IV) leaves a U(VI) residual solution that becomes isotopically lighter, in a Rayleigh-type distillation process. Abiotic reduction has shown less evidence of fractionation, or a slight increase in the lighter isotope in the reduced U(IV) form (Andersen et al., 2017).

Natural $^{238}\text{U}/^{235}\text{U}$ fractionation is limited without redox changes. The ratio is not strongly fractionated by sorption reactions (Brown et al., 2016). Sorption of U(VI) to birnessite has shown only a small, approximately 0.2‰, reduction in $^{238}\text{U}/^{235}\text{U}$ ratio in the sorbed U compared to the aqueous U (Brennecka et al., 2011). Similarly, no $^{238}\text{U}/^{235}\text{U}$ isotopic fractionation was observed in desorption experiments with unconfined Quaternary floodplain sediments from Rifle, Colorado (Shiel et al., 2013). Some small fractionation may occur through preferential leaching of U-rich minerals (Murphy et al., 2014).

The dominant role of the U(IV)/U(VI) transformation, both oxidation and reduction, as the driver for changes in the $^{235}\text{U}/^{238}\text{U}$ ratio has led to its use as a redox proxy: a recorder of past changes in redox conditions, and implicitly in the organic-richness of palaeo-environments (Abshire et al., 2022; Andersen et al., 2017; Chen et al., 2021; Lau et al., 2019; Weyer et al., 2008). Recent applications have addressed the timings of ocean anoxic events (OAEs) (Clarkson et al., 2018; McDonald et al., 2022).

Although minute quantities of ^{236}U occur naturally, ^{236}U is a constituent of spent nuclear fuel and its presence in environmental samples is an indicator of anthropogenic U. It has been detected widely in small amounts but not sufficient to seriously disrupt natural ratios, except potentially locally around nuclear power plants and weapons sites (Andersen et al., 2017). Naturally-occurring U ores have $^{236}\text{U}/^{238}\text{U}$ atom ratios $<10^{-9}$ (Murphy et al., 2015). The presence of $^{236}\text{U}/^{238}\text{U}$ ratios above this may indicate local inputs of anthropogenic U from spent fuel.

7. Uranium chemistry and its speciation

7.1. Introduction

The spatial distributions of U described above ultimately arise from the operation of chemical processes at the atomic scale and over varying time scales, often under the influence of fluid flow, principally of water. The principal processes involved are surprisingly similar in the various environments. Given the importance of U to the nuclear industry and the environment, its chemistry has been studied extensively and documented in many settings, as the studies referenced above indicate. A large body of information has accumulated aided by the ever-increasing scope of sophisticated analytical measurements, databasing and modelling. The aim is to understand reasons for the distributions observed and ideally, to be able to predict future changes, including under changing environmental conditions.

7.2. Redox, hydrolysis and complexation

The two principal oxidation states – U(VI) and U(IV) – are found in oxidizing and reducing conditions, respectively. The uranyl ion, UO_2^{2+} , is the stable species of U(VI) in oxidized environments. The two strongly-

bound O atoms present in the UO_2^{2+} ion are arranged in an axial (vertical) orientation with 5–8 H_2O molecules attached in the equatorial plane (Kubicki et al., 2009; Müller et al., 2019). Grenthe et al. (2021) favour the structure with five water molecules as this is supported by EXAFS data and quantum chemical calculations.

The U^{4+} cation is only stable under strongly reducing conditions with the central cation surrounded by 9 ± 1 water molecules, a conclusion also supported by EXAFS data and quantum chemical calculations (Grenthe et al., 2021; Shor et al., 2020).

Both these cationic species are very susceptible to hydrolysis (loss of protons from bound water molecules) and are only found in extremely acidic solutions. More commonly, they are found in their hydrolyzed forms or complexed with other ligands, especially oxygen-containing ligands such as carbonate, phosphate and silicate as well as a broad range of organic ligands, large and small. Ternary complexes such as $\text{Ca}_2\text{UO}_2(\text{CO}_3)_3$ also form and are very stable (Kubicki et al., 2009; Oher et al., 2020; Shang et al., 2020; Shang and Reiller, 2020). At high U concentrations, this tendency to hydrolyze can lead to polynuclear species, colloids and ultimately, well-defined and rather insoluble minerals such as schoepite or metaschoepite. Most of the ligands that U binds strongly to in solution can also form corresponding U minerals and it is this duality in the role of ligands that adds to the complexity of U chemistry.

The U(V) oxidation state is transient but the UO_2^+ aquo ion has been identified in the laboratory and can be stabilized by various organic ligands and concentrated carbonate solutions (Mizuoka et al., 2005). It has five water molecules in its first coordination sphere. The water molecules are strongly polarized, leading to a particularly strong tendency to hydrolyze (Atta-Fynn et al., 2012; Grenthe et al., 2021). U(V) occurs naturally but rapidly disproportionates to U(IV) or U(VI) and so is now considered unstable and rare. This contrasts with Langmuir's (1978) assertion that it 'has an appreciable field of stability in reduced waters below pH 7'. Uranium(V) can be stabilized briefly by complexation. The $\text{UO}_2(\text{CO}_3)_3^{5-}$ species has been found to be stable for 2 h in aqueous solutions and for up to 2 weeks when sealed in a cuvette (Kubicki et al., 2009). U(V) species may also be important intermediaries in the reduction of U(VI) to U(IV) by microbes. The Fe (III)-reducing bacterium *Shewanella oneidensis* MR1 has been shown to produce U(V) stabilized for up to 120 h (Vettese et al., 2020). U(V) species may also appear as transient species during the reduction of U(VI)–Ca– CO_3 complexes by zero-valent iron (Tsarev et al., 2017). These considerations notwithstanding, the redox chemistry of U in the environment is overwhelmingly about the interplay of the U(IV) and U(VI) oxidation states.

7.3. Thermodynamic databases – 'standing on the shoulders of giants'

Thermodynamic databases encapsulate in a quantitative way the chemical reactions that give rise to the varied suite of U-containing gaseous, solution, mineral and surface species that define the behaviour of U in the environment. Together with the appropriate speciation software, they enable predictions about the behaviour of U to be made for a wide variety of environments: natural, laboratory and industrial. We summarize some of the more important publicly-available databases suitable for environmental applications in Table 10 and provide some idea of the scope of the databases by tabulating the total number of species and number of U species included in each database.

The chemistry of U is particularly complex and thermodynamic data have been derived from a large number of detailed laboratory studies over many years. One of the first systematic compilations for U was by Langmuir (1978). The OECD Nuclear Energy Agency (NEA) Thermochemical Database (TDB) is now the most comprehensive source of critically-reviewed thermodynamic data (Martinez et al., 2019; Ragoussi and Costa, 2019). This project has reviewed data for U and associated elements on a rolling basis since 1986. The reviews by Grenthe et al. (1992) and Guillaumont et al. (2003) were pivotal in defining the

stability of many of the key U species, and the most recent review published in 2021 (Grenthe et al., 2021) has updated these. The electronic database derived from the latest work, the TDB-e database, is based on selected data that are deemed to be highly reliable and well-documented and is deliberately conservative. Therefore, while it provides an excellent foundation, the TDB-e database is notably incomplete (Mühr-Ebert et al., 2019) and often needs to be supplemented to make it suitable for environmental applications. Fortunately, this has been done by others, most recently with the PRODATA database (Reiller and Descostes, 2020) which has been developed specifically for mining applications but should nevertheless have a wider role in environmental studies.

Other modern databases extending the 'official' NEA TDB-e database include those from the ThermoChimie, NAGRA/PSI, JAEA TDB and THEREDA projects (Table 10). There are other more specialized databases such as SOLTHERM for geothermal systems (Alsemgeest et al., 2021), ColdChem (Pitzer) for low temperatures (Toner et al., 2017), CEMDATA for cements (Lothenbach et al., 2019) and phreeqc.dat for gases (Peng-Robinson) (Appelo et al., 2014; Parkhurst and Appelo, 2013). However, none of these databases includes U species. The program SUPPHREEQC has also been developed for generating customized PHREEQC-format databases for high temperatures and pressures from the SUPCRTBL database (G. Zhang et al., 2020).

The PHREEQC-format electronic databases cited above do not include the uncertainties in their data although this could in principle be added as comments. However, none of the popular speciation programs would be able to use these data directly to propagate errors. Monte Carlo (MC) simulations would certainly be feasible and the program MCPHREEQC (AMPHOS21, 2011) has been designed to do just this. Alternatively, the PhreeqcRM interface to PHREEQC (Parkhurst and Wissmeier, 2015) would be ideal for developing customized MC software. Although uncertainty data are not included in the electronic databases, some of the supporting information for the databases does provide this. The NEA-TDB (Grenthe et al., 2021) is notable in this respect.

Some databases maintain an internal consistency: true 'databases' in the sense defined by Hörbrand et al. (2018), while others do not. Overall, the published electronic databases show a somewhat confusing mixture of common and unique data with differing quality standards for inclusion (Lu et al., 2022; Meeussen et al., 2009; Reiller and Descostes, 2020; Wang et al., 2019). Some of these databases are open-source, some proprietary, some actively maintained, others not. Most can in principle be modified or extended to include new data. The original databases are closely linked to the software that uses them but the PHREEQC format has become the *de facto* interchange format; all the databases in Table 10 are available in this format and can be used with the popular PHREEQC software (Lu et al., 2022; Parkhurst and Appelo, 2013). Depending on the database used, PHREEQC can use the ion-association (extended Debye-Hückel, B-dot or Davies equations), Pitzer or SIT (Specific Ion Interaction Theory) models to account for non-idealities in solution (the variation of activity coefficients), and either an enthalpy or a polynomial expression to account for the temperature dependency of $\log K$'s.

The lnl.dat database, which was compiled by the Lawrence Livermore National Laboratory, uses an extended Debye-Hückel model with the B-dot extension, as well as a detailed model for the activity coefficient of $\text{CO}_2(\text{aq})$. The database has been designed specifically to cover a wide range of temperatures and ionic strengths (including seawater). Other approaches designed for medium to high ionic strengths are the Pitzer approach (up to 6 mol/kg water) and the SIT approach (up to 3 mol/kg water). The SIT approach is favoured by the NEA TDB and its siblings. The Pitzer and SIT approaches use semi-empirical corrections to the Debye-Hückel equation through a set of specific ion-ion interaction parameters between pairs or triplets of ions. The Pitzer approach attempts to maintain internal consistency and replaces many of the weak complexes between major ions seen in the other databases with a set of interaction parameters. However, in most cases these parameters are

Table 10
Some of the more important sources of thermodynamic data that are freely available and in PHREEQC format.

Database (country of origin) Institution	Redox states, number of species for all elements and U [aq-min-gas- ads], and minimum solubility ^a	Some of the U species considered	Activity model and scope	Comment	Database and source
NEA TDB-e (many) OECD/NEA	U(III), U(IV), U(V), U(VI) All [522-182-58-0] U [101-63-8-0] log $U_{diss} = -8.47$ [UO ₂ (am,hyd)] 162 (U = 27) SIT interactions	Many U-CO ₃ , Ca, SO ₄ , PO ₄ aq species	SIT – helped to popularize the SIT model. This latest version deliberately lacks less reliable but possibly important species including some minerals of environmental significance	Multi-national, critically reviewed, consistent, traceable and authoritative. The 2021 document elaborates extensively. Minerals defined by chemical formula rather than by name but with suffix such as (cr), (am), (beta) etc	NEA_TDB_phreeqc_Jan2021.dat https://www.oecd-nea.org/download/tdb/NEA_TDB_phreeqc_Jan2021.dat
JAEA (JP) JAEA	GC: All [181-550-13-0] GC: U [0-0-0-0] U(III), U(IV), U(V), U(VI) RN: All [998-1040-133-0] 353 SIT interactions U [106-148-29-0] 52 SITlog $U_{diss} = -15.13$ [UO ₂ (cr)]		LLNL aqueous model, temperature dependence (the erroneous definition of β -Na ₂ UO ₄ was removed)	This latest update has improved internal consistency and temperature dependence. Split into two tdb's with some overlap: GC = geochemistry; RN = radionuclides. Four organic ligands considered: EDTA, Cit, Ox and ISA	PHREEQC19v12.dat (GC) 201203s0.tdb (RN) https://migrationdb.jaea.go.jp/
llnl (US) thermo. com.V8.R6.230 LLNL	U(III), U(IV), U(V), U(VI) All [1326-1119-93-34] U [72-178-31-0] log $U_{diss} = -9.37$ [uraninite]	U-CO ₃ , PO ₄ , SO ₄ (not U-Ca)	LLNL aqueous model, temperature dependence		llnl.dat (12758, PHREEQC 3.7.3) based on thermo. com.V8.R6.230
minteq.v4 (US) US EPA	U(III), U(IV), U(V), U(VI) All [1324-553-15-78] U [44-35-0-0] log $U_{diss} = -10.85$ [uraninite]	U-CO ₃ , PO ₄ , SO ₄ (not U-Ca)	Large number of organic ligands	US EPA originally developed for the US EPA but no longer being actively developed; Gustafsson supplemented with 8 aq (U-Ca) and 6 surface species (CD-MUSIC model) and for organic matter (WHAM/SHM model)	minteq.v4.dat (PHREEQC 3.7.3) https://www.usgs.gov/software/phreeqc-version-3
Thermoddem (FR, US) With CHESS BRGM	U(III), U(IV), U(V), U(VI) All [1005-717-23-0] U [17-3-0-0] log $U_{diss} = -9.38$ [uraninite]	Only protonated U species	LLNL aqueous model, temperature dependence. Broad scope. Latest includes improved temperature dependence data for geothermal applications, and revised major element data	Originally based on EQ3/EQ6. Includes LLNL aqueous model and so capable of modelling a wide range of temperatures (0–35 °C). Similar to ThermoChimie?	PHREEQC_ThermoddemV1.10_06Jun2017.txt https://thermoddem.brgm.fr/databases/chess https://thermoddem.brgm.fr/databases/phreeqc Blanc et al. (2012), Blanc (2017)
Nagra/PSI (CH) Nagra/PSI	U(IV), U(V), U(VI) All [539-122-7-0] U [78-14-0-0] log $U_{diss} = -8.50$ [UO ₂ (am,hyd)] log $U_{diss} = -8.47$ [Uraninite]	U-CO ₃ , Ca, PO ₄ species	Davies 25 °C only	Used by GEMS	PSINA 12 07 110615 DAV s win.dat
Hatches Version 20 (GB) AMEC for NDA	U(IV), U(V), U(VI) All [1384-959-7-0] U [135-80-0-0] log $U_{diss} = -14.89$ [UO ₂ (c)]	U-CO ₃ , Ca, Si, PO ₄	Davies. 25 °C only but has some enthalpy data	No longer being developed (replaced by ThermoChimie)	PCHatches.dat http://www.hatches-database.com/
PRODATA (FR) CEA	U(III), U(IV), U(V), U(VI) All [676-882-30-50] U [90-191-5-5] log $U_{diss} = -14.90$ [UO ₂ (cr)] 269 (U = 47) SIT interactions in SIT version		Davies (SIT available) Extends NEA TDB for mining and other applications	Incorporates results of a detailed review of U chemistry. A SIT version is available with 269 interaction parameters	PRODATA_xxxx_Mine_RedoxO2_1.5.32.dat where xxx = Davies or SIT prodata@cea.fr Reiller and Descostes (2020)

(continued on next page)

Table 10 (continued)

Database (country of origin) Institution	Redox states, number of species for all elements and U [aq-min-gas-ads], and minimum solubility ^a	Some of the U species considered	Activity model and scope	Comment	Database and source
SOLTHERM (US) Univ. of Oregon	U(III), U(IV), U(VI) All [489-372-21-0] U [51-35-0-0] log $U_{diss} = -9.38$ [uraninite]	U-OH, CO ₃ , F, Ac	LLNL aqueous model up to 300 °C. Especially for geothermal systems.	Developed by M H Reed, J. Palandri and colleagues. Used by speciation programs such as SOLVEQ, TOUGHREACT and GeoT	Soltherm.h06 (Jun 2016) converted to PHREEQC format by Alsemgeest et al. (2021) . See paper and SI for details of conversion. For latest see https://pages.uoregon.edu/palandri/data/Soltherm.xpt .
THEREDA (DE, CH) HZDR	All [163-217-4-0] U [32-32-0-0] log $U_{diss} = -8.49$ [U(OH) ₄ (am)] 117 (U = 18) Pitzer interactions	U-CO ₃ , PO ₄ (not U-Ca, no uraninite)	Focus on transuranic elements. High ionic strengths, no redox??	117 Pitzer parameters (18 U)	THEREDA_2020_PHRQ.dat Vsn 1.6 Richter et al. (2015)
ThermoChimie (FR, GB, BE)	U(III), U(IV), U(V), U(VI)	Many U-CO, Ca-P aq species	Extended Debye-Hückel & LLNL (SIT available) Broad scope (56 elements). pH 5–14; high I; 13 organic weak acids and chelates	Critically reviewed; modern. Includes LLNL aqueous model Same as NEA?	ThermoChimie_PHREEQC_eDH_v9b0.dat http://www.thermochimie-tdb.com/ Also see sit.dat (PHREEQC 3.7.3) https://www.usgs.gov/software/phreeqc-version-3 Grivé et al. (2015) , Giffaut et al. (2014)
ANDRA	All [1411-853-10-0] U [109-62-0-0] log $U_{diss} = -14.88$ [uraninite] 374 (U = 39) SIT interactions in SIT version but no surface species				
wateq4f (US) USGS	All [360-311-8-54] U [54-30-0-2] log $U_{diss} = -13.37$ [uraninite(c)]	U-CO ₃ , P (no U-Ca) Dzombak & Morel surface species		Not under active development	wateq4f.dat (PHREEQC 3.7.3) https://www.usgs.gov/software/phreeqc-version-3

^a Count of species defined by species type: aq = aqueous; min = mineral; gas and ads = adsorbed species. "Minimum solubility" is the concentration of U in a strongly reducing system expressed as log₁₀ (dissolved U in mol/kgw): $U_T = 1e-3$ mol/kgw, NaCl = $1e-2$ mol/kgw, 20 °C, pH 7, $PO_2(g) = -70$ atm.

only known for a relatively small subset of major-ion species. The THEREDA database is the most complete Pitzer database and includes parameters for a relatively large number of major ion-U interactions.

For users not closely associated with a specific database, it can be difficult to know which database is best to use for calculations. The first consideration is matching the suite of elements and species of interest to those in the available databases. The second consideration is the appropriate choice of activity model based on the ionic strength of interest as outlined above. Additional factors include the perceived quality of the database, its completeness and transparency. Detailed comparisons between databases are non-trivial because of the lack of use of established conventions for the naming of species, e.g. IUPAC or CODATA for chemical species and IMA/CNMNC for mineral names ([Warr, 2021](#)). Solution species are defined by their chemical formulae but the order of components (e.g. elements), their grouping and the use of parentheses is variable, e.g. Si(OH)₄ or H₄SiO₄. The same mineral may be spelt or labelled differently and may be specified by a chemical formula or a mineral name. A given mineral may actually refer to different polymorphs (e.g. alpha or beta forms) which can have notably different properties, e.g. amorphous or crystalline. Mineral formulae can sometimes even be mistaken for solution species. Uranium suffers from these inconsistencies more than most elements because of the large number of species and minerals involved. The lack of canonical naming means that a simple lexicographic comparison of species by name is not possible and that switching or merging of databases can require significant changes to scripts.

There have been attempts to include sorption processes in generic databases but the task is daunting and progress has been rather slow ([Brendler et al., 2003](#); [Jung et al., 2001](#); [McKinley and Scholits, 1993](#); [Payne et al., 2011](#); [van der Lee and Lomenech, 2004](#)). Notable

achievements include the SDB by the Japanese Atomic Energy Agency, JAEA ([Sugiura et al., 2020](#)) and the RES³T (Rossendorf Expert System for Surface and Sorption Thermodynamics). As with minerals, there is no uniformity in the naming of surface species. In 2011, the JAEA database (Version 3) included 46,669 K_d values of which some 4231 were for U on non-cementitious substrates. By 2017, this had increased to 62,977 K_d 's. However, K_d values are highly conditional not only on the substrate, e.g. its specific surface area ([Mendez et al., 2020](#); [Payne et al., 2011](#)), but also on the solution composition (e.g. pH, PCO_2 , redox, ionic strength, etc.) which makes estimating K_d 's for varying conditions, as required in many simulations, difficult.

The RES³T system adopts a more fundamental approach in that it concentrates on surface complexation data for pure minerals rather than whole soils and sediments. It is being actively maintained and as of 15 May 2022 has data for 150 minerals and 7448 surface-complexation reactions including many for U. This provides the prospect of modelling the behaviour of U in a wide variety of soils and sediments using a linear additive approach but leaves unresolved the challenge of identifying the quantities and detailed properties of the model components present in the system of interest ([Davis et al., 2004](#)). There are presently no data for metal-ion binding to humics in the database. At a more fundamental level, there can be significant interactions amongst the components leading to non-additive behaviour and kinetic effects ([Reiller, 2012](#); [Weng et al., 2008a](#)). Ternary (mineral-humic-metal) interactions are likely to be significant in many environmental settings which has led to various modelling approaches ([Bryan et al., 2012](#)), although none specifically targeting U speciation. Since the derivation of surface-complexation parameters inevitably involves a detailed solution speciation, e.g. for calculating the activity of the uranyl ion, maintaining consistency between the sorption and aqueous databases requires

special care and could, in principle, necessitate a reanalysis of the original sorption data.

As the scope of quantum chemical modelling increases, especially of DFT, it is likely that these methods will provide increased support for the choice of the most stable species and ultimately, the derivation of log K 's and other thermodynamic properties of solution, mineral and surface species, parameters that are often difficult or impossible to measure experimentally. Recent work deriving thermodynamic properties of some uranyl-phosphate aqueous species (Jackson et al., 2013) and uranyl-carbonate minerals (Colmenero, 2020) are examples. Similar calculations have already been used to help constrain the choice of surface species (Hiemstra, 2018; D. Pan et al., 2022) and to design novel uranium adsorbents (W.-W. Zhao et al., 2022). These methods are particularly useful when combined with spectroscopic techniques such as attenuated total reflectance infrared (ATR IR), EXAFS and XANES, which can help to corroborate the derived molecular structures.

7.4. Solution speciation

In oxidizing waters, the uranyl ion, UO_2^{2+} , is dominant but as noted above, this readily hydrolyzes and forms a large set of unusually strong complexes with a wide variety of common ligands (Grenthe et al., 2021; Langmuir, 1978). These include OH^- , CO_3^{2-} , PO_4^{3-} , SiO_4^{2-} , F^- , Na^+ , Ca^{2+} and Mg^{2+} . U(VI) and U(IV) chloride complexes can even be formed under extreme conditions (Hennig et al., 2005; Timofeev et al., 2018).

The speciation embedded within a thermodynamic database is often best-illustrated in terms of species-pH plots and Eh-pH predominance diagrams. All calculations here and in the rest of this review were made with PHREEQC software (Parkhurst and Appelo, 2013) embedded in PhreePlot (Kinniburgh and Cooper, 2004). We have primarily used the PRODATA database as this is a modern database that extends the NEA TDB-e with species that are of potential environmental significance. Reiller and Descostes (2020) give a detailed discussion of the development of this database, its relationship with other databases and how they resolved issues of internal consistency.

Fig. 7(a,b) shows a species-pH plot for U (10^{-6} mol/kg water or 2.4 $\mu\text{g/L}$) in oxidizing and reducing freshwaters respectively, containing the major ligand-forming elements with a Mg/Ca molar ratio of 1 and exposed to atmospheric CO_2 . In Fig. 7(a), three uranyl-carbonate complexes dominate the U speciation above pH 6 and above pH 7.5, two U–Ca– CO_3 ternary complexes are dominant. Even below pH 7.5, uranyl complexes with P and F are more dominant than the bare UO_2^{2+} ion.

The redox conditions imposed for the reducing case (Fig. 7(b)), namely a fixed $\text{O}_2(\text{g})$ partial pressure of 10^{-70} atm, are sufficient to reduce U(VI) to U(IV) below pH 8 but not to reduce $\text{CO}_2(\text{g})$ to $\text{CH}_4(\text{g})$. Above pH 8, U(VI) becomes increasingly important and the ternary U–Ca(Mg)– CO_3 complexes dominate in both oxidizing and moderately reducing freshwaters up to about pH 9.5, after which $\text{UO}_2(\text{CO}_3)_4^{4-}$ becomes dominant. In even more reducing waters, $\text{CO}_2(\text{g})$ is reduced to $\text{CH}_4(\text{g})$ and the U– CO_3 complexes become insignificant.

Speciation of seawater-like solutions (Fig. 7(c)) over the pH range pH 8–9.5 is broadly similar to the oxidizing freshwater case described above but with the U–Mg– CO_3 ternary complex playing a more important role. At the natural seawater pH of 8.1, according to this speciation, U speciation in seawater is dominated by a mixture of the charged species $\text{MgUO}_2(\text{CO}_3)_3^{2-}$, $\text{CaUO}_2(\text{CO}_3)_3^{2-}$, $\text{UO}_2(\text{CO}_3)_4^{4-}$ and the neutral species, $\text{Ca}_2\text{UO}_2(\text{CO}_3)_3$. This speciation is similar to that shown in Shang and Reiller (2020) except that the $\text{MgUO}_2(\text{CO}_3)_3$ species is included here following the most recent update to the PRODATA database. Bernhard et al. (2001), Vercouter et al. (2015) and Reiller and Descostes (2020) have stressed the importance of these ternary complexes in environmental applications, especially where the dissolved organic carbon concentration is low. Jo et al. (2022) provide a recent review of the stability of all the major (Mg, Ca, Se, Ba) ternary alkaline earth-U- CO_3 species. There is still some uncertainty about the relative abundance of these species with some speciation calculations for seawater showing

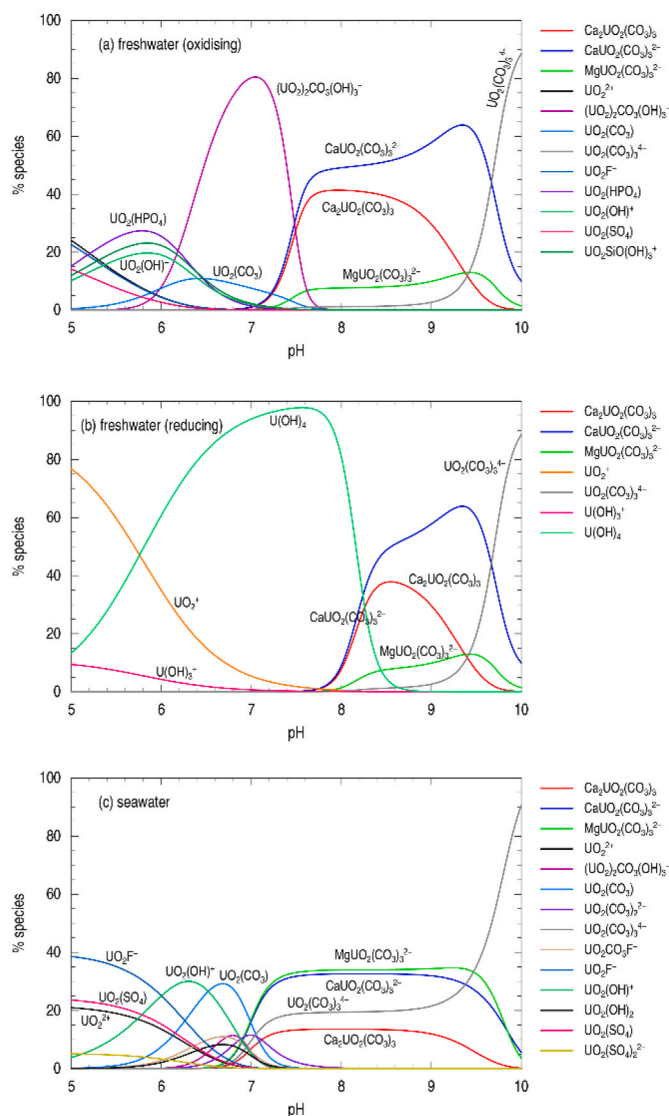


Fig. 7. Distribution of species vs pH for (a) an oxidizing freshwater ($\text{PO}_2(\text{g}) = 0.21$ atm), (b) a reducing freshwater ($\text{PO}_2(\text{g}) = 10^{-70}$ atm), and (c) for standard seawater (SSW76) showing the importance of Ca–Mg–uranyl carbonate species in both freshwater and seawater for pH greater than pH 7.5. Calculations made with the PRODATA database (Davies version for (a) and (b) and SIT for (c)) at 25°C. pH adjustments were made with NaOH and a PCO_2 of $10^{-3.4}$ atm was maintained in all of the calculations. The model freshwaters contained a total concentration of: $1 \cdot 10^{-6}$ U (VI), $2 \cdot 10^{-3}$ Na, $1 \cdot 10^{-3}$ K, Ca, Mg, SO_4 , C and Cl, $1 \cdot 10^{-4}$ Si and NO_3 , $1 \cdot 10^{-5}$ F and P, all concentrations in mol/kg water. All mineral precipitation was suppressed.

$\text{Ca}_2\text{UO}_2(\text{CO}_3)_3$ as the dominant species (Endrizzi et al., 2016; Endrizzi and Rao, 2014; Li et al., 2017; Wu et al., 2016). It is also known that $\text{Ca}_2\text{UO}_2(\text{CO}_3)_3$ forms a strong association with Na^+ in solution, effectively making quaternary species possible (Li et al., 2017; Wu et al., 2016).

In summary, while the importance of uranyl carbonate species has been appreciated for a long time (Langmuir, 1978; Hostetler and Garrels, 1962), it is only relatively recently that stability constants for all the commonly-found Ca–Mg ternary complexes have become available (Grenthe et al., 2021; Jo et al., 2019; Mühr-Ebert et al., 2019; Shang and Reiller, 2020), and even now some uncertainty remains. Note that given the strength of U– CO_3 interactions, U– CO_3 species can be significant under neutral and even mildly acidic conditions which highlights their importance not only in the environment but also in laboratory experiments carried out under open-atmosphere conditions.

Below pH 6–7, the CO_3^{2-} activity diminishes rapidly and other

ligands such as OH^- , PO_4^{3-} , SiO_4^{2-} , SO_4^{2-} and even F^- , if present, combine with the uranyl ion. The bare uranyl ion, UO_2^{2+} , therefore only becomes significant below pH 7, or at even lower pH values, when the concentrations of these ligand-forming anions are low. Uranyl phosphate species do not appear in these diagrams but where P is enhanced due to pollution, mining or natural mineralization, soluble P species can become important especially below pH 7 (Wang et al., 2019). Uranium can also be precipitated as U-phosphate solids under aerobic P-rich conditions with a high U loading. This can also occur via the bio-precipitation of U-P minerals mediated by various organisms which secrete extracellular acid and alkaline phosphatases (Kulkarni et al., 2013, 2016; Nilgiriwala et al., 2008).

Uranyl sulphate species can be significant in acidic sulphate-rich natural waters such as those arising from acid mine drainage (Arnold et al., 2011; Ladeira and Gonçalves, 2007). At higher U concentrations, polynuclear species such as $(\text{UO}_2)_2\text{CO}_3(\text{OH})_3$ can play a significant role especially above pH 6, a feature that may be important in experimental studies. Other complexing ligands such as EDTA may be relevant at contaminated sites.

Eh-pH diagrams are used to show the impact of varying redox potential (Eh) and pH on U speciation and incidentally provide a useful way to compare databases. Diagrams based on the 12 databases included in Table 10 are shown in Fig. 8. Fig. 8(a) shows the predominant species for a simple U-C-Na-Cl system where the precipitation of all minerals has been suppressed, while in Fig. 8(b), the same systems are considered but all minerals that show supersaturation are allowed to precipitate. The upper boundary of these diagrams shows where the oxygen fugacity is above atmospheric (0.21 atm) and the lower boundary is for an oxygen fugacity of 10^{-70} atm, below which the methane partial pressures can become very large. Trying to maintain a fixed PCO_2 above pH 10 leads to high carbonate concentrations.

Although the calculated aqueous speciation varies considerably in detail between the various databases (Fig. 8(a)), the major features are common to all databases, namely in oxidizing waters (Eh > ca. 0.5 V): (i) UO_2^{2+} dominates from pH 3–6; (ii) above pH 9, the carbonate species, $\text{UO}_2(\text{CO}_3)_3^{4-}$, dominates, and (iii) between pH 6–9, the speciation is much more variable with a variety of hydrolyzed uranyl and carbonate species predominating. The speciation under reducing conditions is quite variable. The databases show UO_2^+ and $\text{U}(\text{OH})_4$ dominating under most pH conditions but some databases, notably Minteq and its derivatives, include $\text{U}(\text{OH})_5$ at high pH. Uranyl carbonate species dominate the speciation at higher pH's. If Ca and Mg had been present in these simulations, the ternary species would likely be present as indicated in Fig. 8.

Reduction of U(VI) generally occurs over the Eh range +0.25V to -0.2V which straddles the suboxic-anoxic boundary (Borch et al., 2010) and is similar to the active redox zones of As and V. In an increasingly reducing environment, U(VI) reduction occurs just after Fe^{3+} reduction but before SO_4^{2-} reduction. A more complete redox sequence is: $\text{O}_2 < \text{NO}_3^- < \text{MnO}_2(\text{s}) < \text{Fe}(\text{OH})_3(\text{s}) < \text{AsO}_4^{3-} \approx \text{VO}_3^- \approx \text{UO}_2^{2+} < \text{MoO}_4^{2-} < \text{SO}_4^{2-} < \text{HCO}_3^- < \text{H}_2\text{O}$ with the precise order depending on the redox reaction considered and the extent of mineral precipitation. All such considerations take place against the background that most redox reactions are kinetically-controlled and that thermodynamic equilibrium between redox species is often not attained.

All the databases show supersaturation with one or more minerals under strongly reducing conditions at ambient temperatures (ca. $\text{pe} + \text{pH} < 7$ or $17 \cdot \text{Eh} + \text{pH} < 7$) even, as here, where the total U concentration is only 10^{-6} mol/kg water (Fig. 8(b)). The supersaturated minerals are either uraninite ($\text{UO}_2(\text{cr})$), or in the case of the NEA TDB-e and THEREDA databases, the more soluble 'amorphous' form, $\text{U}(\text{OH})_4(\text{am})$. The amorphous form may be a nano-particulate version of uraninite or closer to the poorly-defined 'non-crystalline' U(IV) precipitates generated by microbes (Alessi et al., 2014b). EXAFS shows that these non-crystalline forms do not have the U-U pair correlations at ca. 3.8–3.9 Å characteristic of $\text{UO}_2(\text{cr})$, perhaps due to co-precipitated

impurities such as P or Fe (Alessi et al., 2014a, 2014b). The ratio of uraninite to non-crystalline UO_2 formed depends on the other ions present during formation: low concentrations of U plus environmentally-relevant concentrations of sulphate, silicate and phosphate favour the formation of non-crystalline UO_2 (Stylo et al., 2013). $\text{U}(\text{OH})_4(\text{am})$ can also be produced by the rapid reduction of U(VI) in the laboratory but care has to be taken during solubility measurements to avoid any partial oxidation to U(VI) since this can lead to anomalously high estimates of U(IV) solubility (Rai et al., 1990). Because of the generally slow kinetics of uraninite dissolution and precipitation in the natural environment, it is usually considered inappropriate to use solubility data for crystalline uraninite, $\text{UO}_2(\text{cr})$ in modelling; some amorphous form is preferred (Alessi et al., 2014b; Richter et al., 2015).

Three of the databases (PRODATA, ThermoChimie and THEREDA) include Na- UO_2 minerals, namely Na-compreignacite or clarkeite, which can also precipitate under oxidizing conditions. With higher U concentrations, aqueous polynuclear uranyl species become important and more minerals begin to precipitate across the whole range of Eh. This includes schoepite under oxidizing conditions and a range of mixed-valence U oxide minerals such as $\text{UO}_{2.34}(\text{s})$ and $\text{UO}_{2.67}(\text{s})$ as the environment becomes increasingly reducing. As the complexity of the water chemistry increases, so the number of possible solution and mineral species increases rapidly.

7.5. Mineral and surface reactions

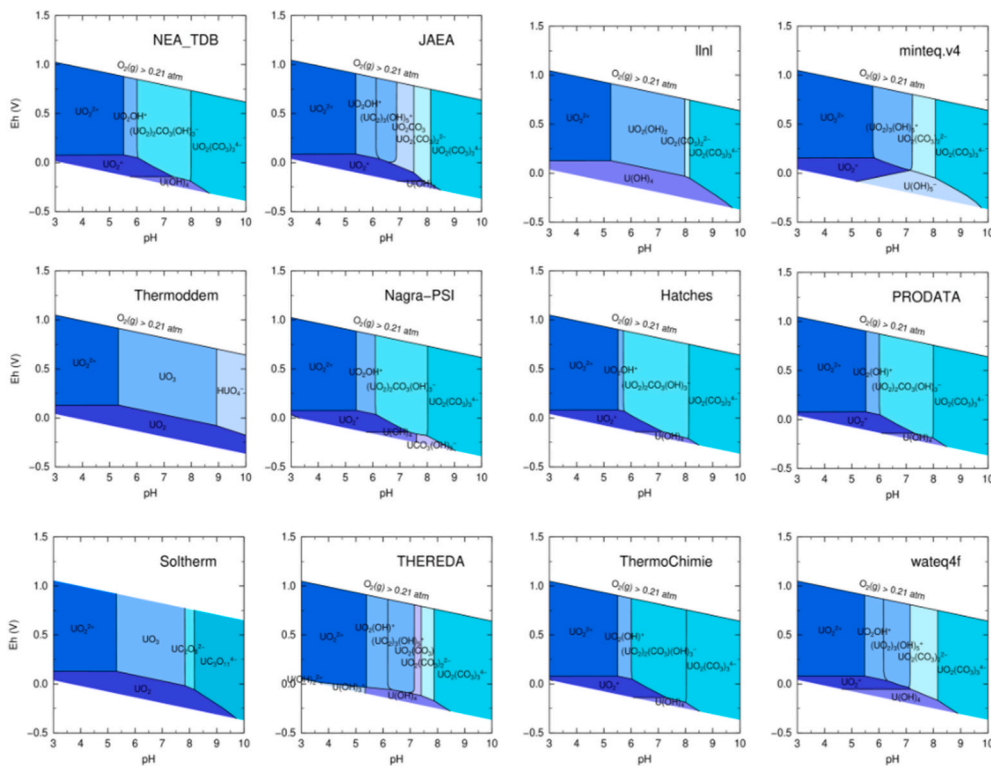
7.5.1. Solid-phase interactions

The propensity of U to precipitate as a wide variety of highly insoluble solids is well known and is widely used in the extraction and purification of U for industrial use. As outlined above, this can occur even with micromolar concentrations of U and major ions. Uranium can also bind to a wide variety of mineral surfaces. Given the high ratio of minerals/U found in sediments and soils, these reactions can dominate U behaviour. These interactions may simply involve U binding to the surface of minerals (sorption; Payne and Waite, 2022), or more complex interactions involving incorporation into the subsurface structure ending up as a solid solution or co-precipitate, or even being intimately bound to an organic component. Chemical analyses show that many minerals contain minor amounts of U (Table 5).

Unlike the 'on-off' nature of mineral precipitation, sorption reactions occur on most surfaces to some extent, the overall amount depending on the surface area involved (Mendez et al., 2020) and the strength of the interaction. These reactions can be highly selective and so are particularly important for trace metals such as U. This highly selective sorption contrasts with the rather non-specific binding by cation exchange as seen on the basal planes of permanently-charged phyllosilicate clays. These cation exchange reactions are important for the major elements, Ca, Mg, Na and K but much less so for trace elements such as U. Sorption reactions are normally rapid, occurring in minutes to hours, and reversible, whereas the kinetics of mineral precipitation/dissolution and solid solution reactions are much more variable and are likely to depend strongly on particle size, structural features and environmental factors. Such differences can provide an empirical basis for speciating trace metals in soils and sediments based on their selective dissolution in various reagents, e.g. the three-step BCR procedure (Dhoum and Evans, 1998). A bicarbonate-based extraction procedure seems particularly appropriate for determining sorbed U in oxidized sediments (Seder-Colomina et al., 2018; Stoliker et al., 2013).

The speciation of U in reduced sediments is more problematic and may benefit from a strong anion exchange resin to separate dissolved U (VI) and U(IV) (Stoliker et al., 2013) or an anaerobic 1.0 M sodium bicarbonate (pH 8.7) extraction to separate biogenically-produced non-crystalline UO_2 from crystalline uraninite (Alessi et al., 2012; Cerrato et al., 2013). The inclusion of an oxidant such as potassium persulphate can also help to resolve the solid forms based on the kinetics of oxidative

(a) Without solids



(b) With solids

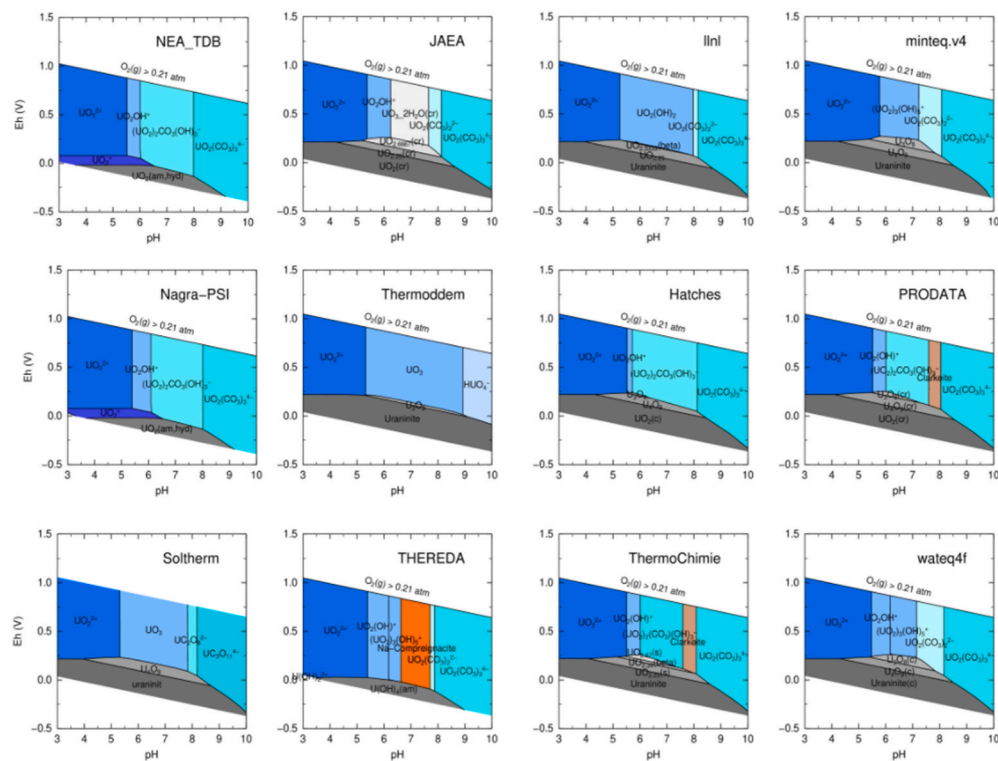


Fig. 8. Eh-pH predominance diagrams for U calculated using the 12 databases tabulated in Table 10. These diagrams are for relatively simple systems with a total U concentration of 10^{-6} mol/kg water in 0.01 mol NaCl/kg water and under a fixed PCO_2 of $10^{-3.4}$ atm, close to atmospheric conditions, shown here assuming (a) no precipitation of minerals and (b) precipitation of any supersaturated minerals included in the indicated database. This illustrates both the chemical speciation of U and the scope and selectivity of the databases.

dissolution (Cerrato et al., 2013). Alternatively, a strong acid ($\text{H}_3\text{PO}_4\text{-HF-H}_2\text{SO}_4$) extraction followed by a U(VI) specific analytical method can help to speciate the U (Luan and Burgos, 2012).

The solubility of the various $\text{UO}_2(\text{s})$ phases is important since they are often suspected of controlling U solubility in reduced waters and sediments. Also, selective dissolution with various organic ligands can help to separate the more soluble biogenic non-crystalline UO_2 forms from chemogenic ones (Chardi et al., 2022) and can thus contribute to understanding the solid phase speciation of U in sediments.

The multiplicity of possible mineral-U reactions, and their overlap, often makes it difficult to determine the most important reactions taking place. It is always going to be difficult to detect trace U minerals at the ppm level. The use of XAS (XANES, EXAFS) has been particularly useful in determining the binding environment of U in minerals (Bargar et al., 1999; Fuller et al., 2002; O'Loughlin et al., 2003; Rossberg et al., 2009; van Veelen et al., 2012) but the methods are not sensitive enough to analyse U in minor phases such as in sediments with average U contents. Nevertheless, with more contaminated sediments, such as at old mine sites, where bulk U concentrations can exceed 400 mg/kg, EXAFS has proven very valuable in identifying the U-binding phases. For example, Lahrouch et al. (2021) used EXAFS combined with other mineralogical and geochemical techniques on samples of granitic waste rock and mine drainage to show that the U was closely associated with iron oxides, particularly with 2-line ferrihydrite. They were even able to identify ternary Fhy-U-P and Fhy-U-C(carboxylate) complexes in the most contaminated samples. EXAFS also identified Fhy and chlorite as the dominant U phases in some Canadian mine wastes (Othmane et al., 2013).

7.5.2. Oxides

The oxides of Fe, Al and Mn are ubiquitous in nature and strongly bind U and many other trace elements. Iron oxides are particularly abundant and reactive and so it is not surprising that there have been numerous studies of the interactions of U with Fe oxides. Iron oxides also undergo redox transformations under similar conditions to that of U. The most abundant iron oxides are ferrihydrite, goethite and hematite under oxidizing conditions, and magnetite and green rusts under reducing conditions. Ferrihydrite is an intrinsically heterogeneous, high-surface-area, metastable form of iron oxide that is favoured in situations where iron oxides have formed relatively recently, as in many soils and sediments, and especially where active weathering is taking place or where redox conditions have fluctuated. It also often forms coatings on other minerals. Iron oxides are also readily synthesized in the laboratory and so have served as model oxides which have been widely used in the development of surface complexation models to quantify sorption (Table 11).

Systematic laboratory studies of U sorption by iron oxides (Table 11) mean that the principal factors controlling the sorption of U by oxides are now quite well understood, at least under oxidizing conditions. pH is the main variable and so the sorption is often reported as a %U adsorbed versus pH curve with U sorption increasing rapidly over the range pH 4–6 (Hiemstra et al., 2009; Kobayashi et al., 2020; Waite et al., 1994). The actual pH range showing this rapid rise (the 'edge') depends on the total amount of U present and the solid/solution ratio. The PCO_2 , which controls dissolved carbonate concentrations, can be another key variable (Fig. 9). Other variables are the specific surface area of the mineral, the concentrations of competitors, ionic strength and temperature. The minimum dissolved U concentration in these studies is in the range 10^{-9} to 10^{-8} M or about 0.24–2.4 $\mu\text{g/L}$ at a pH close to pH 7. While % sorption-pH plots are popular, they can disguise important features especially when the sorption is above 90%. Plots of $\log(\text{dissolved U})$ -pH or of the distribution coefficient-pH can be more revealing and are better suited for archiving purposes.

When a U-containing solution is exposed to the atmosphere, $\text{CO}_2(\text{g})$ is absorbed and carbonate ions are formed. This results in the formation of dissolved uranyl carbonate species, as discussed above (Section 7.3)

and leads to a sharp decline in uranyl activity and hence U sorption. Other co-ions can also lead to a decrease in U sorption, as demonstrated for P sorption on goethite at high pH (T. Cheng et al., 2004) and Si sorption on ferrihydrite (Gustafsson et al., 2009) but here the effects due to complexation in solution must be combined with those due to competition for surface sites and the possible formation of ternary surface species. The presence of Ca above pH 7 decreases U sorption by ferrihydrite probably due to the formation of stable U-Ca- CO_3 ternary species in solution (Fox et al., 2006). These are not favourably adsorbed for both charge and coordination reasons. Payne et al. (1996) noted a strong positive influence of PO_4 sorption to ferrihydrite at pH < 7, with increased sorption of U attributed to the formation of ternary surface complexes with UO_2^{2+} and PO_4^{3-} . These were concluded to be inner-sphere surface complexes at least up to about pH 8. Payne et al. (1994) also noted a reduction in U sorption affinity following the aging of ferrihydrite to more crystalline forms.

The mechanisms of U sorption have been studied extensively with EXAFS and FTIR spectroscopy and by modelling (Table 11). EXAFS is able to reveal bond lengths and provides support for the nature of U binding, including the presence of ternary complexes such as surface-U- CO_3 species. Aging of ferrihydrite to hematite has been found to result in incorporation of U into the hematite structure, with EXAFS and XANES data suggesting incorporation by replacing octahedrally coordinated Fe (III) (Marshall et al., 2014). Surface complexation (i.e. electrostatic) models are required for a detailed understanding since the variable sorption of ions, including H^+ , leads to a change in the surface potential and surface charge and so affects further sorption. Even the sorption of UO_2^{2+} will itself change the surface potential although because it is normally only present at very low concentrations, it is unlikely to be a major potential determining ion.

As shown above (Section 7.1), the predominant U species in solution changes from a cation under acidic conditions (UO_2^{2+}) to an anion at high pH, e.g. $\text{UO}_2(\text{OH})_3$, or to $\text{UO}_2(\text{CO}_3)_3^{4-}$ and $\text{CaUO}_2(\text{CO}_3)_2^{3-}$ in the presence of $\text{CO}_2(\text{g})$ and Ca (Wazne et al., 2003). The point of zero charge (pzc) of ferrihydrite is pH 8.1 and so above this pH, the surface charge becomes negative which combined with the dominance of anionic U species in solution results in a repulsion that tends to inhibit sorption. The pzc's of other iron oxides are also generally in the range pH 7–9.5 (Kosmulski, 2009).

The most successful surface-complexation models for describing this sorption quantitatively are the Diffuse Layer Model (Mahoney et al., 2009; Waite et al., 1994), the CD-MUSIC model (Gustafsson et al., 2009; Hiemstra et al., 2009) and the Extended Triple Layer Model (Kobayashi et al., 2020). These differ in the location of the sorbed charge, the way that this interacts with the surface charge and the change in water dipoles in response to sorption. The latter two models attempt to reconcile their simplified structural models with information obtained from spectroscopy and molecular modelling. This also helps to constrain the number of adjustable parameters during model fitting. These studies indicate that the binding of U is predominantly as a bidentate inner-sphere species.

It has been found that in the presence of $\text{CO}_2(\text{g})$ and high pH, although dissolved carbonate reduces sorption, it is necessary to include one or more ternary surface-U- CO_3 complexes in the model to explain all of the experimental data (Rossberg et al., 2009). Ignoring such species would require either an adjustment to the log K's of solution U- CO_3 species (Hsi and Langmuir, 1985), which is undesirable, or accepting a poorer fit to the observations. The relative importance of these ternary species remains one of the differences between existing models (Kobayashi et al., 2020). Differences between predictions from the different models and experiment generally tend to only become apparent in more complex systems, particularly where the model is tested outside its range of calibration. Somewhat surprisingly, this can include sorption under CO_2 -free conditions at high pH (Kobayashi et al., 2020). Where a sorption model is required for a range of three or more orders of magnitude in dissolved U concentration, the intrinsic

Table 11
Uranium sorption studies with various oxide minerals.

Mineral	Data	SCM ^a	Comment	Reference
Ferrihydrite	Sorption-pH; Variables: $U_T = 1 \mu\text{M}$; 0.02, 0.1, 0.5 M NaNO_3 ; two PCO_2 ; 0/0.1 mM P; humic acid (HA); mass concentration. EXAFS	Two-site (strong-weak) DLM (MINTEQA2), ternary complex with CO_3^{2-}	Inner sphere bidentate binding. Good fit pH 3–10. Surface U polymers not readily formed (c.f. solution). Compared with kaolinite and Fhy + kaolinite mixtures – Fhy dominates. HA increases U sorption at low pH but not at pH > 8	Waite et al. (1994); Payne et al. (1998)
Ferrihydrite	Sorption-pH (3–10) curves varying U_T , P, HA	Discussed possible speciation but not implemented	P increased U sorption, HA increased sorption below pH 7 with little effect for pH > 7	Payne et al. (1996)
Ferrihydrite	Sorption-pH, pH 2–12, $U_T = 10^{-8}$ to 10^{-4} M, variable PCO_2 including CO_2 -free	ETLM	Extensive re-analysis of old and new data including new CO_2 -free data. Good fits throughout	Kobayashi et al. (2020)
Ferrihydrite	Partitioning of U in Fhy/HA(Elliott Soil),FA (Suwanee R) mixtures (pH 4.6 & 7.0), zeta potential Fhy (pH 4–11), HA/FA isotherms on Fhy, EXAFS	Fhy (inner sphere, mononuclear, bidentate), Fhy + NOM (some HA/FA-U complexes)	At pH 4.6, NOM increases total U adsorbed but not at pH 7.0	Dublet et al. (2017)
Ferrihydrite	Reanalysis of literature data (14 data sets/233 data points)	DLM	Revised Dzombak and Morel's estimated log K's for uranyl sorption which tended to overestimate sorption at low pH. Added two log K's for carbonate sorption	Mahoney et al. (2009)
Ferrihydrite	H+ titration; density; reanalysis of literature data; EXAFS	CD-MUSIC; two sites; extensive data fitting. Bidentate inner sphere complex at Fhy edge and corner sites	The SCM is able to fit a wide range of pH- CO_2 data with a relatively small set of surface species including a monodentate Fhy- $\text{OCO}_2\text{UO}_2(\text{CO}_3)_2$ ternary complex	Hiemstra et al. (2009); Hiemstra and Van Riemsdijk (2009); Rossberg et al. (2009)
Ferrihydrite, hematite	Sorption-pH edges, pH 3.5–10, $U_T = 10^{-6}$ M, $I = 0.02, 0.1$ and 0.5 . $\text{PCO}_2 = 10^{-3.5}$ atm	DLM with single site and three adsorbed U species including a U- CO_3 species	Fitted model for hematite was the same as for Fhy after scaling for their different specific surface areas (x5)	Jang et al. (2007)
Ferrihydrite	Measured extraction (e.g. Am-Ox, $\text{NaHCO}_3 + \text{Na}_2\text{CO}_3$) of U and Fe from various Fe-U-(P, Si) coprecipitates over 2 yr; Mössbauer, micro XRD	Coprecipitation combines surface sorption plus bulk incorporation	U preferentially extracted cf. Fe. Extractability decreased with ripening time but increased with extraction time. Fhy gradually transformed to goethite and hematite (except with P).	Smith et al. (2009)
Ferrihydrite	Open air U/Fe coprecipitation at mM concentrations. EXAFS, FTIR	DLM. Bidentate edge-sharing inner sphere complex	Generally good fit to SCM except at high pH where slow CO_2 absorption likely. Metaschoepite precipitation predicted but not found.	Winstanley et al. (2019)
Ferrihydrite, goethite, hematite	Sorption-pH (3–10), ionic strength, CO_3 , Ca, Mg	DLM	Sorption: Fhy > goethite > hematite. Carbonate severely inhibited sorption but Ca/Mg had no effect. Modelling successful but CO_3 systems required adjustments of log K	Hsi and Langmuir (1985)
Ferrihydrite, Lepidocrocite, goethite, hematite	EXAFS (simulated and experimental) for U in goethite and hematite	<i>ab initio</i> molecular dynamics calculations	Calculations consistent with U(V) incorporation into goethite under reducing conditions. Best fit to observations did not quite match minimum energy configuration	Kerisit et al. (2016); McBriarty et al. (2018); Soltis et al. (2019)
Goethite	Effect of PCO_2 , Ca, Mg, P on U_T (0.1, 2 mg/L) sorption by goethite	DLM (FITEQL) Monodentate binding of U	Less sorption at high PCO_2 and high alkalinity because weak sorption of negatively-charged U(VI)- CO_3 species	Duff and Amrhein (1996)
Goethite	U and P sorption on goethite-coated sand. pH 2–10, $U_T = 5 \mu\text{M}$	CC	Phosphate increased U sorption at pH < 7. Speculated that there was formation of a ternary U-P-goethite surface complex	Cheng et al. (2004)
Hematite (nanoscale)	H+ titration; sorption-pH (3–11); EXAFS/XANES; particle size, $U_T = 1,100 \mu\text{M}$	2-site DLM (FITEQL); U(VI) probably sorbed as mononuclear bidentate complexes	log K corrected for particle size (Sverjensky). Precipitation of schoepite at high U	Zeng et al. (2009)
Hematite	ATR FTIR, EXAFS		Hematite-U(VI)- CO_3 predominant adsorbed species (pH 4.5–8.5). Inner sphere bidentate hematite-U(VI)- CO_3 complexes, polymeric at pH ≥ 6.5	Bargar et al. (1999); Bargar et al. (2000)
Hematite	Hematite + U(VI)+Suwanee River HA (IHSS); H+ titration; electrophoresis; batch open air (+ NaHCO_3) U sorption; ion exchange; varying solid/solution ratio; ionic strength 0.001, 0.01, 0.1 M NaClO_4	FITEQL; Non-electrostatic with HA simulated as mixture of monoprotic acids; TLM	Max. sorption of HA at pH 4	Lenhart and Honeyman (1999); Murphy et al. (1999)
Hematite	ATR IR of sorbed U in the presence of an aqueous solution at pH 5–8	None	Detected one peak at 906 cm^{-1} attributable to antisymmetric O=U=O stretching and a single adsorbed species, possibly bidentate	Lefevre et al. (2006)
Hematite	pH 2.8–6.5 in 0.01M NaCl, 15–80 °C, 21.6 & 43.5 $U_T = 22,44 \text{ nM}$	DLM (FITEQL)	Sorption increases with increasing temperature (endothermic) but this was only tested for pH < 6.5 and Kersten maintains that this may not be true at greater pH's because of carbonate-forming side reactions	Estes and Powell (2020); Kersten (2021)

(continued on next page)

Table 11 (continued)

Mineral	Data	SCM ^a	Comment	Reference
Magnetite (nanoparticles)	Lignite HA coated, FTIR, XPS, H ⁺ titration, kinetics, BET	Non-electrostatic, multisite	LHA binds strongly to magnetite surface. Sorption increased pH 2–7 then declined	Zhang et al. (2021)
Green rust	EXAFS, high-res TEM	Number of nearest neighbour U atoms decreases from 12 in UO ₂ to 5.4 in green rust samples	Green rusts readily reduce U(VI) to 2–9 nm diameter UO ₂ nanoparticles	O’Loughlin et al. (2003)
Gibbsite	pH 4–9, two solid/solution ratios, U _T = 9 μM, CO ₂ (g)-free	TLM (FITEQL)	Also measured sorption by silica and montmorillonite	McKinley et al. (1995)

^a SCM (Surface Complexation Model): DLM = Diffuse Layer Model; TLM = Triple Layer Model; ETLM = Extended TLM; CC=Constant Capacitance Model; FITEQL = a program for fitting SCM models to experimental data (Herbelin and Westall, 1999); Fhy: ferrihydrite; NOM: natural organic matter.

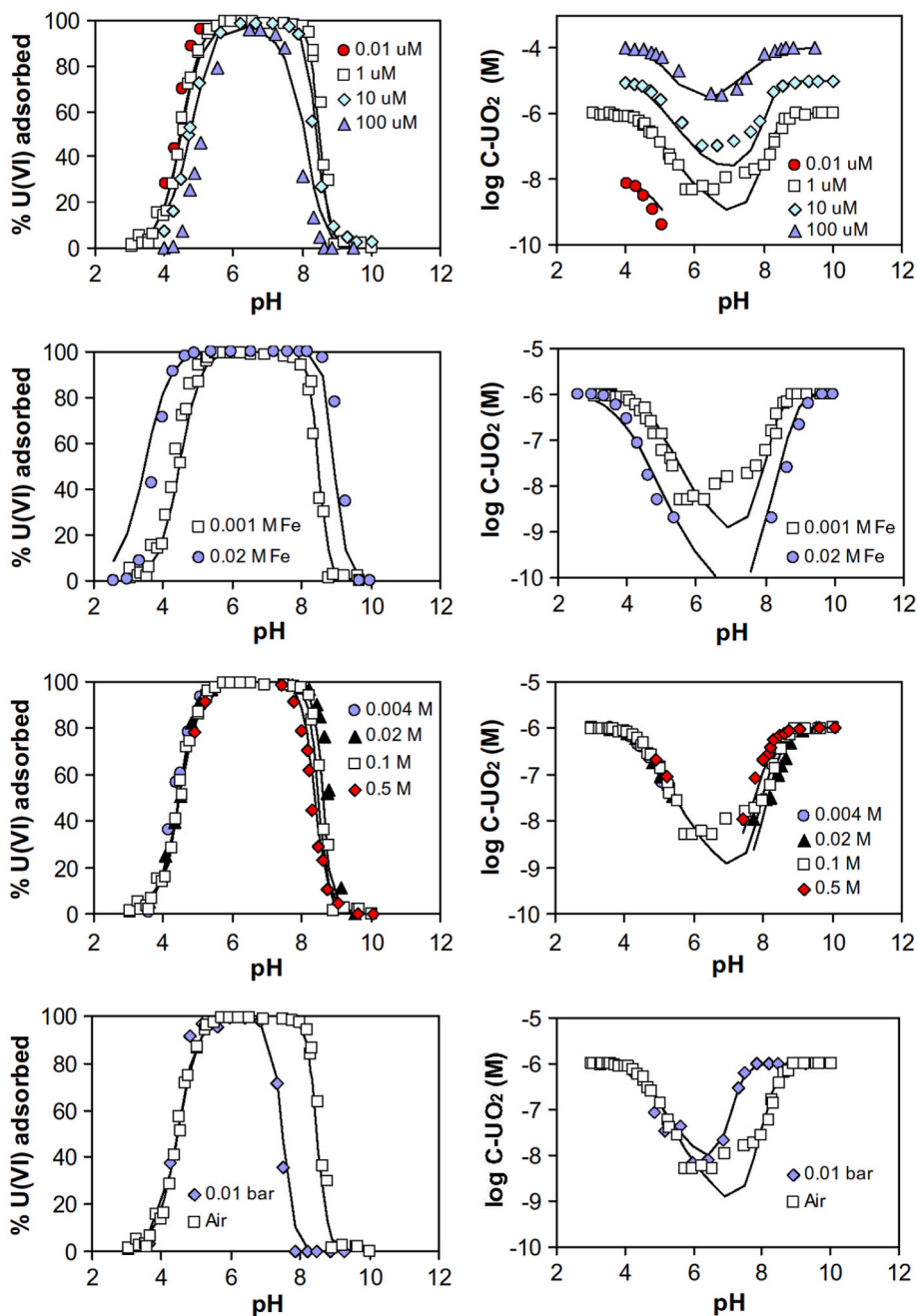


Fig. 9. The percentage of uranyl adsorbed on ferrihydrite as a function of pH (left panels) and the corresponding equilibrium concentrations (right panels). Bottom row shows effect of CO₂(g) partial pressure; reprinted from Hiemstra et al. (2009), ©2009, with permission from Elsevier.

heterogeneity of ferrihydrite might also need to be considered, most simply by resolving into high- and low-affinity sites (Dzombak and Morel, 1991; Mendez and Hiemstra, 2020; Waite et al., 1994). This separation does not necessarily imply that there are just two distinct classes of sites but is an efficient and practical way of capturing the apparent heterogeneity.

The effect of the sorption of other ions such as the strongly-bound phosphate ion is largely untested but laboratory experiments have shown that it can increase U sorption by iron and aluminium oxides at neutral to acidic pH's through the formation of a ternary U–P surface complex (T. Cheng et al., 2004; Guo et al., 2009; Payne et al., 1996). Anecdotal evidence from U transport studies with phosphate-amended sediments supports this, at least in the short-term (Mehta et al., 2015). The impact above pH 8 is less clear.

Sorption of U to iron-oxide minerals under reducing conditions is more difficult to study and is complicated by reductive dissolution, particularly of ferrihydrite which can transform to more stable minerals including goethite, magnetite and green rust. Green rust's major role may also be to catalyze the reduction of U(VI) to U(IV), producing highly insoluble UO₂ nano particles (O'Loughlin et al., 2003). Uranium is also reduced and strongly sorbed by zero-valent Fe which can be incorporated into a permeable reactive barrier to restrict the mobility of soil or groundwater U or used in nanoparticle form as an adsorbent (X. Zhao et al., 2020).

Aluminium oxides and hydroxides such as boehmite (γ -AlOOH) and gibbsite (α -Al(OH)₃) are common minerals in soils and also strongly sorb a wide variety of trace elements including U (Karamalidis and Dzombak, 2011). Most side-by-side comparisons on a weight-weight basis suggest sorption is slightly less strong for Al minerals than for Fe minerals (Wang et al., 2022). The Al minerals are not sensitive to changes in redox which makes their contribution to U binding under moderately reducing conditions, where Fe oxides are unstable, that much more significant. However, they have not received the attention of Fe oxides, probably because the U binding is less strong, perhaps aided by the fact that they are not so brightly coloured and so less visible in soils and sediments! Aluminium oxides are relatively soluble under both moderately acidic and moderately alkaline conditions, which makes them more difficult to study over a wide pH range. They are also more amenable to crystallization and transformation than iron oxides: there is no stable Al equivalent of ferrihydrite, for example.

As a result, the surface acidity of Al oxides is not as well resolved as for iron oxides with pzc's of gibbsite varying from pH 8.7 to 11 (Adekola et al., 2011), indicating a net positive surface charge below pH 9 or so. There can also be considerable hysteresis in acid-base titrations of gibbsite (Adekola et al., 2011) exacerbated by mineral dissolution below pH 5 and above pH 8.5. There is minimal U sorption below pH 4 but this increases rapidly with increasing pH (McKinley et al., 1995; Sylwester et al., 2000). ATR FTIR and EXAFS of U sorbed to gibbsite suggest the formation of an inner-sphere bidentate ternary surface-U(VI)–CO₃ species when equilibrated with the atmosphere (Jo et al., 2018), and the formation of polynuclear species or surface precipitation of U in the absence of substantial carbonate, even at micromolar U concentrations (Froideval et al., 2006; Gückel et al., 2012; Kowal-Fouchard et al., 2004; Müller et al., 2013).

Manganese oxides and oxyhydroxides are redox-active and readily undergo oxidative precipitation and reductive dissolution. They tend to be an order of magnitude less abundant than iron oxides but bind cations more strongly than Fe oxides (O'Reilly and Hochella Jr, 2003; Trivedi and Axe, 1999). Uranium is strongly bound to biogenic and chemically-precipitated manganese oxides, making them a potential sink for U(VI) in the natural environment (Wang et al., 2013a), and as a possible adsorbent in U(VI) recovery schemes (Al-Attar and Dyer, 2002; Ren et al., 2020). Natural and synthetic Mn oxides exist in many forms with a corresponding range of surface acidities (Cristiano et al., 2011; Tan et al., 2008), specific surface areas (Ren et al., 2020) and crystal structures (tunnels and layers). They are normally negatively charged

above pH 1.5–6 and bind U as a bidentate complex with the maximum loading directly related to their specific surface area (Ren et al., 2020).

Sorption of other trace-metal cations to synthetic hydrous Mn oxides tends to increase up to about pH 7–8 and then remains constant up to pH 10 (Tonkin et al., 2004) but for U in the presence of CO₂(g), the maximum sorption is at pH 6 and thereafter diminishes, reflecting the increasing role of dissolved uranyl carbonate species as with Fe oxides (Han et al., 2007). There is a small isotopic fractionation (ca. 0.2‰) during sorption, with the lighter ²³⁵U being favourably adsorbed (Brennecke et al., 2011), a feature also observed in marine ferromanganese crusts (Goto et al., 2014). Sorption of metal ions to Mn oxides often leads to the co-release of Mn²⁺ to solution which points to a more complex mechanism than for Fe oxides.

Silica (SiO₂) comes in various polymorphs ranging in solubility from about 6 to 14 mg/L SiO₂ for quartz to 70–150 mg/L SiO₂ for amorphous silica at 25 °C. It is relatively stable and insensitive to changes in both pH and Eh. Quartz can adsorb U (Prikryl et al., 2001) but is unlikely to be a major adsorbent because of its low specific surface area (<1 m²/g). However amorphous Si, with a specific surface area of several hundred m²/g, can adsorb U quite efficiently (Hou et al., 2021; Kowal-Fouchard et al., 2004; McKinley et al., 1995) and natural opal, a form of amorphous silica, is known to sometimes contain large contents of U (Table 5) (Massey et al., 2014b; Neymark and Paces, 2000). The U in opals and agates may be present as concentric bands showing green luminescence. The U in opals may sometimes be associated with Fe or Ca impurities. TRFLS has shown that the U in opals derived from mineralized rhyolitic lavas in Mexico was sorbed as U-phosphate or polynuclear U–OH species trapped on the internal surfaces of the opal (Othmane et al., 2016). However, pure, synthetic opals can also incorporate U into their structure (Massey et al., 2014b; Schindler et al., 2017). Like the other oxides, U adsorbs to the surface of amorphous SiO₂ via an inner-sphere, bidentate surface complex (Pan et al., 2021; Reich et al., 1998; Sylwester et al., 2000). Using EXAFS, Sylwester et al. (2000) also detected U–U coordination at a pH of about 6.5 and at micromolar U concentrations on amorphous silica. This signal is characteristic of a polynuclear species or of a surface precipitate, albeit in this case, not of schoepite. The stability of U in these forms of microcrystalline silica, including their thermal stability, has led to interest in their use for long-term storage of U-rich wastes.

Other metal oxides also adsorb U and can have superior mechanical properties to the common Fe, Al and Mn oxides for industrial use. For example, an experimental plant was operated in Japan from 1981 to 1988 using a hydrous titanium dioxide sorbent to sorb U from seawater. However, low sorption capacities of approximately 0.1 mg of U/g of sorbent led to the discontinuation of this project (Abney et al., 2017).

7.5.3. Clays

Clay minerals generally have high specific surface areas and so would be expected to adsorb U. However, ion exchange on the exterior basal surfaces and interlayer spaces would be expected to be rather unselective and hence of minor importance, especially when U is complexed with carbonate. Sorption by clays is therefore dominated by inner-sphere complexes with aluminol, silanol, Mg and Fe sites located at the edges (Catalano and Brown, 2005; Chisholm-Brause et al., 2004; D. Pan et al., 2022; Zhang et al., 2018) and the sorption bears some similarities to that found on the corresponding oxides. Maximum sorption occurs at about pH 6–7 and is lower in the presence of CO₂ (Marques Fernandes et al., 2012; Pabalan and Turner, 1997). Pan et al. (2022) found a reversible increase in U(VI) sorption on phlogopite with temperature (25–65 °C), and above pH 10, a marked increase in U uptake probably due to the precipitation of a solid such as metaschoepite. In the presence of high concentrations of Ca, the formation of Ca–UO₂–CO₃ complexes further suppresses U sorption (Joseph et al., 2011; Stockmann et al., 2022). The edges show pH-dependent charging behaviour and for montmorillonite, the surface potential of the edge sites is complicated in that there is an interaction with the adjacent

negatively-charged basal sites, the so-called ‘spillover effect’. This is a significant feature of modelling ion sorption at the edge sites and its inclusion has enabled U sorption to be predicted accurately for a wide variety of conditions using a single-site/three-species sorption model (Tournassat et al., 2018).

The aluminol sites bind U more strongly than the silanol sites on montmorillonite but are different from those on a gibbsite surface for which there is no spillover effect (Turner et al., 1996). Unlike recent models for U sorption on oxides, there is no evidence that ternary surface-U-CO₃ complexes are significantly involved (Stockmann et al., 2022; Tournassat et al., 2018), a conclusion supported by molecular dynamics simulations for kaolinite (Kerisit and Liu, 2014) but contrary to some earlier models (Marques Fernandes et al., 2012). Molecular dynamic calculations also suggest that polynuclear surface complexes may be significant on montmorillonite above pH 8 but these have so far not been identified experimentally (Catalano and Brown, 2005; Zhang et al., 2018).

Bachmaf and Merkel (2011) found that kaolinite adsorbed U more strongly than montmorillonite above pH 5, an observation attributed to the greater abundance and activity of aluminol sites on kaolinite. TiO₂ impurities (especially anatase) are common in kaolinite and these may also influence the sorption of U (Bachmaf and Merkel, 2011; Payne et al., 1998).

Industrially, kaolinite has been investigated for the removal of U impurities from phosphoric acid (40% P₂O₅) produced during fertilizer manufacture. Activating the kaolinite by heat treatment (700 °C) improved the removal efficiency up to about 70% (Taha et al., 2018).

7.5.4. Carbonates

Given the global extent of limestone-rich natural environments, the interactions of U with Ca, Mg and CO₃ are of particular importance. Uranium forms solid solutions with carbonate minerals such as calcite, aragonite and vaterite, giving U concentrations in carbonate rocks typically in the range 0.1–10 mg/kg (Kelly et al., 2003) (Table 5). Minor minerals such as apatite and pyrite can also contribute to the U content of carbonate sediments. Although carbonate minerals are not normally associated with high-U groundwaters, the release of U from the dissolution of carbonates has been implicated as the source of U in some German groundwaters following treatment and reinjection of CO₂-rich groundwater into shallow Quaternary sediments (Banning et al., 2017).

Calcite is the most abundant carbonate mineral worldwide but the large UO₂²⁺ cation fits better into the octahedrally-coordinated environment of aragonite than that of calcite. The coordination of U in aragonite matches that of the UO₂(CO₃)₃⁴⁻ ion which favours U incorporation into aragonite (Smrzka et al., 2019) but this does mean that U can be released from aragonite if it recrystallizes to calcite (Lachniet et al., 2012). The incorporation in aragonite can be achieved both abiotically (Chen et al., 2016; Reeder et al., 2001) and biotically (Drysdale et al., 2019). The U content of aragonitic fossil corals has been used in various palaeo-environmental reconstructions (Gothmann et al., 2019; Smrzka et al., 2019). The U contents of marine foraminera are believed to reflect past seawater U concentrations (Russell et al., 1994) and the U content of an annually-banded stalagmite showed a variation related to the monsoonal cycles (Johnson et al., 2006). However, unlike for foraminifer and corals, the U/Ca ratio in bivalves does not appear to be simply related to ocean chemistry (Gillikin and Dehairs, 2013). The smaller U⁴⁺ ion found in reduced environments is more readily incorporated into calcite and can lead to U concentrations in calcite of up to 35 mg/kg (Sturchio et al., 1998).

Originally it was thought that the UO₂²⁺ cation was too large and of dissimilar coordination to substitute for Ca²⁺ in the calcite structure but EXAFS evidence now suggests that natural calcite can grow sufficiently slowly for U to be incorporated in a relatively stable position (Kelly et al., 2003). Synthetic calcites grown rapidly in the laboratory are more likely to concentrate U in defects and other disordered sites.

Uranium can also be adsorbed onto pre-existing mineral carbonate

surfaces with preferential binding to step edges over flat surfaces (Reeder et al., 2004; Rihs et al., 2004). Molecular dynamics calculations suggest that an outer-sphere complex is most likely (Doudou et al., 2012) indicating rather weak and non-specific binding. The overall extent of sorption is likely limited by the relatively low specific surface areas of natural calcites (<1 m²/g) (Cubillas et al., 2005) and their low affinity for U (Tran et al., 2021). The indirect effects of calcite in blocking access to potential high-affinity sorbing sites, such as those on the edges of phyllosilicate minerals, combined with its role in maintaining high concentrations of neutral Ca₂UO₂(CO₃)₃ or negatively-charged UO₂(CO₃)₃⁴⁻ dissolved species, are likely to be more important than its direct role as an adsorbent (Dong et al., 2005).

Uranium can also form many carbonate-containing minerals, such as liebigite, Ca₂UO₂(CO₃)₃·10H₂O (Alwan and Williams, 1980), but these are relatively soluble and are unlikely to control U concentrations in most natural waters. However, there may be exceptions (Nolan et al., 2021). They are occasionally found as secondary minerals in U-rich environments such as oxidized ore bodies and as efflorescences on mine walls.

7.5.5. Phosphates

Uranium is a common minor component in phosphate minerals such as apatite, hydroxyapatite and fluorapatite and in phosphate-rich rocks (Table 5), especially those of ‘younger’ (Ordovician-Neogene) marine sedimentary origin (Sun et al., 2020). Phosphate forms strong bonds with both U(VI) and U(IV) and is responsible for the reversible sorption of U to primary phosphate minerals such as natural and synthetic apatite (Thomson et al., 2003) and amorphous calcium phosphate (Mehta et al., 2016), as well as the less-reversible uptake by derivatives such as bone charcoal (Fuller et al., 2003) and synthetic Cu-substituted hydroxyapatite (Szenknect et al., 2020). Dissolution of phosphates can also affect U indirectly through the formation of autinite-type minerals and ternary Fhy-U(VI)-P complexes on minerals such as ferrihydrite (Lahrouch et al., 2021). It also enhances the production of non-crystalline UO₂ during U(VI) to U(IV) reduction (Alessi et al., 2014b). Phosphate groups on cell walls are also able to sorb uranium (‘biosorption’) and certain fungi are able to use phosphatases to precipitate various exotic U-P minerals on hyphal surfaces (Liang et al., 2015). Phosphate minerals, directly or indirectly, can therefore aid the immobilization of U in many ways.

7.5.6. Sulphides

Dissolved U(VI) is rapidly immobilized in a wide range of natural and synthetic sulphide minerals (Descostes et al., 2010; Ma et al., 2015; Wersin et al., 1994; Xiao et al., 2017). Amorphous FeS has been found to rapidly reduce U(VI) to a reduced UO₂, U₄O₉ or U₃O₈ solid phase with a consequent lowering of U solubility and release of Fe²⁺ (Hua and Deng, 2008). Hyun et al. (2012) showed that the reduction and formation of uraninite could be initiated by sorption to a fine-grained mackinawite (FeS). Fine-grained mackinawite is an early product of sulphide reduction and not only instigates U reduction but can provide a redox buffer against future oxidation of the reduced U phases. However, when there is a large amount of oxygen available, the reverse may happen: oxidation of FeS can catalyze the oxidation of non-crystalline U(IV) (Lorregian et al., 2020).

The reactivity of crystalline pyrite (FeS₂) is low but fine-grained pyrite is considerably more reactive, and in natural pyrite is increased by the presence of trace-element impurities such as As (B. Ma et al., 2020). Uranium(VI) can also adsorb to pyrite surfaces and transform to UO₂(s) especially in the pH range around 5–7 (Descostes et al., 2010; Wersin et al., 1994), but U(IV) can also be precipitated as a hyperstoichiometric UO_{2+x} solid (Bruggeman and Maes, 2010; Descostes et al., 2010). The surface of pyrite can adsorb a wide variety of ions including H⁺ and Fe²⁺ which compete for surface sites and can reduce U sorption.

7.6. Natural organic matter (NOM)

7.6.1. Metal-ion-NOM interactions

Natural organic matter is found in almost all natural waters, sediments and soils and gives rise to their brown colour. This ubiquity combined with their inherently high and selective metal-binding capacity makes them important materials in the speciation of all trace metals, including U, in natural environments.

Given this intrinsic reactivity towards a wide range of ligands, it is not surprising that U binds very strongly to many NOMs ranging from humic-type compounds and cell surfaces to synthetic organics (Davis et al., 2000; Gustafsson et al., 2009; Higgs et al., 1993; Lofts et al., 2015; Reiller and Buckau, 2012). The uranyl ion, UO_2^{2+} , is one of the most strongly bound divalent cations, and normally binds more strongly to NOM than Cu^{2+} and even Pb^{2+} (Milne et al., 2003). This binding is important since it can affect U toxicity and mobility as well as presenting the possibility of using these materials for the extraction of U from water or for immobilizing U in contaminated soils.

Not surprisingly, given the complexity of uranium chemistry and the experimental difficulty of determining the individual activities of U species, most of the present understanding of humic-metal ion interactions has come from laboratory studies not directly involving U, although some reviews have targeted U and other radionuclides specifically (Reiller, 2012; Reiller and Buckau, 2012).

Sometimes NOM can be responsible for the natural accumulation of U to high levels. For example, Lefebvre et al. (2022) describe a small, pristine alpine wetland catchment in southern France where U has accumulated to concentrations of up to 1000–5000 mg/kg in the shallow, organic-rich soils. They used a variety of techniques including isotope ratios, μ -XRF, SEM-EDX, EPMA, XANES and EXAFS to identify the nature of the U and concluded that it was predominantly U(VI) bound to NOM (HA). It appears that the U had accumulated over the course of some 14,500 years as a result of the prolonged input from some unidentified but probably mineralized source in the adjacent granitic landscape.

NOM is often operationally divided into dissolved organic matter (DOM) and particulate organic matter (POM). The distinction between the two is based on some form of separation: filtration, centrifugation, or dialysis, and can depend on environmental conditions such as pH. An alternative classification is based on chemical extraction. The most reactive components of the NOMs found in soils and natural waters are humic acid (HA) and fulvic acid (FA). These are the relatively stable end products of the decomposition or oxidation of fresh organic. They are separated from each other by their solubility under acid and alkaline conditions: HA is soluble in alkali but insoluble ('floculated') in acid, while FA is soluble ('dispersed') in both alkali and acid. Humic is the organic fraction that is insoluble in both alkali and acid. It is relatively unreactive.

An estimate of the DOM concentrations in natural waters can be made using various empirical relations including those based on UV–Vis spectroscopy (Li and Hur, 2017). The Cu complexation by DOM-containing natural waters suggested that the effective FA concentration was 65% of the DOM concentration but only after the impact of measured EDTA and NTA concentrations, a feature of some urban waters, had been included (Ahmed et al., 2014). Soil and sediment organic C is made up of approximately 40% FA + HA with HA/FA ca. 3 (Ukalska-Jaruga et al., 2021).

Measuring the free UO_2^{2+} ion concentration in the presence of NOM-U species is difficult, especially at trace concentrations. Several approaches are possible (Pesavento et al., 2009). One is to use the Donnan Membrane Technique (DMT) which has two aqueous compartments separated by a cation-exchange resin. The donor side contains the free metal ion of interest and its complexes while the acceptor side contains the metal ion at some fixed activity, possibly including a ligand with well-known properties to increase the sensitivity of the method. Pure minerals, such as $\text{UO}_2(\text{s})$, are also able to 'fix' activities in solution and if

the solubility product was well known, could in principle be used to fix the uranyl activity. Cations transfer across the resin until a Donnan equilibrium is achieved. This may take many days and so more rapid, dynamic variations have been devised (Marang et al., 2006). Reiller et al. (2011) used such a technique to derive NICA-Donnan parameters for U(VI) binding to Gorleben HA and an insolubilized HA. Another approach is the Diffuse Gradient in Thin film (DGT) method which relies on the diffusion of the free metal ion through a gel and onto a resin that acts as a sink for the ion. This has also been applied to U binding by HA/FA solutions (J. Zhao et al., 2020).

HA and FA are variously described as colloids, polyelectrolytes or as a polydisperse mixture of molecules with a variable molecular weight. They have a variable net negative charge under all conditions. This charge arises from the dissociation of a wide variety of weak acid sites broadly classified as 'carboxylic-type' sites and 'phenolic-type' sites (Milne et al., 2001; Reiller and Buckau, 2012). The separation into HA and FA relates to more fundamental structural features; FA generally has a slightly higher charge and lower average molecular weight than HA and these properties tend to keep it in solution rather than in an aggregated state. There are more carboxylic-type sites than phenolic-type sites, especially in FA's that contain a greater number of oxygen-containing groups than HA's. Carboxylic-type sites are likely to dominate U binding especially under acidic conditions (Schmeide et al., 2003). Metal-ion binding generally increases with increasing ionic strength (Kinniburgh et al., 1999) but the effect is rather small, especially for FA, and is not universally observed (Glaus et al., 1997).

Humic substances have almost linear proton titration (charge-pH) curves and while they vary in detail when derived from different sources, they also show broadly similar charging behaviour (Milne et al., 2001) and cation binding (Milne et al., 2003). In simple systems, the binding of most multivalent cations increases monotonically with increasing pH. UO_2^{2+} would be expected to be bound very strongly by both HA and FA based on its tendency to hydrolyze (Milne et al., 2003) and this has indeed been observed (Glaus et al., 1997; Reiller et al., 2011). At a molecular level, EXAFS has demonstrated the similarity between the binding of U to HA and to various uranyl carboxylates (Denecke et al., 1997).

Modelling the binding of uranium to NOM is complex. Prerequisites for capturing metal-ion binding behaviour over a wide range of environmental conditions must consider that: (i) there is an intrinsic binding heterogeneity of NOM and this heterogeneity is *a priori* unknown both in form and in detail (requires a multisite model); (ii) different ions behave differently and there is site competition between them (requires a multicomponent model); (iii) binding of ions involves variable charging of the NOM and associated electrostatic interactions (requires an electrostatic model); (iv) humic substances adsorb to mineral surfaces but this varies with solution chemistry (requires a ternary model), and (v) there may be kinetic effects with some of the bound ions slowly becoming irreversibly bound to the humic substance (kinetic model).

The heterogeneity is most readily seen in the almost linear proton titration curves over a broad range of pH (pH 3–10). This cannot be described with a single-site model, i.e. with one log K. It can be explained either by assuming a small number of discrete proton-binding sites with varying log K's, or by assuming some form of continuation distribution, or distributions of sites. A number of models of varying complexity and scope have been developed for describing metal-ion binding by such heterogeneous humic substances, but the two most successful are Model VI/VII of Tipping (Tipping, 1998; Tipping et al., 2011) and the NICA-Donnan model of Kinniburgh et al. (1999). The former is an example of a discrete site model incorporating multidentate binding and specifically designed for humic materials, while the latter is a general-purpose continuous distribution model based on monodentate binding. In practice, proton charging curves and metal-ion binding can usually be described almost equally well with either model. An elementary analysis of the proton charging curve indicates some form of bimodal distribution and so the continuous distribution approach works

best if binding is described as the sum of two distributions corresponding to a spread in log K 's for the carboxylic-type and phenolic-type sites described above. In the NICA-Donnan model, these distributions are based on Sips distributions (Koopal et al., 2020). There is considerable overlap of the two distributions at near neutral pH's.

The different behaviour of different ions is reflected in the 'non-ideal' behaviour of the ions: it is not possible to simulate the behaviour of one cation by simply adjusting the log K of another cation as in the competitive Langmuir isotherm. The affinity distributions are not fully correlated and a single cation-specific shift of the median log K simply does not work. Also, the binding isotherms remain nonlinear at very low metal concentrations, a feature that is uniquely characteristic of NOM, and difficult to reproduce with many models. Bidentate binding at high loadings and high pH, a feature confirmed for Pb binding using EXAFS (Xiong et al., 2013), may also account for some of the apparent non-ideality seen in the NICA-Donnan approach. Furthermore, while there are similarities in behaviour between different humic substances (HS), there are also important differences and so optimization of at least some of the isotherm parameters will be required for accurately describing interactions with specific HS's (Xiong et al., 2013). Equally, parameters derived from the analysis of specific HS's may not be appropriate for generic modelling.

The variable charging induced by different cations is revealed in the non-stoichiometric nature of the binding: for example, binding a divalent cation, such as Cd^{2+} , on a H^+ -saturated sample of NOM does not release two H^+ but somewhat fewer (Kinniburgh et al., 1999), a feature that has a direct relationship with the observed pH dependency of ion binding. This results in a change in surface charge and surface potential that will affect the binding of all cations and so contribute to competitive interactions. The simplest model to account for this non-specific electrostatic effect and the requirement for overall charge balance in the adsorbed phase is the Donnan model. More complex, and potentially more realistic, models are possible (Koopal et al., 2020; Pinheiro et al., 2021; Town et al., 2019) but the simplicity of the Donnan model is attractive. A key parameter of the Donnan model is the Donnan volume which is the volume that contains the charge-neutralizing cations. This increases with decreasing ionic strength, especially for HA's, and is reflected in the swelling and gel-like characteristics of humic substances, a feature that is both observed and that plays a role in modelling its interactions with mineral surfaces.

This overall complexity results in a large number of model parameters which requires an extensive range of well-spaced experimental data to resolve. When such datasets are not available, some parameters may need to be estimated independently, or the model simplified. Care must be taken not to replace these poorly-defined parameters with arbitrary, post-hoc assumptions.

Unlike many metals, U is found to be bound most strongly to humic substances in mildly acidic conditions ($\text{pH} < 6$), at least under open atmospheric conditions (Gustafsson et al., 2009; Lofts et al., 2015; Reiller et al., 2011). At higher pH's, increasing carbonate concentrations limit the amount of U bound as the activity of uranyl rapidly decreases and the dominant U species becomes either neutral or negatively charged as with the oxides (Section 7.5.2). This accounts for the rather unusual behaviour of U in that U can become less strongly bound above pH 7 and reflects the fact that in most experimental studies, the systems are open to the atmosphere and so contain dissolved U-CO_3 species (Gustafsson et al., 2009). Also pH can affect the apparent 'solubility' of HA's and so reduce the apparent binding of U at high pH when the speciation is based on a size-sensitive separation technique such as centrifugation (Dublet et al., 2017). In terms of the percentage of U bound to NOM and hence its relative importance, this is greatest for very low U concentrations and high NOM concentrations.

Accounting for possible competitive effects between U and multiple macro- and trace cations is obviously important and not yet well tested. The impact on U binding would be expected to be greatest for low concentrations of dissolved U relative to the other metal ions. At higher

U concentrations, as in mine-impacted waters, co-contaminants may have very little impact on the overall speciation especially in neutral to alkaline waters where carbonate complexes will dominate the speciation (Lofts et al., 2015).

7.6.2. NOM-mineral interactions

Humic and fulvic acids adsorb to the surfaces of many minerals (Philippe and Schaumann, 2014) and this is of importance both for the overall binding of uranium and its mobility. Humic substances can be considered as large anions that can adsorb to mineral surface sites rather like other ions and so there are also sorption isotherms for these humic substances that respond to various environmental conditions. Sorption increases with increasing HA/FA concentration in a Langmuir-like fashion and ultimately can lead to a reversal of the apparent surface charge (Ho and Miller, 1985). Sorption is greatest at low pH (2–3 mg/m^2 at pH 4 on goethite) and decreases by a factor 2–3 on going from pH 4 to 10, a feature that can be modelled, although not simply (Weng et al., 2006a, 2007). Sorption in terms of mass is several times greater for the larger HA molecules compared with FA. It is also more pH- and ionic-strength-dependent for HA compared with FA, reflecting a conformational change in the shape of the adsorbed HA when it is close to a mineral surface (Weng et al., 2007).

pH can also affect the interactions between NOM and U and result in the precipitation of U minerals. An analysis of the interaction between U and Suwannee River NOM found that soluble U-DOM complexes were observed at pH 7 while at pH 4, a nanocrystalline U(VI) solid had formed (Velasco et al., 2021).

7.6.3. Metal-ion-NOM-mineral interactions

In many natural environments, minerals such as ferrihydrite (Fhy) or goethite are also present alongside NOM and understanding the overall binding must consider all these components as well as their possible interactions. Payne et al. (1996) found that HA was strongly sorbed by Fhy and in a Fhy-HA-U mixture, increased U sorption by Fhy below pH 5 with little effect at higher pH. Dublet et al. (2017) also found that NOM increased the overall binding of U in acid conditions (pH 4.6), probably via a ternary Fhy-NOM-U complex (supported by EXAFS), but that at pH 7, the adsorbed U was dominantly associated with Fhy alone. These experiments were performed in open air conditions and so at neutral and higher pH would have been susceptible to U-CO_3 formation in solution.

Adsorbed NOM coatings can partially cover mineral surfaces and potentially block sorption sites, but the interactions can be complicated as seen clearly with PO_4 sorption on goethite: below pH 5, FA reduces PO_4 sorption by goethite but above that pH and in the presence of Ca, it increases PO_4 sorption because the Ca^{2+} ion is also bound to the FA and reduces the net negative surface charge, thereby facilitating PO_4 sorption (Weng et al., 2012). The LCD model (Van Riemsdijk et al., 2006; Weng et al., 2007, 2008b) attempts to account for these interactions by combining the CD-MUSIC model for ion binding to mineral surfaces with the NICA-Donnan model for the humic substances (Van Riemsdijk et al., 2006) along with a factor that accounts for the spatial distribution of the sorbed NOM charge in relation to the mineral surface charge (Weng et al., 2007). The smaller size of FA molecules means that they can interact more closely (in the Stern layer) with positively-charged mineral surfaces such as goethite whereas bound HA extends beyond the Stern layer (Weng et al., 2006b) and has weaker electrostatic interactions and a smaller competitive effect with ions such as PO_4 (Weng et al., 2008b, 2009).

The size of the larger HA molecules increases with decreasing ionic strength and this swelling prevents the molecules coming close enough to the mineral surface to compete with other adsorbed counterions and so affect the surface potential. This effect diminishes with increasing ionic strength, accounting for the relatively large ionic strength dependency of HA binding. The size of the much smaller FA molecules is less dependent on ionic strength (Weng et al., 2007). As the extent of NOM binding to mineral surfaces increases, the impact of the underlying

mineral will be increasingly masked and so become less important with the ternary behaviour eventually becoming dominated by the NOM (Li et al., 2022). The magnitude of these interactions has yet to be established for U.

An additional complication in modelling ternary mineral-metal ion-NOM interactions is that there can be fractionation of the HS during sorption, e.g. preferential sorption of the higher-molecular-weight fractions, as can be seen by changes in the apparent molecular masses and UV-visible and luminescence spectra as well as the complexation properties of the dissolved component (Bryan et al., 2012; Reiller and Buckau, 2012; Van de Weerd et al., 2002). It is also possible that the apparent molecular weight of humic substances can change with ionic strength perhaps explaining in part the ionic strength dependency of HA binding to mineral surfaces (Weng et al., 2007). There may also be significant kinetic effects in humic systems with the slow, possibly irreversible, binding of metals to organic matter (Bryan et al., 2012). HA's often show hysteresis in their charge-pH curves during their first full titration (Milne et al., 1995) suggesting significant conformational changes may take place following the strong acid step used to isolate and purify them.

The complex modelling that is reflected in these attempts to provide a comprehensive view of the ternary interactions requires appropriate software to make the necessary calculations. Most of the popular geochemical modelling packages include at best a few of the published surface complexation models, and they usually cannot be easily modified to include new ones. An exception is the ORCHESTRA program (Meeussen, 2003) which has been quite widely used to develop these complex models (e.g. Weng et al., 2008a). It has a modular and hierarchical design with a text-based definition of all its chemical models, including surface complexation models. This can be quite easily edited and extended. It includes both chemical speciation and reactive transport, and is fast.

7.6.4. Laboratory and field observations

Experimentally, the interaction of metal ions with HS has often been studied in the presence of minerals, such as ferrihydrite or clay (Beneš et al., 1998; Dublet et al., 2017; Evans et al., 2011; Ho and Miller, 1985; Ivanov et al., 2012; Joseph et al., 2011; Lenhart and Honeyman, 1999; Payne et al., 1996; Schmeide et al., 2000; Zhang et al., 2021; Zhiwei et al., 2009). This addresses the question, does the presence of HS increase or decrease the binding of the metal ion to the solid phase? The answer is that this will depend in part on the fate of the HS which itself will depend on the pH and nature of the HS (HA or FA) as discussed above. Minerals such as ferrihydrite and goethite are potentially positively charged below pH 8 and so can retain HS under neutral or acidic conditions by charge neutralization.

Uranium porewater concentrations sometimes show a correlation with DOM (Cumberland et al., 2016) but interestingly porewater profiles from contaminated lake sediments in Canada showed no evidence for the release of U by reductive dissolution of Fe or Mn oxides (Novotnik et al., 2018), as often shown by other oxyanions such as As and inferred from some aquifer studies (Section 9.2).

Most experiments have been based on U(VI) but U(IV) also binds strongly to NOM with the partition coefficient increasing linearly with pH over the range pH 3.5–8.5 (Evans et al., 2011). Somewhat bizarrely, the amount of binding of U(IV) in ternary systems can depend on the order of addition of the components, especially for U(IV) (Reiller and Buckau, 2012). In U-kaolin-HA mixtures, the overall binding of U to the >0.2 μm kaolin-dominated fraction decreased as the concentration of added HA increased demonstrating that if HA remains soluble, it is capable of effectively solubilizing some of the U (Evans et al., 2011).

Field evidence also suggests that U(IV) is strongly bound to NOM. This is derived from a detailed analysis of Swiss peats which showed that U accumulates in part as U(IV) bound to the peat organic matter (Mikutta et al., 2016). In fact, the complexation was so strong that it prevented solid UO_2 of any form being created.

The concentration of ligands including DOM in natural waters can also affect the bioavailability and toxicity of U (Markich, 2002; Riethmüller et al., 2001). The Biotic Ligand Model (BLM) states that the bioavailability of a dissolved element, such as UO_2^{2+} , is best predicted by the activity of the free ion rather than its total dissolved concentration. The importance of carbonate complexation in classifying the bioavailability of U in stream waters has already been noted (Lartigue et al., 2020). Numerous studies of freshwater organisms such as *Chlorella* sp. have shown that increasing dissolved organic carbon (DOC) in waters is associated with the decreasing uptake and toxicity of metals, including that of U, and that DOC is often one of the best predictors of U toxicity (Markich and Twining, 2012). pH can also be important since it is a master variable in terms of speciation and affects the binding of most metal ions to cell surfaces. Uranium tends to concentrate in or near the cell wall of microbes by both active and passive mechanisms. For example, U (and Cu) toxicity to *Chlorella* spp. in synthetic (DOC-free) solutions decreased in going from pH 5.7 to 6.5 (Franklin et al., 2000), in line with the protective effect of cation binding to cell surfaces. Metal-reducing bacteria such as *Geobacter* spp. can immobilize U by the extracellular reduction of U(VI) to U(IV), possibly aided by electrically conductive pili ('hairs') attached to the cell surface, thereby protecting the internal integrity of the cell (Cologgi et al., 2011). Lopez-Fernandez et al. (2018) used time-resolved laser fluorescence spectrometry (TRLFS), scanning transmission electron microscopy (STEM) and EXAFS to show that U was initially bound to the surface carboxyl groups of the yeast *Rhodotorula mucigilana* BII-R8 but that this later bound to neighbouring surface phosphate ligands in the phospholipid bilayer of the cytoplasmic membrane.

7.7. Synthetic adsorbents

As a result of the recent interest in the removal of U from wastewaters and the mining of U from the oceans, many studies have investigated adsorbents that adsorb U strongly but also have more robust physical and chemical properties than the traditional mineral adsorbents such as ferrihydrite and hydrous titanium oxide. These have focused on porous amidoxime-based polymer adsorbents which contain both amide ($-\text{NH}_2$) and oxime ($-\text{NOH}$) functional groups (Abney et al., 2017; Aguila et al., 2019; Chen et al., 2017; Sun et al., 2018). These are efficient adsorbents, even in the presence of ambient carbonate concentrations, and have the advantage that they are amenable to both column filtration and passive collection. However, they co-adsorb significant quantities of V, Fe and major cations, with potential unintended consequences if used on a large scale, and are susceptible to biofouling (Haji et al., 2019). Much research continues into the optimal design of synthetic U adsorbents.

7.8. Factors controlling dissolved U concentrations

While the calculated solution speciation of U varies depending on the species considered and their thermodynamic properties (and hence database), a critical factor in terms of the mobility of U is how the total dissolved concentration of U varies under varying conditions irrespective of the detailed speciation. Two scenarios are of particular importance in the natural environment: (i) a change from mildly reducing to strongly reducing conditions which can lead to extremely low dissolved U concentrations, and (ii) a change in the concentration of potential ligands under oxidizing conditions, especially that of carbonate, which can lead to relatively high dissolved U concentrations.

To illustrate these scenarios, the total dissolved U concentration was calculated for a simple U–Na–Cl system with each of the 12 databases under mildly to strongly reducing conditions (Eh from +0.4V to –0.4V). In each case, it was assumed that all the mineral phases defined in their respective databases were able to precipitate if their saturation indices exceeded zero. These calculations (Fig. 10) show a wide range in the calculated dissolved concentrations demonstrating the sensitivity to

these parameters as well as to the great range in the solubility of the minerals selected for inclusion in the various databases. As expected, all databases show a dramatic decline in U solubility over the Eh range +0.2V to -0.2V reflecting the U(VI) to U(IV) conversion (Fig. 10(a)). The limiting concentration at low Eh (-0.4V) depends on the most stable form of $\text{UO}_2(\text{s})$ included in the database with a cluster at 10^{-8} to 10^{-10} mol/kg water assuming an 'amorphous' form, $\text{UO}_2(\text{am})$, and another cluster at 10^{-13} to 10^{-15} mol/kg water for those including the more stable crystalline $\text{UO}_2(\text{cr})$ (uraninite) phase. This accounts for the major differences at very low Eh. Under less-strongly reducing conditions, the differences reflect the absence or presence of minerals such as schoepite, metaschoepite, clarkeite, and minerals with an intermediate oxidation state such as U_3O_8 .

For the simple system considered here, the NEA TDB-e database is unique in that it includes just one mineral capable of precipitating under these conditions, $\text{UO}_2(\text{am, hydr})$, and this remains completely soluble at $\text{Eh} > 0.0\text{V}$, thus giving rise to the horizontal lines in Fig. 10. The NEA review of Grenthe et al. (2021) includes recommended data for $\text{UO}_2(\text{cr})$ but this is not included in the NEA TDB-e database. Although the THEREDA database only includes $\text{UO}_2(\text{am})$, it also includes a $\text{Na}_2\text{U}_2\text{O}_7 \cdot \text{H}_2\text{O}$ phase which can precipitate over a wide range of conditions and so limit U solubility (Endrizzi et al., 2019). The response to increasing pH (Fig. 10(b)) is generally not much change below pH 6 but increasing U solubility above pH 7. The detailed response depends on the minerals present. The solubility can vary by several orders of magnitude between databases.

The variation with increasing temperature is not surprisingly more variable (Fig. 10(c)). The NEA TDB-e database shows no variation because no mineral precipitates over the range of conditions considered; the Nagra/PSI database also shows no variation because there is no enthalpy data or analytical equation to describe the temperature dependence of metaschoepite solubility, the controlling phase. The JAEA database appears to be an outlier with declining solubility with increasing temperature. This reflects the negative enthalpy defined for the $\text{UO}_2(\text{cr})$ and $\text{UO}_{2.25}(\text{cr})$ phases. In general, the temperature dependence under these reducing conditions is poorly defined, reflecting the challenging experimental conditions required to obtain such data.

Fig. 10 is for a CO_2 -free environment, but in oxidizing environments, the role of carbonate, and hence the role of PCO_2 and pH, is likely to be a critical factor in controlling dissolved U concentrations through its impact on sorption/desorption reactions. This can be demonstrated by calculating how the PCO_2 and pH control the dissolved U concentration for various U loadings (Fig. 11). In the absence of $\text{CO}_2(\text{g})$ and carbonates, U sorption on ferrihydrite steadily reduces dissolved U concentrations in the pH range 3.5–7 (Fig. 11(a)). At higher pH's, concentrations plateau out and then increase (Lofts et al., 2015). This increase in the calculated dissolved U concentrations at high pH in the CO_2 -free case reflects the influence and stability of uranyl hydrolysis

species which prevent sorption. A similar effect is seen with U(VI) sorption by kaolinite (Křepelová et al., 2006) and smectite (McKinley et al., 1995) in the absence of $\text{CO}_2(\text{g})$. This is similar to the behaviour of Hg^{2+} which also strongly hydrolyzes (Kinniburgh and Jackson, 1978). At the highest U loading (100 $\mu\text{mol}/\text{kg}$ water), albeit still at very low U loadings and unexceptional Na concentrations, clarkeite ($\text{Na}(\text{UO}_2)\text{O}(\text{OH})$) precipitation occurs and prevents the U concentration from increasing. At atmospheric PCO_2 and ten times higher (Fig. 11(b), (c)), the role of carbonate dramatically reduces sorption above pH 7.5 and also inhibits clarkeite precipitation.

These calculations demonstrate the effect that dissolved carbonate can have on dissolved U concentrations through its impact on sorption reactions, here exemplified by U sorption on ferrihydrite. In soils and sediments, the concentration of ferrihydrite and other sorbing minerals can be one or two orders of magnitude greater than the 1 g/kg water used in these calculations with a corresponding increase in the amount of sorption. The CO_2 -free calculations demonstrate that not only does U(VI) reduction have an impact on reducing dissolved U concentrations because of the precipitation of $\text{UO}_2(\text{s})$ but also indirectly through its impact on the conversion of carbonate to methane and consequent loss of competitive effects. The precipitation of clarkeite ($\text{Na}(\text{UO}_2)\text{O}(\text{OH})$) and related minerals could also be affected.

Selecting the set of possible minerals involved is often the most important decision that must be made when performing speciation calculations. This has to be guided by the environment being considered and any additional information about the type of minerals likely to be found or actually observed. For example, a comparison of measured and dissolved U concentrations for three lakes in U-enriched natural analogue sites by Giffaut et al. (2014) suggested that an amorphous variant of $\text{UO}_2(\text{s})$ was controlling U concentrations at 10^{-9} to 10^{-7} M. Much recent evidence points increasingly to the importance and stability of a non-crystalline, biotically-reduced U(IV) component in U-rich environments such as roll-front deposits (Bhattacharyya et al., 2017). This might not necessarily be the case in other environments, e.g. freshwater aquifers, where dissolution rather than precipitation is occurring.

Even for dissolution reactions, considerable extrapolation may be required. The thermodynamic data for uraninite dissolution has often necessarily been established experimentally at very low or very high pH and high Cl concentrations (Grenthe et al., 2021) since the extremely low dissolved U concentrations that uraninite can impose at near neutral pH's are well below the detection limit of present-day analytical techniques. In natural waters, the presence of small amounts of dissolved organic matter with bound U, or of colloidal material, could enhance the apparent uraninite solubility if not carefully excluded.

In most environmental systems, such as natural waters, sediments, soils and aquifers, a wide variety of U minerals could play a role in controlling U concentrations. This includes interactions with most major

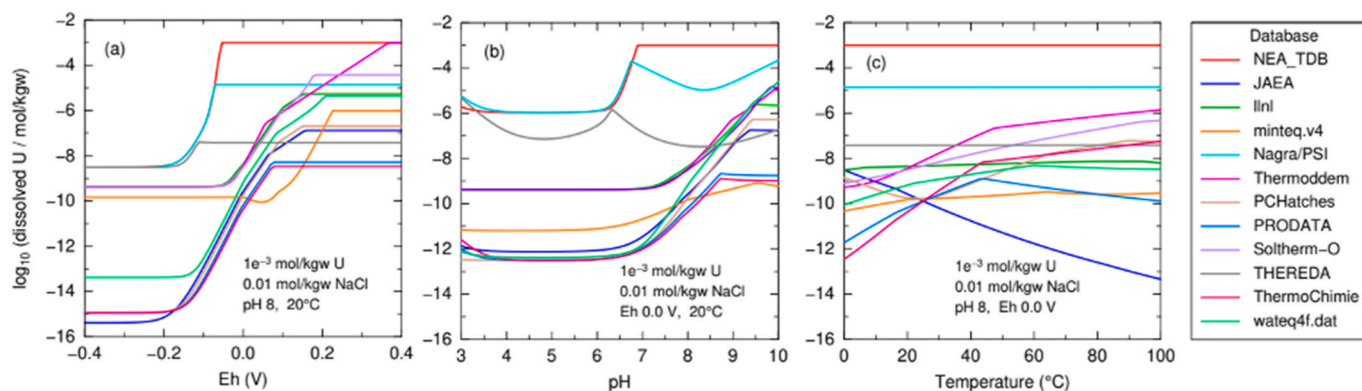


Fig. 10. Variation in the calculated dissolved concentration of U under reducing to strongly reducing conditions for 12 publicly-available thermodynamic databases as a function of varying (a) Eh, (b) pH and (c) temperature. The total U in all systems is 10^{-3} mol/kg water. The atmosphere is CO_2 -free.

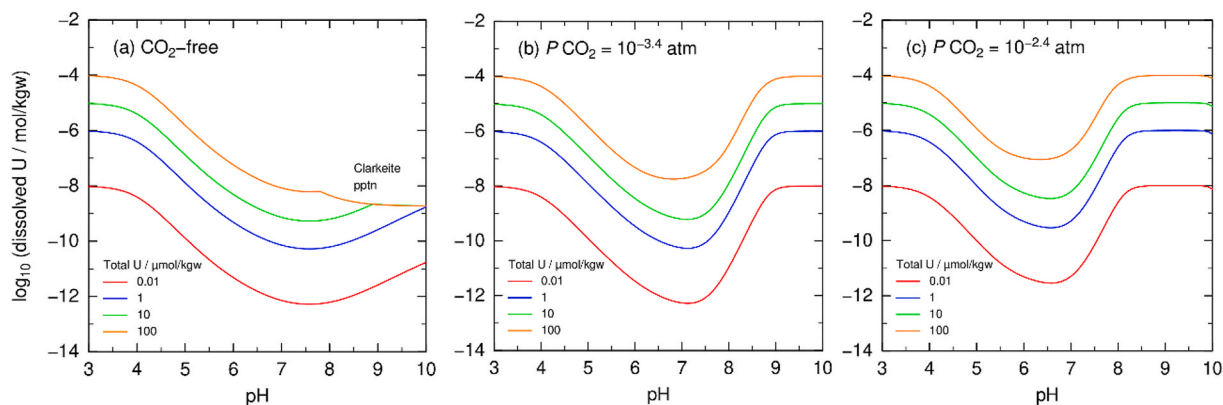


Fig. 11. Effect of $\text{CO}_2(\text{g})$ and pH on the dissolved U concentration in systems containing 0.01, 1, 10 and 100 $\mu\text{mol U/kg}$ water and 1 g/kg water of ferrihydrite in 0.01 mol NaCl/kg water. All calculations were made with the CD-MUSIC surface complexation model with parameters taken from [Hiemstra et al. \(2009\)](#).

ions as well as other trace elements in mineralized or contaminated environments. The only way to know which interactions might be important is to calculate the speciation using a comprehensive thermodynamic database, such as PRODATA or ThermoChimie, and then to look carefully at the minerals that are precipitating, dissolving or have saturation indices close to or greater than zero. Of course, direct observation of the mineral species present provides the strongest evidence.

7.9. Mechanisms of uranium(VI) reduction

Uranium(VI) reduction is a key process governing the mobility of U in the environment, the accumulation of U in ore bodies and the isotopic fractionation of U. The driving force for reduction in the natural environment is often the introduction of fresh organic matter combined with a mechanism for limiting oxygen transport such as waterlogging in soils or the deposition of an impermeable fine-grained layer in sediments. Reduction of U(VI) to U(IV) may be either abiotic or biotic ([Borch et al., 2010](#)). Some of the possible mechanisms include: (i) direct reduction by Fe^{2+} in solution; (ii) reduction by iron minerals; (iii) bioreduction by various organisms, especially metal-reducing bacteria, and (iv) reduction by sulphides. We discuss these below.

7.9.1. Reduction by ferrous iron

Thermodynamics, DFT calculations and limited experimental evidence support the pH-dependent homogeneous reduction of U(VI) by Fe^{2+} in solution ([Collins and Rosso, 2017](#); [Du et al., 2011](#)). [Fig. 12\(a\)](#) shows the calculated variation in U solubility in a mixture of UO_2^{2+} and Fe^{2+} as the pH increases and solids begin to precipitate. This results in a UO_2 solid phase somewhere between pH 4.5–8 depending on the solubility of the assumed solid UO_2 solid phase. The more insoluble the $\text{UO}_2(\text{s})$ phase, the more it drives further reduction ([Fig. 12\(a\)](#)) and the lower the pH where UO_2 precipitation occurs. This is seen in the rapid decline of U(VI) concentrations above pH 7.5 when $\text{UO}_2(\text{cr})$ precipitates, whereas if $\text{UO}_2(\text{am})$ is formed, this begins at just below pH 8 but is much less dramatic and most of the U(VI) remains in solution even at high pH. Therefore, the extent of reduction is strongly dependent on the U(IV) solid formed ([Stetten et al., 2018](#)). $\text{Fe}(\text{OH})_2(\text{s})$ precipitation occurs at pH 8.0 reducing dissolved Fe^{2+} concentrations in line with observations ([Du et al., 2011](#)). In more complex environments, including seawater, the presence of Ca and Mg leads to the formation of ternary Ca(Mg)– UO_2 – CO_3 species which hinder the reduction of U(VI) by Fe^{2+} ([Bender and Becker, 2020](#); [Dewey et al., 2020](#)).

7.9.2. Role of iron minerals

Given the ubiquity of iron minerals in the environment and the redox-sensitive nature of Fe under moderately reducing conditions, it is

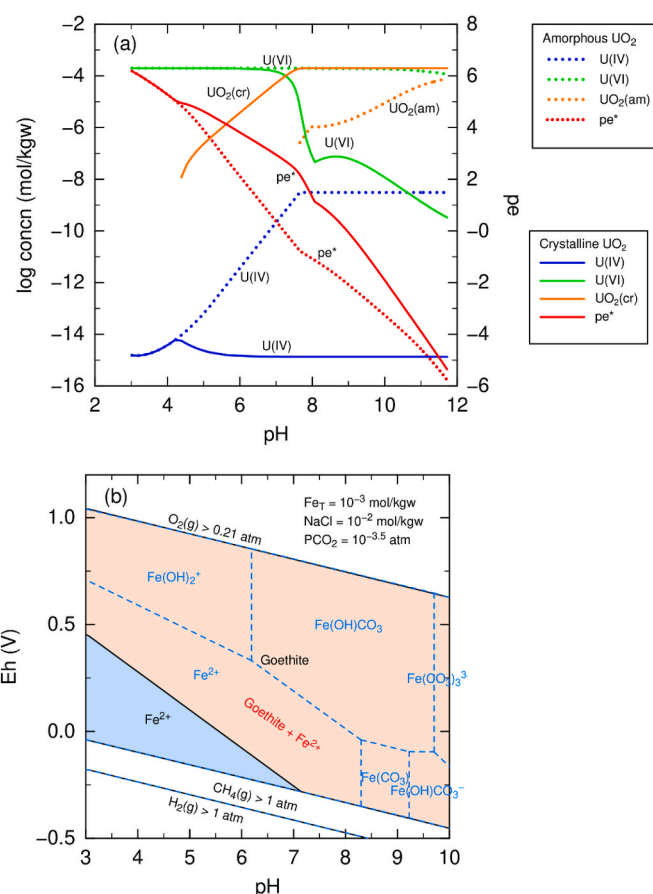


Fig. 12. (a) Calculated speciation demonstrating the homogeneous reduction of UO_2^{2+} by Fe^{2+} in solution in an inert atmosphere as the pH is adjusted. This diagram shows the sensitivity to pH and the solubility of the UO_2 phase formed (amorphous or crystalline, U(VI) = 2e-4 mol/kg water; Fe(II) = 1e-3 mol/kg water, pH adjusted with NaOH, 25C). Concentrations are the total dissolved concentrations of the various redox states plus the concentration of the UO_2 solid phase formed; (b) Eh-pH diagram for iron showing the large field occupied by goethite. The dashed lines in blue show the underlying predominant aqueous Fe species. Note the overlap in the centre of the diagram where goethite coexists with Fe^{2+} , an area where Fe^{2+} -catalyzed U(VI) reduction might be feasible (all calculations using the PRODATA database).

not surprising that Fe minerals often play a key part in the redox chemistry of U ([Belli and Taillefert, 2018](#); [Massey et al., 2014a](#)). There is an area in the Eh-pH diagram for Fe where goethite ($\alpha\text{-FeOOH}$) (and

other iron oxides) can co-exist with relatively high concentrations of Fe^{2+} (Fig. 12(b)). This provides opportunities for the Fe^{2+} -promoted surface catalysis of U(VI) reduction. Such a process has been demonstrated in the laboratory during the Fe^{2+} -catalyzed transformation of ferrihydrite to goethite (Boland et al., 2014) and possibly also following the sorption of U(VI) by colloidal hematite (Du et al., 2011; Liger et al., 1999). Adsorbed U can also be incorporated into other iron oxides during mineral transformations (Marshall et al., 2014; McBriarty et al., 2018) but incorporation into goethite is favoured over lepidocrocite (McBriarty et al., 2017). Above pH 8 and exposed to the atmosphere, Fe-CO_3 species become dominant in solution which combined with the similar dominance of aqueous U-CO_3 species and the possible precipitation of siderite (FeCO_3), are likely to hinder U(VI) reduction and even lead to reoxidation of U(IV) (Belli et al., 2015; Belli and Taillefert, 2018). In aerobic systems, sorption is likely to remain the preferred binding mechanism for U (Soltis et al., 2019).

Unlike in solution, U(V) species can be stabilized in mineral structures and have been identified by XANES during various mineral redox transformations, e.g. during the Fe^{2+} -catalyzed transformation of ferrihydrite to goethite in the presence of U(VI) (Boland et al., 2014; Massey et al., 2014a). Massey et al. (2014a) suggest that U(V), rather than U(IV) or U(VI), is the major form of U incorporated into goethite during these transformations. Also following the coprecipitation of uranyl (VI) with $\text{FeCl}_2/\text{FeCl}_3$ to form magnetite, U(V) was likely stabilized in octahedral sites of the magnetite (Pidchenko et al., 2017) and these inclusions have been shown to be isotopically heavy (Z. Pan et al., 2022). Molecular dynamics calculations also suggest that U(V) in octahedral coordination may substitute for structural Fe(III) during the transformation of ferrihydrite to goethite (Kerisit et al., 2016).

U(VI) can be reduced by Fe(II)-containing minerals such as green rusts, magnetite, siderite and mackinawite. The coprecipitation of U(VI) with FeCl_2 to form magnetite has been studied in detail by a variety of nano-scale spectroscopic and microscopic techniques (Pan et al., 2020). This has indicated a sequence of events involving a surface-bound U(V) species and isotopic fractionation. The overall formation of a stable $\text{UO}_2(\text{s})$ phase involved a sequence of transformations starting with sorption of U(VI) to the magnetite surface, then reduction to U(V) and (IV) species, production of UO_2 nanoparticles, self-assembly of these to strings or 'nanowires' and finally aggregation of these nanowires to UO_2 nanoclusters, all over a few weeks (Pan et al., 2020). Green rusts, a type of mixed Fe(II)/Fe(III) layered hydroxide formed naturally under reducing conditions, have also been found to readily reduce U(VI) to nanometer-sized $\text{UO}_2(\text{s})$ of unknown solubility (O'Loughlin et al., 2003).

The possible oxidation of solid-phase U(IV) by iron(III) minerals is also important. The oxidation of U(IV) in $\text{UO}_2(\text{bio})$ by ferrihydrite produces dissolved Fe^{2+} and U(VI) and the rate depends on the rate of $\text{UO}_2(\text{bio})$ dissolution which in turn depends on the pH and HCO_3^- concentration (Ginder-Vogel et al., 2010). Oxidation is fastest when the pH is far from neutral and for high HCO_3^- concentrations.

7.9.3. Biosorption and bioprecipitation

Uranium may be sorbed and precipitated by microorganisms under both reducing and oxidizing conditions. Lovley et al. (1991) were the first to show that dissimilatory Mn(IV) and Fe(III)-reducing microorganisms could gain energy by directly reducing U(VI) to insoluble U(IV). Bioreduction of U refers to the reduction of U(VI) to U(V) or U(IV) by a wide variety of microorganisms including SO_4^- and Fe-reducing bacteria (Abdelouas et al., 2000; Borch et al., 2010; Lovley and Phillips, 1992; Myers and Neilson, 1988), and is a feature that can now be confirmed by the identification of an isotopically-heavy U phase (Stylo et al., 2015). It is a key process that is used in *in-situ* bioremediation strategies for U-contaminated sites (Cerrato et al., 2013).

Certain strains of bacteria that have evolved in U-contaminated environments such as mining waste have developed particularly efficient methods of binding U(VI) to cell walls and proteinaceous cell surfaces. Merroun et al. (2005) used EXAFS to study U binding by *Bacillus*

sphaericus JG-A12 and found that the U was bound in a bidentate fashion to carboxyl groups and in a monodentate fashion to phosphate groups.

Under reducing conditions, the U can be precipitated both within the periplasm and outside the cell often as very fine-grained (<2 nm diameter) uraninite particles or some form of sorbed U attached to mineral surfaces or organic matter (Alessi et al., 2012; Cerrato et al., 2013; Stetten et al., 2018). EXAFS often indicates shorter U-U distances (3.80 Å) than in bulk uraninite (3.87 Å), implying a possible displacement of surface U(IV) ions (Suzuki et al., 2002) or a non-uraninite source. Phosphate may play a crucial role since a U(IV)-phosphate species may be formed (Boyanov et al., 2011), possibly involving a polymerized phosphate polymer or even the mineral ningyoite, $\text{CaU}(\text{PO}_4)_2$ (Alessi et al., 2014b). A variety of techniques including XANES analyses point to a U(V) intermediate species in the reduction by the versatile microorganism *Shewanella oneidensis* MR1 (Vettese et al., 2020).

As shown above, the reduction of U(VI) to U(IV) is usually accompanied by a dramatic reduction in U solubility. This bioreduction of U in the environment takes place against a background of the redox transformations of major components especially those of C, N, Fe, Mn and S and not surprisingly, both Fe- and SO_4^- -reducing bacteria are often found to be taking part in these reactions. The role of major ions such as Ca^{2+} and HCO_3^- are also important because of the stability and abundance of bio-unavailable ternary complexes such as $\text{Ca}_2\text{UO}_2(\text{CO}_3)_3$ (Luo et al., 2007). The presence of nitrate (Borch et al., 2010) and phosphate (Cerrato et al., 2013) can also hinder the formation of $\text{UO}_2(\text{s})$.

Laboratory experiments have followed many of these transformations in detail while field experiments, often involving the addition of a C-source such as acetate to stimulate reduction, have been undertaken with a view to monitoring the reduction in U solubility. As with mineral weathering, bioreduction rates are strongly scale-dependent with rates measured in the laboratory being several orders of magnitude faster than those measured in the field (Bao et al., 2014). This reflects the averaging effect of mixed microbial cultures in the field compared with laboratory experiments where the most effective microbes are favoured. There is also extensive mixing in laboratory systems which facilitates access of the biostimulant to the principal terminal electron acceptor such as Fe(III) oxides (Li et al., 2011). There could even be a form of microbe-induced 'self-sealing' whereby biofouling preferentially reduces flow through formerly active reduction zones. This sealing is likely to be more significant for field observations compared with constant-flow laboratory conditions (Komlos et al., 2008). It has been modelled successfully (Li et al., 2011).

The overall effect of this bioreduction on U solubility and transport depends not only on the extent of bioreduction but also the concentration of ligands capable of keeping U(IV) in solution including bicarbonate (Long et al., 2015), low-molecular-weight organic acids such as citrate (Francis and Dodge, 2008) and fulvic acids. Francis and Dodge (2008) found that while *Clostridia* sp. could reduce dinuclear U(VI)-citrate to a mononuclear U(IV) citrate, the microorganisms did not metabolize the citrate itself reflecting the unavailability of the tridentate citrate ligand. The impact of NOM is particularly complex because it can both stimulate reduction and reoxidation of U as well as strongly binding U(IV) and U(VI) in either a solid or soluble phase (Gu et al., 2005). Colloidal transport of such organic complexes as well as colloidal-sized uraninite particles are also possible complications (Suzuki et al., 2002).

Although the principal role of organic matter in uranium reduction is to initiate the microbial processes that lead to the consumption of oxygen and nitrate, the remaining organic matter, including HA and FA, are themselves redox-active through their electron-donating phenolic moieties and electron-accepting quinone moieties. Light-sensitive redox reactions may also be relevant for dissolved organic matter in lakewater. HA/FA can therefore operate as a limited redox buffer and as an electron shuttle between microorganisms and redox reactions including those of U reduction. This overall capacity can be measured by redox titration

(Kappler et al., 2004; Peretyazhko and Sposito, 2006). A variety of humic substances have electron-donating and electron-accepting capacities on the order of 1–2 mol/kg under near-neutral conditions (Aeschbacher et al., 2012). Reiller (2005) estimated that U(VI) is reduced to U(IV) by 100 mg/L HA suspensions when $E_h \leq -20$ mV.

7.9.4. Reduction by sulphides

Uranium(VI) can be rapidly reduced abiotically by sulphide in solution and by sulphide minerals such as pyrite (FeS_2) (Wersin et al., 1994) and mackinawite (FeS). The rate of reduction is inhibited by dissolved carbonate at millimolar concentrations, especially at high pH (Hua et al., 2006), and also by the formation of uranyl carbonates and ternary Ca–U–CO₃ complexes. This retardation is likely to account for the lack of U(VI) reduction in modern anoxic waters such as those of the Cariaco Basin and Black Sea (Hua et al., 2006; Stewart et al., 2007). It can also lead to U isotope fractionation (Brown et al., 2016).

7.10. Transport of uranium

7.10.1. Mechanisms

Many aspects of U chemistry in the environment involve the transport of U, whether it is at the molecular scale, across cell membranes, or at the aquifer scale. Many of the same principles apply at these different scales: transport can be either by movement along electrochemical gradients as with diffusion, or be carried by convection along pressure gradients following the mass flow of water. Diffusive transport can even be important in aquifers, for example, by transferring solutes between fissures and pores.

Convective transport of solutes is controlled by the amount of time the solute spends in the water flow rather than adsorbed to a stationary particle surface or precipitated as a mineral. The solid/solution partition coefficient, K_d , determines the former and the mineral solubility the latter. This is why the chemical speciation outlined above is important. A recurring theme from both field observations and laboratory experiments is the important role of U(IV) to U(VI) oxidation combined with carbonate complexation in mobilizing U. Hostetler and Garrels (1962) were the first to appreciate the importance of U–CO₃ species in U transport in aquifers. These species are now known to be primarily either U–CO₃ or U–Ca/Mg–CO₃ complexes (Section 7.4). The buildup of dissolved carbonate is therefore a key process. This is controlled by microbial activity in the soil followed by weathering reactions and evaporation. Carbonate concentrations are usually measured in groundwaters by acid titration and recorded as the alkalinity. In alkaline

groundwaters, the alkalinity is made up primarily of the bicarbonate ion (HCO_3^-) with a small amount of carbonate (CO_3^{2-}) at high pH plus a minor contribution from other weak acids including borate, phosphate and DOM.

The overall role that these reactions play in controlling U transport can be seen through their effect on the uranyl activity in solution and the K_d in a system with a U-adsorbing solid. This is demonstrated in Fig. 13 which shows the impact of changing the total alkalinity and pH in a simple U–NaCl–Ca–Fhy system on uranyl activity and the K_d . The uranyl activity is reduced by many orders of magnitude by the complexation (Fig. 13(a)). Even at pH 8 and a typical groundwater alkalinity of $10^{-2.5}$ eq/kg water (3.1 meq/L or ca. 180 mg HCO_3^- /L), the uranyl activity is approximately 10^{-15} for a total U concentration of 10^{-6} mol/kg water, or a decrease by about a factor of 10^{-9} . It steadily decreases even further with both increasing pH and alkalinity. This impacts on the sorption of U as seen in the variation of the K_d (Fig. 13(b)) which shows the K_d varying by 5 orders of magnitude. This varies in a more complex way than the uranyl activity since ternary Fhy–U–CO₃ surface complexes are formed. The transformation from a strongly sorbed, immobile species at low pH and low alkalinity to a weakly sorbed and mobile species at high pH and high alkalinity is clear.

Sorption is at a maximum between pH 6 and 8 with $\log K_d$ values of 6–7, signifying very strong sorption, similar to that obtained with synthetic amidoxime-based polymers (Aguila et al., 2019; Sun et al., 2018). Estimates of $\log K_d$'s for montmorillonite are also maximal (5.1) near pH 7, dropping to about 4.1 at pH 10 and in the absence of CO₂ (Zhang et al., 2018).

Laboratory measurements of the $\log K_d$ for γ -alumina ($131 \text{ m}^2/\text{g}$) are more than two orders of magnitude lower (ca. 1.6 at pH 4.45) (Guo et al., 2009). The $\log K_d$ of soils reflects their constituent components. In one study, the $\log K_d$ of organic soils was the highest (3.1), loams intermediate (2.5) and sands (2.1) and clays (1.1) the lowest (Vandenhove et al., 2009), generally following the trend noted by Sheppard et al. (2006). Measured $\log K_d$'s for a range of uncontaminated freshwater sediments showed a maximum $\log K_d$ in the range 3.0–4.2 at pH 6–7 with a significant reduction at higher pH (Crawford et al., 2017). Another study of 25 sandy sediments from Virginia, USA, showed that $\log K_d$ varied from 0.5 to 2.9 with an increase of roughly 0.47 per pH unit (Rosentreter et al., 1998). These partition coefficients show that the movement of U in soils and sediments is normally several orders of magnitude slower than that of the mass flow of water.

Transport experiments at laboratory or field scale can be used to infer interaction factors such as the K_d and reaction kinetics (Avasarala et al.,

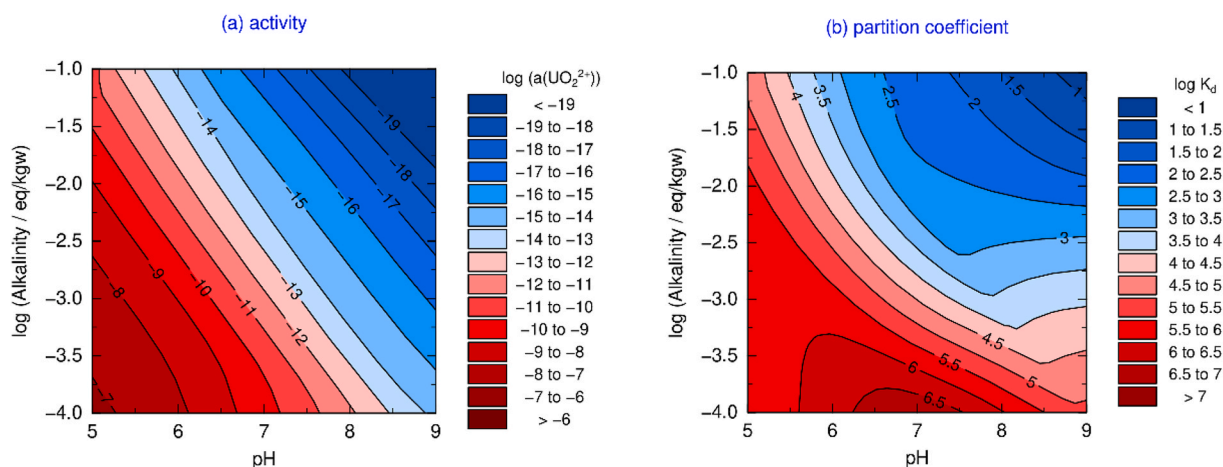


Fig. 13. (a) Variation in $\log(UO_2^{2+})$ activity as a function of pH and total alkalinity (initial solution = 1 μM U, 2 mM NaCl, 2 mM $CaCl_2$; alkalinity adjusted with Na_2CO_3 , pH adjusted with NaOH); (b) variation in $\log K_d$ for the sorption of U by 1 g/L ferrihydrite (Fhy) as a function of pH and alkalinity with the initial solution the same as in (a); units for the partition coefficient, K_d , are kg water/kg Fhy; PRODATA database with sorption modelling using the CD-MUSIC model and parameters from Hiemstra et al. (2009).

2017; Curtis et al., 2006; Dangelmayr et al., 2017, 2018; Hou et al., 2021; Mehta et al., 2015; Nitzsche and Merkel, 1999). Although transport in aquifers is generally slow, and over long timescales, it can separate elements as in a chromatography column. Ultimately, this can lead to ore bodies such as roll fronts (Section 5.1, 8.1). The transport of U away from contaminated sites and potential waste repositories is also of great interest and many studies have been undertaken to try to predict the magnitude of this movement (Avasarala et al., 2017; Hennig et al., 2020; Seigneur et al., 2021) and to devise approaches to minimize it, such as permeable reactive barriers (Henderson and Demond, 2007). The transport of U at many contaminated sites, e.g. Hanford, USA have been studied extensively (Section 8.6).

In the application of ISL, transport of U needs to be maximized (Abzalov, 2012) (Section 5.1). Chemical speciation plays an important role here too. Acid leaching (H_2SO_4) used in sandstone formations with a low carbonate content involves the injection of native groundwater mixed with a substantial quantity of acid into the host formation, potentially with addition of an oxidant (e.g. $\text{O}_2(\text{g})$ or H_2O_2). This promotes the dissolution of U minerals such as pitchblende and coffinite. Strong complexes are formed with SO_4 which reduce U sorption and so increase transport to the collector sites. Where carbonates are present, the acid required would be excessive and an alkaline (Na_2CO_3) leach solution can be used. Here, the high pH and large concentration of dissolved CO_3^{2-} aids transport by minimizing sorption. These conditions also reduce the undesired dissolution of gangue minerals. Various reactive-transport models have been used to analyse these processes and to aid the planning of post-mining restoration when the transport must be reduced (Lagneau et al., 2019).

7.10.2. Colloid-facilitated transport

The role of colloids in facilitating the transport of U and other highly insoluble radionuclides has long been a major concern for regulatory agencies responsible for the containment of sites contaminated with radioelements. This was highlighted by a study of Pu migration from the underground nuclear test site in Nevada. This showed that low levels of Pu had migrated 1.3 km downgradient from the test site over about 40 years when conventional wisdom suggested that dissolved Pu concentrations were too low to account for this (Kersting et al., 1999). In this case, various mineral colloids were implicated, but organic 'colloids' are also of concern. Transport of actinides associated with colloids has also been implicated at the Savannah River nuclear materials processing site in South Carolina, USA (Kaplan et al., 1994).

Simply having colloids transported in the groundwater flow is not sufficient to ensure enhanced transport since if equilibrium with the surrounding environment is maintained, the excess U will eventually be stripped from any U-laden colloid. This has been demonstrated in laboratory column experiments with Am-laden bentonite colloids (Dittrich et al., 2015). The extent of any facilitated transport will depend on many factors including the strength of binding, the ratio of mobile/immobile binding capacity (Crançon and Van der Lee, 2003; Emerson et al., 2016; Kretzschmar et al., 1999; Mibus et al., 2007) and the kinetics and reversibility of the binding (Yang et al., 2013). There can also be physical factors at play such as fracture flow, particle filtration, colloid stability, and in the unsaturated zone, attachment to the air-water interface (Flury and Qiu, 2008).

8. Case studies: areas with high aqueous uranium concentrations

8.1. Roll fronts: Wyoming basins, USA

Intermontane basins of Wyoming, Colorado and Nebraska, USA, range in size up to several thousand square kilometres and contain continental sediments of Cenozoic to Quaternary age (Dahlkamp, 2010). The basins host a number of economic-grade U roll-front deposits and the Great Divide Basin in Wyoming also hosts tabular U deposits. The

deposits lend themselves to U extraction by ISL (ISR) and five ISL plants operated across the region until recent closures. The U deposits are aligned parallel to the groundwater flow direction, though may crosscut bedding; original U sources in the commonly arkosic sandstone are inferred to be proximal or parental granitic and rhyolitic volcanic rocks (Bullock and Parnell, 2017; Dahlkamp, 2010; Seeland, 1976; Wolde-Gabriel et al., 2014).

The mineralogy of the roll fronts characteristically changes downgradient, with partial or complete destruction of pyrite and magnetite and smaller contents of organic matter and calcite in the upgradient oxidized zone. Downgradient of the roll front, two generations of pyrite commonly exist, comprising a diagenetic form derived from biogenic reactions, and pyrite in the mineralized zones related to ore formation. The U occurs typically as coffinite and pitchblende, along with less common coconinoite, tyuyamunite, torbernite and autunite (Table 4). A biogenic, non-crystalline form of U(IV) has also been identified (Bhat-tacharyya et al., 2017). Uranium minerals occur as grain coatings, interstitial infills and replacements of organic carbon. Other trace elements can also occur, for example, native selenium or ferroselite on the concave upgradient side of the roll front, and molybdenite on the convex downgradient side (Dahlkamp, 2010).

The Smith Ranch-Highland plant in the southern Powder River Basin of eastern Wyoming is a former ISL U plant and mine complex, which when active constituted the largest U facility in the USA. The site consists of two mines which were operated together, and a single processing plant. Ore grades at the complex are about 0.10% U_3O_8 (Cameco, 2021). The method of U extraction involved pumping groundwater into the aquifer with addition of O_2 and Na-HCO_3 or H_2SO_4 and pumping dissolved U back to the surface for processing into yellowcake (U oxide) (Dangelmayr et al., 2017). The operator suspended operations at the Smith Ranch plant in 2018, citing mainly market conditions (Cameco, 2021). Current activities at the complex are focused on site restoration (Dangelmayr et al., 2017).

The roll-front U deposits at the Smith Ranch site (Fig. 14) occur in fluvial sandstones of the Paleocene Fort Union Formation and sandstones of the Eocene Wasatch Formation (Seeland, 1976). The sandstone units are rich in organic carbon and pyrite and are intercalated with fluvial or lacustrine silt, clay and coal deposits (Dahlkamp, 2010). The Powder River Basin is bordered to the south by the Laramie Mountains, to the west by the Big Horn Mountains and to the east by the Black Hills. Basal Palaeocene deposits are dominantly argillaceous but later Palaeocene deposits include intercalations of arkosic sandstone derived from erosion of the crystalline rocks of the Laramie range. Subsidence during the late Palaeocene to early Eocene resulted in deposition of fluvial deposits, and swamps produced coal deposits. The Eocene Wasatch Formation shows sedimentary cycles alternating from coarse fluvial sandstone to finer deposits (Seeland, 1976).

The sandstone deposits of the Smith Ranch-Highland complex dip gently eastwards ($<0.5^\circ$) with eastwards groundwater flow (Brown et al., 2016). The U mineral accumulation at the redox front (up to 25,000 mg/kg) (WoldeGabriel et al., 2014) is of the order of 2–8 m wide in an arcuate form in cross section, over a depth range of 61–366 m (4 km² study area).

Groundwater samples upgradient of the redox front were reported to have U concentrations of 11–16 $\mu\text{g/L}$ and of 5–17 $\mu\text{g/L}$, mostly $<10 \mu\text{g/L}$, downgradient. Concentrations at the roll front mineralized zone were 13,000–40,000 $\mu\text{g/L}$. The higher concentrations in the ore zone were taken to be due to residual oxidation and complexation of U with CO_3 (Brown et al., 2016).

Brown et al. (2016) investigated the U isotopic compositions of groundwater across the redox front at the Smith Ranch site and noted a 3‰ drop in the $^{238}\text{U}/^{235}\text{U}$ ratio ($\delta^{238}\text{U} -0.88$ to -1.08‰ upgradient, -0.41 to -0.15‰ in the ore zone and -1.5 to -2.8‰ downgradient), corresponding with the decrease in U concentration beyond the front. Activity ratios of $^{234}\text{U}/^{238}\text{U}$ were 5.12–5.61 in the upgradient oxic zone and taken to be controlled by the balance between ^{234}U release by alpha

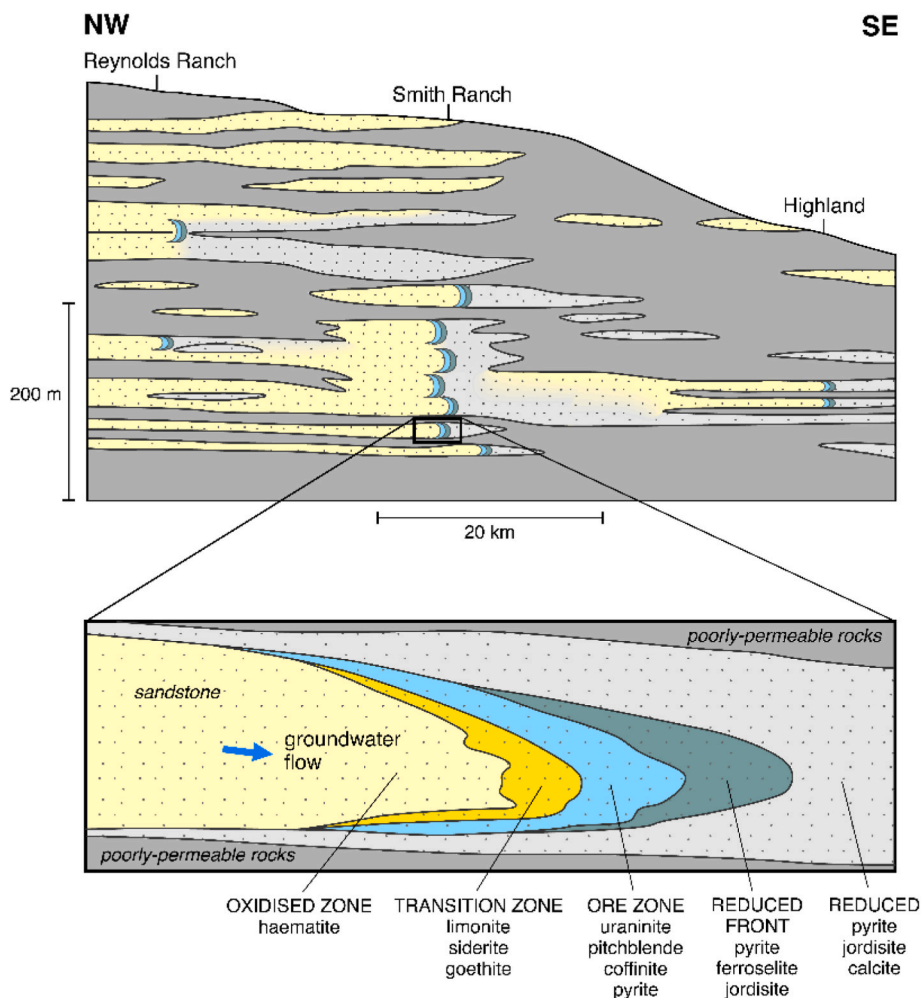


Fig. 14. Schematic diagram of the Smith Ranch-Highland roll-front uranium deposit, eastern Wyoming, USA; adapted with permission from Brown et al. (2016), ©2016 American Chemical Society.

recoil and U release by silicate weathering. Ratios were around 1.0 in the ore zone, and between 2.3 and 3.7 further downgradient. The variation in U isotopic ratios across the roll front was inferred to be indicative of reduction of U(VI) to U(IV), either enzymatically by microbes or in combination with an abiotic reduction process (Brown et al., 2016). Distributions of other analytes, including dissolved Fe and SO_4 , supported the evidence for redox reactions across the roll front. The authors used the spatial distributions of the changing $^{234}\text{U}/^{238}\text{U}$ ratio to estimate the degree to which U is transported downgradient of the ore body.

8.2. Koongarra uranium deposit, Alligator Rivers project, Australia

Uranium deposits of the Alligator Rivers field of Northern Territory, Australia, some 220 km east of Darwin, are of unconformity-type. The field is highly prospective and includes the Ranger, Koongarra, Jabiluka and Nabarlek U deposits (Raffensperger and Garven, 1995). At all sites where previous mining took place, activities have now ceased, though some rehabilitation works remain. The Koongarra deposit has a U_3O_8 grade of 0.8%. It is perhaps the most studied U deposit in the region, having been adopted especially during the 1980s and 1990s as a natural analogue site for assessing the safety of radioactive waste disposal (Payne and Airey, 2006). Koongarra was never mined and in 2013, protection of the site was secured when it became part of the Kakadu National Park World Heritage area.

The unconformity at Koongarra separates steeply-dipping early Proterozoic metasediments of the Cahill Formation from middle

Proterozoic sediments of the Kombolgie Formation (Fig. 15). The Cahill Formation itself overlies Archaean granite and granite-gneiss (Komninou and Sverjensky, 1995). The Cahill Formation is composed of brecciated amphibolite facies metasediments, including a lower carbonaceous partly graphitic schist, passing upwards into feldspathic schist. The overlying Kombolgie Formation consists of terrestrial sandstone and conglomerate deposits, including some evaporite, with interbedded volcanic rocks. The mineralization age is inferred as around 1.6 Ga, shortly after the deposition of the Kombolgie Formation (Komninou and Sverjensky, 1995; Maas, 1989). Formation of the U deposits is likely to have involved reaction of hot, oxidizing, U-bearing fluids from the Kombolgie Formation with reducing metasediments of the Cahill Formation (Maas, 1989).

Pre-ore hydrothermal alteration of the type observed in the Koongarra unconformity-related U deposit is demonstrated by chloritization of metamorphic minerals (Komninou and Sverjensky, 1995). Syn-ore mineralization involved subsequent more intense alteration around breccia zones, veins and the unconformity itself. This involved formation of chlorite, hematite and phengitic white mica, along with uraninite (Maas, 1989).

Primary uraninite ore occurs as lenses below the weathered zone at around 25–30 m depth to around 100 m depth (Fig. 15). Secondary U minerals occur in a 'dispersion fan' as a result of oxidation of the primary uraninite and mobilization probably as U(VI)-carbonate complexes, before redeposition in the fan as uranyl adsorbed to iron oxides, clays and possibly Al oxides, and subsequently as uranyl phosphates (Payne

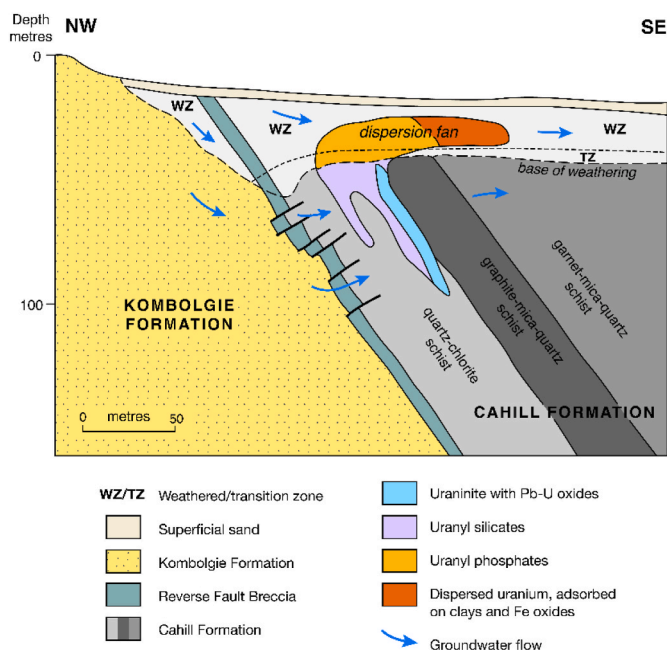


Fig. 15. Koongarra deposit, adapted from Payne and Airey (2006), ©2006 with permission from Elsevier.

and Airey, 2006; Yanase et al., 1991). The age of the secondary deposits in the fan has been placed around 1–1.5 Ma (Payne and Airey, 2006).

Saléite ($Mg(UO_2)_2(PO_4)_2 \cdot 10H_2O$) is the dominant secondary mineral in the upgradient oxalic section of the Koongarra deposit, where it replaces the secondary mineral sklodowskite ($Mg(UO_2)_2(SiO_3OH)_2 \cdot 6H_2O$) and apatite. Within and downgradient of the deposit, saléite and metatorbernite ($Cu(UO_2PO_4)_2 \cdot 8H_2O$) occur as microcrystals in veins of hematite and goethite (Murakami et al., 1997, 2005). The microcrystals likely originate from U and PO_4 released from ferrihydrite on aging (Murakami et al., 1997).

EXAFS investigations of uranyl sorption onto ferrihydrite from Koongarra showed uranyl occurred as a mononuclear bidentate surface complex. Best-fit modelling required a ternary uranyl-carbonate on both weak and strong surface sites (Waite et al., 1994). More crystalline oxides (goethite, hematite) showed decreased U affinity compared to ferrihydrite although some U is likely transformed into the crystalline phases during the aging process (Ohnuki et al., 1997).

Uranium concentrations across the ore body vary from $<1 \mu\text{g/L}$ in groundwater from the Komolgie Formation upstream, to $440 \mu\text{g/L}$ in the central part of the ore body, to $<1 \mu\text{g/L}$ some 200 m downstream (Fig. 16) (Payne, 1991). $^{234}\text{U}/^{238}\text{U}$ activity ratios in easily extractable secondary phases (Fe oxides, clays) from the Koongarra deposit were below 1.0 in the shallow ($<20 \text{ m}$) weathered zone and were similar to values in the circulating shallow groundwaters (Fig. 16). By contrast, activity ratios in resistate minerals (quartz) were above 1.0, as were many of the deeper groundwaters ($>30 \text{ m}$) (Payne and Airey, 2006; Yanase et al., 1995). The reasons for the variation and secular disequilibrium are unclear, but values greater than 1.0 in groundwater have been variously attributed to damage to the mineral structure, location of daughter atoms on weakly bound sites, oxidation of U(IV) to U(VI) during alpha decay resulting in enhanced mobility, or alpha recoil (Payne and Airey, 2006; Yanase et al., 1995).

The low $^{234}\text{U}/^{238}\text{U}$ activity ratios (<1.0) in the shallow groundwaters have been inferred as possibly favoured in unsaturated conditions, where daughter ^{234}U is thought more likely to vacate the pore space and enter into a mineral (Yanase et al., 1995). An alternative explanation for the low ratios is sorption of short-lived daughter ^{234}Th to clay or ferrihydrite, with subsequent fixation to the mineral on decay to ^{234}U . The low activity ratio from the deeper groundwater from borehole PH88 may be due to localized more deep weathering (Fig. 16) (Yanase et al., 1995).

8.3. Natural nuclear fission: Oklo, Okélobondo and Bangombé, Gabon

The Oklo, Okélobondo and Bangombé group of U deposits in the Republic of Gabon, West Africa, are the only known examples of natural nuclear fission. At the sites, uraninite ore occurs as discrete lenses within

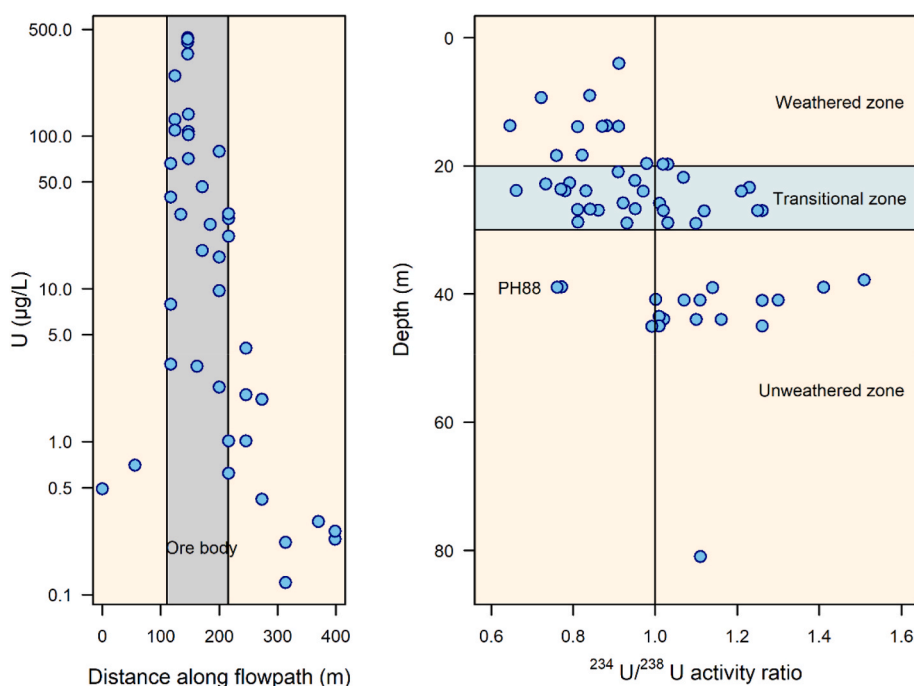


Fig. 16. Uranium concentrations in groundwater along the flow path across the Koongarra uranium ore body; data from Payne (1991); and activity ratio of $^{234}\text{U}/^{238}\text{U}$ against depth for groundwater from the Koongarra uranium deposit; samples from PH88 described in the text; after Yanase et al. (1995).

Lower Proterozoic (2.3 Ga) sandstone. Aged around 2 Ga, these are the earliest redox-controlled sandstone-hosted deposits in the world (Cuney, 2010). Known as natural reactors, the ore deposits have anomalously low ²³⁵U activities (0.62% compared to natural 0.72%) and the isotopic ratios of some other elements are also perturbed (Miller et al., 2000). Before 2 Ga, natural U would have had a larger abundance of ²³⁵U, around 3.7%. The deposits post-date the GOE (around 2.4 Ga) when surface conditions on earth became gradually more oxidizing (Andersen et al., 2017) and where U was mobilized and redistributed. This allowed greater concentrations to accumulate (up to 60% U) on reduction and redeposition in organic-rich sediments higher in the rock strata (Miller et al., 2000). Accumulation of U was sufficient to achieve radioactive criticality (sufficient critical mass that each fission releases sufficient neutrons to sustain ongoing nuclear reactions) and over the following hundreds of thousands of years, host rocks were then subjected to fission as well as radioactive decay. Natural radioactive decay reduced the ²³⁵U to <3% of the total by 1.7 Ga, and conditions for natural fission have not existed on earth since then.

The ore bodies consist of a central core of uraninite and outer aureole of uraninite, coffinite and pitchblende. The heat of nuclear reactions led to hydrothermal alteration with the formation of outer zones enriched in illite and chlorite. Temperatures would have been up to 600 °C and pressures up to 30–40 MPa (Miller et al., 2000). Criticality stopped when ²³⁵U eventually diminished. Over the long time period since then, most transuranic fission products have decayed to small amounts. Radioactive daughters such as plutonium remain immobilized at the locations.

The Okélobondo uraninite deposit occurs at about 300 m depth.

Groundwater at this depth is oxic and alkaline (pH 7.0–8.5) and U concentrations are reported in the range 0.32–332 µg/L. Shallow groundwater at the site has lower concentrations as it occurs in association with black shale and is more reducing (Salas and Ayora, 2004). The Oklo mine complex closed in the 1990s and is now flooded.

8.4. La Pampa quaternary loess aquifer, Argentina

Groundwater from the semi-arid northern La Pampa Province of central Argentina has neutral to alkaline pH, is overwhelmingly oxic, is mainly of Na–HCO₃ or Na-mixed-anion composition, and commonly contains high concentrations of U (up to 250 µg/L), along with high alkalinity (up to 1440 mg/L as HCO₃), variable but often high salinity (SEC up to 17.5 mS/cm) and with high concentrations of a number of dissolved anion and oxyanion species (e.g. F up to 29 mg/L, V up to 5.4 mg/L, As up to 5300 µg/L, Mo up to 990 µg/L). The groundwater is hosted by a Quaternary loess aquifer which is dominated by silt and fine sand and which contains a component of Andean rhyolitic volcanic ash as disseminated or thin discrete layers. The loess deposits also contain secondary calcium carbonate as calcrite layers, nodules or cements (Smedley et al., 2002). High groundwater alkalinity is inferred to be due to silicate hydrolysis (weathering) reactions with carbonate equilibrium and likely some ion exchange. High concentrations of U as well as As, V and F are related to the oxic and alkaline conditions, sources including volcanic ash, and poor sorption of these elements to metal oxides in the loess deposits (Smedley et al., 2002, 2005).

Uranium concentrations in the groundwater show poor correlations

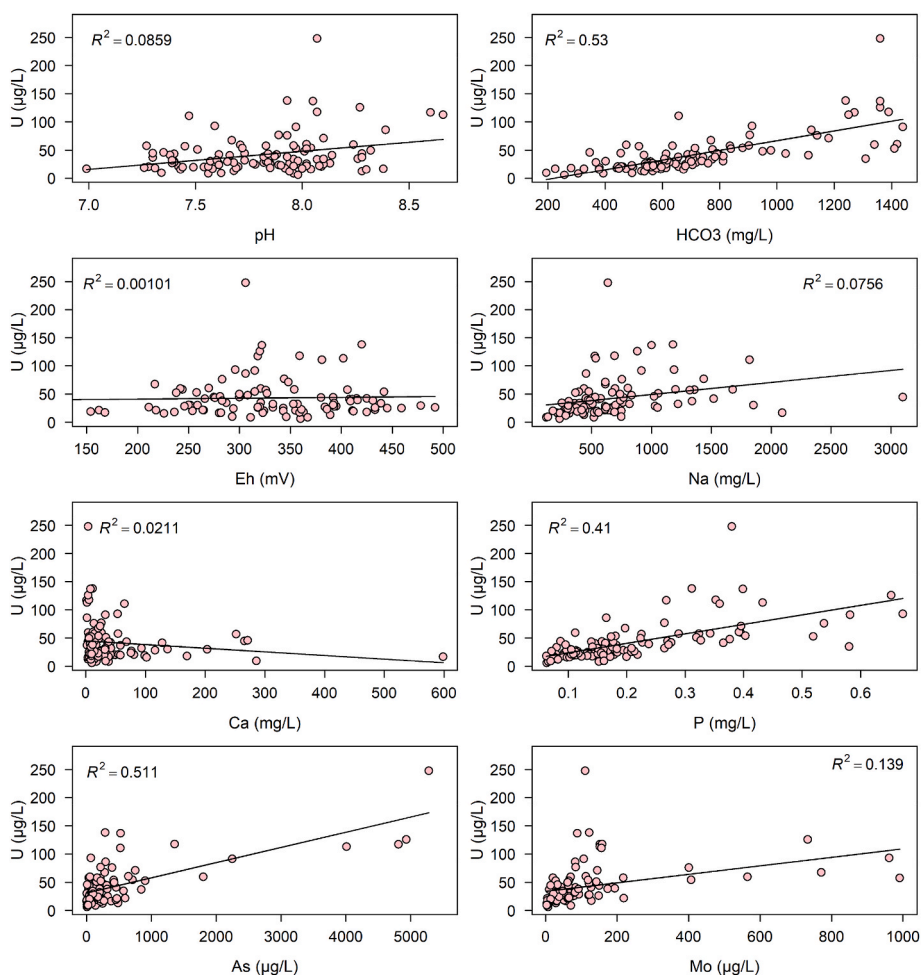


Fig. 17. Relationship between dissolved uranium and selected analytes in groundwaters from La Pampa, Argentina; regression lines and R² also shown (data from Smedley et al., 2002).

with pH, Eh and salinity (e.g. Na) (Fig. 17), but better positive correlations with alkalinity (HCO_3^-), P, As and Mo. The relationship with Ca is weak and if anything negative. Modelling (PHREEQC with the PRODATA database and Davies activity model) suggests that dissolved U is present in the groundwaters predominantly as $\text{UO}_2(\text{CO}_3)_3^{4-}$ species, although the few samples at the low end of the pH range are dominated by $\text{UO}_2(\text{HPO}_4)_2^{2-}$. Model results do not find predominant Ca(Mg) ternary complexes.

La Pampa Province forms part of the Chaco-Pampean Plain, a vast 1 million km^2 area of Argentina with similar superficial geology and hydrogeochemical features. Groundwater As problems in the region are well-documented (Martinez and Carrillo-Rivera, 2006; Nicolli et al., 2012b, Nicolli et al., 1989). Associated high concentrations of U are often also recorded but with much less emphasis on studying their distributions and controls.

8.5. Platte River Valley, Nebraska, USA

Relatively high concentrations of U in the Platte River system of Nebraska, Colorado and Wyoming (average 24 $\mu\text{g/L}$) are attributed to weathering of U-rich rocks in the Front Range and Laramie Mountains (Snow and Spalding, 1994). Samples of river water collected at different times under different rainfall conditions along the stretch have a concentration range of 0.27–31.7 $\mu\text{g/L}$ and $^{234}\text{U}/^{238}\text{U}$ activity ratios showing varying degrees of disequilibrium from 1.03 to 1.72. Both concentrations and ratios were generally higher under low-flow (base-flow) conditions. From one round of sampling, Snow and Spalding (1994) found concentrations of U of 22.8 and 31.7 $\mu\text{g/L}$ in the North and South Platte Rivers respectively, decreasing downstream beyond the confluence along the Platte River, a distance of some 600 km.

Groundwater from private wells in the Platte River valley of Nebraska had groundwater U concentrations in the range 0.3–99.3 $\mu\text{g/L}$, though concentrations up to 550 $\mu\text{g/L}$ have been reported for the valley alluvium (Snow and Spalding, 1994). Wells close to the Platte River system derive a contribution of their U from river water via irrigation. At times of low river flow, the alluvial aquifer returns U-bearing irrigation water back to the river forming a semi-closed loop. The contribution of U from phosphate fertilizers is thought to be negligible (Snow and Spalding, 1994).

A range of chemical and isotopic tools used to investigate groundwaters from the alluvial aquifer of the North Platte River valley (Dutch

Flats area) also pointed to a significant influence of surface-water irrigation on groundwater compositions (Böhlke et al., 2007). Uranium concentrations in the groundwater were 9.52–19.0 $\mu\text{g/L}$ and $^{234}\text{U}/^{238}\text{U}$ activity ratios 1.4–1.8. Each was similar to river water and local canal water compositions. Enriched ^{234}U indicating disequilibrium conditions, suggested a U origin from mineral reactions rather than phosphate fertilizer, which might have contributed a ratio closer to equilibrium (Zielinski et al., 1997). Böhlke et al. (2007) concluded that large quantities of U with low $^{234}\text{U}/^{238}\text{U}$ ratios (1.4–1.8) were present in the alluvial aquifer as a result of irrigation with U-bearing river water, alongside smaller amounts of U with higher $^{234}\text{U}/^{238}\text{U}$ activity ratios (closer to 2), contributed from underlying volcanic-rich and alluvial sediments.

The high U uranium concentrations in groundwater and the effects of recycling of irrigation flows in the Platte River valley of Colorado, Wyoming and Nebraska are easily picked out as the east-west-trending line ($\text{U} > 30 \mu\text{g/L}$) on the USGS U map produced from the NAWQA data sets (Ayotte et al., 2011) (Fig. 18).

8.6. Hanford Department of Energy nuclear site, USA

The DOE Hanford nuclear site, Washington, USA, hosts some 210 million litres of hazardous nuclear waste, the largest such site in the world. The waste was produced as a result of weapons processing for World War II and the Cold War over the period 1943–1989 (Reynolds et al., 2018; Um et al., 2009); U forms a substantial component of the waste. The 1500 km^2 site consists of distinct areas which hosted different processing activities and had differing waste streams (McKinley et al., 2007). In the 200 Area in the central part of the site, U-bearing alkaline (pH around 10) liquid waste and sludge has been stored in 177 underground tanks, several of which have leaked over the lifetime of the operations (Christensen et al., 2010; Zachara et al., 2013). In the 300 Area to the south of the site, both strongly alkaline (sodium aluminate) and acidic (copper uranyl nitrate) solutions were released to surface process ponds, which over their lifetime had pH values ranging between 1.8 and 11.4, leaching from which also contributed to the site groundwater and river water contamination plume (Stubbs et al., 2009; Zachara et al., 2013). Restoration works have been ongoing since production ceased, including pre-2004 removal of a surface layer of heavily contaminated sediment at 300 Area to reduce contaminant loads to groundwater.

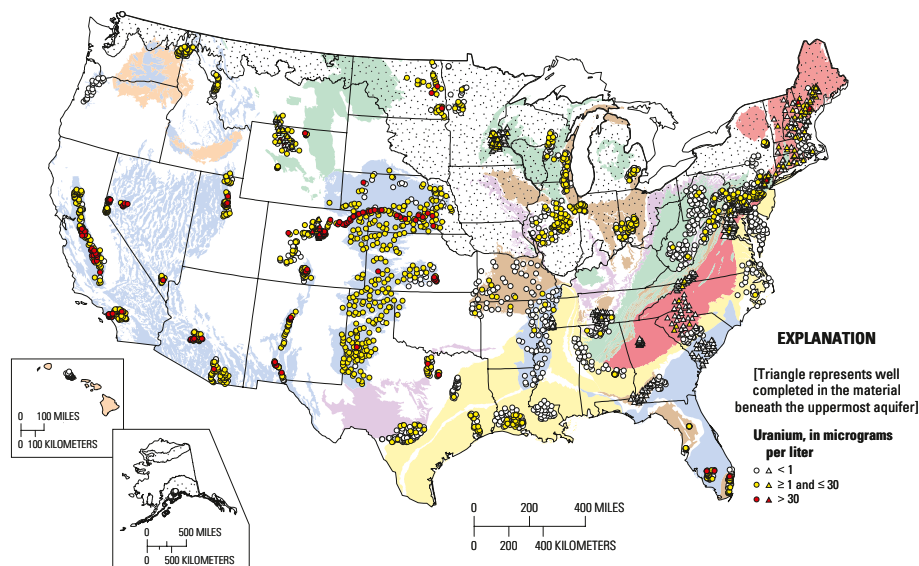


Fig. 18. Uranium in groundwater from the USGS's National Water Quality Assessment Program (NAWQA) (1992–2003). Colour washes denote principal aquifers and stipple denotes distribution of glacial unconsolidated sand and gravel aquifers (from Ayotte et al., 2011), with permission; also available at <http://pubs.usgs.gov/sir/2011/5059>).

The Hanford site sits on the floodplain of the Columbia River and is underlain by Pleistocene fluvio-glacial sands and gravels and Pliocene fluvio-lacustrine deposits, above Miocene Columbia River Basalt (Gartman et al., 2015; McKinley et al., 2007). The Pleistocene sediments form an unconfined aquifer and host the U contaminant plume. The 200 Area has a thick unsaturated zone with groundwater level about 60–80 m below surface; the 300 Area is proximal to the Columbia River with a thinner unsaturated zone.

The mineral associations of the contaminant U vary spatially. In the 300 Area, contaminated surface sediments that had been removed as part of site remediation contained U coprecipitated with calcite. Remaining underlying sediments contain metatorbernite, cuprosklovdowskite ($\text{Cu}(\text{UO}_2)_2(\text{SiO}_4)(\text{H}_3\text{O})_2 \cdot 2\text{H}_2\text{O}$), and U adsorbed to phyllosilicates including chlorite and metal oxides (Catalano et al., 2006; Stubbs et al., 2009). In the 200 East tank farm Area, secondary boltwoodite and uranophane have been found at 15–16 m depth, adsorbed U(VI) phases and polynuclear U(VI) surface precipitates at 20–25 m depth, with only natural U in granite lithic fragments present within the sediment at >28 m depth. Adsorbed forms were found to be more mobile than these mineral hosts (McKinley et al., 2006; Um et al., 2009).

Hanford shallow groundwater is oxic and dissolved U is present as U(VI). Concentrations around 18–205 mg/L have been recorded in the 300 Area with HCO_3^- of 150–230 mg/L, SEC up to 500 $\mu\text{S}/\text{cm}$ and pH of 7.1–8.7 (Zachara et al., 2013). Uranium concentrations up to 524 $\mu\text{g}/\text{L}$ were reported from the site by Dresel et al. (2002). Aqueous species are dominated by $\text{UO}_2(\text{CO}_3)_3^{4-}$ with a smaller proportion of $\text{Ca}_2\text{UO}_2(\text{CO}_3)_3$ (Wang et al., 2004). Groundwater U concentration increases with spring recharge as the water level rises and U is mobilized from the contaminated lower unsaturated zone beneath surface sites. Slow site remediation has been attributed to slow desorption of U held within micropores and grain fractures in the aquifer sediments and diffusive release to groundwater (Zachara et al., 2013). Desorption is also dependent on the aqueous HCO_3^- concentration and pH which vary according to the extent of groundwater-river interaction (Um et al., 2007). Small mass loss of U(VI) to the Columbia River is also noted as a factor. This has been attributed to the complex topography of the Pleistocene base of the aquifer, restricting flow to the river, and complex changes in river-groundwater flow directions in response to river stage (Zachara et al., 2013). Diverse mineral associations with differing U(VI) solubilities also play a large role in prolonging U release to aqueous solution and removal from the system.

9. High-uranium groundwater provinces

The above accounts of U occurrence in water and the environment demonstrate the predominant controls on its speciation and mobility. While some natural high-U occurrences clearly exist in all water types, they are uncommon in surface waters and generally restricted to areas of U mineralization and alkaline lakes. They also have limited concentrations in marine water. Uranium concentrations appreciably above the WHO provisional guideline value of 30 $\mu\text{g}/\text{L}$ are also unusual in groundwater as U(VI) is readily sorbed to metal oxides, clays and NOM and U(IV) is also strongly immobilized by reduction with precipitation or sorption. However, a large and growing number of documented occurrences indicate the types of environment where high dissolved U concentrations are most likely to occur. These natural occurrences and their dominant features are outlined below; occurrences with an anthropogenic control (nuclear processing, munitions and other contaminated land) are not included. Factors producing current high-U groundwaters have many overlaps with the recognized processes that mobilized (and immobilized) U during the creation of ore deposits albeit with lower intensity.

9.1. Granitic and felsic volcanic aquifers

Many of the documented occurrences have been reported in

groundwater from granites, granite-gneisses and felsic volcanic rocks. These are rocks with a relatively high Si content, including an abundance of feldspars. These have relatively large U contents (up to around 70 mg/kg) compared to many other rock types (typical 1–4 mg/kg), with U residing in primary minerals such as monazite, apatite, ilmenite, magnetite and zircon, potentially micas and amphiboles, and in their alteration products including clay minerals (Section 3.1). Some contain uraninite. Documented examples of high-U groundwater from these sources include parts of peninsular India, USA, Ireland, Sweden, Finland, Burundi and South Korea (Andrews et al., 1989; Cho and Choo, 2019; Coyte et al., 2019; Gross and Brown, 2020; Lapworth et al., 2021; Linhoff et al., 2016; Papageorgiou et al., 2022; Post et al., 2017; Prat et al., 2009; Warner et al., 2011; Wathen, 1987). Alkaline rhyolites have been inferred as a source of U in groundwater from Mongolia (Linhoff et al., 2011) and rhyolitic ashes as the ultimate source in groundwater from volcanogenic sediments in Argentina and Ethiopia (Nicolli et al., 2012a; Rango et al., 2010; Smedley et al., 2002). Ultimately, granitic rocks and their volcanic equivalents are the sources of all terrestrial U.

Common features of the high-U groundwaters in such bedrock terrains are typically oxic conditions, often but not always with associated high salinity, and high alkalinity (HCO_3^-). Indeed, a positive correlation between dissolved U and HCO_3^- concentrations is one of the most commonly observed relationships (e.g. Cho and Choo, 2019; Matteoda et al., 2019; Warner et al., 2011). These oxic, alkaline waters also commonly have associated increased concentrations of other anion and oxyanion-forming species (e.g. F, As, V, Mo) (e.g. Rango et al., 2010). Increased salinity in some has been linked in part to evapotranspiration (Post et al., 2017). Although ^{222}Rn is a daughter in the ^{238}U decay chain, the correlations between dissolved U and dissolved Rn are typically poor because of the differing behaviour of the two elements, U being a reactive solute and Rn a dissolved gas.

As the mobility of U is favoured in the neutral to alkaline pH range with dissolved carbonate species exerting a strong control, e.g. as $\text{UO}_2(\text{CO}_3)_2^{2-}$, $\text{UO}_2(\text{CO}_3)_3^{4-}$ (Cumberland et al., 2016), the ability to generate alkalinity in groundwater has a bearing on dissolved U concentrations. Silicate hydrolysis induced by weathering reactions and carbonate mineral reactions in aquifers can increase alkalinity and pH, especially where throughflow is limited.

Uranium-rich groundwaters (>30 $\mu\text{g}/\text{L}$) in the granitic aquifers of Rajasthan have pH values in the range 6.7–7.7 and high HCO_3^- in the range 344–1690 mg/L (Coyte et al., 2018). The presence of Ca can also have an important influence because of the capacity to form U–Ca– CO_3 ternary complexes. These have reduced affinity for sorption to surfaces (Section 7.4). For example, the $\text{Ca}_2\text{UO}_2(\text{CO}_3)_3^0$ complex is uncharged which limits sorption (Lopez et al., 2020); other anionic ternary complexes also enhance U mobility. Groundwater sampled from granite in southern Finland with U concentrations up to 3400 $\mu\text{g}/\text{L}$ had pH values of 7.9–9.0 and HCO_3^- of 67–216 mg/L; the dominant species were $\text{Ca}_2\text{UO}_2(\text{CO}_3)_3^0$ and $\text{CaUO}_2(\text{CO}_3)_3^{2-}$ (Prat et al., 2009). In that study, the dominance of Ca-uranil-carbonate complexes was considered an important factor in reducing the U toxicity of the groundwater. Groundwaters from granite-gneiss in Karnataka, India, are calcite-saturated (pH 6.3–7.5, HCO_3^- 200–500 mg/L), with $\text{Ca}_2\text{UO}_2(\text{CO}_3)_3^0$ becoming the dominant U species (Lapworth et al., 2021). Although groundwaters in the Leinster granite of Ireland have $\text{UO}_2(\text{CO}_3)_2^{2-}$ and $\text{UO}_2(\text{CO}_3)_3^{4-}$ as the dominant species, the highest U concentrations occurred where overlain by Quaternary limestone-bearing till (pH 7–8, HCO_3^- 30–70 mg/L). Calcite was considered to be an important control on mobilization (Papageorgiou et al., 2022). Also, gneiss and schist in the Yukon, Canada, was found to contribute more Ca alongside alkalinity (pH 7.6–8.4, HCO_3^- 50–608 mg/L) to groundwater than did granite, with higher dissolved U concentrations resulting from the formation of uranyl-Ca-carbonate ternary complexes (Skierszkan et al., 2020b).

These observations contrast with those from the granite of south-west England which has groundwater with low pH (4.7–6.8) and

HCO₃ (5.6–83 mg/L) concentrations due to absence of calcite and returns some relatively low observed concentrations of U (Fig. 5).

9.2. Oxidic and sub-oxidic, neutral to alkaline groundwater in sandstone aquifers

Oxidic and neutral to alkaline conditions are also a predominant feature of high-U groundwaters from sedimentary aquifers. These are typically continental alluvial, lacustrine or aeolian silicate aquifers; many though not all are of Cenozoic or Quaternary age. Examples are seen in the Quaternary alluvial aquifers of the Indo-Gangetic Basin, India and Pakistan (Coyte et al., 2018; Sahoo et al., 2022), the Cenozoic alluvial aquifers of the High Plains, USA (Nolan and Weber, 2015), Cenozoic-Quaternary alluvial/lacustrine aquifers of Central Valley, USA (Jurgens et al., 2010), Miocene alluvial/lacustrine aquifers of Española Basin, New Mexico, USA (Linhoff et al., 2016) and the Quaternary loess Chaco-Pampean aquifer of Argentina (Smedley et al., 2002). Some are extremely well-documented (e.g. the Ganga Basin of India), others less so (e.g. Indus Basin of Pakistan). Data can be sparse even for these aquifer types in developed countries, for example data for private wells in the USA (Vengosh et al., 2022).

The ultimate sources of U in many of these sedimentary silicate aquifers are also likely to be granitic or felsic volcanic precursors, which would have formed an important component of the products of unroofing of large mountain massifs such as the Rocky Mountains which provided the sediments for the High Plains aquifer, USA, the Himalaya as the sources of the Indo-Gangetic Plain sediments of India and Pakistan and the Andes as the source of sediments and volcanic rocks of the Pampean Plain, Argentina. The high-U groundwaters typically occur in arid or semi-arid areas and some of the groundwaters have increased salinity, although many are major productive aquifers used for agriculture and many also contain high concentrations of NO₃ which is retained under the ambient oxidic conditions (e.g. Nolan and Weber, 2015).

As with the igneous aquifers, a correlation of U with HCO₃ is well-documented in these groundwaters (Alkinani et al., 2016; Jurgens et al., 2010; Linhoff et al., 2016) and mobilization of U(VI) in oxidic, alkaline conditions accounts for many of the documented occurrences (Fig. 4). Binary or ternary (with Ca) U-carbonate complexes are likely involved (e.g. Warner et al., 2011). Associations with other anion/oxo-anion species (F, As, V, Mo) are also prevalent (Linhoff et al., 2016; Nicolli et al., 2012a; Smedley et al., 2002; Welch and Lico, 1998).

Increased U concentrations have also been reported in groundwaters from such aquifers under Mn-reducing conditions. Reductive dissolution of metal oxides was inferred to explain some of the high U concentrations observed in groundwaters from the Carson Desert of Nevada, USA (Welch and Lico, 1998) where mildly reducing conditions were suggested from a number of the groundwaters having dissolved-oxygen concentrations <1 mg/L and dissolved Mn concentrations up to 4 mg/L. Increased concentrations were also found in Mn-reducing groundwaters from Germany (Riedel and Kübeck, 2018). This may involve release of U(VI), known to sorb to MnO₂ surfaces (Brennecka et al., 2011), or redox interaction between UO₂ and MnO₂ (Wang et al., 2013b).

As discussed in detail in Section 7, uranium is immobilized when reduced to U(IV), and in young alluvial aquifers, immobilization is observed under Fe- and SO₄-reducing conditions such as are observed in the lower Bengal Basin of Bangladesh, Mekong delta of Vietnam and Cambodia and Yellow River Basin of China (e.g. BGS et al., 2001; Buschmann et al., 2008; Frisbie et al., 2009; Smedley et al., 2003). These tend to be in areas with superficial deposits dominated by clay-rich alluvial overbank and deltaic deposits and where confined conditions in the underlying sands facilitate the development of strongly reducing groundwater conditions in the presence of relatively-fresh NOM.

Increased salinity in some high-U alluvial groundwaters under the arid conditions has been linked to evaporation. Examples include the

San Joaquin Valley, California and Carson Desert, Nevada (Fujii and Swain, 1995; Welch and Lico, 1998). A correlation of U(VI) with salinity would suggest either conservative behaviour of uranyl as water undergoes evaporation or increased competition for sorption sites between uranyl and other solutes (Sahoo et al., 2022).

Occurrences of high U concentrations in groundwater seem not to be a feature of limestone aquifers. While U(VI) is sequestered in calcite either in structural or adsorbed sites (Section 7.4.4), and is one mechanism for attenuating U (Nolan et al., 2021), contents are typically relatively small (Table 5). Marine carbonates precipitating from oxidic marine water in equilibrium with aqueous U–CO₃ complexes and a U concentration typically around 3 µg/L would not be expected to accumulate large U contents in the solid carbonate. Accumulations of U observed in calcretes and speleothems are of local extent and unlikely to impact on a regional groundwater scale.

9.3. Uranium-mineralized areas

Some of the best-documented groundwater U occurrences are in locations of known U mineralization. Examples include the Koongarra U deposit, Australia (Payne and thesis, 1991; Payne and Airey, 2006; Yanase et al., 1995), U deposits of the Yilgarn Craton, Australia (Noble et al., 2011), deposits of southern China (B. Zhang et al., 2020), Pinhal do Souto U mine, Portugal (Neiva et al., 2014), Smith Ranch-Highland, Wyoming, USA (Brown et al., 2016), Palmotto U deposit, Finland (Ahonen et al., 2004) and Königstein mine, Germany (Arnold et al., 2011). Case studies are also given in Section 8. Uranium concentrations in groundwater from these areas can reach extremes in the mg/L range in the vicinity of the mineralization. Mobility is enhanced under oxidic, alkaline conditions in the presence of HCO₃ but high-U zones may be local depending on changing redox conditions across a given deposit. Low U concentrations have been observed in groundwater near U deposits where secondary minerals include phosphates (e.g. autunite, Table 4) as these retain U as solid uranyl phosphate (Jerden and Sinha, 2003, 2006) even under oxidizing conditions.

Uranium ores may also be present in association with acid-generating ores such as pyrite. Examples include the Iberian Pyrite Belt of south-west Spain and Pocos de Caldas U mine, Brazil. Although U (IV) ore minerals are sparingly soluble over much of the natural range of pHs, mobilization can occur at pH < 3, which can occur in acid mine drainage. In such conditions, U may be mobilized as the free uranyl ion, UO₂²⁺; alternatively, SO₄ complexes can become important, for example UO₂SO₄ (Arnold et al., 2011) or UO₂(SO₄)₃⁴⁻ (Ladeira and Gonçalves, 2007). The mobility of U in sulphate-rich acidic conditions is also made use of in U in-situ leaching operations by the circulation of sulphuric acid. Although pyrite is ubiquitous in U mineralized areas, generation of acid drainage is dependent on the absence of substantial quantities of acid-neutralizing minerals. Acid drainage may be neutralized effectively in the presence of calcite, as occurs in the Dawson Range, Yukon, Canada (Skierszkan et al., 2021).

10. Conclusions

The fate of U in the environment is both complex and much studied. Its distribution in freshwater, seawater, minerals, rocks and soils is well-documented but its reactivity and sensitivity to environmental conditions mean that surprises can still occur. This is seen in the not infrequent discovery of U concentrations of more than 30 µg/L, the current provisional WHO guideline value, in some drinking water. Surface water can contain high U concentrations in places, but groundwater much more so. Key areas vulnerable to mobilization are: granitic and felsic volcanic rocks where U contents are relatively large (up to around 70 mg/kg compared to many other rock types with around 1–4 mg/kg U), continental sandstones, especially in alluvial plains, and U-mineralized and mined areas.

Examples from granitic and felsic volcanic terrains are documented

in peninsular India, eastern USA, Canada, South Korea, southern Finland, Norway, Switzerland and Burundi. Alluvial sediments with high-U groundwater are found in several parts of the USA, India, Pakistan, China and parts of Iraq and wind-blown loess deposits occur in the Chaco-Pampean Plain, Argentina. In these terrains, granitic and felsic volcanic precursors are often inferred as the original provenance of the mobilized U. Areas of U mineralization are also documented in parts of Australia, Brazil, Canada, China, Egypt, Germany, Portugal and USA. Many high-U groundwater provinces occur in arid and semi-arid areas where evaporation of solutes may increase U concentrations further.

The percentage exceedances of U above the WHO provisional guideline value sampled in groundwater from these areas vary significantly. For example, studies in granitic basement areas of peninsular India have shown up to 78% exceedance in Karnataka, while others showed 33% in Rajasthan and 5% in Gujarat. Around 29% were in excess in a survey from Burundi. In alluvial aquifers, exceedance statistics were around 8% in one study from the High Plains alluvial aquifer and 29% in a study from the Edwards-Trinity aquifer, USA; another showed 24% exceedance in groundwater from the Datong Basin of China. While the use of these groundwaters as sources of drinking water cannot be confirmed in all documented studies and the statistical representativeness of the survey designs cannot be verified, the figures indicate some substantial exceedances. However, even in high-U groundwater provinces, the occurrence of groundwater sources with low concentrations can still be significant. Further testing to identify safe drinking-water sources is therefore warranted. This is especially important in arid and semi-arid areas where water resources are likely to be already scarce.

The documented distributions of U in groundwater highlight not only the high-U occurrences but also the regions where little testing has taken place. Examples include parts of large alluvial plains where oxic conditions are likely to prevail (e.g. the upper portions of the Indus of Pakistan) and numerous areas of the world with recognized U mineralization (e.g. Russia, Kazakhstan and southern Africa). Many private groundwater supplies have not been tested for U, including in many developed countries (e.g. USA, Europe). Uranium is also less commonly reported in areas where concentrations are low or expected to be low.

A legacy of U-contaminated sites arises from both industrial and military uses that need to be contained and possibly decontaminated. Despite many detailed studies of such sites, there remains considerable uncertainty in how to prevent downstream contamination over the long term. Uranium solubility and transport are sensitive to its environment and responds to the key variables controlling the major-ion water quality: redox, pH, alkalinity and hardness, all factors that are difficult to manipulate on a large scale and over a long timescale.

There is also a need to dispose of, or recycle, the waste from existing and future nuclear reactors in a safe way. This has spurred the need for simple (but reliable) performance assessment models of U containment and in closed-cycle schemes to recover the most valuable elements (U and Pu). In recent years, the relatively high and constant concentration of U in seawater (3.3 µg/L) and the renewed interest in nuclear power by nations without sizeable land-based U reserves has led to interest in the possible 'mining' of U from seawater. Any expansion of the nuclear power industry will require additional safe places to dispose of the resulting waste.

These issues all require a deep understanding of U chemistry to be able to manage the resultant waste safely and to not contaminate the environment. This is reflected in the dominant role that redox reactions and complexation play. Under reducing conditions, the reduction of U (VI) to U(IV) occurs readily under conditions that are broadly similar to that of Fe reduction, and invariably results in a dramatic immobilization of U in some form of non-crystalline UO₂ solid, possibly microbially-mediated and still not that well-defined, especially in terms of its solubility.

The behaviour of U(VI) in oxidizing environments is largely determined by the 'battle of the ligands', notably the competition between

surface ligands especially of iron, aluminium and manganese oxides and humic substances, and in solution, dissolved carbonate. These reactions largely determine its solubility and whether or not it will move. Uranium is also bound strongly to humic substances but these have a 'Jekyll and Hyde' character in that they can both be soluble, and hence mobile, or insoluble and immobile, sometimes even switching between the two depending on the chemical environment.

Relatively few laboratory experiments (e.g. sorption, solubility) are carried out in a CO₂-free environment, and even fewer in a genuinely 'O₂-free' environment ($P_{O_2}(g) < 10^{-65}$ atm), even though this would often provide useful new information, albeit at the expense of added experimental complexity.

Ultimately, to be of use in making predictions about the fate of U, the controlling reactions must be incorporated into models and databases and accessed with software. Other than for the simplest reactions, such as complexation in solution and the precipitation of pure minerals, there is little agreement on the best way to do this, at least in detail. This is seen in the numerous variations in surface complexation models with their different treatments of the electrostatic interactions. Consequently, the available modelling software often fails to reflect the latest understanding and so practitioners are often deprived of the most effective tools. The interactions between mineral-NOM-U are central to many applications but are complex and need state-of-the-art experimentation and modelling to unravel. Even with the precipitation of pure U-containing minerals, of which there are many, the kinetics and other factors controlling dissolution and precipitation are often poorly understood or documented, leaving the choice of a set of the most relevant minerals as a major challenge in modelling. The factors controlling the kinetics of 'slow' reactions involving surface and mineral rearrangements are important for long-term simulations but are rather poorly understood.

In cases where drinking water contains excessive concentrations of U, complexes of U-CO₃ clearly play a major role in maintaining its mobility. These complexes are so stable that they are likely to dominate U speciation even in aqueous systems close to pH 7 and open to the atmosphere. This dominance probably reduces the chemical toxicity to microorganisms. The effect of complexation on the toxicity of U in drinking water for humans is less clear as major changes in chemical speciation occur *in vivo* (e.g. within the stomach at around pH 1.3–2.5). Nonetheless, the lack of evidence for clinical symptoms of chemical toxicity of U among communities drinking water (groundwater) at concentrations above international guidelines and limits is at once encouraging and indicative of a need for further research.

Declaration of competing interest

The authors declare that they have no known competing financial interests or personal relationships that could have appeared to influence the work reported in this paper.

Data availability

Review article - data sources cited

Acknowledgments

Acknowledgements are due to BGS library staff and the BGS and Oxford Bodleian libraries online services for provision of references. Joseph Ayotte and John Böhlke (USGS) are thanked for information on the Platte River data, USA. We also thank Energy Resources of Australia (ERA) and Geomartin for making their photographs available. The manuscript has benefited from reviews by two anonymous reviewers and by Jenny Bearcock of BGS, to whom we extend our thanks. This research did not receive any specific grant from funding agencies in the public, commercial, or not-for-profit sectors. For the purpose of open access, the author has applied a Creative Commons Attribution (CC BY) licence to this article.

References

- Abdelouas, A., Lutze, W., Gong, W., Nuttall, E.H., Strietelmeier, B.A., Travis, B.J., 2000. Biological reduction of uranium in groundwater and subsurface soil. *Sci. Tot. Environ.* 250, 21–35. [https://doi.org/10.1016/S0048-9697\(99\)00549-5](https://doi.org/10.1016/S0048-9697(99)00549-5).
- Abney, C.W., Mayes, R.T., Saito, T., Dai, S., 2017. Materials for the recovery of uranium from seawater. *Chem. Rev.* 117, 13935–14013. <https://doi.org/10.1021/acs.chemrev.7b00355>.
- Abshire, M.L., Riedinger, N., Clymer, J.M., Scott, C., Severmann, S., Romaniello, S.J., Puckette, J.O., 2022. Reconstructing the paleoceanographic and redox conditions responsible for variations in uranium content in North American Devonian black shales. *Palaeogeogr. Palaeoclimatol.* 587, 110763.
- Abzalov, M., 2012. Sandstone-hosted uranium deposits amenable for exploitation by in situ leaching technologies. *Appl. Earth Sci.* 121, 55–64.
- Adekola, F., Fedoroff, M., Geckeis, H., Kupcik, T., Lefevre, G., Lützenkirchen, J., Plaschke, M., Preocanin, T., Rabung, T., Schild, D., 2011. Characterization of acid-base properties of two gibbsite samples in the context of literature results. *J. Colloid. Interf. Sci.* 354, 306–317.
- Adithya, V., Chidambaram, S., Keesari, T., Mohokar, H., Prasanna, M., 2019. Occurrence of uranium in groundwater along the lithological contacts in central Tamilnadu, India: an isotope hydrogeochemical perspective. *Expos. Health* 11, 277–290. <https://doi.org/10.1007/s12403-017-0269-3>.
- Aeschbacher, M., Graf, C., Schwarzenbach, R.P., Sander, M., 2012. Antioxidant properties of humic substances. *Environ. Sci. Technol.* 46, 4916–4925.
- Aguila, B., Sun, Q., Cassidy, H., Abney, C., Li, B., Ma, S., 2019. Design strategies to enhance amidoxime chelators for uranium recovery. *ACS Appl. Mater. Inter.* 11, 30919–30926. <https://doi.org/10.1021/acsami.9b09532>.
- Ahmed, I.A., Hamilton-Taylor, J., Bierzo, M., Zhang, H., Davison, W., 2014. Improving and testing geochemical speciation predictions of metal ions in natural waters. *Water Res.* 67, 276–291.
- Ahonen, L., Kaija, J., Paananen, M., Ruskeeniemi, T., Hakkarainen, V., 2004. Palmottu Natural Analogue: a Summary of the Studies, Tiedonanto YST-121. Geological Survey of Finland, Espoo, Finland.
- Akram, M., Khattak, N.U., Qureshi, A.A., Iqbal, A., Tufail, M., Qureshi, I.E., 2004. Fission track estimation of uranium concentrations in drinking water from Azad Kashmir, Pakistan. *Health Physics* 86.
- Al-Attar, L., Dyer, A., 2002. Sorption behaviour of uranium on birnessite, a layered manganese oxide. *J. Mater. Chem.* 12, 1381–1386.
- Alessi, D.S., Uster, B., Veeramani, H., Suvorova, E.I., Lezama-Pacheco, J.S., Stubbs, J.E., Bargar, J.R., Bernier-Latmani, R., 2012. Quantitative separation of monomeric U(VI) from UO₂ in products of U(VI) reduction. *Environ. Sci. Technol.* 46, 6150–6157. <https://doi.org/10.1021/es204123z>.
- Alessi, D.S., Lezama-Pacheco, J.S., Janot, N., Suvorova, E.I., Cerrato, J.M., Giammar, D. E., Davis, J.A., Fox, P.M., Williams, K.H., Long, P.E., Handley, K.M., Bernier-Latmani, R., Bargar, J.R., 2014a. Speciation and reactivity of uranium products formed during *in situ* bioremediation in a shallow alluvial aquifer. *Environ. Sci. Technol.* 48, 12842–12850. <https://doi.org/10.1021/es502701u>.
- Alessi, D.S., Lezama-Pacheco, J.S., Stubbs, J.E., Janusch, M., Bargar, J.R., Persson, P., Bernier-Latmani, R., 2014b. The product of microbial uranium reduction includes multiple species with U (IV)–phosphate coordination. *Geochim. Cosmochim. Acta* 131, 115–127.
- Alexandre, P., Thomas, D., Polito, P., Marlat, J., 2007. Geochronology of unconformity-related uranium deposits in the Athabasca Basin, Saskatchewan, Canada and their integration in the evolution of the basin. *Miner. Deposita* 44, 41–59. <https://doi.org/10.1007/s00126-007-0153-3>.
- Ali, W., Aslam, M.W., Feng, C., Junaid, M., Ali, K., Li, S., Chen, Z., Yu, Z., Rasool, A., Zhang, H., 2019. Unraveling prevalence and public health risks of arsenic, uranium and co-occurring trace metals in groundwater along riverine ecosystem in Sindh and Punjab, Pakistan. *Env. Geochem. Health* 41, 2223–2238. <https://doi.org/10.1007/s10653-019-00278-7>.
- Alkinani, M., Kanoua, W., Merkel, B., 2016. Uranium in groundwater of the Al-Batin Alluvial Fan aquifer, south Iraq. *Environmental Earth Sciences* 75, 869. <https://doi.org/10.1007/s12665-016-5685-3>.
- Alloway, B.J., 2013. Uranium. In: Alloway, B.J. (Ed.), *Chapter 26 in Heavy Metals in Soils, Environmental Pollution*. Springer, Dordrecht, pp. 565–577.
- Alsemgeest, J., Auqué, L., Gimeno, M., 2021. Verification and comparison of two thermodynamic databases through conversion to PHREEQC and multicomponent geothermometrical calculations. *Geothermics* 91, 102036.
- Altschuler, Z.S., Clarke Jr., R.S., Young, E.J., 1957. The Geochemistry of Uranium in Apatite and Phosphorite (Report No. 701), Trace Elements Investigations. <https://doi.org/10.3133/tei701>.
- Alwan, A.K., Williams, P.A., 1980. The aqueous chemistry of uranium minerals. Part 2. Minerals of the liebigite group. *Mineralogical Magazine* 43, 665–667.
- AMPHOS21, 2011. MCFpreeqc: a Tool for PHREEQC Monte-Carlo Simulations.
- Andersen, M.B., Stirling, C.H., Weyer, S., 2017. Uranium isotope fractionation. *Rev. Min. Geochem.* 82, 799–850.
- Anderson, R.F., 1987. Redox behavior of uranium in an anoxic marine basin. *Uranium* 3, 145–164.
- Anderson, R.F., Fleisher, M.Q., LeHuray, A.P., 1989. Concentration, oxidation state, and particulate flux of uranium in the Black Sea. *Geochim. Cosmochim. Acta* 53, 2215–2224. [https://doi.org/10.1016/0016-7037\(89\)90345-1](https://doi.org/10.1016/0016-7037(89)90345-1).
- Anderson, R.T., Vrionis, H.A., Ortiz-Bernad, I., Resch, C.T., Long, P.E., Dayvault, R., Karp, K., Marutzky, S., Metzler, D.R., Peacock, A., White, D.C., Lowe, M., Lovley, D. R., 2003. Stimulating the *in situ* activity of *Geobacter* species to remove uranium from the groundwater of a uranium-contaminated aquifer. *Appl. Environ. Microbiol.* 69, 5884. <https://doi.org/10.1128/AEM.69.10.5884-5891.2003>.
- Andrews, J.N., Lee, D.J., 1979. Inert gases in groundwater from the Bunter Sandstone of England as indicators of age and palaeoclimatic trends. *J. Hydrol.* 41, 233–252.
- Andrews, J.N., Ford, D.J., Hussain, N., Trivedi, D., Youngman, M.J., 1989. Natural radioelement solution by circulating groundwaters in the Stripa granite. *Geochim. Cosmochim. Acta* 53, 1791–1802.
- Ansoberlo, E., Prat, O., Moisy, P., Den Auwer, C., Guilbaud, P., Carriere, M., Gouget, B., Duffield, J., Doizi, D., Vercouter, T., Moulin, C., Moulin, V., 2006. Actinide speciation in relation to biological processes. *Biochimie* 88, 1605–1618. <https://doi.org/10.1016/j.biochi.2006.06.011>.
- Appelo, C., Parkhurst, D.L., Post, V., 2014. Equations for calculating hydrogeochemical reactions of minerals and gases such as CO₂ at high pressures and temperatures. *Geochim. Cosmochim. Acta* 125, 49–67.
- Arey, J.S., Seaman, J.C., Bertsch, P.M., 1999. Immobilization of uranium in contaminated sediments by hydroxyapatite addition. *Environ. Sci. Technol.* 33, 337–342. <https://doi.org/10.1021/es980425+>.
- Arnold, T., Baumann, N., Krawczyk-Bärsch, E., Brockmann, S., Zimmermann, U., Jenk, U., Weiß, S., 2011. Identification of the uranium speciation in an underground acid mine drainage environment. *Geochim. Cosmochim. Acta* 75, 2200–2212. <https://doi.org/10.1016/j.gca.2011.01.037>.
- Arzuaga, X., Rieth, S., Bathija, A., Cooper, G., 2010. Renal effects of exposure to natural and depleted uranium: a review of the epidemiologic and experimental data. *J. Toxicol. Env. Heal. B* 13, 527–545. <https://doi.org/10.1080/10937404.2010.509015>.
- Asikainen, M., Kahlos, H., 1979. Anomalously high concentrations of uranium, radium and radon in water from drilled wells in the Helsinki region. *Geochim. Cosmochim. Acta* 43, 1681–1686. [https://doi.org/10.1016/0016-7037\(79\)90187-X](https://doi.org/10.1016/0016-7037(79)90187-X).
- Atkins, M.L., Santos, I.R., Perkins, A., Maher, D.T., 2016. Dissolved radon and uranium in groundwater in a potential coal seam gas development region (Richmond River Catchment, Australia). *J. Environ. Radioactiv.* 154, 83–92. <https://doi.org/10.1016/j.jenvrad.2016.01.014>.
- Atta-Fynn, R., Johnson, D.F., Bylaska, E.J., Ilton, E.S., Schenter, G.K., De Jong, W.A., 2012. Structure and hydrolysis of the U (IV), U (V), and U (VI) aqua ions from ab initio molecular simulations. *Inorg. Chem.* 51, 3016–3024.
- Avasarala, S., Lichtner, P.C., Ali, A.-M.S., González-Pinzón, R., Blake, J.M., Cerrato, J.M., 2017. Reactive transport of U and V from abandoned uranium mine wastes. *Environ. Sci. Technol.* 51, 12385–12393. <https://doi.org/10.1021/acs.est.7b03823>.
- Avivar, J., Ferrer, L., Casas, M., Cerda, V., 2012. Fully automated lab-on-valve-multisyringe flow injection analysis-ICP-MS system: an effective tool for fast, sensitive and selective determination of thorium and uranium at environmental levels exploiting solid phase extraction. *J. Anal. Atom. Spectrom.* 27, 327–334.
- Ayotte, J.D., Gronberg, J.A.M., Apodaca, L.E., 2011. Trace Elements and Radon in Groundwater across the United States, 1992-2003 (Scientific Investigations Report No. 2011-5059), National Water-Quality Assessment Program. United States Geological Survey, Reston, Virginia, USA.
- Babu, M.N.S., Somashekar, R.K., Kumar, S.A., Shivanna, K., Krishnamurthy, V., Eappen, K.P., 2008. Concentration of uranium levels in groundwater. *Int. J. Environ. Sci. Technol.* 5, 263–266. <https://doi.org/10.1007/BF03326020>.
- Bachmaf, S., Merkel, B.J., 2011. Sorption of uranium(VI) at the clay mineral-water interface. *Environ. Earth Sci.* 63, 925–934. <https://doi.org/10.1007/s12665-010-0761-6>.
- Baik, M.H., Jung, E.C., Jeong, J., 2015. Determination of uranium concentration and speciation in natural granitic groundwater using TRLFS. *J. Radioanal. Nucl. Chem.* 305, 589–598. <https://doi.org/10.1007/s10967-015-3971-2>.
- Bajwa, B.S., Kumar, S., Singh, S., Sahoo, S.K., Tripathi, R.M., 2017. Uranium and other heavy toxic elements distribution in the drinking water samples of SW-Punjab, India. *J. Rad. Res. Appl. Sci.* 10, 13–19. <https://doi.org/10.1016/j.jrras.2015.01.002>.
- Balaram, V., Rani, A., Rathore, D., 2022. Uranium in groundwater in parts of India and world: a comprehensive review of sources, impact to the environment and human health, analytical techniques, and mitigation technologies. *Geosys. Geoenviron.* 100043.
- Balbudhe, A.Y., Srivastava, S.K., Vishwaprasad, K., Srivastava, G.K., Tripathi, R.M., Puranik, V.D., 2012. Assessment of age-dependent uranium intake due to drinking water in Hyderabad, India. *Radiat. Prot. Dosim.* 148, 502–506. <https://doi.org/10.1093/rpd/ncr193>.
- Balcaen, L., Bolea-Fernandez, E., Resano, M., Vanhaecke, F., 2015. Inductively coupled plasma – tandem mass spectrometry (ICP-MS/MS): a powerful and universal tool for the interference-free determination of (ultra)trace elements – a tutorial review. *Analytica Chimica Acta* 894, 7–19. <https://doi.org/10.1016/j.aca.2015.08.053>.
- Ball, T.K., Miles, J.C.H., 1993. Geological and geochemical factors affecting the radon concentration in homes in Cornwall and Devon, UK. *Environ. Geochem. Health* 15, 27–36. <https://doi.org/10.1007/BF00146290>.
- Ball, T.K., Cameron, D.G., Colman, T.B., 1992. Aspects of radon potential mapping in Britain. *Radiat. Prot. Dosim.* 45, 211–214. <https://doi.org/10.1093/rpd/45.1-4.211>.
- Bankole, O.M., El Albani, A., Meunier, A., Rouzel, O.J., Gauthier-Lafaye, F., Bekker, A., 2016. Origin of red beds in the Paleoproterozoic Franceville Basin, Gabon, and implications for sandstone-hosted uranium mineralization. *Amer. J. Sci.* 316, 839–872.
- Banks, D., Røyset, O., Strand, T., Skarphagen, H., 1995. Radioelement (U, Th, Rn) concentrations in Norwegian bedrock groundwaters. *Environ. Geol.* 25, 165–180.
- Banning, A., Benfer, M., 2017. Drinking water uranium and potential health effects in the German federal state of Bavaria. *International Journal of Environmental Research & Public Health* 18, 927. <https://doi.org/10.3390/ijerph14080927>.
- Banning, A., Pawletko, N., Röder, J., Kübeck, C., Wisotzky, F., 2017. Ex situ groundwater treatment triggering the mobilization of geogenic uranium from aquifer sediments. *Sci. Tot. Environ.* 587–588, 371–380. <https://doi.org/10.1016/j.scitotenv.2017.02.162>.

- Bao, C., Wu, H., Li, L., Newcomer, D., Long, P.E., Williams, K.H., 2014. Uranium bioreduction rates across scales: biogeochemical hot moments and hot spots during a biostimulation experiment at Rifle, Colorado. *Environ. Sci. Technol.* 48, 10116–10127. <https://doi.org/10.1021/es501060d>.
- Bargar, J.R., Reitmeyer, R., Davis, J.A., 1999. Spectroscopic confirmation of uranium (VI)–carbonato adsorption complexes on hematite. *Environ. Sci. Technol.* 33, 2481–2484. <https://doi.org/10.1021/es990048g>.
- Bargar, J.R., Reitmeyer, R., Lenhart, J.J., Davis, J.A., 2000. Characterization of U(VI)–carbonato ternary complexes on hematite: EXAFS and electrophoretic mobility measurements. *Geochim. Cosmochim. Acta* 64, 2737–2749. [https://doi.org/10.1016/S0016-7037\(00\)00398-7](https://doi.org/10.1016/S0016-7037(00)00398-7).
- Barisić, D., Lulić, S., Miletić, P., 1992. Radium and uranium in phosphate fertilizers and their impact on the radioactivity of waters. *Water Res* 26, 607–611. [https://doi.org/10.1016/0043-1354\(92\)90234-U](https://doi.org/10.1016/0043-1354(92)90234-U).
- Barker, R.A., Bush, P.W., Baker, E.T.J., 1994. *Geologic History and Hydrogeologic Setting of the Edwards-Trinity Aquifer System, West Central Texas* (No. 94-4039), Water-Resources Investigations Report. United States Geological Survey, Austin, Texas.
- Barnes, C.E., Cochran, J.K., 1990. Uranium removal in oceanic sediments and the oceanic U balance. *Earth Planet. Sci. Lett.* 97, 94–101. [https://doi.org/10.1016/0012-821X\(90\)90101-3](https://doi.org/10.1016/0012-821X(90)90101-3).
- Barnes, C.E., Cochran, J.K., 1993. Uranium geochemistry in estuarine sediments: controls on removal and release processes. *Geochim. Cosmochim. Acta* 57, 555–569.
- Belitz, K., Dubrovsky, N.M., Burow, K.R., Jurgen, B., Johnson, T., 2003. *Framework for a Ground-Water Quality Monitoring and Assessment Program for California* (No. 03-4166), Water-Resources Investigations Report. United States Geological Survey, Sacramento, California.
- Bell, K.G., 1963. Uranium in Carbonate Rocks. USGS Professional Paper 474-A. United States Geological Survey, Washington, D.C.
- Belli, K.M., Taillefert, M., 2018. Geochemical controls of the microbially mediated redox cycling of uranium and iron. *Geochim. Cosmochim. Acta* 235, 431–449.
- Belli, K.M., DiChristina, T.J., Van Cappellen, P., Taillefert, M., 2015. Effects of aqueous uranyl speciation on the kinetics of microbial uranium reduction. *Geochim. Cosmochim. Acta* 157, 109–124.
- Bender, W.M., Becker, U., 2020. Resolving the kinetics of individual aqueous reaction steps of actinyl (AnO^{2+} and AnO_2^+ ; An = U, Np, and Pu) tricarbonate complexes with ferrous iron and hydrogen sulfide from first principles. *Radiochim. Acta* 108, 165–184.
- Beneš, P., Kratzer, K., Vičková, Š., Šebestová, E., 1998. Adsorption of uranium on clay and the effect of humic substances. *Radiochim. Acta* 82, 367–374.
- Berisha, F., Goessler, W., 2013. Uranium in Kosovo's drinking water. *Chemosphere* 93, 2165–2170. <https://doi.org/10.1016/j.chemosphere.2013.07.078>.
- Bernhard, G., Geipel, G., Reich, T., Brendler, V., Amayri, S., Nitsche, H., Uranyl, null, 2001. Uranyl(VI) carbonate complex formation: validation of the $\text{Ca}_2\text{UO}_2(\text{CO}_3)_3$ (aq) species. *Radiochim. Acta* 89, 511.
- BGS and DPHE, 2001. Technical Report WC/00/19. In: Kinniburgh, D.G., Smedley, P.L. (Eds.), *Arsenic Contamination of Groundwater in Bangladesh*. British Geological Survey, Keyworth, UK.
- Bhargava, R., Tiwari, M., Ajmal, P., Sahu, S., Pandit, G., 2013. Laser fluorimetric analysis of uranium in water from Vishakhapatnam and estimation of health risk. *Radiat. Prot. Environ.* 36, 128–132. <https://doi.org/10.4103/0972-0464.137478>.
- Bhattacharyya, A., Campbell, K.M., Kelly, S.D., Roebbert, Y., Weyer, S., Bernier-Latmani, R., Borch, T., 2017. Biogenic non-crystalline U(IV) revealed as major component in uranium ore deposits. *Nat. Comm.* 8, 15538 <https://doi.org/10.1038/ncomms15538>.
- Birke, M., Rauch, U., Lorenz, H., 2009. Uranium in stream and mineral water of the Federal Republic of Germany. *Environ. Geochem. Health* 31, 693. <https://doi.org/10.1007/s10653-009-9247-4>.
- Blanc, P., 2017. *Thermomodem : Update for the 2017 Version*, BRGM/RP-66811-FR. Bureau de Recherches Géologiques et Minières (BRGM), Orléans, France.
- Blanc, P., Lassin, A., Piantone, P., Azaroual, M., Jacquemet, N., Fabbri, A., Gaucher, E.C., 2012. Thermomodem: a geochemical database focused on low temperature water/rock interactions and waste materials. *Appl. Geochem.* 27, 2107–2116.
- Böhlke, J.K., Verstraeten, I.M., Kraemer, T.F., 2007. Effects of surface-water irrigation on sources, fluxes, and residence times of water, nitrate, and uranium in an alluvial aquifer. *Appl. Geochem.* 22, 152–174. <https://doi.org/10.1016/j.apgeochem.2006.08.019>.
- Boland, D.D., Collins, R.N., Glover, C.J., Payne, T.E., Waite, T.D., 2014. Reduction of U (VI) by Fe(II) during the Fe (II)-accelerated transformation of ferrihydrite. *Environ. Sci. Technol.* 48, 9086–9093.
- Bonnetti, C., Zhou, L., Riegler, T., Brugger, J., Fairclough, M., 2020. Large S isotope and trace element fractionations in pyrite of uranium roll front systems result from internally-driven biogeochemical cycle. *Geochim. Cosmochim. Acta* 282, 113–132.
- Borch, T., Kretzschmar, R., Kappler, A., Cappellen, P.V., Ginder-Vogel, M., Voegelin, A., Campbell, K., 2010. Biogeochemical redox processes and their impact on contaminant dynamics. *Environ. Sci. Technol.* 44, 15–23. <https://doi.org/10.1021/es9026248>.
- Bottrell, S.H., 1993. Redistribution of uranium by physical processes during weathering and implications for radon production. *Environ. Geochem. Health* 15, 21–25. <https://doi.org/10.1007/BF00146289>.
- Boulyga, S.F., Becker, J.S., 2002. Isotopic analysis of uranium and plutonium using ICP-MS and estimation of burn-up of spent uranium in contaminated environmental samples. *J. Anal. At. Spectrom.* 17, 1143–1147.
- Bowell, R.J., Grogan, J., Hutton-Ashkeny, M., Brough, C., Penman, K., Sapsford, D.J., 2011. Geometallurgy of uranium deposits. *Miner. Eng.* 24, 1305–1313. <https://doi.org/10.1016/j.mineng.2011.05.005>.
- Bowen, H.J.M., 1979. *Environmental Chemistry of the Elements*. Academic Press, London.
- Bowie, S.H.U., Parker, A., Raynor, E.J., 1979. Uranium reconnaissance survey of British Lower Palaeozoic shales: trace elements related to clay mineralogy. *Trans. Inst. Min. Metall. B* 88, B61–B64.
- Boyantov, M.I., Fletcher, K.E., Kwon, M.J., Rui, X., O'Loughlin, E.J., Löffler, F.E., Kemmer, K.M., 2011. Solution and microbial controls on the formation of reduced U (IV) species. *Environ. Sci. Technol.* 45, 8336–8344.
- Bradtmiller, L.L., Anderson, R.F., Sachs, J., Fleisher, M.Q., 2010. A deeper respired carbon pool in the glacial equatorial Pacific Ocean. *Earth Planet. Sci. Lett.* 299, 417–425. <https://doi.org/10.1016/j.epsl.2010.09.022>.
- Brendler, V., Vahle, A., Arnold, T., Bernhard, G., Fanghänel, T., 2003. RES³T-Rosendorf expert system for surface and sorption thermodynamics. *J. Contam. Hydrol.* 61, 281–291.
- Brennecke, G.A., Wasylenki, L.E., Bargar, J.R., Weyer, S., Anbar, A.D., 2011. Uranium isotope fractionation during adsorption to Mn-oxhydroxides. *Environ. Sci. Technol.* 45, 1370–1375. <https://doi.org/10.1021/es103061v>.
- Brincat, N.A., Parker, S.C., Molinari, M., Allen, G.C., Storr, M.T., 2015. Density functional carbon pool in the layered uranium oxides U₃O₈ and U₂O₅. *Dalton Trans* 44, 2613–2622. <https://doi.org/10.1039/C4DT02493A>.
- Brindha, K., Elango, L., Nair, R.N., 2011. Spatial and temporal variation of uranium in a shallow weathered rock aquifer in southern India. *J. Earth Syst. Sci.* 120, 911–920.
- Brown, P.L., Guerin, M., Hankin, S.I., Lowson, R.T., 1998. Uranium and other contaminant migration in groundwater at a tropical Australian Uranium Mine. *J. Contam. Hydrol.* 35, 295–303. [https://doi.org/10.1016/S0169-7722\(98\)00129-6](https://doi.org/10.1016/S0169-7722(98)00129-6).
- Brown, S.T., Basu, A., Christensen, J.N., Reimus, P.W., Heikoop, J.M., Simmons, A.M., Woldegabriel, G., Maher, K., Weaver, K.L., Clay, J.T., DePaolo, D.J., 2016. Isotopic evidence for reductive immobilization of uranium across a roll-front mineral deposit. *Environ. Sci. Technol.* 50, 6189–6198.
- Bruce, M., Kreuzer, O., Wilde, A., Buckingham, A., Butera, K., Bierlein, F., 2020. Unconformity-type uranium systems: a comparative review and predictive modelling of critical genetic factors. *Minerals* 10, 738. <https://doi.org/10.3390/min10090738>.
- Brugge, D., Buchner, V., 2011. Health effects of uranium: new research findings. *Reviews on Environmental Health* 26, 231–249. <https://doi.org/10.1515/REVEH.2011.032>.
- Bruggeman, C., Maes, N., 2010. Uptake of uranium(VI) by pyrite under Boom clay conditions: influence of dissolved organic carbon. *Environ. Sci. Technol.* 44, 4210–4216. <https://doi.org/10.1021/es100919p>.
- Bryan, N.D., Abrahamsen, L., Evans, N., Warwick, P., Buckau, G., Weng, L., Van Riemsdijk, W.H., 2012. The effects of humic substances on the transport of radionuclides: recent improvements in the prediction of behaviour and the understanding of mechanisms. *Appl. Geochem.* 27, 378–389.
- Bullock, L.A., Parnell, J., 2017. Selenium and molybdenum enrichment in uranium roll-front deposits of Wyoming and Colorado, USA. *J. Geochem. Explor.* 180, 101–112. <https://doi.org/10.1016/j.gexplo.2017.06.013>.
- Burns, P.C., Finch, R.J., 1999. Wyartite: crystallographic evidence for the first pentavalent-uranium mineral. *Amer. Mineral.* 84, 1456–1460.
- Buschmann, J., Berg, M., Stengel, C., Winkel, L., Sampson, M.L., Trang, P.T.K., Viet, P.H., 2008. Contamination of drinking water resources in the Mekong delta floodplains: arsenic and other trace metals pose serious health risks to population. *Environ. Int.* 34, 756–764. <https://doi.org/10.1016/j.envint.2007.12.025>.
- Butt, C.R.M., Horwitz, R.C., Mann, A.W., 1977. *Uranium Occurrences in Calcrete and Associated Sediments in Western Australia*, FP16, Minerals Research Laboratories. CSIRO, Australia.
- Byerley, J.J., Schärer, J.M., Atkinson, G.F., 1987. Determination of uranium(VI) in process liquors by ion chromatography. *Analyst* 112, 41–44. <https://doi.org/10.1039/AN9871200041>.
- Cameco, 2021. *Mineral Reserves and Resources* [WWW Document]. Reserves and Resources (Measured and Indicated). URL: <https://www.cameco.com/businesses/uranium-operations/suspended/smith-ranch-highland/reserves-resources>, 1.2.22.
- Campbell, K.M., Gallejos, T.J., Landa, E.R., 2015. Biogeochemical aspects of uranium mineralization, mining, milling, and remediation. *Appl. Geochem.* 57, 206–235. <https://doi.org/10.1016/j.apgeochem.2014.07.022>.
- Carvalho, F., Oliveira, J.M., Malta, M., 2015. Radiological quality of water in areas with old uranium mines in the District of Viseu, Portugal. *J. Nucl. Energy Sci. Power Gen. Technol.* 4, 1–5. <https://doi.org/10.4172/2325-9809.1000134>.
- Castor, S.B., Henry, C.D., 2000. Geology, geochemistry, and origin of volcanic rock-hosted uranium deposits in northwestern Nevada and southeastern Oregon, USA. *Ore Geol. Rev.* 16, 1–40. [https://doi.org/10.1016/S0169-1368\(99\)00021-9](https://doi.org/10.1016/S0169-1368(99)00021-9).
- Catalano, J.G., Brown, G.E., 2005. Uranyl adsorption onto montmorillonite: evaluation of binding sites and carbonate complexation. *Geochim. Cosmochim. Acta* 69, 2995–3005. <https://doi.org/10.1016/j.gca.2005.01.025>.
- Catalano, J.G., Heald, S.M., Zachara, J.M., Brown, G.E., 2004. Spectroscopic and diffraction study of uranium speciation in contaminated vadose zone sediments from the Hanford site, Washington state. *Environ. Sci. Technol.* 38, 2822–2828. <https://doi.org/10.1021/es049963e>.
- Catalano, J.G., McKinley, J.P., Zachara, J.M., Heald, S.M., Smith, S.C., Brown, G.E., 2006. Changes in uranium speciation through a depth sequence of contaminated Hanford sediments. *Environ. Sci. Technol.* 40, 2517–2524. <https://doi.org/10.1021/es0520969>.
- Cerrato, J.M., Ashner, M.N., Alessi, D.S., Lezama-Pacheco, J.S., Bernier-Latmani, R., Bargar, J.R., Giammar, D.E., 2013. Relative reactivity of biogenic and chemogenic uraninite and biogenic noncrystalline U(IV). *Environ. Sci. Technol.* 47, 9756–9763. <https://doi.org/10.1021/es401663t>.
- Chandrasekaran, K., Karunasagar, D., Arunachalam, J., 2011. Dispersive liquid-liquid micro extraction of uranium(VI) from groundwater and seawater samples and determination by inductively coupled plasma–optical emission spectrometry and

- flow injection-inductively coupled plasma mass spectrometry. *Anal. Meth.* 3, 2140–2147. <https://doi.org/10.1039/C1AY05329A>.
- Charalambous, C., Aletrari, M., Piera, P., Nicolaidou-Kanari, P., Efstathiou, M., Pashalidis, I., 2013. Uranium levels in Cypriot groundwater samples determined by ICP-MS and α -spectroscopy. *J. Environ. Radioactiv.* 116, 187–192.
- Chardi, K.J., Satpathy, A., Schenkeveld, W.D., Kumar, N., Noël, V., Kraemer, S.M., Giammar, D.E., 2022. Ligand-induced U mobilization from chemogenic uraninite and biogenic noncrystalline U(IV) under anoxic conditions. *Environ. Sci. Technol.* 56, 6369–6379. <https://doi.org/10.1021/acs.est.1c07919>.
- Charette, M.A., Sholkovitz, E.R., 2006. Trace element cycling in a subterranean estuary: Part 2. Geochemistry of the pore water. *Geochim. Cosmochim. Acta* 70, 811–826. <https://doi.org/10.1016/j.gca.2005.10.019>.
- Chen, J.H., Wasserburg, G.J., Damm, K.L. von, Edmond, J.N., 1986. The U-Th-Pb systematics in hot springs on the east pacific rise at 21 deg N and guaymas basin. *Geochim. Cosmochim. Acta* 50, 2467–2479.
- Chen, X., Romaniello, S.J., Herrmann, A.D., Wasylenki, L.E., Anbar, A.D., 2016. Uranium isotope fractionation during coprecipitation with aragonite and calcite. *Geochim. Cosmochim. Acta* 188, 189–207. <https://doi.org/10.1016/j.gca.2016.05.022>.
- Chen, L., Bai, Z., Zhu, L., Zhang, L., Cai, Y., Li, Y., Liu, W., Wang, Y., Chen, Lanhua, Diwu, J., Wang, J., Chai, Z., Wang, S., 2017. Ultrafast and efficient extraction of uranium from seawater using an amidoxime appended metal-organic framework. *ACS Appl. Mater. Interf.* 9, 32446–32451. <https://doi.org/10.1021/acsami.7b12396>.
- Chen, X., Romaniello, S.J., McCormick, M., Sherry, A., Havig, J.R., Zheng, W., Anbar, A.D., 2021. Anoxic depositional overprinting of 238U/235U in calcite: when do carbonates tell black shale tales? *Geology* 49, 1193–1197.
- Cheng, T., Barnett, M.O., Roden, E.E., Zhuang, J., 2004. Effects of phosphate on uranium (VI) adsorption to goethite-coated sand. *Environ. Sci. Technol.* 38, 6059–6065. <https://doi.org/10.1021/es040388o>.
- Cheng, Z., Zheng, Y., Mortlock, R., van Geen, A., 2004. Rapid multi-element analysis of groundwater by high-resolution inductively coupled plasma mass spectrometry. *Anal. Bioanal. Chem.* 379, 512–518. <https://doi.org/10.1007/s00216-004-2618-x>.
- Chentsov, I.G., 1961. The entry of uranium into some rock-forming minerals. *Int. Geol. Rev.* 3, 5–8. <https://doi.org/10.1080/00206816109474646>.
- Chi, G., Li, Z., Chu, H., Bethune, K., Quirt, D., Ledru, P., Normand, C., Card, C., Bosman, S., Davis, W., 2018. A shallow-burial mineralization model for the unconformity-related uranium deposits in the Athabasca Basin. *Econ. Geol.* 113, 1209–1217.
- Chisholm-Brause, C.J., Berg, J.M., Little, K.M., Matzner, R.A., Morris, D.E., 2004. Uranyl sorption by smectites: spectroscopic assessment of thermodynamic modeling. *J. Colloid. Interf. Sci.* 277, 366–382. <https://doi.org/10.1016/j.jcis.2004.04.047>.
- Cho, B.W., Choo, C.O., 2019. Geochemical behavior of uranium and radon in groundwater of Jurassic granite area, Icheon, Middle Korea. *Water* 11, 1–17. <https://doi.org/10.3390/w11061278>.
- Christensen, J.N., Dresel, P.E., Conrad, M.E., Patton, G.W., DePaolo, D.J., 2010. Isotopic tracking of Hanford 300 area derived uranium in the Columbia river. *Environ. Sci. Technol.* 44, 8855–8862. <https://doi.org/10.1021/es1025799>.
- Clarkson, M.O., Stirling, C.H., Jenkyns, H.C., Dickson, A.J., Porcelli, D., Moy, C.M., Pogge von Strandmann, P.A.E., Cooke, I.R., Lenton, T.M., 2018. Uranium isotope evidence for two episodes of deoxygenation during Oceanic Anoxic Event 2. *P. Natl. Acad. Sci. USA* 115, 2918–2923. <https://doi.org/10.1073/pnas.1715278115>.
- Colley, S., Thomson, J., 1985. Recurrent uranium relocations in distal turbidites emplaced in pelagic conditions. *Geochim. Cosmochim. Acta* 49, 2339–2348. [https://doi.org/10.1016/0016-7037\(85\)90234-0](https://doi.org/10.1016/0016-7037(85)90234-0).
- Colley, S., Thomson, J., Toole, J., 1989. Uranium relocations and derivation of quasi-isochrons for a turbidite pelagic sequence in the north-east Atlantic. *Geochim. Cosmochim. Acta* 53, 1223–1234. [https://doi.org/10.1016/0016-7037\(89\)90058-6](https://doi.org/10.1016/0016-7037(89)90058-6).
- Collins, R.N., Rosso, K.M., 2017. Mechanisms and rates of U(VI) reduction by Fe(II) in homogeneous aqueous solution and the role of U(V) disproportionation. *J. Phys. Chem. A* 121, 6603–6613.
- Collins, G.E., Lu, Q., Abubeker, S., Vajs, E., 2002. Remote fiber-optic flow cell for the detection of uranium(VI) in groundwater. *Appl. Spectrosc.* 56, 464–468. <https://doi.org/10.1366/0003702021955123>.
- Colmenero, F., 2020. Thermodynamic properties of the uranyl carbonate minerals roubaultite, fontanite, wiedenmannite, grimselite, cejkaite and bayleyite. *Inorg. Chem. Front.* 7, 4160–4179.
- Cologgi, D.L., Lampa-Pastirk, S., Speers, A.M., Kelly, S.D., Reguera, G., 2011. Extracellular reduction of uranium via *Geobacter* conductive pili as a protective cellular mechanism. *Proc. Natl. Acad. Sci. USA* 108, 15248. <https://doi.org/10.1073/pnas.1108616108>.
- Corkhill, C.L., Crean, D.E., Bailey, D.J., Makepeace, C., Stennett, M.C., Tappero, R., Grolimund, D., Hyatt, N.C., 2017. Multi-scale investigation of uranium attenuation by arsenic at an abandoned uranium mine. *South Terras. npj Mater. Degrad.* 1, 19. <https://doi.org/10.1038/s41529-017-0019-9>.
- Cot-Auriol, M., Virost, M., Micheau, C., Dumas, T., Le Goff, X., Den Auwer, C., Diat, O., Moisy, P., Nikitenko, S.I., 2021. Ultrasonically assisted conversion of uranium trioxide into uranium(VI) intrinsic colloids. *Dalton Trans* 50, 11498–11511. <https://doi.org/10.1039/d1dt01609a>.
- Council of the European Union, 2013. Council Directive Laying Down Requirements for the Protection of the Health of the General Public with Regard to Radioactive Substances in Water Intended for Human Consumption. Council Directive 2013/51/EURATOM. European Commission, Brussels.
- Council of the European Union, 2020. Directive 2020/2184 on the Quality of Water Intended for Human Consumption (Recast), Directive (EU) 2020/2184 of the European Parliament and of the Council (European Commission, Brussels).
- Cowart, J.B., Osmond, J.K., 1980. Uranium Isotopes in Ground Water as a Prospecting Technique. Dept Geology, Florida State University, Tallahassee.
- Coyte, R.M., Jain, R.C., Srivastava, S.K., Sharma, K.C., Khalil, A., Ma, L., Vengosh, A., 2018. Large-scale uranium contamination of groundwater resources in India. *Environ. Sci. Technol. Lett.* 5, 341–347. <https://doi.org/10.1021/acs.estlett.8b00215>.
- Coyte, R.M., Singh, A., Furst, K.E., Mitch, W.A., Vengosh, A., 2019. Co-occurrence of geogenic and anthropogenic contaminants in groundwater from Rajasthan, India. *Sci. Tot. Environ.* 688, 1216–1227. <https://doi.org/10.1016/j.scitotenv.2019.06.334>.
- Cramer, J.J., 1986. A Natural Analog for a Fuel Waste Disposal Vault. Presented at the Proceedings of the Canadian Nuclear Society 2nd International Conference on Radioactive Waste Management, Sept. 7–11, 1986, Winnipeg, Canada. Canadian Nuclear Society, Toronto, Canada, p. 821.
- Crançon, P., Van der Lee, J., 2003. Speciation and mobility of uranium (VI) in humic-containing soils. *Radiochim. Acta* 91, 673–679.
- Crawford, S.E., Loftis, S., Liber, K., 2017. The role of sediment properties and solution pH in the adsorption of uranium(VI) to freshwater sediments. *Environ. Pollut.* 220, 873–881. <https://doi.org/10.1016/j.envpol.2016.10.071>.
- Cristiano, E., Hu, Y.-J., Siegfried, M., Kaplan, D., Nitsche, H., 2011. A comparison of point of zero charge measurement methodology. *Clays Clay Miner* 59, 107–115.
- Cubillas, P., Köhler, S., Prieto, M., Chairat, C., Oelkers, E.H., 2005. Experimental determination of the dissolution rates of calcite, aragonite, and bivalves. *Chem. Geol.* 216, 59–77.
- Cumberland, S.A., Douglas, G., Grice, K., Moreau, J.W., 2016. Uranium mobility in organic matter-rich sediments: a review of geological and geochemical processes. *Earth-Sci. Rev.* 159, 160–185. <https://doi.org/10.1016/j.earscirev.2016.05.010>.
- Cumberland, S.A., Etschmann, B., Bruggen, J., Douglas, G., Evans, K., Fisher, L., Kappen, P., Moreau, J.W., 2018. Characterization of uranium redox state in organic-rich Eocene sediments. *Chemosphere* 194, 602–613. <https://doi.org/10.1016/j.chemosphere.2017.12.012>.
- Cuney, M.L., 2005. World-class unconformity-related uranium deposits: key factors for their genesis. In: Mao, J., Bierlein, F.P. (Eds.), *Mineral Deposit Research: Meeting the Global Challenge*. Springer, Berlin & Heidelberg, pp. 245–248.
- Cuney, M., 2008. The extreme diversity of uranium deposits. *Miner. Deposita* 44, 3–9. <https://doi.org/10.1007/s00126-008-0223-1>.
- Cuney, M., 2010. Evolution of uranium fractionation processes through time: driving the secular variation of uranium deposit types. *Econ. Geol.* 105, 553–569. <https://doi.org/10.2113/gsecongeo.105.3.553>.
- Curtis, G.P., Davis, J.A., Naftz, D.L., 2006. Simulation of reactive transport of uranium (VI) in groundwater with variable chemical conditions. *Water Resour. Res.* 42, W04404. <https://doi.org/10.1029/2005WR003979>, 1–15.
- Cuttell, J.C., Ivanovich, M., Tellam, J.H., Lloyd, J.W., 1988. Uranium-series isotopes in the groundwater of the Permo-Triassic sandstone aquifer, Lower-Mersey Basin. *U.K. Appl. Geochem.* 3, 255–271.
- Dabous, A.A., Osmond, J.K., Dawood, Y.H., 2002. Uranium/Thorium isotope evidence for ground-water history in the Eastern Desert of Egypt. *J. Arid. Environ.* 50, 343–357. <https://doi.org/10.1006/jare.2001.0861>.
- Dahlkamp, F.J., 1993. *Uranium Ore Deposits*. Springer, Berlin & Heidelberg.
- Dahlkamp, F.J., 2009. *Uranium Deposits of the World: Asia*. Springer, Berlin & Heidelberg.
- Dahlkamp, F.J., 2010. *Uranium Deposits of the World: USA and Latin America*. Springer, Berlin & Heidelberg.
- Dahlkamp, F.J., 2016. *Uranium Deposits of the World: Europe*. Springer, Berlin & Heidelberg.
- Dai, S., Sereidin, V., Ward, C., Hower, J., Xing, Y., Zhang, W., Song, W., Wang, P., 2015. Enrichment of U-Se-Mo-Re-V in coals preserved within marine carbonate successions: geochemical and mineralogical data from the Late Permian Guiding Coalfield, Guizhou, China. *Miner. Deposita* 50, 159–186. <https://doi.org/10.1007/s00126-014-0528-1>.
- Dangelmayr, M.A., Reimus, P.W., Wasserman, N.L., Punsal, J.J., Johnson, R.H., Clay, J. T., Stone, J.J., 2017. Laboratory column experiments and transport modeling to evaluate retardation of uranium in an aquifer downgradient of a uranium in-situ recovery site. *Appl. Geochem.* 80, 1–13. <https://doi.org/10.1016/j.apgeochem.2017.02.018>.
- Dangelmayr, M.A., Reimus, P.W., Johnson, R.H., Clay, J.T., Stone, J.J., 2018. Uncertainty and variability in laboratory derived sorption parameters of sediments from a uranium in situ recovery site. *J. Contam. Hydrol.* 213, 28–39.
- Davis, J.R., Higgs, J.J.W., Noy, D.J., Hooker, P.J., 2000. Complexation studies of uranium and thorium with a natural fulvic acid. In: Buckau, G. (Ed.), *Effects of Humic Substances on the Migration of Radionuclides: Complexation and Transport of Actinides*. Institut für Nukleare Entsorgung, Karlsruhe, pp. 85–100.
- Davis, J.A., Meece, D.E., Kohler, M., Curtis, G.P., 2004. Approaches to surface complexation modeling of uranium(VI) adsorption on aquifer sediments. *Geochim. Cosmochim. Acta* 68, 3621–3641. <https://doi.org/10.1016/j.gca.2004.03.003>.
- Degens, E.T., Khoo, F., Michaelis, W., 1977. Uranium anomaly in Black Sea sediments. *Nature* 269, 566–569. <https://doi.org/10.1038/269566a0>.
- Delaney, M.L., Boyle, E.A., 1983. Uranium and thorium isotope concentrations in foraminiferal calcite. *Earth Planet. Sci. Lett.* 62, 258–262. [https://doi.org/10.1016/0012-821X\(83\)90088-2](https://doi.org/10.1016/0012-821X(83)90088-2).
- Denecke, M.A., Pompe, S., Reich, T., Moll, H., Bubner, M., Heise, K., Nicolai, R., Nitsche, H., 1997. Measurements of the structural parameters for the interaction of uranium (VI) with natural and synthetic humic acids using EXAFS. *Radiochim. Acta* 79, 151–160.

- Descostes, M., Schlegel, M.L., Eglizaud, N., Descamps, F., Miserque, F., Simoni, E., 2010. Uptake of uranium and trace elements in pyrite (FeS₂) suspensions. *Geochim. Cosmochim. Acta* 74, 1551–1562. <https://doi.org/10.1016/j.gca.2009.12.004>.
- Dewey, C., Sokaras, D., Kroll, T., Bargar, J.R., Fendorf, S., 2020. Calcium-uranyl-carbonate species kinetically limit U(VI) reduction by Fe(II) and lead to U(V)-bearing ferrihydrite. *Environ. Sci. Technol.* 54, 6021–6030.
- Dhoom, R.T., Evans, G.J., 1998. Evaluation of uranium and arsenic retention by soil from a low level radioactive waste management site using sequential extraction. *Appl. Geochem.* 13, 415–420. [https://doi.org/10.1016/S0883-2927\(97\)00091-7](https://doi.org/10.1016/S0883-2927(97)00091-7).
- Diez-Fernández, S., Jaegler, H., Bresson, C., Chartier, F., Evrard, O., Hubert, A., Nonell, A., Pointurier, F., Isnard, H., 2020. A new method for determining ²³⁶U/²³⁸U isotope ratios in environmental samples by means of ICP-MS/MS. *Talanta* 206, 120221. <https://doi.org/10.1016/j.talanta.2019.120221>.
- Dinis, M. de L., Fiúza, A., 2021. Mitigation of uranium mining impacts—a review on groundwater remediation technologies. *Geosci* 11, 250.
- Dissanayake, C., Chandrajith, R., 2009. Phosphate mineral fertilizers, trace metals and human health. *J. Natl. Sci. Found. Sri* 37, 153–165.
- Dittrich, T.M., Boukhalfa, H., Ware, S.D., Reimus, P.W., 2015. Laboratory investigation of the role of desorption kinetics on americium transport associated with bentonite colloids. *J. Environ. Radioactiv.* 148, 170–182. <https://doi.org/10.1016/j.jenvrad.2015.07.001>.
- Dong, W., Brooks, S.C., 2008. Formation of aqueous MgUO₂(CO₃)₂²⁻ complex and uranium anion exchange mechanism onto an exchange resin. *Environ. Sci. Technol.* 42, 1979–1983. <https://doi.org/10.1021/es0711563>.
- Dong, W., Ball, W.P., Liu, C., Wang, Z., Stone, A.T., Bai, J., Zachara, J.M., 2005. Influence of calcite and dissolved calcium on uranium(VI) sorption to a Hanford subsurface sediment. *Environ. Sci. Technol.* 39, 7949–7955. <https://doi.org/10.1021/es0505088>.
- Doudou, S., Vaughan, D.J., Livens, F.R., Burton, N.A., 2012. Atomistic simulations of calcium uranyl(VI) carbonate adsorption on calcite and stepped-calcite surfaces. *Environ. Sci. Technol.* 46, 7587–7594. <https://doi.org/10.1021/es300034k>.
- Douglas, G.B., Butt, C.R.M., Gray, D.J., 2011. Geology, geochemistry and mineralogy of the lignite-hosted Ambassador palaeochannel uranium and multi-element deposit, Gunbarrel Basin, Western Australia. *Miner. Deposita* 46, 761–787. <https://doi.org/10.1007/s00126-011-0349-4>.
- Dresel, P.E., Evans, J.C., Farmer, O.T.I., 2002. Investigation of Isotopic Signatures for Sources of Groundwater Contamination at the Hanford Site, PNNL-13763. Pacific Northwest National Laboratory (PNNL), Richland, WA (USA).
- Drever, J.I., 1997. *The Geochemistry of Natural Waters: Surface and Groundwater Environments*, third ed. Prentice Hall, Englewood Cliffs, New Jersey.
- Drysdale, R.N., Zanchetta, G., Baneschi, L., Guidi, M., Isola, I., Couchoud, L., Piccini, L., Greig, A., Wong, H., Woodhead, J.D., Regattieri, E., Corrick, E., Paul, B., Spötl, C., Denson, E., Gordon, J., Jaillot, S., Dux, F., Hellstrom, J.C., 2019. Partitioning of Mg, Sr, Ba and U into a subaqueous calcite speleothem. *Geochim. Cosmochim. Acta* 264, 67–91. <https://doi.org/10.1016/j.gca.2019.08.001>.
- Du, X., Boonchayaanant, B., Wu, W.-M., Fendorf, S., Bargar, J., Criddle, C.S., 2011. Reduction of uranium(VI) by soluble iron(II) conforms with thermodynamic predictions. *Environ. Sci. Technol.* 45, 4718–4725. <https://doi.org/10.1021/es2006012>.
- Dublet, G., Lezama Pacheco, J., Bargar, J.R., Fendorf, S., Kumar, N., Lowry, G.V., Brown, G.E., 2017. Partitioning of uranyl between ferrihydrite and humic substances at acidic and circum-neutral pH. *Geochim. Cosmochim. Acta* 215, 122–140. <https://doi.org/10.1016/j.gca.2017.07.013>.
- Duff, M.C., Amrhein, C., 1996. Uranium(VI) adsorption on goethite and soil in carbonate solutions. *Soil Sci. Soc. Amer. J.* 60, 1393–1400. <https://doi.org/10.2136/sssaj1996.03615995006000050014x>.
- Duff, M.C., Coughlin, J.U., Hunter, D.B., 2002. Uranium co-precipitation with iron oxide minerals. *Geochim. Cosmochim. Acta* 66, 3533–3547.
- Durand, J.F., 2012. The impact of gold mining on the Witwatersrand on the rivers and karst system of Gauteng and North West Province, South Africa. *J. Afr. Earth Sci.* 68, 24–43. <https://doi.org/10.1016/j.jafrearsci.2012.03.013>.
- Dzombak, D.A., Morel, F.M.M., 1991. *Surface Complexation Modeling: Hydrous Ferric Oxide*. John Wiley & Sons, New York.
- Ebaid, Y., 2010. Use of gamma-ray spectrometry for uranium isotopic analysis in environmental samples. *Rom Journ Phys* 55.
- Eggs, S.M., Kinsley, L.P.J., Shelley, J.M.G., 1998. Deposition and element fractionation processes during atmospheric pressure laser sampling for analysis by ICP-MS. *Appl. Surf. Sci.* 127–129, 278–286. [https://doi.org/10.1016/S0169-4332\(97\)00643-0](https://doi.org/10.1016/S0169-4332(97)00643-0).
- Eisenbud, M., Gesell, T., 1997. *Environmental Radioactivity from Natural, Industrial and Military Sources*, fourth ed. Academic Press, California, USA.
- Elhewany, O.A., 2017. A new optical sensor for spectrophotometric determination of uranium (VI) and thorium (IV) in acidic medium. *Radiochimica Acta* 105, 993–1004. <https://doi.org/10.1515/ract-2017-2772>.
- Emerson, H.P., Hickok, K.A., Powell, B.A., 2016. Experimental evidence for ternary colloid-facilitated transport of Th(IV) with hematite (α-Fe₂O₃) colloids and Suwannee River fulvic acid. *J. Environ. Radioactiv.* 165, 168–181. <https://doi.org/10.1016/j.jenvrad.2016.10.001>.
- Endrizzi, F., Rao, L., 2014. Chemical speciation of uranium(VI) in marine environments: complexation of calcium and magnesium ions with [(UO₂)(CO₃)₃]⁴⁻ and the effect on the extraction of uranium from seawater. *Chem-Eur. J.* 20, 14499–14506. <https://doi.org/10.1002/chem.201403262>.
- Endrizzi, F., Leggett, C.J., Rao, L., 2016. Scientific basis for efficient extraction of uranium from seawater. I: understanding the chemical speciation of uranium under seawater conditions. *Ind. Eng. Chem. Res.* 55, 4249–4256. <https://doi.org/10.1021/acs.iecr.5b03679>.
- Endrizzi, F., Gaona, X., Zhang, Z., Xu, C., Rao, L., Garcia-Perez, C., Altmaier, M., 2019. Thermodynamic description of U (VI) solubility and hydrolysis in dilute to concentrated NaCl solutions at T= 25, 55 and 80° C. *Radiochimica Acta* 107, 663–678.
- EPA, 1991. *Diffuse NORM Wastes: Waste Characterization and Preliminary Risk Assessment (Draft)*. US Environmental Protection Agency, Washington, D.C.
- Estes, S.L., Powell, B.A., 2020. Enthalpy of uranium adsorption onto hematite. *Environ. Sci. Technol.* 54, 15004–15012. <https://doi.org/10.1021/acs.est.0c04429>.
- Evans, N., Warwick, P., Lewis, T., Bryan, N., 2011. Influence of humic acid on the sorption of uranium(IV) to kaolin. *Environ. Chem. Lett.* 9, 25–30.
- Fahey, A.J., Groopman, E.E., Grabowski, K.S., Fazel, K.C., 2016. Measurement of uranium isotopes in particles of U₃O₈ by secondary ion mass spectrometry—single-stage accelerator mass spectrometry (SIMS-SSAMS). *Anal. Chem.* 88, 7145–7153. <https://doi.org/10.1021/acs.analchem.6b01209>.
- Fairclough, M.C., Irvine, J.A., Katona, L.F., Simmon, W.L., 2018. *World Distribution of Uranium Deposits*. Map by the International Atomic Energy Agency, Vienna.
- Fedotov, P.S., Fedyunina, N.N., Filosofov, D.V., Yakushev, E.A., Warot, G., 2019. A novel combined countercurrent chromatography – inductively coupled plasma mass spectrometry method for the determination of ultra trace uranium and thorium in Roman lead. *Talanta* 192, 395–399. <https://doi.org/10.1016/j.talanta.2018.09.071>.
- Ferrari, C.R., de Azevedo, H., Wisniewski, M.J.S., Rodger, S., Roque, C.V., Nascimento, M.R.L., 2015. An overview of an acidic uranium mine pit lake (Caldas, Brazil): composition of the zooplankton community and limnocochemical aspects. *Mine Water Environ* 34, 343–351. <https://doi.org/10.1007/s10230-015-0333-9>.
- Fiedor, J.N., Bostick, W.D., Jarabek, R.J., Farrell, J., 1998. Understanding the mechanism of uranium removal from groundwater by zero-valent iron using X-ray photoelectron spectroscopy. *Environ. Sci. Technol.* 32, 1466–1473. <https://doi.org/10.1021/es970385u>.
- Filippidis, A., Misaelides, P., Clouvas, A., Godelitsas, A., Barbayiannis, N., Anousis, I., 1997. Mineral, chemical and radiological investigation of a black sand at Touzla Cape, near Thessaloniki, Greece. *Env. Geochem. Health* 19, 83–88. <https://doi.org/10.1023/A:1018498404922>.
- Fleischer, R.L., 1982. Alpha-recoil damage and solution effects in minerals: uranium isotopic disequilibrium and radon release. *Geochim. Cosmochim. Acta* 46, 2191–2201. [https://doi.org/10.1016/0016-7037\(82\)90194-6](https://doi.org/10.1016/0016-7037(82)90194-6).
- Fleischer, R.L., Alter, H.W., Furman, S.C., Price, P.B., Walker, R.M., 1972. Particle track etching. *Science* 178, 255–263. <https://doi.org/10.1126/science.178.4058.255>.
- Flury, M., Qiu, H., 2008. Modeling colloid-facilitated contaminant transport in the vadose zone. *Vadose Zone J* 7, 682–697.
- Fox, P.M., Davis, J.A., Zachara, J.M., 2006. The effect of calcium on aqueous uranium (VI) speciation and adsorption to ferrihydrite and quartz. *Geochim. Cosmochim. Acta* 70, 1379–1387. <https://doi.org/10.1016/j.gca.2005.11.027>.
- Francis, A.J., Dodge, C.J., 2008. Bioreduction of uranium(VI) complexed with citric acid by *Clostridia* affects its structure and solubility. *Environ. Sci. Technol.* 42, 8277–8282. <https://doi.org/10.1021/es801045m>.
- Franklin, N.M., Stauber, J.L., Markich, S.J., Lim, R.P., 2000. pH-dependent toxicity of copper and uranium to a tropical freshwater alga (*Chlorella* sp.). *Aquat. Toxicol.* 48, 275–289. [https://doi.org/10.1016/S0166-445X\(99\)00042-9](https://doi.org/10.1016/S0166-445X(99)00042-9).
- Frengstad, B., Midtgård Skrede, A.K., Banks, D., Reidar Krog, J., Siewers, U., 2000. The chemistry of Norwegian groundwaters: III. The distribution of trace elements in 476 crystalline bedrock groundwaters, as analysed by ICP-MS techniques. *Sci. Tot. Environ.* 246, 21–40. [https://doi.org/10.1016/S0048-9697\(99\)00413-1](https://doi.org/10.1016/S0048-9697(99)00413-1).
- Frisbie, S.H., Mitchell, E.J., Mاستera, L.J., Maynard, D.M., Yusuf, A.Z., Siddiqi Mohammad, Yusuf, Ortega, Richard, Dunn Richard, K., Westerman David, S., Thomas, Bacquart, Sarkar, Bibudhendra, 2009. Public health strategies for western Bangladesh that address arsenic, manganese, uranium, and other toxic elements in drinking water. *Environ. Health Persp.* 117, 410–416. <https://doi.org/10.1289/ehp.11886>.
- Froideval, A., Del Nero, M., Gaillard, C., Barillon, R., Rossini, I., Hazemann, J., 2006. Uranyl sorption species at low coverage on Al-hydroxide: TRLFS and XAFS studies. *Geochim. Cosmochim. Acta* 70, 5270–5284.
- Fujii, R., Swain, W.C., 1995. Areal Distribution of Selected Trace Elements, Salinity, and Major Ions in Shallow Ground Water, Tulare Basin, Southern San Joaquin Valley, California, Water Resources Investigations Report. U.S. Geological Survey, Sacramento, California.
- Fuller, C.C., Bargar, J.R., Davis, J.A., Piana, M.J., 2002. Mechanisms of uranium interactions with hydroxyapatite: implications for groundwater remediation. *Environ. Sci. Technol.* 36, 158–165. <https://doi.org/10.1021/es0108483>.
- Fuller, C., Bargar, J., Davis, J., 2003. Molecular-scale characterization of uranium sorption by bone apatite materials for a permeable reactive barrier demonstration. *Environmental science & technology* 37, 4642–4649.
- Gäbler, H.-E., 2002. Applications of magnetic sector ICP-MS in geochemistry. *J. Geochem. Explor.* 75, 1–15. [https://doi.org/10.1016/S0375-6742\(01\)00197-2](https://doi.org/10.1016/S0375-6742(01)00197-2).
- Galhardi, J.A., Bonotto, D.M., 2017. Radionuclides (²²²Rn, ²²⁶Ra, ²³⁴U, and ²³⁸U) release in natural waters affected by coal mining activities in southern Brazil. *Water Air Soil Poll* 228, 207. <https://doi.org/10.1007/s11270-017-3381-x>.
- Gallagher, M.J., Michie, U.M., Smith, R.T., Haynes, L., 1971. New evidence of uranium and other mineralization in Scotland. *T. I. Min. Metall. B* 80, B150–B173.
- Ganesh, S., Khan, F., Ahmed, M., Velavendan, P., Pandey, N., Mudali, U., Pandey, S., 2012. Determination of ultra traces amount of uranium in raffinate of Purex process by laser fluorimetry. *J. Rad. Nucl. Chem.* 292, 331–334. <https://doi.org/10.1007/s10967-011-1431-1>.
- Garg, V., Yadav, A., Singh, K., Singh, M., Bishnoi, M., Pulhani, V., 2014. Uranium Concentration in Groundwater in Hisar City, India, 5, pp. 112–114.
- Gartman, B.N., Qafoku, N.P., Szecsody, J.E., Kukkadapu, R.K., Wang, Z., Wellman, D.M., Truex, M.J., 2015. Uranium fate in Hanford sediment altered by simulated acid

- waste solutions. *Appl. Geochem.* 63, 1–9. <https://doi.org/10.1016/j.apgeochem.2015.07.010>.
- Gascoyne, M., 1989. High levels of uranium and radium in groundwaters at Canada's underground research laboratory, Lac du Bonnet, Manitoba, Canada. *Appl. Geochem.* 4, 577–591. [https://doi.org/10.1016/0883-2927\(89\)90068-1](https://doi.org/10.1016/0883-2927(89)90068-1).
- Gavrilescu, M., Pavel, L.V., Cretescu, I., 2009. Characterization and remediation of soils contaminated with uranium. *J. Hazard Mater.* 163, 475–510. <https://doi.org/10.1016/j.jhazmat.2008.07.103>.
- Geipel, G., Reich, T., Brendler, V., Bernhard, G., Nitsche, H., 1997. Laser and X-ray spectroscopic studies of uranium-calcite interface phenomena. *J. Nucl. Mater.* 248, 408–411. [https://doi.org/10.1016/S0022-3115\(97\)00136-0](https://doi.org/10.1016/S0022-3115(97)00136-0).
- Gezahegne, W.A., Hennig, C., Tsushima, S., Planer-Friedrich, B., Scheinost, A.C., Merkel, B.J., 2012. EXAFS and DFT investigations of uranyl arsenate complexes in aqueous solution. *Environ. Sci. Technol.* 46, 2228–2233. <https://doi.org/10.1021/es203284s>.
- Giffaut, E., Grivé, M., Blanc, Ph, Vieillard, Ph, Colàs, E., Gailhanou, H., Gaboreau, S., Marty, N., Madé, B., Duro, L., 2014. Andra thermodynamic database for performance assessment: ThermoChimie. *Appl. Geochem.* 49, 225–236. <https://doi.org/10.1016/j.apgeochem.2014.05.007>.
- Gillikin, D.P., Dehairs, F., 2013. Uranium in aragonitic marine bivalve shells. *Palaeogeography, Palaeoclimatology, Palaeoecology* 373, 60–65. <https://doi.org/10.1016/j.palaeo.2012.02.028>.
- Ginder-Vogel, M., Stewart, B., Fendorf, S., 2010. Kinetic and mechanistic constraints on the oxidation of biogenic uraninite by ferrihydrite. *Environ. Sci. Technol.* 44, 163–169. <https://doi.org/10.1021/es902452u>.
- Glaus, M.A., Hummel, W., Van Loon, L.R., 1997. Experimental Determination and Modelling of Trace Metal-Humate Interactions: A Pragmatic Approach for Applications in Groundwater, PSI 97-13. Paul Scherrer Institut, Villigen, Switzerland.
- Godoy, J.M., Ferreira, P.R., de Souza, E.M., Silva, L.I. da, Bittencourt, I.C.S., 2019. High uranium concentrations in the groundwater of the Rio de Janeiro State, Brazil, mountainous region. *J. Braz. Chem. Soc.* 30, 224–233.
- Gony, J.-N., 1971. Etude cristallographique du phosphate uranifère de Bakouma (République Centrafricaine), Rapport CEA-R-4003. Commissariat à l'Energie Atomique (Fontenay-Aux-Roses).
- Gothmann, A.M., Higgins, J.A., Adkins, J.F., Broecker, W., Farley, K.A., McKeon, R., Stolarski, J., Planavsky, N., Wang, X., Bender, M.L., 2019. A Cenozoic record of seawater uranium in fossil corals. *Geochim. Cosmochim. Acta* 250, 173–190.
- Goto, K.T., Anbar, A.D., Gordon, G.W., Romaniello, S.J., Shimoda, G., Takaya, Y., Tokumaru, A., Nozaki, T., Suzuki, K., Machida, S., 2014. Uranium isotope systematics of ferromanganese crusts in the Pacific Ocean: implications for the marine 238U/235U isotope system. *Geochim. Cosmochim. Acta* 146, 43–58.
- Götze, J., Gaff, M., Möckel, R., 2015. Uranium and uranyl luminescence in agate/chalcedony. *Min. Mag.* 79, 985–995. <https://doi.org/10.1180/minmag.2015.079.4.08>.
- Grenthe, I., Fuger, J., Konings, R.J., Lemire, R.J., Muller, A.B., Nguyen-Trung, C., Wanner, H., 1992. *Chemical Thermodynamics of Uranium*. Elsevier, Amsterdam.
- Grenthe, I., Gaona, X., Plyasunov, A.V., Rao, L., Runde, W.H., Grambow, B., Konings, R.J.M., Smith, A.L., Moore, E.E., 2021. Second Update on the Chemical Thermodynamics of Uranium, Neptunium, Plutonium, Americium and Technetium, Chemical Thermodynamics, 14. Nuclear Energy Agency, OECD, Paris, France. <https://doi.org/10.1787/bf86a907-en>.
- Grivé, M., Duro, L., Colàs, E., Giffaut, E., 2015. Thermodynamic data selection applied to radionuclides and chemotoxic elements: an overview of the ThermoChimie-TDB. *Appl. Geochem.* 55, 85–94. <https://doi.org/10.1016/j.apgeochem.2014.12.017>.
- Gross, E.L., Brown, C.J., 2020. Arsenic and Uranium Occurrence in Private Wells in Connecticut, 2013–18 — A Spatially Weighted and Bedrock Geology Assessment, Open-File Report 2020–1111. United States Geological Survey, Reston, VA.
- Groudev, S., Spasova, I., Nicolova, M., Georgiev, P., 2007. Acid mine drainage cleanup in a uranium deposit by means of a passive treatment system. *Physicochem. Probl. Mi.* 41, 265–274.
- Groza, N., Manescu, A., Panturu, E., Filcenco-Olteanu, A., Panturu, R.-I., Jinescu, C., 2010. Uranium wastewater treatment using wetland system. *Rev. Chim.* 61, 680–684.
- Gu, B., Ku, Y.-K., Jardine, P.M., 2004. Sorption and binary exchange of nitrate, sulfate, and uranium on an anion-exchange resin. *Environ. Sci. Technol.* 38, 3184–3188. <https://doi.org/10.1021/es034902m>.
- Gu, B., Yan, H., Zhou, P., Watson, D.B., Park, M., Istok, J., 2005. Natural humics impact uranium bioreduction and oxidation. *Environ. Sci. Technol.* 39, 5268–5275. <https://doi.org/10.1021/es050350r>.
- Gückel, K., Rossberg, A., Brendler, V., Foerstendorf, H., 2012. Binary and ternary surface complexes of U(VI) on the gibbsite/water interface studied by vibrational and EXAFS spectroscopy. *Chem. Geol.* 326–327, 27–35. <https://doi.org/10.1016/j.chemgeo.2012.07.015>.
- Guillaumont, R., Fanghänel, T., Fuger, J., Grenthe, I., Neck, V., Palmer, D.A., Rand, M.H., 2003. Update on the Chemical Thermodynamics of Uranium, Neptunium, Plutonium, Americium and Technetium, Chemical Thermodynamics, ume 5. Nuclear Energy Agency (NEA), Issy-les-Moulineaux, France.
- Guo, Z., Yan, C., Xu, J., Wu, W., 2009. Sorption of U(VI) and phosphate on γ -alumina: binary and ternary sorption systems. *Colloid Surface A* 336, 123–129. <https://doi.org/10.1016/j.colsurfa.2008.11.032>.
- Gupta, S.K., Thulasidas, S.K., Goyal, N., Godbole, S.V., 2014. A modular-type atomic absorption instrument with the graphite furnace in a glove box for nuclear applications. *Instrum. Sci. Technol.* 42, 161–172. <https://doi.org/10.1080/10739149.2013.845848>.
- Gustafsson, J.P., Dässon, E., Bäckström, M., 2009. Towards a consistent geochemical model for prediction of uranium(VI) removal from groundwater by ferrihydrite. *Appl. Geochem.* 24, 454–462.
- Haas, J.R., Northup, A., 2004. Effects of aqueous complexation on reductive precipitation of uranium by *Shewanella putrefaciens*. *Geochem. T.* 5, 41–48. <https://doi.org/10.1063/1.1803971>.
- Haddad, Kh, Al-Masri, M.S., Al-Haleem, M.A., Sarhil, A., 2021. Comparison of three analytical techniques for determination of Th and U in environmental samples. *Appl. Radiat. Isotopes* 168, 109489. <https://doi.org/10.1016/j.apradiso.2020.109489>.
- Hain, K., Martschini, M., Gülce, F., Honda, M., Lachner, J., Kern, M., Pitters, J., Quinto, F., Sakaguchi, A., Steier, P., Wiederin, A., Wieser, A., Yokoyama, A., Golsner, R., 2022. Developing accelerator mass spectrometry capabilities for anthropogenic radionuclide analysis to extend the set of oceanographic tracers. *Front. Marine Sci.* 9 <https://doi.org/10.3389/fmars.2022.837515>.
- Haji, M.N., Drysdale, J.A., Buesseler, K.O., Slocum, A.H., 2019. Results of an ocean trial of the symbiotic machine for ocean uranium extraction. *Environ. Sci. Technol.* 53, 2229–2237. <https://doi.org/10.1021/acs.est.8b05100>.
- Hamamo, H., Landsberger, S., Harbottle, G., Panno, S., 1995. Studies of radioactivity and heavy metals in phosphate fertilizer. *J. Radioanal. Nucl. Chem.* 194, 331–336. <https://doi.org/10.1007/BF02038431>.
- Han, R., Zou, W., Wang, Y., Zhu, L., 2007. Removal of uranium(VI) from aqueous solutions by manganese oxide coated zeolite: discussion of adsorption isotherms and pH effect. *J. Environ. Radioactiv.* 93, 127–143. <https://doi.org/10.1016/j.jenvrad.2006.12.003>.
- Haneklaus, N., Sun, Y., Bol, R., Lottemoser, B., Schnug, E., 2017. To extract, or not to extract uranium from phosphate rock, that is the question. *Environ. Sci. Technol., Viewpoint* 51, 753–754.
- Haneklaus, S.H., Windmann, H., Maekawa, M., Zhang, L., Schnug, E., 2021. Diet controls uranium intake and aggravates health hazards. *Medical Research Archives* 9.
- Harguindeguy, S., Crançon, P., Pointurier, F., Potin-Gautier, M., Lespes, G., 2014. Isotopic investigation of the colloidal mobility of depleted uranium in a podzolic soil. *Chemosphere* 103, 343–348.
- Haslam, H.W., Sandon, P.T.S., 1991. *The Geochemistry of Some Red-Bed Formations in the United Kingdom*, Technical Report WP/90/2. British Geological Survey, Keyworth, UK.
- Hassan, N., Amin, A.S., 2017. Membrane optode for uranium (VI) preconcentration and colorimetric determination in real samples. *RSC Adv* 7, 46566–46574.
- Henderson, G.M., Anderson, R.F., 2003. The U-series toolbox for paleoceanography. *Rev. Min. Geochem.* 52, 493–531. <https://doi.org/10.2113/0520493>.
- Henderson, A.D., Demond, A.H., 2007. Long-term performance of zero-valent iron permeable reactive barriers: a critical review. *Environ. Eng. Sci.* 24, 401–423.
- Hennessy, J., 1981. A classification of British Caledonian granites based on uranium and thorium contents. *Min. Mag.* 44, 449–454.
- Hennig, C., Tutschku, J., Rossberg, A., Bernhard, G., Scheinost, A.C., 2005. Comparative EXAFS investigation of uranium(VI) and -(IV) aquo chloro complexes in solution using a newly developed spectroelectrochemical cell. *Inorg. Chem.* 44, 6655–6661. <https://doi.org/10.1021/ic048422n>.
- Hennig, T., Stockmann, M., Kühn, M., 2020. Simulation of diffusive uranium transport and sorption processes in the Opalinus Clay. *Appl. Geochem.* 123, 104777.
- Herbelin, A.L., Westall, J.C., 1999. FITEQL: A Computer Program for the Determination of Chemical Equilibrium Constants from Experimental Data, Version 4.0 (No. 99–01). Chemistry Department, Oregon State University, Corvallis, OE.
- Hess, C., Michel, J., Horton, T., Prichard, H., Coniglio, W., 1985. The occurrence of radioactivity in public water supplies in the United States. *Health Phys* 48, 553–586. <https://doi.org/10.1097/00004032-198505000-00002>.
- Hiemstra, T., 2018. Ferrihydrite interaction with silicate and competing oxyanions: geometry and hydrogen bonding of surface species. *Geochim. Cosmochim. Acta* 238, 453–476.
- Hiemstra, T., Van Riemsdijk, W.H., 2009. A surface structural model for ferrihydrite I: sites related to primary charge, molar mass, and mass density. *Geochim. Cosmochim. Acta* 73, 4423–4436. <https://doi.org/10.1016/j.gca.2009.04.032>.
- Hiemstra, T., Riemsdijk, W.H.V., Rossberg, A., Ulrich, K.-U., 2009. A surface structural model for ferrihydrite II: adsorption of uranyl and carbonate. *Geochim. Cosmochim. Acta* 73, 4437–4451. <https://doi.org/10.1016/j.gca.2009.04.035>.
- Hierro, A., Martín, J.E., Ollás, M., García, C., Bolívar, J.P., 2013. Uranium behavior during a tidal cycle in an estuarine system affected by acid mine drainage (AMD). *Chem. Geol.* 342, 110–118. <https://doi.org/10.1016/j.chemgeo.2013.01.021>.
- Higgo, J.J.W., Kinniburgh, D., Smith, B., Tipping, E., 1993. Complexation of Co^{2+} , Ni^{2+} , UO_2^{2+} and Ca^{2+} by humic substances in groundwaters. *Radiochim. Acta* 61, 91–104.
- Ho, C.H., Miller, N.H., 1985. Effect of humic acid on uranium uptake by hematite particles. *J. Colloid. Interf. Sci.* 106, 281–288.
- Holland, H.D., 2005. 100th Anniversary Special Paper: sedimentary mineral deposits and the evolution of earth's near-surface environments. *Econ. Geol.* 100, 1489–1509. <https://doi.org/10.2113/gsecongeo.100.8.1489>.
- Hörbrand, T., Baumann, T., Moog, H.C., 2018. Validation of hydrogeochemical databases for problems in deep geothermal energy. *Geoth. Energy* 6, 20. <https://doi.org/10.1186/s40517-018-0106-3>.
- Hostetler, P.B., Garrels, R.M., 1962. Transportation and precipitation of uranium and vanadium at low temperatures, with special reference to sandstone-type uranium deposits. *Economic Geology* 57, 137–167.
- Hotchkis, M., Child, D., Tumlz, C., 2002. Application of accelerator mass spectrometry for 236U analysis. *J. Nucl. Sci. Technol.* 39, 532–536. <https://doi.org/10.1080/00223131.2002.10875524>.

- Hou, W., Lei, Z., Hu, E., Wang, H., Wang, Q., Zhang, R., Li, H., 2021. Cotransport of uranyl carbonate loaded on amorphous colloidal silica and strip-shaped humic acid in saturated porous media: behavior and mechanism. *Environ. Pollut.* 285, 117230.
- Hsi, C.-K.D., Langmuir, D., 1985. Adsorption of uranyl onto ferric oxyhydroxides: application of the surface complexation site-binding model. *Geochim. Cosmochim. Acta* 49, 1931–1941. [https://doi.org/10.1016/0016-7037\(85\)90088-2](https://doi.org/10.1016/0016-7037(85)90088-2).
- Hua, B., Deng, B., 2008. Reductive immobilization of uranium(VI) by amorphous iron sulfide. *Environ. Sci. Technol.* 42, 8703–8708. <https://doi.org/10.1021/es801225z>.
- Hua, B., Xu, H., Terry, J., Deng, B., 2006. Kinetics of uranium(VI) reduction by hydrogen sulfide in anoxic aqueous systems. *Environ. Sci. Technol.* 40, 4666–4671. <https://doi.org/10.1021/es051804n>.
- Hudak, P.F., 2018. Associations between dissolved uranium, nitrate, calcium, alkalinity, iron, and manganese concentrations in the Edwards-Trinity Plateau Aquifer, Texas, USA. *Environ. Proc.* 5, 441–450. <https://doi.org/10.1007/s40710-018-0296-5>.
- Hussain, N., 1997. Flux of ⁴He from Carmanellis granite: modelling of an HDR geothermal reservoir. *Appl. Geochem.* 12, 1–8.
- Hyun, S.P., Davis, J.A., Sun, K., Hayes, K.F., 2012. Uranium(VI) reduction by iron(II) monosulfide mackinawite. *Environ. Sci. Technol.* 46, 3369–3376. <https://doi.org/10.1021/es203786p>.
- Ilani, S., Kronfeld, J., Pinchasov, A., 1987. Uranium distribution in iron veins in Israel. *Uranium* 4, 159–174.
- Ilani, S., Minster, T., Kronfeld, J., Even, O., 2006. The source of anomalous radioactivity in the springs bordering the Sea of Galilee. *Israel. J. Environ. Radioactiv.* 85, 137–146.
- Ivanov, P., Griffiths, T., Bryan, N.D., Bozhikov, G., Dmitriev, S., 2012. The effect of humic acid on uranyl sorption onto bentonite at trace uranium levels. *J. Environ. Monit.* 14, 2968–2975.
- Ivanovich, M., Alexander, J., 1985. Uranium Series Disequilibrium: Application to Studies of the Groundwater Regime of the Harwell Region, AERE Report 11688. AERE, Harwell.
- Jackson, V.E., Gutowski, K.E., Dixon, D.A., 2013. Density functional theory study of the complexation of the uranyl dication with anionic phosphate ligands with and without water molecules. *J. Phys. Chem. A* 117, 8939–8957. <https://doi.org/10.1021/jp405470k>.
- Jaireth, S., Roach, I.C., Bastrakov, E., Liu, S., 2016. Basin-related uranium mineral systems in Australia: a review of critical features. *Ore Geol. Rev.* 76, 360–394. <https://doi.org/10.1016/j.oregeorev.2015.08.006>.
- Jambhulkar, H., Shaikh, S., Kumar, M., 2018. Fly ash toxicity, emerging issues and possible implications for its exploitation in agriculture; Indian scenario: a review. *Chemosphere* 213, 333–344. <https://doi.org/10.1016/j.chemosphere.2018.09.045>.
- Jang, J.-H., Dempsey, B.A., Burgos, W.D., 2007. A model-based evaluation of sorptive reactivities of hydrous ferric oxide and hematite for U(VI). *Environ. Sci. Technol.* 41, 4305–4310.
- Jerden, J.L., Sinha, A.K., 2003. Phosphate based immobilization of uranium in an oxidizing bedrock aquifer. *Appl. Geochem.* 18, 823–843. [https://doi.org/10.1016/S0883-2927\(02\)00179-8](https://doi.org/10.1016/S0883-2927(02)00179-8).
- Jerden, J.L., Sinha, A.K., 2006. Geochemical coupling of uranium and phosphorous in soils overlying an unmined uranium deposit: Coles Hill, Virginia. *J. Geochem. Explor.* 91, 56–70. <https://doi.org/10.1016/j.gexplo.2005.12.003>.
- Jerden, J.L., Sinha, A.K., Zelazny, L., 2003. Natural immobilization of uranium by phosphate mineralization in an oxidizing saprolite–soil profile: chemical weathering of the Coles Hill uranium deposit, Virginia. *Chem. Geol.* 199, 129–157. [https://doi.org/10.1016/S0009-2541\(03\)00080-9](https://doi.org/10.1016/S0009-2541(03)00080-9).
- Jia, G., Belli, M., Sansone, U., Rosamilia, S., Occone, R., Gaudino, S., 2002. Determination of uranium isotopes in environmental samples by alpha-spectrometry. *J. Radioanal. Nucl. Chem.* 253, 395–406. <https://doi.org/10.1023/A:1020413302019>.
- Jo, B.U., Choo, C.O., Kim, M., Lee, Y.-J., Yun, U., Lee, B.-D., 2011. Uranium and radon concentrations in groundwater near the Icheon Granite. *J. Eng. Geol.* 21, 259–269. <https://doi.org/10.9720/KSEG.2011.21.3.259>.
- Jo, Y., Lee, J.-Y., Yun, J.-I., 2018. Adsorption of uranyl tricarbonate and calcium uranyl carbonate onto γ -alumina. *Appl. Geochem.* 94, 28–34. <https://doi.org/10.1016/j.apgeochem.2018.05.004>.
- Jo, Y., Kirishima, A., Kimuro, S., Kim, H.-K., Yun, J.-I., 2019. Formation of $\text{CaUO}_2(\text{CO}_3)_2^{2-}$ and $\text{Ca}_2\text{UO}_2(\text{CO}_3)_3(\text{aq})$ complexes at variable temperatures (10–70 °C). *Dalton Trans* 48, 6942–6950. <https://doi.org/10.1039/C9DT01174A>.
- Jo, Y., Lee, J.-Y., Yun, J.-I., 2022. Chemical thermodynamics of ternary M-An (VI)-CO₃ system (M= Mg, Ca, Sr, and Ba). *Radiochimica Acta* 110 (11), 873–889. <https://doi.org/10.1515/ract-2021-1133>.
- Johnson, K.R., Hu, C., Belshaw, N.S., Henderson, G.M., 2006. Seasonal trace-element and stable-isotope variations in a Chinese speleothem: the potential for high-resolution paleomonsoon reconstruction. *Earth Planet. Sci. Lett.* 244, 394–407.
- Joseph, C., Schmeide, K., Sachs, S., Brendler, V., Geipel, G., Bernhard, G., 2011. Sorption of uranium(VI) onto Opalinus Clay in the absence and presence of humic acid in Opalinus Clay pore water. *Chem. Geol.* 284, 240–250. <https://doi.org/10.1016/j.chemgeo.2011.03.001>.
- Jroundi, F., Merroun, M.L., Arias, J.M., Rossberg, A., Selenska-Pobell, S., González-Muñoz, M.T., 2007. Spectroscopic and microscopic characterization of uranium biomineralization in *Myxococcus xanthus*. *Geomicrobiol. J.* 24, 441–449. <https://doi.org/10.1080/01490450701437651>.
- Juanjuan, S., Zhigang, Y., Bochao, X., Wenhua, D., Dong, X., Xueyan, J., 2014. Concentrations and fluxes of dissolved uranium in the Yellow River estuary: seasonal variation and anthropogenic (Water-Sediment Regulation Scheme) impact. *J. Environ. Radioactiv.* 128, 38–46. <https://doi.org/10.1016/j.jenvrad.2013.11.003>.
- Jung, J., Lee, J., Hahn, P., 2001. Development and application of a sorption data base for the performance assessment of a radwaste repository. *Waste Management* 21, 363–369.
- Jurgens, B.C., Burow, K.R., Dalgish, B.A., Shelton, J.L., 2008. Hydrogeology, Water Chemistry, and Factors Affecting the Transport of Contaminants in the Zone of Contribution of a Public-Supply Well in Modesto, Eastern San Joaquin Valley, California, Scientific Investigations Report 2008–5156. United States Geological Survey, Reston, Virginia, USA.
- Jurgens, B.C., Fram, M.S., Belitz, K., Burow, K.R., Landon, M.K., 2010. Effects of groundwater development on uranium: central Valley, California, USA. *Groundwater* 48, 913–928. <https://doi.org/10.1111/j.1745-6584.2009.00635.x>.
- Kahle, S.C., Welch, W.B., Tecca, A.E., Eliason, D.M., 2018. Uranium Concentrations in Groundwater, Northeastern Washington (Report), Scientific Investigations Map, Report 3401. United States Geological Survey, Reston, VA. <https://doi.org/10.3133/sim3401>.
- Kansal, S., Mehra, R., Singh, N.P., 2011. Uranium concentration in ground water samples belonging to some areas of Western Haryana, India using fission track registration technique. *J. Public Health Epidem.* 3, 352–357.
- Kaplan, D.I., Bertsch, P.M., Adriano, D.C., Orlandini, K.A., 1994. Actinide association with groundwater colloids in a Coastal Plain aquifer. *Radiochim. Acta* 66–67, 181. <https://doi.org/10.1524/ract.1994.6667.special-issue.181>.
- Kaplan, D.I., Buettner, S.W., Li, D., Huang, S., Koster van Groos, P.G., Jaffé, P.R., Seaman, J.C., 2017. *In situ* porewater uranium concentrations in a contaminated wetland: effect of seasons and sediment depth. *Appl. Geochem.* 85, 128–136. <https://doi.org/10.1016/j.apgeochem.2016.11.017>.
- Kappler, A., Benz, M., Schink, B., Brune, A., 2004. Electron shuttling via humic acids in microbial iron(III) reduction in a freshwater sediment. *FEMS Microbiol. Ecol.* 47, 85–92.
- Karamalidis, A.K., Dzombak, D.A., 2011. Surface Complexation Modeling: Gibbsite. John Wiley & Sons, New York.
- Katsoyiannis, I.A., Hug, S.J., Ammann, A., Zikoudi, A., Hatziliontos, C., 2007. Arsenic speciation and uranium concentrations in drinking water supply wells in Northern Greece: correlations with redox indicative parameters and implications for groundwater treatment. *Sci. Tot. Environ.* 383, 128–140. <https://doi.org/10.1016/j.scitotenv.2007.04.035>.
- Kawabata, Y., Aparin, V., Nagai, M., Yamamoto, M., Shiraishi, K., Katayama, Y., 2008. Uranium and thorium isotopes from Kazakhstan. *J. Radioanal. Nucl. Chem.* 278, 459–462. <https://doi.org/10.1007/s10967-008-0904-3>.
- Keesari, T., Mohokar, H.V., Sahoo, B.K., Mallesh, G., 2014. Assessment of environmental radioactive elements in groundwater in parts of Nalgonda district, Andhra Pradesh, South India using scintillation detection methods. *J. Radioanal. Nucl. Chem.* 302, 1391–1398. <https://doi.org/10.1007/s10967-014-3566-3>.
- Keith, S., Faroon, O., Roney, N., Scinicariello, F., Wilbur, S., Ingerman, L., Lladós, F., Plewak, D., Wohlers, D., Diamond, G., 2013. Toxicological Profile for Uranium. Agency for Toxic Substances and Disease Registry, Atlanta, GA, USA.
- Kelly, S.D., Newville, M.G., Cheng, L., Kemner, K.M., Sutton, S.R., Fenter, P., Sturchio, N., Spötl, C., 2003. Uranyl incorporation in natural calcite. *Environ. Sci. Technol.* 37, 1284–1287.
- Kerist, S., Liu, C., 2014. Molecular dynamics simulations of uranyl and uranyl carbonate adsorption at aluminosilicate surfaces. *Environ. Sci. Technol.* 48, 3899–3907. <https://doi.org/10.1021/es405387c>.
- Kerist, S., Bylaska, E.J., Massey, M.S., McBriarty, M.E., Ilton, E.S., 2016. Ab Initio molecular dynamics of uranium incorporated in goethite (α -FeOOH): interpretation of X-ray absorption spectroscopy of trace polyvalent metals. *Inorg. Chem.* 55, 11736–11746. <https://doi.org/10.1021/acs.inorgchem.6b01773>.
- Kersten, M., 2021. Comment on “Enthalpy of uranium adsorption onto hematite. *Environ. Sci. Technol.* 55, 3442–3443.
- Kersting, A.B., Efurud, D.W., Finnegan, D.L., Rokop, D.J., Smith, D.K., Thompson, J.L., 1999. Migration of plutonium in ground water at the Nevada Test Site. *Nature* 397, 56.
- Khan, M.H., Warwick, P., Evans, N., 2006. Spectrophotometric determination of uranium with arsenazo-III in perchloric acid. *Chemosphere* 63, 1165–1169. <https://doi.org/10.1016/j.chemosphere.2005.09.060>.
- Kienzler, B., Metz, V., Brendebach, B., Finck, N., Plaschke, M., Rabung, T., Rothe, J., Schild, D., 2010. Chemical status of U(VI) in cemented waste forms under saline conditions. *Radiochim. Acta* 98, 675–684. <https://doi.org/10.1524/ract.2010.1768>.
- Kimura, T., Serrano, J., Nakayama, S., Takahashi, K., Takeishi, H., 1992. Speciation of uranium in aqueous solutions and in precipitates by photoacoustic spectroscopy. *Radiochim. Acta* 58, 173–173.
- Kimura, T., Kato, Y., Meinrath, G., Yoshida, Z., Choppin, G.R., 1995. Speciation of actinides in aqueous solution by time-resolved laser-induced fluorescence spectroscopy (TRLFS). In: Innovative Laser Technologies in Nuclear Energy. Presented at the Proceedings of the 6th International Symposium on Advanced Nuclear Energy Research, Advanced Science Research Center. Japan Atomic Energy Research Institute, Japan.
- Kinniburgh, D.G., Cooper, D.M., 2004. Predominance and mineral stability diagrams revisited. *Environ. Sci. Technol.* 38, 3641–3648. <https://doi.org/10.1021/es034927l>.
- Kinniburgh, D.G., Jackson, M.L., 1978. Adsorption of mercury (II) by iron hydrous oxide gel. *Soil Sci. Soc. Amer. J.* 42, 45–47.
- Kinniburgh, D.G., van Riemsdijk, W.H., Koopal, L.K., Borkovec, M., Benedetti, M.F., Avena, M.J., 1999. Ion binding to natural organic matter: competition, heterogeneity, stoichiometry and thermodynamic consistency. *Colloid Surface A* 151, 147–166.
- Kirishima, A., Kimura, T., Tochiyama, O., Yoshida, Z., 2003. Luminescence study of tetravalent uranium in aqueous solution. *Chem. Commun.* 910–911. <https://doi.org/10.1039/B300583F>.
- Klinkhammer, G., Palmer, M., 1991. Uranium in the oceans: where it goes and why. *Geochim. Cosmochim. Acta* 55, 1799–1806.

- Knox, A.S., Brimon, R.L., Kaplan, D.I., Paller, M.H., 2008. Interactions among phosphate amendments, microbes and uranium mobility in contaminated sediments. *Sci. Tot. Environ.* 395, 63–71. <https://doi.org/10.1016/j.scitotenv.2008.01.061>.
- Kobayashi, Y., Fukushi, K., Kosugi, S., 2020. A robust model for prediction of U(VI) adsorption onto ferrihydrite consistent with spectroscopic observations. *Environ. Sci. Technol.* 54, 2304–2313. <https://doi.org/10.1021/acs.est.9b06556>.
- Kochhar, N., Gill, G.S., Tuli, N., Dadwal, V., Balaram, V., 2007. Chemical quality of ground water in relation to incidence of cancer in parts of SW Punjab, India. *Asian J. Water Environ. Pollut.* 4, 107–112.
- Komlos, J., Moon, H.S., Jaffé, P.R., 2008. Effect of sulfate on the simultaneous bioreduction of iron and uranium. *J. Environ. Qual.* 37, 2058–2062. <https://doi.org/10.2134/jeq2007.0665>.
- Kominou, A., Sverjensky, D.A., 1995. Pre-ore hydrothermal alteration in an unconformity-type uranium deposit. *Contrib. Mineral. Petr.* 121, 99. <https://doi.org/10.1007/s004100050092>.
- Koopal, L., Tan, W., Avena, M., 2020. Equilibrium mono- and multicomponent adsorption models: from homogeneous ideal to heterogeneous non-ideal binding. *Adv. Colloid Interf.* 280, 102138.
- Korkisch, J., Gödl, L., 1974. Determination of uranium in natural waters after anion-exchange separation. *Anal. Chim. Acta* 71, 113–121. [https://doi.org/10.1016/S0003-2670\(01\)82876-2](https://doi.org/10.1016/S0003-2670(01)82876-2).
- Kosmulski, M., 2009. pH-dependent surface charging and points of zero charge. IV. Update and new approach. *J. Colloid. Interf. Sci.* 337, 439–448.
- Kowal-Fouchard, A., Drot, R., Simoni, E., Ehrhardt, J.J., 2004. Use of spectroscopic techniques for uranium(VI)/montmorillonite interaction modeling. *Environ. Sci. Technol.* 38, 1399–1407. <https://doi.org/10.1021/es0348344>.
- Kratz, S., Schnug, E., 2006. Rock phosphates and P fertilizers as sources of U contamination in agricultural soils. In: Merkel, B.J., Hasche-Berger, A. (Eds.), *Uranium in the Environment*. Springer, Berlin & Heidelberg, pp. 57–67.
- Kratz, S., Schick, J., Schnug, E., 2016. Trace elements in rock phosphates and P containing mineral and organo-mineral fertilizers sold in Germany. *Sci. Tot. Environ.* 542, 1013–1019.
- Křepelová, A., Sachs, S., Bernhard, G., 2006. Uranium(VI) sorption onto kaolinite in the presence and absence of humic acid. *Radiochim. Acta* 94, 825. <https://doi.org/10.1524/ract.2006.94.12.825>.
- Kretzschmar, R., Borkovec, M., Grolimund, D., Elimelech, M., 1999. Mobile subsurface colloids and their role in contaminant transport. *Adv. Agron.* 66, 121–193.
- Kubicki, J.D., Halada, G.P., Jha, P., Phillips, B.L., 2009. Quantum mechanical calculation of aqueous uranium complexes: carbonate, phosphate, organic and biomolecular species. *Chem. Cent. J.* 3, 1–29.
- Kulkarni, S., Ballal, A., Apte, S.K., 2013. Bioprecipitation of uranium from alkaline waste solutions using recombinant *Deinococcus radiodurans*. *J. Hazard Mater.* 262, 853–861.
- Kulkarni, S., Misra, C.S., Gupta, A., Ballal, A., Apte, S.K., 2016. Interaction of uranium with bacterial cell surfaces: inferences from phosphate-mediated uranium precipitation. *Appl. Environ. Microbiol.* 82, 4965–4974.
- Kumar, S.S., Dhara, S., 2022. Energy dispersive X-ray fluorescence determination of uranium in different uranates using Rh K α scattered peaks for matrix correction. *Spectrochim. Acta B* 193, 106427. <https://doi.org/10.1016/j.sab.2022.106427>.
- Kumar, A., Tripathi, R.M., Sabiyasachi, R., Mishra, M.K., Ravi, P.M., Ghosh, A.K., 2014. Characterization of groundwater composition in Punjab state with special emphasis on uranium content, speciation and mobility. *Radiochim. Acta* 102, 239. <https://doi.org/10.1515/ract-2014-2109>.
- Kumar, M.P., Purna, S., Akash, K., Prasad, M.K., 2015. Uranium in ground water of eastern Uttar Pradesh, India: a preliminary study. *Int. Res. J. Env. Sci.* 4, 70–74.
- Kumar, D., Singh, A., Jha, R.K., Sahoo, S.K., Jha, V., 2018. Using spatial statistics to identify the uranium hotspot in groundwater in the mid-eastern Gangetic plain, India. *Environ. Earth Sci.* 77, 702. <https://doi.org/10.1007/s12665-018-7889-1>.
- Kunze, C., Kiessig, G., Kuchler, A., 2007. Management of passive biological water treatment systems for mine effluents. In: *Advanced Science and Technology for Biological Decontamination of Sites Affected by Chemical and Radiological Nuclear Agents*. Springer, Berlin & Heidelberg, pp. 177–195.
- Kurttila, P., Auvinen, A., Salonen, L., Saha, H., Pekkanen, I., Väisänen, S.B., Penttilä, I., Komulainen, H., Hannu, Komulainen, 2002. Renal effects of uranium in drinking water. *Environ. Health Persp.* 110, 337–342. <https://doi.org/10.1289/ehp.02110337>.
- Kurttila, P., Komulainen, H., Leino, A., Salonen, L., Auvinen, A., Saha, H., 2005. Bone as a possible target of chemical toxicity of natural uranium in drinking water. *Environ. Health Persp.* 113, 68–72. <https://doi.org/10.1289/ehp.7475>.
- Kurttila, P., Harmoinen, A., Saha, H., Salonen, L., Karpas, Z., Komulainen, H., Auvinen, A., 2006. Kidney toxicity of ingested uranium from drinking water. *Am. J. Kidney Dis.* 47, 972–982. <https://doi.org/10.1053/j.ajkd.2006.03.002>.
- Lachniet, M.S., Bernal, J.P., Asmerom, Y., Polyak, V., 2012. Uranium loss and aragonite-calcite age discordance in a calcitized aragonite stalagmite. *Quat. Geochronol.* 14, 26–37.
- Ladeira, A.C.Q., Gonçalves, C.R., 2007. Influence of anionic species on uranium separation from acid mine water using strong base resins. *J. Hazard Mater.* 148, 499–504. <https://doi.org/10.1016/j.jhazmat.2007.03.003>.
- Lagneau, V., Regnault, O., Descostes, M., 2019. Industrial deployment of reactive transport simulation: an application to uranium *in situ* recovery. *Rev. Min. Geochem.* 85, 499–528.
- Lahrouch, F., Guo, N., Hunault, M.O., Solari, P.L., Descostes, M., Gerard, M., 2021. Uranium retention on iron oxyhydroxides in post-mining environmental conditions. *Chemosphere* 264, 128473.
- Landsberger, S., Kapsimalis, R., 2013. Comparison of neutron activation analysis techniques for the determination of uranium concentrations in geological and environmental materials. *J. Environ. Radioactiv.* 117, 41–44. <https://doi.org/10.1016/j.jenvrad.2011.08.014>.
- Langmuir, D., 1978. Uranium solution-mineral equilibria at low temperatures with applications to sedimentary ore deposits. *Geochim. Cosmochim. Acta* 42, 547–569. [https://doi.org/10.1016/0016-7037\(78\)90001-7](https://doi.org/10.1016/0016-7037(78)90001-7).
- Lanzoni, M., 2019. Rain Events and Recharge Processes in the San Luis Valley of Southern Colorado (D. Phil thesis). University of Oxford, Oxford, UK.
- Lapworth, D.J., Brauns, B., Chattopadhyay, S., Goody, D.C., Loveless, S.E., MacDonald, A.M., McKenzie, A.A., Muddu, S., Nara, S.N.V., 2021. Elevated uranium in drinking water sources in basement aquifers of southern India. *Appl. Geochem.* 133, 105092. <https://doi.org/10.1016/j.apgeochem.2021.105092>.
- Lartigue, J.E., Charrasse, B., Reile, B., Descostes, M., 2020. Aqueous inorganic uranium speciation in European stream waters from the FOREGS dataset using geochemical modelling and determination of a U bioavailability baseline. *Chemosphere* 251, 126302. <https://doi.org/10.1016/j.chemosphere.2020.126302>.
- Lau, K.V., Romaniello, S.J., Zhang, F., 2019. The Uranium Isotope Paleoredox Proxy. Cambridge University Press, Cambridge, UK.
- Lee, M.H., Choi, G.S., Cho, Y.H., Lee, C.W., Shin, H.S., 2001. Concentrations and activity ratios of uranium isotopes in the groundwater of the Okchun Belt in Korea. *J. Environ. Radioactiv.* 57, 105–116. [https://doi.org/10.1016/S0265-931X\(01\)00014-5](https://doi.org/10.1016/S0265-931X(01)00014-5).
- Lefebvre, P., Le Pape, P., Mangeret, A., Gourgiotis, A., Sabatier, P., Louvat, P., Diez, O., Mathon, O., Hunault, M.O., Baya, C., 2022. Uranium sorption to organic matter and long-term accumulation in a pristine alpine wetland. *Geochimica et Cosmochimica Acta* 338, 322–346. <https://doi.org/10.1016/j.gca.2022.10.018>.
- Lefevre, G., Noinville, S., Fédroff, M., 2006. Study of uranyl sorption onto hematite by *in situ* attenuated total reflection-infrared spectroscopy. *J. Colloid. Interf. Sci.* 296, 608–613.
- Lenhart, J.J., Honeyman, B.D., 1999. Uranium(VI) sorption to hematite in the presence of humic acid. *Geochim. Cosmochim. Acta* 63, 2891–2901. [https://doi.org/10.1016/S0016-7037\(99\)00269-0](https://doi.org/10.1016/S0016-7037(99)00269-0).
- Leventhal, J.S., Daws, T.A., Frye, J.S., 1986. Organic geochemical analysis of sedimentary organic matter associated with uranium. *Appl. Geochem.* 1, 241–247.
- Leybourne, M.I., Cameron, E.M., 2008. Source, transport, and fate of rhenium, selenium, molybdenum, arsenic, and copper in groundwater associated with porphyry-Cu deposits, Atacama Desert, Chile. *Chem. Geol.* 247, 208–228. <https://doi.org/10.1016/j.chemgeo.2007.10.017>.
- Li, P., Hur, J., 2017. Utilization of UV-Vis spectroscopy and related data analyses for dissolved organic matter (DOM) studies: a review. *Crit. Rev. Env. Sci. Tec.* 47, 131–154.
- Li, L., Gawande, N., Kowalsky, M.B., Steefel, C.I., Hubbard, S.S., 2011. Physicochemical heterogeneity controls on uranium bioreduction rates at the field scale. *Environ. Sci. Technol.* 45, 9959–9966. <https://doi.org/10.1021/es201111y>.
- Li, Z., Chi, G., Bethune, K., 2016. The effects of basement faults on thermal convection and implications for the formation of unconformity-related uranium deposits in the Athabasca Basin, Canada. *Geofluids* 16, 729–751. <https://doi.org/10.1111/gfl.12180>.
- Li, B., Zhou, J., Priest, C., Jiang, D., 2017. Effect of salt on the uranyl binding with carbonate and calcium ions in aqueous solutions. *J. Phys. Chem. B* 121, 8171–8178.
- Li, X., Xiong, C., Sun, K., Fang, F., Zhang, Q., 2021. Optimization of ICP-OES's parameters for uranium analysis of rock samples. *J. Korean Phys. Soc.* 78, 737–742.
- Li, J., Weng, L., Deng, Y., Ma, J., Chen, Y., Li, Y., 2022. NOM-mineral interaction: significance for speciation of cations and anions. *Sci. Tot. Environ.* 820, 153259. <https://doi.org/10.1016/j.scitotenv.2022.153259>.
- Liang, X., Hillier, S., Pendrowski, H., Gray, N., Ceci, A., Gadd, G.M., 2015. Uranium phosphate biomineralization by fungi. *Environmental Microbiology* 17, 2064–2075. <https://doi.org/10.1111/1462-2920.12771>.
- Liesch, T., Hinrichsen, S., Goldscheider, N., 2015. Uranium in groundwater — fertilizers versus geogenic sources. *Sci. Tot. Environ.* 536, 981–995. <https://doi.org/10.1016/j.scitotenv.2015.05.133>.
- Liger, E., Charlet, L., Van Cappellen, P., 1999. Surface catalysis of uranium(VI) reduction by iron(II). *Geochim. Cosmochim. Acta* 63, 2939–2955.
- Linhoff, B.S., Bennett, P.C., Puntsgag, T., Gerel, O., 2011. Geochemical evolution of uraniumiferous soda lakes in Eastern Mongolia. *Environ. Earth Sciences* 62, 171–183. <https://doi.org/10.1007/s12665-010-0512-8>.
- Linhoff, B., Longmire, P., Rearick, M., McQuillan, D., Perkins, G., 2016. Water quality and hydrogeochemistry of a basin and range watershed in a semi-arid region of northern New Mexico. *Environ. Earth Sci.* 75. <https://doi.org/10.1007/s12665-015-5179-8>.
- Liu, J., Brown, A.K., Meng, X., Cropek, D.M., Istok, J.D., Watson, D.B., Lu, Y., 2007. A catalytic beacon sensor for uranium with parts-per-trillion sensitivity and millionfold selectivity. *Proc. Natl. Acad. Sci. USA* 104, 2056–2061.
- Lofts, S., Fevrier, L., Horemans, N., Gilbin, R., Bruggeman, C., Vandenhove, H., 2015. Assessment of co-contaminant effects on uranium and thorium speciation in freshwater using geochemical modelling. *J. Environ. Radioactiv.* 149, 99–109. <https://doi.org/10.1016/j.jenvrad.2015.07.011>.
- Long, P.E., Williams, K.H., Davis, J.A., Fox, P.M., Wilkins, M.J., Yabusaki, S.B., Fang, Y., Waicher, S.R., Berman, E.S., Gupta, M., 2015. Bicarbonate impact on U(VI) bioreduction in a shallow alluvial aquifer. *Geochim. Cosmochim. Acta* 150, 106–124.
- Lopez, A.M., Wells, A., Fendorf, S., 2020. Soil and aquifer properties combine as predictors of groundwater uranium concentrations within the Central Valley, California. *Environ. Sci. Technol.* 55, 352–361.
- Lopez-Fernandez, M., Romero-González, M., Günther, A., Solari, P.L., Merroun, M.L., 2018. Effect of U(VI) aqueous speciation on the binding of uranium by the cell surface of *Rhodotorula mucilaginosa*, a natural yeast isolate from bentonites. *Chemosphere* 199, 351–360.

- Loreggian, L., Sorwat, J., Byrne, J.M., Kappler, A., Bernier-Latmani, R., 2020. Role of iron sulfide phases in the stability of noncrystalline tetravalent uranium in sediments. *Environ. Sci. Technol.* 54, 4840–4846.
- Lothenbach, B., Kulik, D.A., Matschel, T., Balonis, M., Baquerizo, L., Dilnesa, B., Miron, G.D., Myers, R.J., 2019. Cemdata18: a chemical thermodynamic database for hydrated Portland cements and alkali-activated materials. *Cement Concrete Res* 115, 472–506.
- Lovley, D.R., Phillips, E.J., 1992. Reduction of uranium by *Desulfovibrio desulfuricans*. *Appl. Environ. Microbiol.* 58, 850–856. <https://doi.org/10.1128/aem.58.3.850-856.1992>.
- Lovley, D.R., Phillips, E.J., Gorby, Y.A., Landa, E.R., 1991. Microbial reduction of uranium. *Nature* 350, 413–416.
- Lu, G., Haes, A.J., Forbes, T.Z., 2018. Detection and identification of solids, surfaces, and solutions of uranium using vibrational spectroscopy. *Coord. Chem. Rev.* 374, 314–344.
- Lu, P., Zhang, G., Apps, J., Zhu, C., 2022. Comparison of thermodynamic data files for PHREEQC. *Earth-Sci. Rev.* 225, 103888 <https://doi.org/10.1016/j.earsci.2021.103888>.
- Luan, F., Burgos, W.D., 2012. Sequential extraction method for determination of Fe(II/III) and U(IV/VI) in suspensions of iron-bearing phyllosilicates and uranium. *Environ. Sci. Technol.* 46, 11995–12002.
- Luo, J., Weber, F.-A., Cirpka, O.A., Wu, W.-M., Nyman, J.L., Carley, J., Jardine, P.M., Criddle, C.S., Kitanidis, P.K., 2007. Modeling in-situ uranium(VI) bioreduction by sulfate-reducing bacteria. *J. Contam. Hydrol.* 92, 129–148. <https://doi.org/10.1016/j.jconhyd.2007.01.004>.
- Luo, Q., Zhong, N., Qin, J., Li, K., Zhang, Y., Wang, Y., Ma, L., 2014. Thucholite in Mesoproterozoic shales from northern north China: occurrence and indication for thermal maturity. *Int. J. Coal Geol.* 125, 1–9. <https://doi.org/10.1016/j.coal.2014.01.009>.
- Luo, J.-C., Hu, R.-Z., Fayek, M., Li, C.-S., Bi, X.-W., Abdu, Y., Chen, Y.-W., 2015. In-situ SIMS uraniumite U–Pb dating and genesis of the Xianshi granite-hosted uranium deposit, South China. *Ore Geol. Rev.* 65, 968–978. <https://doi.org/10.1016/j.oregeorev.2014.06.016>.
- Lyons, W.B., Gardner, C.B., Welch, S.A., Israel, S., 2020. Uranium in Ohio, USA surface waters: implications for a fertilizer source in waters draining agricultural lands. *Sci. Rep.-UK* 10, 5151. <https://doi.org/10.1038/s41598-020-61922-2>.
- Ma, R., Zheng, C., Prommer, H., Greskowiak, J., 2011. Modelling Field-Scale Uranium Mass Transfer at the Hanford IFRC Site. IAHS-AISH Publication.
- Ma, R., Liu, C., Greskowiak, J., Prommer, H., Zachara, J., Zheng, C., 2014. Influence of calcite on uranium(VI) reactive transport in the groundwater-river mixing zone. *J. Contam. Hydrol.* 156, 27–37. <https://doi.org/10.1016/j.jconhyd.2013.10.002>.
- Ma, S., Huang, L., Ma, L., Shim, Y., Islam, S.M., Wang, P., Zhao, L.-D., Wang, S., Sun, G., Yang, X., Kanatzidis, M.G., 2015. Efficient uranium capture by polysulfide/layered double hydroxide composites. *J. Am. Chem. Soc.* 137, 3670–3677. <https://doi.org/10.1021/jacs.5b00762>.
- Ma, B., Fernandez-Martinez, A., Kang, M., Wang, K., Lewis, A.R., Maffei, T.G., Findling, N., Salas-Colera, E., Tisserand, D., Bureau, S., 2020. Influence of surface compositions on the reactivity of pyrite toward aqueous U(VI). *Environ. Sci. Technol.* 54, 8104–8114.
- Maas, R., 1989. Nd-Sr isotope constraints on the age and origin of unconformity-type uranium deposits in the Alligator Rivers uranium field, Northern Territory, Australia. *Econ. Geol.* 84, 64–90. <https://doi.org/10.2113/gsecongeo.84.1.64>.
- Maher, K., Bargar, J.R., Brown, G.E., 2013. Environmental speciation of actinides. *Inorg. Chem.* 52, 3510–3532. <https://doi.org/10.1021/ic301686d>.
- Mahoney, J.J., Cadle, S.A., Jakubowski, R.T., 2009. Uranyl adsorption onto hydrous ferric oxide—a re-evaluation for the diffuse layer model database. *Environ. Sci. Technol.* 43, 9260–9266. <https://doi.org/10.1021/es901586v>.
- Makubalo, S.S., Diamond, R.E., 2020. Hydrochemical evolution of high uranium, fluoride and nitrate groundwaters of Namakwaland, South Africa. *J. Afr. Earth Sci.* 172, 104002.
- Mangini, A., Sonntag, C., Bertsch, G., Müller, E., 1979. Evidence for a higher natural uranium content in world rivers. *Nature* 278, 337–339. <https://doi.org/10.1038/278337a0>.
- Marang, L., Reiller, P., Pepe, M., Benedetti, M.F., 2006. Donnan membrane approach: from equilibrium to dynamic speciation. *Environ. Sci. Technol.* 40, 5496–5501.
- Markich, S.J., 2002. Uranium speciation and bioavailability in aquatic systems: an overview. *The Scientific World* 2.
- Markich, S.J., Twining, J.R., 2012. Radioecology of tropical freshwater ecosystems: mechanisms and kinetics of bioaccumulation and the importance of water chemistry. In: Twining, J.R. (Ed.), *Tropical Radioecology, Radioactivity in the Environment*. Elsevier, pp. 231–280.
- Marques Fernandes, M., Baeyens, B., Dähn, R., Scheinost, A.C., Bradbury, M.H., 2012. U(VI) sorption on montmorillonite in the absence and presence of carbonate: a macroscopic and microscopic study. *Geochim. Cosmochim. Acta* 93, 262–277. <https://doi.org/10.1016/j.gca.2012.04.017>.
- Marshall, T.A., Morris, K., Law, G.T.W., Livens, F.R., Mosselmans, J.F.W., Bots, P., Shaw, S., 2014. Incorporation of uranium into hematite during crystallization from ferrihydrite. *Environ. Sci. Technol.* 48, 3724–3731. <https://doi.org/10.1021/es500212a>.
- Martinez, S.E., Carrillo-Rivera, J.J., 2006. Socio-economic constraints of groundwater in capital La Rioja, Argentina. *Environ. Geol.* 49, 875–886. <https://doi.org/10.1007/s00254-006-0183-7>.
- Martinez, J.S., Santillan, E.-F., Bossant, M., Costa, D., Ragoussi, M.-E., 2019. The new electronic database of the NEA thermochemical database project. *Appl. Geochem.* 107, 159–170. <https://doi.org/10.1016/j.apgeochem.2019.05.007>.
- Martinez-Aguirre, A., Garcialeon, M., Ivanovich, M., 1994. The distribution of U, Th and Ra-226 derived from the phosphate fertilizer industries on an estuarine system in southwest Spain. *J. Environ. Radioact.* 22, 155–177. [https://doi.org/10.1016/0265-931X\(94\)90020-5](https://doi.org/10.1016/0265-931X(94)90020-5).
- Massey, M.S., Lezama-Pacheco, J.S., Jones, M.E., Ilton, E.S., Cerrato, J.M., Bargar, J.R., Fendorf, S., 2014a. Competing retention pathways of uranium upon reaction with Fe(II). *Geochim. Cosmochim. Acta* 142, 166–185. <https://doi.org/10.1016/j.gca.2014.07.016>.
- Massey, M.S., Lezama-Pacheco, J.S., Nelson, J.M., Fendorf, S., Maher, K., 2014b. Uranium incorporation into amorphous silica. *Environ. Sci. Technol.* 48, 8636–8644. <https://doi.org/10.1021/es501064m>.
- Matteoda, E., Blarasin, M., Lutri, V., Giacobone, D., Maldonado, L., Quinodoz, F.B., Albo, J.G., Cabrera, A., 2019. Uranium in groundwater in the sedimentary aquifer of the eastern sector of Valle de la Cruz, Córdoba, Argentina. *Int. J. Eng. Appl. Sci.* 6, 20–25.
- McBriarty, M.E., Soltis, J.A., Kerisit, S., Qafoku, O., Bowden, M.E., Bylaska, E.J., De Yoreo, J.J., Ilton, E.S., 2017. Trace uranium partitioning in a multiphase nano-FeOOH system. *Environ. Sci. Technol.* 51, 4970–4977. <https://doi.org/10.1021/acs.est.7b00432>.
- McBriarty, M.E., Kerisit, S., Bylaska, E.J., Shaw, S., Morris, K., Ilton, E.S., 2018. Iron vacancies accommodate uranyl incorporation into hematite. *Environ. Sci. Technol.* 52, 6282–6290.
- McDonald, B.S., Partin, C.A., Sageman, B., Holmden, C., 2022. Uranium isotope reconstruction of ocean deoxygenation during OAE 2 hampered by uncertainties in fractionation factors and local U-cycling. *Geochim. Cosmochim. Acta*. <https://doi.org/10.1016/j.gca.2022.05.010>.
- McKinley, I., Scholits, A., 1993. A comparison of radionuclide sorption databases used in recent performance assessments. *J. Contam. Hydrol.* 13, 347–363.
- McKinley, J.P., Zachara, J.M., Smith, S.C., Turner, G.D., 1995. The influence of uranyl hydrolysis and multiple site-binding reactions on adsorption of U(VI) to montmorillonite. *Clays Clay Miner* 43, 586.
- McKinley, J., Zachara, J., Liu, C., Heald, S., Prenitzer, B., Kempshall, B., 2006. Microscale controls on the fate of contaminant uranium in the vadose zone, Hanford Site, Washington. *Geochim. Cosmochim. Acta* 70, 1873–1887. <https://doi.org/10.1016/j.gca.2005.10.037>.
- McKinley, J.P., Zachara, J.M., Wan, J., McCready, D.E., Heald, S.M., 2007. Geochemical controls on contaminant uranium in vadose Hanford formation sediments at the 200 area and 300 area, Hanford site, Washington. *Vadose Zone J* 6, 1004–1017. <https://doi.org/10.2136/vzj2006.0184>.
- McManus, J., Berelson, W.M., Klinkhammer, G.P., Hammond, D.E., Holm, C., 2005. Authigenic uranium: relationship to oxygen penetration depth and organic carbon rain. *Geochim. Cosmochim. Acta* 69, 95–108.
- Meeussen, J.C., 2003. ORCHESTRA: an object-oriented framework for implementing chemical equilibrium models. *Environ. Sci. Technol.* 37, 1175–1182.
- Meeussen, J., van der Sloot, H., Dijkstra, J., Kosson, D., 2009. Review of Thermodynamic and Adsorption Databases. CBP-TR-2009-002.
- Mehra, R., Singh, S., Singh, K., 2007. Uranium studies in water samples belonging to Malwa region of Punjab, using track etching technique. *Radiat. Meas.* 42, 441–445. <https://doi.org/10.1016/j.radmeas.2007.01.040>.
- Mehta, V.S., Maillot, F., Wang, Z., Catalano, J.G., Giammar, D.E., 2015. Transport of U(VI) through sediments amended with phosphate to induce *in situ* uranium immobilization. *Water Res* 69, 307–317. <https://doi.org/10.1016/j.watres.2014.11.044>.
- Mehta, V.S., Maillot, F., Wang, Z., Catalano, J.G., Giammar, D.E., 2016. Effect of reaction pathway on the extent and mechanism of uranium(VI) immobilization with calcium and phosphate. *Environ. Sci. Technol.* 50, 3128–3136. <https://doi.org/10.1021/acs.est.5b06212>.
- Meinrath, G., 1997. Uranium(VI) speciation by spectroscopy. *J. Radioanal. Nucl. Chem.* 224, 119–126. <https://doi.org/10.1007/BF02034623>.
- Mendez, J.C., Hiemstra, T., 2020. High and low affinity sites of ferrihydrite for metal ion adsorption: data and modeling of the alkaline-earth ions Be, Mg, Ca, Sr, Ba, and Ra. *Geochim. Cosmochim. Acta* 286, 289–305.
- Mendez, J.C., Hiemstra, T., Koopmans, G.F., 2020. Assessing the reactive surface area of soils and the association of soil organic carbon with natural oxide nanoparticles using ferrihydrite as proxy. *Environ. Sci. Technol.* 54, 11990–12000.
- Merroun, M.L., Raff, J., Rossberg, A., Hennig, C., Reich, T., Selenska-Pobell, S., 2005. Complexation of uranium by cells and S-layer sheets of *Bacillus sphaericus* JG-A12. *Applied and Environmental Microbiology* 71, 5532–5543.
- Metzger, S.C., Rogers, K.T., Bostick, D.A., McBay, E.H., Ticknor, B.W., Manard, B.T., Hexel, C.R., 2019. Optimization of uranium and plutonium separations using TEVA and UTEVA cartridges for MC-ICP-MS analysis of environmental swipe samples. *Talanta* 198, 257–262. <https://doi.org/10.1016/j.talanta.2019.02.034>.
- Mibus, J., Sachs, S., Pflingsten, W., Nebelung, C., Bernhard, G., 2007. Migration of uranium(IV)/(VI) in the presence of humic acids in quartz sand: a laboratory column study. *J. Contam. Hydrol.* 89, 199–217. <https://doi.org/10.1016/j.jconhyd.2006.08.005>.
- Michie, U.M., 1970. Uranium in the Old Red Sandstone of Caithness, WF/AG/70/30. British Geological Survey, Keyworth, Nottingham.
- Michon, J., Frelon, S., Garnier, C., Coppin, F., 2010. Determinations of uranium(VI) binding properties with some metalloproteins (transferrin, albumin, metallothionein and ferritin) by fluorescence quenching. *Journal of Fluorescence* 20, 581–590. <https://doi.org/10.1007/s10895-009-0587-3>.
- Mikutka, C., Langner, P., Bargar, J.R., Kretzschmar, R., 2016. Tetra- and hexavalent uranium forms bidentate-monoanuclear complexes with particulate organic matter in a naturally uranium-enriched peatland. *Environ. Sci. Technol.* 50, 10465–10475. <https://doi.org/10.1021/acs.est.6b03688>.

- Miller, W., Alexander, R., Chapman, N., McKinley, I., Smellie, J., 2000. Geological Disposal of Radioactive Wastes and Natural Analogues, 2. Pergamon, Amsterdam.
- Milne, C.J., Kinniburgh, D.G., De Wit, J.C.M., Van Riemsdijk, W.H., Koopal, L.K., 1995. Analysis of proton binding by a peat humic acid using a simple electrostatic model. *Geochim. Cosmochim. Acta* 59, 1101–1112.
- Milne, C.J., Kinniburgh, D.G., Tipping, E., 2001. Generic NICA-Donnan model parameters for proton binding by humic substances. *Environ. Sci. Technol.* 35, 2049–2059.
- Milne, C.J., Kinniburgh, D.G., Van Riemsdijk, W.H., Tipping, E., 2003. Generic NICA-Donnan model parameters for metal-ion binding by humic substances. *Environ. Sci. Technol.* 37, 958–971.
- Milvey, P., Cothorn, C.R., 1990. Scientific background for the development of regulations for radionuclides in drinking water. In: Cothorn, C.R., Rebers, P.A. (Eds.), *Radon, Radium and Uranium in Drinking Water*. Lewis Publishers, Chelsea, Michigan, pp. 1–16.
- Missana, T., García-Gutiérrez, M., Maffiotte, C., 2003. Experimental and modeling study of the uranium(VI) sorption on goethite. *J. Colloid. Interf. Sci.* 260, 291–301. [https://doi.org/10.1016/S0021-9797\(02\)00246-1](https://doi.org/10.1016/S0021-9797(02)00246-1).
- Missimer, T.M., Teaf, C., Maliva, R.G., Danley-Thomson, A., Covert, D., Hegy, M., 2019. Natural radiation in the rocks, soils, and groundwater of southern Florida with a discussion on potential health impacts. *International Journal of Environmental Research and Public Health* 16. <https://doi.org/10.3390/ijerph16101793>.
- Mizuoka, K., Grenthe, I., Ikeda, Y., 2005. Structural and kinetic studies on uranyl(V) carbonate complex using ¹³C NMR spectroscopy. *Inorg. Chem.* 44, 4472–4474.
- Mochizuki, A., Hosoda, K., Sugiyama, M., 2016. Characteristic seasonal variation in dissolved uranium concentration induced by the change of lake water pH in Lake Biwa, Japan. *Limnology* 17, 127–142. <https://doi.org/10.1007/s10201-015-0469-0>.
- Moncur, M.C., Paktunc, D., Thibault, Y., Birks, S.J., Wieser, M., 2011. *Uranium and Arsenic Sources in Shallow Groundwater Near Bonnyville, Alberta: a Mineralogy Study*. Government of Alberta.
- Morales-Arredondo, J.I., Hernandez, M.A.A., Hernandez-Mendiola, E., Estrada-Hernandez, R.E., Bermea, O.M., 2018. Hydrogeochemical behavior of uranium and thorium in rock and groundwater samples from southeastern of El Bajío Guanajuatense, Guanajuato, Mexico. *Env. Earth Sci* 77, 567. <https://doi.org/10.1007/s12665-018-7749-z>.
- Morrison, S.J., Metzler, D.R., Dwyer, B.P., 2002. Removal of As, Mn, Mo, Se, U, V and Zn from groundwater by zero-valent iron in a passive treatment cell: reaction progress modeling. *J. Contam. Hydrol.* 56, 99–116. [https://doi.org/10.1016/S0169-7722\(01\)00205-4](https://doi.org/10.1016/S0169-7722(01)00205-4).
- Moulin, C., Beaucaire, C., Decambox, P., Mauchien, P., 1990. Determination of uranium in solution at the ng l⁻¹ level by time-resolved laser-induced spectrofluorimetry: application to geological samples. *Analytica Chimica Acta* 238, 291–296. [https://doi.org/10.1016/S0003-2670\(00\)80550-4](https://doi.org/10.1016/S0003-2670(00)80550-4).
- Mudd, G.M., 2014. The future of Yellowcake: a global assessment of uranium resources and mining. *Sci. Tot. Environ.* 472, 590–607. <https://doi.org/10.1016/j.scitotenv.2013.11.070>.
- Mühr-Ebert, E.L., Wagner, F., Walther, C., 2019. Speciation of uranium: compilation of a thermodynamic database and its experimental evaluation using different analytical techniques. *Appl. Geochem.* 100, 213–222. <https://doi.org/10.1016/j.apgeochem.2018.10.006>.
- Müller, K., Brendler, V., Foerstendorf, H., 2008. Aqueous uranium(VI) hydrolysis species characterized by attenuated total reflection fourier-transform infrared spectroscopy. *Inorg. Chem.* 47, 10127–10134. <https://doi.org/10.1021/ic8005103>.
- Müller, K., Foerstendorf, H., Brendler, V., Rossberg, A., Stolze, K., Gröschel, A., 2013. The surface reactions of U(VI) on γ -Al₂O₃ — *In situ* spectroscopic evaluation of the transition from sorption complexation to surface precipitation. *Chem. Geol.* 357, 75–84. <https://doi.org/10.1016/j.chemgeo.2013.08.033>.
- Müller, K., Foerstendorf, H., Steudtner, R., Tsushima, S., Kumke, M.U., Lefevre, G., Rothe, J., Mason, H., Szabó, Z., Yang, P., 2019. Interdisciplinary round-robot test on molecular spectroscopy of the U(VI) acetate system. *ACS Omega* 4, 8167–8177.
- Murakami, T., Ohnuki, T., Isobe, H., Sato, T., 1997. Mobility of uranium during weathering. *Amer. Mineral.* 82, 888–899. <https://doi.org/10.2138/am-1997-9-1006>.
- Murakami, T., Sato, T., Ohnuki, T., Isobe, H., 2005. Field evidence for uranium nanocrystallization and its implications for uranium transport. *Chem. Geol.* 221, 117–126. <https://doi.org/10.1016/j.chemgeo.2005.04.004>.
- Murphy, A.M., 1998. *Sediment and Groundwater Geochemistry of the Chalk in Southern England* (Ph.D Thesis). Kingston University. Kingston University, Kingston Upon Thames.
- Murphy, R.J., Lenhart, J.J., Honeyman, B.D., 1999. The sorption of thorium(IV) and uranium(VI) to hematite in the presence of natural organic matter. *Colloid Surface A* 157, 47–62. [https://doi.org/10.1016/S0927-7757\(99\)00115-6](https://doi.org/10.1016/S0927-7757(99)00115-6).
- Murphy, M.J., Stirling, C.H., Kaltenbach, A., Turner, S.P., Schaefer, B.F., 2014. Fractionation of ²³⁸U/²³⁵U by reduction during low temperature uranium mineralisation processes. *Earth Planet. Sci. Lett.* 388, 306–317. <https://doi.org/10.1016/j.epsl.2013.11.034>.
- Murphy, M.J., Froehlich, M.B., Fifield, L.K., Turner, S.P., Schaefer, B.F., 2015. *In-situ* production of natural ²³⁶U in groundwaters and ores in high-grade uranium deposits. *Chem. Geol.* 410, 213–222. <https://doi.org/10.1016/j.chemgeo.2015.06.024>.
- Myers, C.R., Nealson, K.H., 1988. Bacterial manganese reduction and growth with manganese oxide as the sole electron acceptor. *Science* 240, 1319–1321.
- NEA and OECD, 2020. *Uranium 2020: Resources, Production and Demand*, 28th Edition. Nuclear Energy Agency and Organisation for Economic Co-operation and Development, Paris, France. NEA No. 7551.
- Neiva, A.M.R., Carvalho, P.C.S., Antunes, I.M.H.R., Silva, M.M.V.G., Santos, A.C.T., Cabral Pinto, M.M.S., Cunha, P.P., 2014. Contaminated water, stream sediments and soils close to the abandoned Pinhal do Souto uranium mine, central Portugal. *J. Geochem. Explor.* 136, 102–117. <https://doi.org/10.1016/j.gexplo.2013.10.014>.
- Nelson, A.W., Eitheim, E.S., Knight, A.W., May, D., Mehrhoff, M.A., Shannon, R., Litman, R., Laughlin, W.C., Forbes, T.Z., Schultz, M.K., 2015. Understanding the radioactive ingrowth and decay of naturally occurring radioactive materials in the environment: an analysis of produced fluids from the marcellus shale. *Environmental Health Perspectives* 123, 689–696. <https://doi.org/10.1289/ehp.1408855>.
- Neymark, L.A., Paces, J.B., 2000. Consequences of slow growth for ²³⁰Th/U dating of Quaternary opals, Yucca Mountain, NV, USA. *Chem. Geol.* 164, 143–160. [https://doi.org/10.1016/S0009-2541\(99\)00142-4](https://doi.org/10.1016/S0009-2541(99)00142-4).
- Nicolli, H.B., Bundschuh, J., Blanco, M., del, C., Tujchneider, O.C., Panarello, H.O., Dapeña, C., Rusansky, J.E., 2012a. Arsenic and associated trace-elements in groundwater from the Chaco-Pampean plain, Argentina: results from 100 years of research. *Sci. Tot. Environ.* 429, 36–56. <https://doi.org/10.1016/j.scitotenv.2012.04.048>.
- Nicolli, H.B., Garcia, J., Falcon, C., Smedley, P., 2012b. Mobilization of arsenic and other trace elements of health concern in groundwater from the Sali River Basin, Tucuman Province, Argentina. *Environ. Geochem. Health* 34, 251–262. <https://doi.org/10.1007/s10653-011-9429-8>.
- Nicolli, H.B., Suriano, J.M., Gomez Peral, M.A., Ferpozzi, L.H., Baleani, O.A., 1989. Groundwater contamination with arsenic and other trace elements in an area of the Pampa, province of Córdoba, Argentina. *Environ. Geol. Water S* 14, 3–16. <https://doi.org/10.1007/BF01740581>.
- Nilgirwal, K.S., Alahari, A., Rao, A.S., Apte, S.K., 2008. Cloning and overexpression of alkaline phosphatase PhoK from *Sphingomonas* sp. strain BSAR-1 for bioprecipitation of uranium from alkaline solutions. *Appl. Environ. Microbiol.* 74, 5516–5523.
- Nitzsche, O., Merkel, B., 1999. Reactive transport modeling of uranium 238 and radium 226 in groundwater of the Königstein uranium mine, Germany. *Hydrogeol. J.* 7, 423–430. <https://doi.org/10.1007/s100400050215>.
- Noble, R.R.P., Gray, D.J., Reid, N., 2011. Regional exploration for channel and playa uranium deposits in Western Australia using groundwater. *Appl. Geochem.* 26, 1956–1974.
- Nolan, J., Weber, K.A., 2015. Natural uranium contamination in major U.S. aquifers linked to nitrate. *Environ. Sci. Technol. Lett.* 2, 215–220. <https://doi.org/10.1021/acs.estlett.5b00174>.
- Nolan, P., Bone, S.E., Campbell, K.M., Pan, D., Healy, O.M., Stange, M., Bargar, J.R., Weber, K.A., 2021. Uranium(VI) attenuation in a carbonate-bearing oxic alluvial aquifer. *J. Hazard Mater.* 412, 125089. <https://doi.org/10.1016/j.jhazmat.2021.125089>.
- Novotnik, B., Chen, W., Evans, R.D., 2018. Uranium bearing dissolved organic matter in the porewaters of uranium contaminated lake sediments. *Appl. Geochem.* 91, 36–44. <https://doi.org/10.1016/j.apgeochem.2018.01.009>.
- Nriagu, J., Nam, D.-H., Ayanwola, T.A., Dinh, H., Erdenechimeg, E., Ochir, C., Bolormaa, T.A., 2012. High levels of uranium in groundwater of Ulaanbaatar, Mongolia. *Sci. Tot. Environ.* 414, 722–726. <https://doi.org/10.1016/j.scitotenv.2011.11.037>.
- Nriagu, J., Johnson, J., Samurkas, C., Erdenebayar, E., Ochir, C., Chandaga, U., 2013. Co-occurrence of high levels of uranium, arsenic and molybdenum in groundwater of Dornogobi, Mongolia. *Global Health Persp* 1, 45–54. <https://doi.org/10.5645/ghp2013.01.01.07>.
- Oher, H., Vercoeur, T., Réal, F., Shang, C., Reiller, P.E., Vallet, V., 2020. Influence of alkaline earth metal ions on structures and luminescent properties of NamMnUO₂(CO₃)₃(4-m-2-n) (M= Mg, Ca; m, n= 0–2): time-Resolved Fluorescence Spectroscopy and Ab Initio Studies. *Inorg. Chem.* 59, 15036–15049.
- Ohnuki, T., Isobe, H., Yanase, N., Nagano, T., Sakamoto, Y., Sekine, K., 1997. Change in sorption characteristics of uranium during crystallization of amorphous iron minerals. *J. Nucl. Sci. Technol.* 34, 1153–1158.
- Orloff, K.G., Mistry, K., Charp, P., Metcalf, S., Marino, R., Shelly, T., Melaro, E., Donohoe, A.M., Jones, R.L., 2004. Human exposure to uranium in groundwater. *Environ. Res.* 94, 319–326. [https://doi.org/10.1016/S0013-9351\(03\)00115-4](https://doi.org/10.1016/S0013-9351(03)00115-4).
- Ortega, R., Devès, G., Maire, R., 2003. Nuclear microprobe analysis of uranium-rich speleothems: methodological aspects. *Nucl. Instrum. Meth. B* 210, 455–458. [https://doi.org/10.1016/S0168-583X\(03\)01075-9](https://doi.org/10.1016/S0168-583X(03)01075-9).
- Osmond, J.K., Cowart, J.B., Ivanovich, M., 1983. Uranium isotopic disequilibrium in ground water as an indicator of anomalies. *Int. J. App. Radiat. Is.* 34, 283–308. [https://doi.org/10.1016/0020-708X\(83\)90132-1](https://doi.org/10.1016/0020-708X(83)90132-1).
- Othmane, G., Allard, T., Morin, G., Sélo, M., Brest, J., Llorens, I., Chen, N., Bargar, J.R., Fayek, M., Calas, G., 2013. Uranium association with iron-bearing phases in mill tailings from gunnar, Canada. *Environ. Sci. Technol.* 47, 12695–12702. <https://doi.org/10.1021/es401437y>.
- Othmane, G., Allard, T., Vercoeur, T., Morin, G., Fayek, M., Calas, G., 2016. Luminescence of uranium-bearing opals: origin and use as a pH record. *Chemical Geology* 423, 1–6.
- Owen, D.E., Otton, J.K., 1995. Mountain wetlands: efficient uranium filters — potential impacts. *Ecol. Eng.* 5, 77–93. [https://doi.org/10.1016/0925-8574\(95\)00013-9](https://doi.org/10.1016/0925-8574(95)00013-9).
- O'Connor, P.J., Hennessy, J., Bruck, P.M., Williams, C.T., 1982. Abundance and distribution of uranium and thorium in the northern units of the Leinster granite, Ireland. *Geol. Mag.* 119, 581–592. <https://doi.org/10.1017/S0016756800027060>.
- O'Loughlin, E.J., Kelly, S.D., Cook, R.E., Csencsits, R., Kemner, K.M., 2003. Reduction of uranium(VI) by mixed iron(II)/iron(III) hydroxide (Green Rust): formation of UO₂ nanoparticles. *Environ. Sci. Technol.* 37, 721–727. <https://doi.org/10.1021/es0208409>.
- O'Reilly, S.E., Hochella Jr., M.F., 2003. Lead sorption efficiencies of natural and synthetic Mn and Fe-oxides. *Geochim. Cosmochim. Acta* 67, 4471–4487.

- Pabalan, R.T., Turner, D.R., 1997. Uranium(6+) sorption on montmorillonite: experimental and surface complexation modeling study. *Aquat. Geochem.* 2, 203–226.
- Palme, H., O'Neill, H.St.C., 2007. Cosmochemical estimates of mantle composition. In: Holland, H.D., Turekian, K.K. (Eds.), *Treatise on Geochemistry*. Pergamon, Oxford, pp. 1–38. <https://doi.org/10.1016/B0-08-043751-6/02177-0>.
- Pan, Z., Giammar, D.E., Mehta, V., Troyer, L.D., Catalano, J.G., Wang, Z., 2016. Phosphate-induced immobilization of uranium in Hanford sediments. *Environ. Sci. Technol.* 50, 13486–13494. <https://doi.org/10.1021/acs.est.6b02928>.
- Pan, Z., Bártová, B., LaGrange, T., Butorin, S.M., Hyatt, N.C., Stennett, M.C., Kvashnina, K.O., Bernier-Latmani, R., 2020. Nanoscale mechanism of UO₂ formation through uranium reduction by magnetite. *Nat. Commun.* 11, 1–12. <https://doi.org/10.1038/s41467-020-17795-0>.
- Pan, Y., Li, D., Feng, R., Wiens, E., Chen, N., Chernikov, R., Götz, J., Lin, J., 2021. Uranyl binding mechanism in microcrystalline silicas: a potential missing link for uranium mineralization by direct uranyl co-precipitation and environmental implications. *Geochimica et Cosmochimica Acta* 292, 518–531. <https://doi.org/10.1016/j.gca.2020.10.017>.
- Pan, D., Zhao, X., Wang, P., Li, P., Li, Y., Wu, W., Wang, Z., Fan, Q., 2022. Insights into sorption speciation of uranium on phlogopite: evidence from TRLFS and DFT calculation. *Journal of Hazardous Materials* 427, 128164. <https://doi.org/10.1016/j.jhazmat.2021.128164>.
- Pan, Z., Roebbert, Y., Beck, A., Bartova, B., Vitova, T., Weyer, S., Bernier-Latmani, R., 2022. Persistence of the isotopic signature of pentavalent uranium in magnetite. *Environ. Sci. Technol.* 56, 1753–1762. <https://doi.org/10.1021/acs.est.1c06865>.
- Pandey, A., Khan, F.A., Kelkar, A., Purohit, P., Kumar, P., Sathe, D.B., Bhatt, R.B., Behere, P.G., 2020. Determination of trace amounts of uranium in plutonium oxide by wavelength dispersive X-ray fluorescence spectrometry. *J. Radioanal. Nucl. Chem.* 324, 731–736. <https://doi.org/10.1007/s10967-020-07116-6>.
- Papageorgiou, F., McDermott, F., Van Acken, D., 2022. Uranium in groundwaters: insights from the leinster granite, SE Ireland. *Appl. Geochem.* 139, 105236. <https://doi.org/10.1016/j.apgeochem.2022.105236>.
- Papastefanou, C., 2010. Escaping radioactivity from coal-fired power plants (CPPs) due to coal burning and the associated hazards: a review. *J. Environ. Radioactiv.* 101, 191–200. <https://doi.org/10.1016/j.jenvrad.2009.11.006>.
- Papp, Z., Dezso, Z., Daroczy, S., 2002. Significant radioactive contamination of soil around a coal-fired thermal power plant. *J. Environ. Radioactiv.* 59, 191–205. [https://doi.org/10.1016/S0265-931X\(01\)00071-6](https://doi.org/10.1016/S0265-931X(01)00071-6).
- Parkhurst, D.L., Appelo, C.A.J., 2013. Description of input and examples for PHREEQC version 3—a computer program for speciation, batch-reaction, one-dimensional transport, and inverse geochemical calculations. In: *U.S. Geological Survey Techniques and Methods, Book 6, Chap. A43*. United States Geological Survey, Reston, VA, p. 497.
- Parkhurst, D.L., Wissmeier, L., 2015. PhreeqcRM: a reaction module for transport simulators based on the geochemical model PHREEQC. *Advances in Water Resources* 83, 176–189. <https://doi.org/10.1016/j.advwatres.2015.06.001>.
- Patel, S., Upadhyay, D., Mishra, B., Abhinav, K., Sarangi, A.K., 2021. Multiple episodes of hydrothermal alteration and uranium mineralization in the Singhbhum Shear Zone, eastern India: constraints from chemical and boron isotope composition of tourmaline. *Lithos* 388–389, 106084. <https://doi.org/10.1016/j.lithos.2021.106084>.
- Payne, T.E., Airey, P.L., 2006. Radionuclide migration at the Koongarra uranium deposit, Northern Australia – lessons from the Alligator Rivers analogue project. *Phys. Chem. Earth Pt. A/B/C* 31, 572–586. <https://doi.org/10.1016/j.pce.2006.04.008>.
- Payne, T.E., 1991. A Study of Uranium and Thorium Migration at the Koongarra Uranium Deposit with Application to Actinide Transport from Nuclear Waste Repositories (M. Env. Stud. thesis). Macquarie University, Sydney.
- Payne, T.E., Waite, T.D., 2022. Uranium adsorption—a review of progress from qualitative understanding to advanced model development. *Radiochimica Acta* 110 (6–9), 549–559. <https://doi.org/10.1515/ract-2022-0003>.
- Payne, T., Davis, J., Waite, T., 1994. Uranium retention by weathered schists - the role of iron minerals. *Radiochim. Acta* 66 (7), 297–303.
- Payne, T.E., Davis, J.A., Waite, T.D., 1996. Uranium adsorption on ferrihydrite-effects of phosphate and humic acid. *Radiochim. Acta* 74, 239–243.
- Payne, T., Lumpkin, G., Waite, T., 1998. Uranium(VI) adsorption on model minerals. In: Jenne, E.A. (Ed.), *Adsorption of Metals by Geomedia*. Academic Press, San Diego, pp. 75–97.
- Payne, T.E., Brendler, V., Comarmond, M.J., Nebelung, C., 2011. Assessment of surface area normalisation for interpreting distribution coefficients (K_d) for uranium sorption. *J. Environ. Radioactiv.* 102, 888–895.
- Peng, B., Tang, X., Yu, C., Xie, S., Xiao, M., Song, Z., Tu, X., 2009. Heavy metal geochemistry of the acid mine drainage discharged from the Hejiacun uranium mine in central Hunan, China. *Environ. Geol.* 57, 421–434. <https://doi.org/10.1007/s00254-008-1313-1>.
- Peñkin, M., Boulyga, S., Dabbs, B., Fischer, D., Humphrey, M., Kochetkov, A., Koepf, A., Sturm, M., 2018. Isotopic composition of commercially available uranium chemicals and elemental analysis standards. *J. Radioanal. Nucl. Chem.* 316, 791–798. <https://doi.org/10.1007/s10967-018-5740-5>.
- Peretyazhko, T., Sposito, G., 2006. Reducing capacity of terrestrial humic acids. *Geoderma* 137, 140–146.
- Pérez, I., Casas, I., Martín, M., Bruno, J., 2000. The thermodynamics and kinetics of uranophane dissolution in bicarbonate test solutions. *Geochim. Cosmochim. Acta* 64, 603–608. [https://doi.org/10.1016/S0016-7037\(99\)00337-3](https://doi.org/10.1016/S0016-7037(99)00337-3).
- Perry, D.L., Klainer, S.M., Bowman, H.R., Milanovich, F.P., Hirschfeld, T., Miller, S., 1981. Detection of ultratrace levels of uranium in aqueous samples by laser-induced fluorescence spectrometry. *Anal. Chem.* 53, 1048–1050.
- Pesavento, M., Alberti, G., Biesuz, R., 2009. Analytical methods for determination of free metal ion concentration, labile species fraction and metal complexation capacity of environmental waters: a review. *Anal. Chim. Acta* 631, 129–141.
- Philippe, A., Schaumann, G.E., 2014. Interactions of dissolved organic matter with natural and engineered inorganic colloids: a review. *Environ. Sci. Technol.* 48, 8946–8962.
- Phrommavanh, V., Leermakers, M., de Boissezon, H., Nos, J., Koko, M.-B., Descostes, M., 2013. Characterizing the transport of natural uranium and its decay product ²²⁶Ra, downstream from former mines in France. *Procedia Earth and Planetary Science* 7, 693–696. <https://doi.org/10.1016/j.proeps.2013.03.064>.
- Pidchenko, I., Kvashnina, K.O., Yokosawa, T., Finck, N., Bahl, S., Schild, D., Polly, R., Bohnert, E., Rossberg, A., Göttlicher, J., Dardenne, K., Rothe, J., Schäfer, T., Geckeis, H., Vitova, T., 2017. Uranium redox transformations after U(VI) coprecipitation with magnetite nanoparticles. *Environ. Sci. Technol.* 51, 2217–2225. <https://doi.org/10.1021/acs.est.6b04035>.
- Pinheiro, J.P., Rotureau, E., Duval, J.F., 2021. Addressing the electrostatic component of protons binding to aquatic nanoparticles beyond the Non-Ideal Competitive Adsorption (NICA)-Donnan level: theory and application to analysis of proton titration data for humic matter. *J. Colloid. Interf. Sci.* 583, 642–651.
- Poole, J., 2001. Radon Release from Granites in South-West England (PhD thesis). University of Reading, Reading, UK.
- Popit, A., Vaupotic, J., Kukar, N., 2004. Systematic radium survey in spring waters of Slovenia. *J. Environ. Radioactiv.* 76, 337–347. <https://doi.org/10.1016/j.jenvrad.2003.12.010>.
- Porcelli, D., Swarzenski, P.W., 2003. The behavior of U- and Th-series nuclides in groundwater. *Rev. Min. Geochem.* 52, 317–361. <https://doi.org/10.2113/0520317>.
- Post, V., Vassolo, S., Tiberghien, C., Baranyikwa, D., Miburo, D., 2017. Weathering and evaporation controls on dissolved uranium concentrations in groundwater—A case study from northern Burundi. *Sci. Tot. Environ.* 607, 281–293.
- Pownceby, M.I., Johnson, C., 2014. Geometallurgy of Australian uranium deposits. *Ore Geol. Rev.* 56, 25–44. <https://doi.org/10.1016/j.oregeorev.2013.07.001>.
- Prat, O., Vercouter, T., Ansoborlo, E., Fichet, P., Perret, P., Kurttio, P., Salonen, L., 2009. Uranium speciation in drinking water from drilled wells in southern Finland and its potential links to health effects. *Environ. Sci. Technol.* 43, 3941–3946. <https://doi.org/10.1021/es803658e>.
- Priestley, S.C., Payne, T.E., Harrison, J.J., Post, V.E.A., Shand, P., Love, A.J., Wohling, D. L., 2018. Use of U-isotopes in exploring groundwater flow and inter-aquifer leakage in the south-western margin of the Great Artesian Basin and Arckaringa Basin, central Australia. *Appl. Geochem.* 98, 331–344. <https://doi.org/10.1016/j.apgeochem.2018.10.002>.
- Prikryl, J.D., Jain, A., Turner, D.R., Pabalan, R.T., 2001. Uranium^{VI} sorption behavior on silicate mineral mixtures. *J. Contam. Hydrol.* 47, 241–253.
- Proctor, G., Wang, H., Larson, S.L., Ballard, J.H., Knotek-Smith, H., Waggoner, C., Unz, R., Li, J., McComb, J., Jin, D., 2020. Rapid screening for uranium in soils using field-portable X-ray fluorescence spectrometer: a comparative study. *ACS Earth Space Chem* 4, 211–217.
- Qafoku, N.P., Kukkadapu, R.K., McKinley, J.P., Arey, B.W., Kelly, S.D., Wang, C., Resch, C.T., Long, P.E., 2009. Uranium in framboidal pyrite from a naturally bio-reduced alluvial sediment. *Environ. Sci. Technol.* 43, 8528–8534. <https://doi.org/10.1021/es9017333>.
- Qiao, J., Xu, Y., 2018. Direct measurement of uranium in seawater by inductively coupled plasma mass spectrometry. *Talanta* 183, 18–23.
- Qiao, J., Lagerkvist, P., Rodushkin, I., Salminen-Paatero, S., Roos, P., Lierhagen, S., Jensen, K.A., Engstrom, E., Lahaye, Y., Skipperud, L., 2018. On the application of ICP-MS techniques for measuring uranium and plutonium: a Nordic inter-laboratory comparison exercise. *J. Radioanal. Nucl. Chem.* 315, 565–580.
- Quemet, A., Ruas, A., Dalier, V., Rivier, C., 2019. Development and comparison of high accuracy thermal ionization mass spectrometry methods for uranium isotope ratios determination in nuclear fuel. *Int. J. Mass Spectrom.* 438, 166–174. <https://doi.org/10.1016/j.ijms.2019.01.008>.
- Radhamani, R., Mahanta, P., Murugesan, P., Chakrapani, G., 2010. Novel fusion method for direct determination of uranium in ilmenite, rutile, columbite, tantalite, and xenotime minerals by laser induced fluorimetry. *J. Radioanal. Nucl. Chem.* 285, 287–292. <https://doi.org/10.1007/s10967-010-0579-4>.
- Raffensperger, J.P., Garven, G., 1995. The formation of unconformity-type uranium ore deposits 2. Coupled hydrochemical modeling. *Amer. J. Sci.* 295, 639–696. <https://doi.org/10.2475/ajs.295.6.639>.
- Raghavendra, T., Srilatha, K., Mahender, C., Elander, M., Vijayalakshmi, T., Himabindu, V., Prasad, V., Padma Savithri, P., Datta, D., Arunachalam, J., 2014. Distribution of uranium concentration in groundwater samples from the Peddagattu/Nambapur and Seripally regions using laser fluorimetry. *Radiat. Prot. Dosim.* 158, 325–330. <https://doi.org/10.1093/rpd/nct228>.
- Ragoussi, M.-E., Costa, D., 2019. Fundamentals of the NEA Thermochemical Database and its influence over national nuclear programs on the performance assessment of deep geological repositories. *J. Environ. Radioactiv.* 196, 225–231.
- Rai, D., Felmy, A., Ryan, J., 1990. Uranium (IV) hydrolysis constants and solubility product of UO₂. *Chem. Abstr.* 112, 260–264.
- Ramadan, R.S., Dawood, Y.H., Yehia, M.M., Gad, A., 2022. Environmental and health impact of current uranium mining activities in southwestern Sinai, Egypt. *Environ. Earth Sci.* 81, 213. <https://doi.org/10.1007/s12665-022-10341-9>.
- Ramdoss, K., Amma, B., Umashankar, V., Rangaswamy, R., 1997. Cold dissolution method for the determination of uranium in various geological materials at trace levels by laser fluorimetry. *Talanta* 44, 1095–1098. [https://doi.org/10.1016/S0039-9140\(96\)02201-1](https://doi.org/10.1016/S0039-9140(96)02201-1).

- Ramola, R.C., Singh, S., Virk, H.S., 1988. Uranium and radon estimation in some water samples from Himalayas. *Int. J. Radiat. App. Instrum. D* 15, 791–793. <https://doi.org/10.1016/j.jfaresci.1988.09.0252-X>.
- Rana, B.K., Dhumale, M.R., Lenka, P., Sahoo, S.K., Ravi, P.M., Tripathi, R.M., 2016. A study of natural uranium content in groundwater around Tummalapalle uranium mining and processing facility, India. *J. Radioanal. Nucl. Chem.* 307, 1499–1506.
- Rango, T., Bianchini, G., Beccaluva, L., Tassinari, R., 2010. Geochemistry and water quality assessment of central Main Ethiopian Rift natural waters with emphasis on source and occurrence of fluoride and arsenic. *J. Afr. Earth Sci.* 57, 479–491. <https://doi.org/10.1016/j.jfaresci.2009.12.005>.
- Rani, A., Mehra, R., Duggal, V., Balaram, V., 2013a. Analysis of uranium concentration in drinking water samples using ICPMS. *Health Phys* 104, 251–255.
- Rani, A., Singh, S., Duggal, V., Balaram, V., 2013b. Uranium estimation in drinking water samples from some areas of Punjab and Himachal Pradesh, India using ICP-MS. *Radiat. Prot. Dosim.* 157, 146–151.
- Rathore, D.P.S., 2008. Advances in technologies for the measurement of uranium in diverse matrices. *Talanta* 77, 9–20.
- Rawlins, B.G., McGrath, S.P., Scheib, A.J., Bredard, N., Cave, M., Lister, T.R., Ingham, M., Gowing, C., Carter, S., 2012. The Advanced Soil Geochemical Atlas of England and Wales. British Geological Survey, Keyworth, Nottingham.
- Read, D., Bennett, D.G., Hooker, P.J., Ivanovich, M., Longworth, G., Milodowski, A.E., Noy, D.J., 1993. The migration of uranium into peat-rich soils at Broustler, Caithness, Scotland, U.K. *J. Contam. Hydrol.* 13, 291–308. [https://doi.org/10.1016/0169-7722\(93\)90067-3](https://doi.org/10.1016/0169-7722(93)90067-3).
- Reeder, R., Nugent, M., Tait, C.D., Morris, D.E., Heald, S.M., Beck, K.M., Hess, W.P., Lanzirrotti, A., 2001. Coprecipitation of uranium(VI) with calcite: XAFS, micro-XAS, and luminescence characterization. *Geochim. Cosmochim. Acta* 65, 3491.
- Reeder, R.J., Elzinga, E.J., Tait, C.D., Rector, K.D., Donohoe, R.J., Morris, D.E., 2004. Site-specific incorporation of uranyl carbonate species at the calcite surface. *Geochim. Cosmochim. Acta* 68, 4799–4808. <https://doi.org/10.1016/j.gca.2004.05.031>.
- Regenspurg, S., Margot-Roquier, C., Harfouche, M., Froidevaux, P., Steinmann, P., Junier, P., Bernier-Latmani, R., 2010. Speciation of naturally-accumulated uranium in an organic-rich soil of an alpine region (Switzerland). *Geochim. Cosmochim. Acta* 74, 2082–2098. <https://doi.org/10.1016/j.gca.2010.01.007>.
- Reich, T., Moll, H., Arnold, T., Denecke, M.A., Hennig, C., Geipel, G., Bernhard, G., Nitsche, H., Allen, P.G., Bucher, J.J., Edelstein, N.M., Shuh, D.K., 1998. An EXAFS study of uranium(VI) sorption onto silica gel and ferrihydrite. *J. Electron Spectrosc.* 96, 237–243. [https://doi.org/10.1016/S0368-2048\(98\)00242-4](https://doi.org/10.1016/S0368-2048(98)00242-4).
- Reiller, P.E., 2005. Prognosticating the humic complexation for redox sensitive actinides through analogy, using the charge neutralisation model. *Radiochim. Acta* 93, 43–55.
- Reiller, P.E., 2012. Modelling metal-humic substances-surface systems: reasons for success, failure and possible routes for peace of mind. *Min. Mag.* 76, 2643–2658.
- Reiller, P.E., Buckau, G., 2012. Impacts of humic substances on the geochemical behaviour of radionuclides. In: Poinssot, C., Geckeis, H. (Eds.), *Radionuclide Behaviour in the Natural Environment*. Woodhead Publishing, Oxford, pp. 103–160.
- Reiller, P.E., Descostes, M., 2020. Development and application of the thermodynamic database PRODATA dedicated to the monitoring of mining activities from exploration to remediation. *Chemosphere* 251, 126301. <https://doi.org/10.1016/j.chemosphere.2020.126301>.
- Reiller, P.E., Marang, L., Jouvin, D., Benedetti, M.F., 2011. Uranium(VI) binding to humic substances: speciation, estimation of competition, and application to independent data. In: Merkel, B., Schipek, M. (Eds.), *The New Uranium Mining Boom*. Springer, Berlin & Heidelberg, pp. 565–572.
- Ren, Y., Bao, H., Wu, Q., Wang, H., Gai, T., Shao, L., Wang, S., Tang, H., Li, Y., Wang, X., 2020. The physical chemistry of uranium(VI) immobilization on manganese oxides. *J. Hazard Mater.* 391, 122207. <https://doi.org/10.1016/j.jhazmat.2020.122207>.
- Rentería Villalobos, M., Montero Cabrera, M.E., Reyes Cortés, M., Herrera Peraza, E.F., Rodríguez Pineda, A., Manjón Collado, G., García Tenorio, R., Crespo, T., Valenzuela Hernández, M., 2007. Characterization of source rocks and groundwater radioactivity at the Chihuahua valley. *Mex. J. Phys.* 53, 16–22.
- Reynolds, R.L., Goldhaber, M.B., 1983. Iron disulfide minerals and the genesis of roll-type uranium deposits. *Econ. Geol.* 78, 105–120.
- Reynolds, J.G., Cooke, G.A., Page, J.S., Warrant, R.W., 2018. Uranium-bearing phases in Hanford nuclear waste. *J. Radioanal. Nucl. Chem.* 316, 289–299. <https://doi.org/10.1007/s10967-018-5724-5>.
- Richter, S., Kühn, H., Aregbe, Y., Hedberg, M., Horta-Domenech, J., Mayer, K., Zuleger, E., Bürger, S., Boulyga, S., Köpf, A., Poths, J., Mathew, K., 2011. Improvements in routine uranium isotope ratio measurements using the modified total evaporation method for multi-collector thermal ionization mass spectrometry. *J. Anal. At. Spectrom.* 26, 550–564. <https://doi.org/10.1039/C0JA00173B>.
- Richter, A., Bok, F., Brendler, V., 2015. Data Compilation and Evaluation of U(IV) and U(VI) for Thermodynamic Reference Database THEREDA, HZDR-065. Helmholtz-Zentrum Dresden, Rossendorf.
- Richter, C., Müller, K., Drobot, B., Steudtner, R., Großmann, K., Stockmann, M., Brendler, V., 2016. Macroscopic and spectroscopic characterization of uranium (VI) sorption onto orthoclase and muscovite and the influence of competing Ca²⁺. *Geochim. Cosmochim. Acta* 189, 143–157.
- Riedel, T., Kübeck, C., 2018. Uranium in groundwater – a synopsis based on a large hydrogeochemical data set. *Water Res* 129, 29–38. <https://doi.org/10.1016/j.watres.2017.11.001>.
- Riethmüller, N., Markich, S.J., Van Dam, R.A., Parry, D., 2001. Effects of water hardness and alkalinity on the toxicity of uranium to a tropical freshwater hydra (*Hydra viridissima*). *Biomarkers* 6, 45–51. <https://doi.org/10.1080/1354750011452788>.
- Rihs, S., Sturchio, N.C., Orlandini, K., Cheng, L., Teng, H., Fenter, P., Bedzyk, M.J., 2004. Interaction of uranyl with calcite in the presence of EDTA. *Environ. Sci. Technol.* 38, 5078–5086. <https://doi.org/10.1021/es049847b>.
- Ring, R.J., Holden, P., McCulloch, J.K., Tapsell, G.J., Collier, D.E., Russell, R., Macnaughton, S., Marshall, K., Stimson, D., 2004. Treatment of Liquid Effluent from Uranium Mines and Mills during and after Operation. International Atomic Energy Agency, Vienna.
- Riotte, J., Chabaux, F., 1999. (234U/238U) activity ratios in freshwaters as tracers of hydrological processes: the Strengbach watershed (Vosges, France). *Geochim. Cosmochim. Acta* 63, 1263–1275. [https://doi.org/10.1016/S0016-7037\(99\)00009-5](https://doi.org/10.1016/S0016-7037(99)00009-5).
- Roessler, C.E., Smith, Z.A., Bolch, W.F., Prince, R.J., 1979. Uranium and radium-226 in Florida phosphate minerals. *Health Phys* 37, 269–277.
- Rosentreter, J.J., Quarder, S., Smith, R.W., McLing, T., 1998. Uranium sorption onto natural sands as a function of sediment characteristics and solution pH. In: Jenne, E. A. (Ed.), Chapter 7. Adsorption of Metals by Geomedia. American Chemical Society, Washington, D.C., pp. 182–192.
- Rossberg, A., Ulrich, K.-U., Weiss, S., Tsushima, S., Hiemstra, T., Scheinost, A.C., 2009. Identification of uranyl surface complexes on ferrihydrite: advanced EXAFS data analysis and CD-MUSIC modeling. *Environ. Sci. Technol.* 43, 1400–1406. <https://doi.org/10.1021/es801727w>.
- Rothbaum, H.P., McGaveston, D.A., Wall, T., Johnston, A.E., Mattingly, G.E.G., 1979. Uranium accumulation in soils from long-continued applications of superphosphate. *J. Soil Sci.* 30, 147–153. <https://doi.org/10.1111/j.1365-2389.1979.tb00972.x>.
- Rovan, L., Strok, M., 2019. Optimization of the sample preparation and measurement protocol for the analysis of uranium isotopes by MC-ICP-MS without spike addition. *J. Anal. At. Spectrom.* 34, 1882–1891. <https://doi.org/10.1039/C9JA00144A>.
- Ruan, C., Luo, W., Wang, W., Gu, B., 2007. Surface-enhanced Raman spectroscopy for uranium detection and analysis in environmental samples. *Anal. Chim. Acta* 605, 80–86. <https://doi.org/10.1016/j.aca.2007.10.024>.
- Russell, A.D., Emerson, S., Nelson, B.K., Erez, J., Lea, D.W., 1994. Uranium in foraminiferal calcite as a recorder of seawater uranium concentrations. *Geochim. Cosmochim. Acta* 58, 671–681. [https://doi.org/10.1016/0016-7037\(94\)90497-9](https://doi.org/10.1016/0016-7037(94)90497-9).
- Rutherford, P.M., Dudas, M.J., Samek, R.A., 1994. Environmental impacts of phosphogypsum. *Sci. Tot. Environ.* 149, 1–38. [https://doi.org/10.1016/0048-9697\(94\)90002-7](https://doi.org/10.1016/0048-9697(94)90002-7).
- Saenko, Y.V., Shiranov, A.M., Nevzorov, A.L., 2021. Geotechnical properties of hemihydrate and dihydrate phosphogypsum. *J. Phys. Conf. Ser.* 1928, 012017. <https://doi.org/10.1088/1742-6596/1928/1/012017>.
- Sahoo, P., Mallika, C., Ananthanarayanan, R., Lawrence, F., Murali, N., Kamachi Mudali, U., 2012. Potentiometric titration in a low volume of solution for rapid assay of uranium: application to quantitative electro-reduction of uranium(VI). *J. Radioanal. Nucl. Chem.* 292, 1401–1409. <https://doi.org/10.1007/s10967-012-1622-4>.
- Sahoo, S.K., Jha, V.N., Patra, A.C., Jha, S.K., Kulkarni, M.S., 2020. Scientific background and methodology adopted on derivation of regulatory limit for uranium in drinking water – a global perspective. *Environ. Adv.* 2, 100020. <https://doi.org/10.1016/j.envadv.2020.100020>.
- Sahoo, S., Jha, S., Jha, V., Patra, A., Kulkarni, M., 2021. Survey of uranium in drinking water sources in India: interim observations. *Curr. Sci.* 120, 1482–1490. <https://doi.org/10.18520/cs/v120/i9/1482-1490>.
- Sahoo, P.K., Virk, H.S., Powell, M.A., Kumar, R., Pattanaik, J.K., Salomão, G.N., Mittal, S., Chouhan, L., Nandabalan, Y.K., Tiwari, R.P., 2022. Meta-analysis of uranium contamination in groundwater from the alluvial plains of Punjab, northwest India: status, health risk, and hydrogeochemical processes. *Sci. Tot. Environ.* 807, 151753. <https://doi.org/10.1016/j.scitotenv.2021.151753>.
- Sahu, S.K., Maity, S., Bhargava, R.C., Pandit, G.G., Sharma, D.N., 2014. Determination of Uranium in Ground Water Using Different Analytical Techniques. BARC/2014/E/011, Department of Atomic Energy, Bhabha Atomic Research Centre, Mumbai, India.
- Sakuragi, Y., Meason, J.L., Kuroda, P.K., 1983. Uranium and plutonium isotopes in the atmosphere. *Journal of Geophysical Research: Oceans* 88, 3718–3724. <https://doi.org/10.1029/JC088iC06p03718>.
- Salas, J., Ayora, C., 2004. Groundwater chemistry of the Okélobondo uraninite deposit area (Oklo, Gabon): two-dimensional reactive transport modelling. *J. Contam. Hydrol.* 69, 115–137.
- Salminen, R., Batista, M.J., Bidovec, M., Demetriades, A., De Vivo, B., De Vos, W., Duris, M., Gilucis, A., Gregorauskiene, V., Halamić, J., 2005. Geochemical Atlas of Europe, Part 1, Background Information, Methodology and Maps. The Association of the Geological Surveys of The European Union (EuroGeoSurveys), The Geological Survey of Finland, Espoo, Finland.
- Sanders, C.J., Santos, I.R., Sadat-Noori, M., Maher, D.T., Holloway, C., Schnetger, B., Brumsack, H.-J., 2017. Uranium export from a sandy beach subterranean estuary in Australia. *Estuar. Coast Shelf S.* 198, 204–212. <https://doi.org/10.1016/j.ecss.2017.09.002>.
- Sanding, A., Bruno, J., 1992. The solubility of (UO₂)₃(PO₄)₂·4H₂O(s) and the formation of U(VI) phosphate complexes: their influence in uranium speciation in natural waters. *Geochim. Cosmochim. Acta* 56, 4135–4145. [https://doi.org/10.1016/0016-7037\(92\)90256-1](https://doi.org/10.1016/0016-7037(92)90256-1).
- Sarin, M.M., Church, T.M., 1994. Behaviour of uranium during mixing in the Delaware and Chesapeake estuaries. *Estuar. Coast Shelf S.* 39, 619–631. [https://doi.org/10.1016/00272-7714\(06\)80013-2](https://doi.org/10.1016/00272-7714(06)80013-2).
- Sato, T., Murakami, T., Yanase, N., Isobe, H., Payne, T.E., Airey, P.L., 1997. Iron nodules scavenging uranium from groundwater. *Environ. Sci. Technol.* 31, 2854–2858. <https://doi.org/10.1021/es970058m>.

- Schimmack, W., Gerstmann, U., Schultz, W., Geipel, G., 2007. Long-term corrosion and leaching of depleted uranium (DU) in soil. *Radiat. Environ. Bioph.* 46, 221–227. <https://doi.org/10.1007/s00411-007-0114-3>.
- Schindler, M., Fayek, M., Hawthorne, F.C., 2010. Uranium-rich opal from the Nopal I uranium deposit, Peña Blanca, Mexico: evidence for the uptake and retardation of radionuclides. *Geochimica et Cosmochimica Acta* 74, 187–202. <https://doi.org/10.1016/j.gca.2009.09.017>.
- Schindler, M., Fayek, M., Courchesne, B., Kyser, K., Hawthorne, F.C., 2017. Uranium-bearing opals: products of U-mobilization, diffusion, and transformation processes. *Amer. Mineral.* 102, 1154–1164.
- Schmeide, K., Pompe, S., Bubner, M., Heise, K.H., Bernhard, G., Nitsche, H., 2000. Uranium(VI) sorption onto phyllite and selected minerals in the presence of humic acid. *Radiochim. Acta* 88, 723–728.
- Schmeide, K., Sachs, S., Bubner, M., Reich, T., Heise, K.H., Bernhard, G., 2003. Interaction of uranium(VI) with various modified and unmodified natural and synthetic humic substances studied by EXAFS and FTIR spectroscopy. *Inorg. Chim. Acta* 351, 133–140.
- Schneider, P., Voerkelius, S., Nindel, K., Forster, M., Schreyer, J., 2001. Release of contaminants from uranium mine waste – laboratory and field experiments. *Mine Water and the Environment* 20, 30–38. <https://doi.org/10.1007/s10230-001-8077-0>.
- Schnug, E., Haneklaus, N., 2015. Uranium in phosphate fertilizers – review and outlook. In: Merkel, B.J., Arab, A. (Eds.), *Uranium – Past and Future Challenges*. Presented at the Proceedings of the 7th International Conference on Uranium Mining and Hydrogeology. Springer, Berlin & Heidelberg, pp. 123–130. https://doi.org/10.1007/978-3-319-11059-2_14.
- Schnug, E., Lottermoser, B.G., 2013. Fertilizer-derived uranium and its threat to human health. *Environ. Sci. Technol.* 47, 2433–2434. <https://doi.org/10.1021/es4002357>.
- Schult, M.K., Burnett, W., Inn, K.G.W., Smith, G., 1998. Geochemical partitioning of actinides using sequential extractions: comparison to stable elements. *J. Radioanal. Nucl. Chem.* 251–256.
- Seder-Colomina, M., Mangeret, A., Stetten, L., Merrot, P., Diez, O., Julien, A., Barker, E., Thouvenot, A., Bargar, J., Cazala, C., Morin, G., 2018. Carbonate facilitated mobilization of uranium from lacustrine sediments under anoxic conditions. *Environ. Sci. Technol.* 52, 9615–9624. <https://doi.org/10.1021/acs.est.8b01255>.
- Seeland, D.A., 1976. Relationships between early Tertiary sedimentation patterns and uranium mineralization in the Powder River Basin, Wyoming. In: 28th Annual Field Conference Guidebook. Presented at the Geology and Energy Resources of the Powder River, Wyoming. Geological Association, pp. 53–64.
- Seigneur, N., De Windt, L., Déjeant, A., Lagneau, V., Descostes, M., 2021. Long-term evolution of uranium mobility within sulfated mill tailings in arid regions: a reactive transport study. *Minerals* 11, 1201.
- Seldén, A.I., Lundholm, C., Edlund, B., Högdahl, C., Ek, B.-M., Bergström, B.E., Ohlson, C.-G., 2009. Nephrotoxicity of uranium in drinking water from private drilled wells. *Environ. Res.* 109, 486–494. <https://doi.org/10.1016/j.envres.2009.02.002>.
- Selvi, B., Vijayakumar, B., Rana, B., Ravi, P., 2016. Distribution of natural uranium in groundwater around Kudankulam. *Radiat. Prot. Environ.* 39 (1), 25–29. <https://doi.org/10.4103/0972-0464.185164>.
- Serenjeh, F.N., Hashemi, P., Ghiasvand, A.R., Rasolzadeh, F., 2016. A new optical sensor for selective quantitation of uranium by the immobilization of arsenazo III on an agarose membrane. *Anal. Methods* 8, 4181–4187. <https://doi.org/10.1039/C6AY00104A>.
- Shand, P., Edmunds, W.M., Lawrence, A.R., Smedley, P.L., Burke, S., 2007. *The Natural (Baseline) Quality of Groundwater in England and Wales*, Research Report RR/07/06. British Geological Survey, Keyworth.
- Shang, C., Reiller, P.E., 2020. Determination of formation constants and specific ion interaction coefficients for $\text{Ca}_n\text{UO}_2(\text{CO}_3)_3^{(4-2n)-}$ complexes in NaCl solution by time-resolved laser-induced luminescence spectroscopy. *Dalton Trans* 49, 466–481. <https://doi.org/10.1039/C9DT03543E>.
- Shang, C., Reiller, P.E., Vercouter, T., 2020. Spectroluminescence measurements of the stability constants of $\text{Ca}_n\text{UO}_2(\text{CO}_3)_3^{(4-2n)-}$ complexes in NaClO_4 medium and the investigation of interaction effects. *Dalton Trans* 49, 15443–15460.
- Shang, D., Geissler, B., Mew, M., Satalkina, L., Zenk, L., Tulsidas, H., Barker, L., El-Yahyaoui, A., Hussein, A., Taha, M., 2021. Unconventional uranium in China's phosphate rock: review and outlook. *Renewable and Sustainable Energy Reviews* 140, 110740.
- Sheppard, S.C., Sheppard, M.I., Tait, J.C., Sanipelli, B.L., 2006. Revision and meta-analysis of selected biosphere parameter values for chlorine, iodine, neptunium, radium, radon and uranium. *J. Environ. Radioactiv.* 89, 115–137.
- Shi, S., Tang, X., Yang, Y., Liu, Z., 2021. Biological effects of uranium in water, soil and rice in uranium deposits in southern China. *J. Radioanal. Nucl. Chem.* 328, 507–517. <https://doi.org/10.1007/s10967-021-07689-w>.
- Shiel, A.E., Laubach, P.G., Johnson, T.M., Lundstrom, C.C., Long, P.E., Williams, K.H., 2013. No measurable changes in $^{238}\text{U}/^{235}\text{U}$ due to desorption-adsorption of U(VI) from groundwater at the Rifle, Colorado, integrated field research challenge site. *Environ. Sci. Technol.* 47, 2535–2541. <https://doi.org/10.1021/es303913y>.
- Shin, W., Oh, J., Choung, S., Cho, B.-W., Lee, K.-S., Yun, U., Woo, N.-C., Kim, H.K., 2016. Distribution and potential health risk of groundwater uranium in Korea. *Chemosphere* 163, 108–115. <https://doi.org/10.1016/j.chemosphere.2016.08.021>.
- Shleweit, H., Alibrahim, M., 2008. Recovery of uranium from phosphate by carbonate solutions. *J. Radioanal. Nucl. Chem.* 275, 97–100.
- Shor, A.M., Ivanova-Shor, E.A., Chiorescu, I., Krüger, S., Rösch, N., 2020. Hydration structure and hydrolysis of U(IV) and Np(IV) ions: a comparative density functional study using a modified continuum solvation approach. *J. Phys. Chem. A* 124, 3805–3814.
- Shrivastava, V.K., Parthasarathy, T.N., Sinha, K.K., 1992. Geochemical study of the uraniumiferous granites from Lambapur area, Nalgonda district, Andhra Pradesh, India. *Explor. Res. At. Miner* 41–52.
- Simon, F.G., Biermann, V., Peplinski, B., 2008. Uranium removal from groundwater using hydroxyapatite. *Appl. Geochem.* 23, 2137–2145. <https://doi.org/10.1016/j.apgeochem.2008.04.025>.
- Simpson, P.R., Brown, G.C., Plant, J., Ostle, D., 1979. Uranium mineralization and granite magmatism in the British Isles. *Philos. T. R. Soc. S-A* 291, 385–412.
- Simpson, H.J., Trier, R.M., Toggweiler, J.R., Mathieu, G., Deck, B.L., Olsen, C.R., Hammond, D.E., Fuller, C., Ku, T.L., 1982. Radionuclides in mono lake, California. *Science* 216, 512–514. <https://doi.org/10.1126/science.216.4545.512>.
- Singh, J., Singh, L., Singh, S., 1995. High U-contents observed in some drinking waters of Punjab, India. *J. Environ. Radioactiv.* 26, 217–222. [https://doi.org/10.1016/0265-931X\(94\)00037-W](https://doi.org/10.1016/0265-931X(94)00037-W).
- Singh, P., Rana, N.S., Azam, A., Naqvi, A.H., Srivastava, D.S., 1996. Levels of uranium in waters from some Indian cities determined by fission track analysis. *Radiat. Meas.* 26, 683–687.
- Singh, B., Singh, G., Sandhu, A.S., Singh, S., 1999. Uranium estimation in water samples collected from some areas of Himachal Pradesh, India. *Radiat. Meas.* 31, 683–685. [https://doi.org/10.1016/S1350-4487\(99\)00172-9](https://doi.org/10.1016/S1350-4487(99)00172-9).
- Singh, S., Malhotra, R., Kumar, J., Singh, B., Singh, L., 2001. Uranium analysis of geological samples, water and plants from Kulu Area, Himachal Pradesh, India. *Radiation Measurements* 34, 427–431. [https://doi.org/10.1016/S1350-4487\(01\)00200-1](https://doi.org/10.1016/S1350-4487(01)00200-1).
- Singh, S., Rani, A., Mahajan, R.K., Walia, T.P.S., 2003. Analysis of uranium and its correlation with some physico-chemical properties of drinking water samples from Amritsar, Punjab. *J. Environ. Monit.* 5, 917–921. <https://doi.org/10.1039/B309493F>.
- Singh, H., Singh, J., Singh, S., Bajwa, B.S., 2009. Uranium concentration in drinking water samples using the SSNTDs. *Indian J. Phys.* 83, 1039–1044.
- Singh, J., Singh, H., Singh, S., Bajwa, B.S., 2009. Estimation of uranium and radon concentration in some drinking water samples of Upper Siwaliks, India. *Environ. Monit. Assess.* 154, 15–22.
- Singh, M., Tapadia, K., Jhariya, D., Sahu, P., 2021. Evaluation of uranium containing ground water quality and non-carcinogenic risk assessment in inhabitant of Bijapur District of Chhattisgarh, Central India. *J. Radioanal. Nucl. Chem.* 327, 939–947.
- Singhal, R.K., Basu, H., Bassan, M.K.T., Pimple, M.V., Manisha, V., Avhad, D.K., Sharma, P.K., Reddy, A.V.R., 2012. Rapid and interference free determination of ultra trace level of uranium in potable water originating from different geochemical environments by ICP-OES. *J. Radioanal. Nucl. Chem.* 292, 675–681. <https://doi.org/10.1007/s10967-011-1494-z>.
- Skierszkan, E.K., Dockrey, J.W., Mayer, K.U., Beckie, R.D., 2020a. Release of geogenic uranium and arsenic results in water-quality impacts in a subarctic permafrost region of granitic and metamorphic geology. *Journal of Geochemical Exploration* 217, 106607. <https://doi.org/10.1016/j.jexplo.2020.106607>.
- Skierszkan, E.K., Dockrey, J.W., Mayer, K.U., Bondici, V.F., McBeth, J.M., Beckie, R.D., 2020b. Geochemical controls on uranium release from neutral-pH rock drainage produced by weathering of granite, gneiss, and schist. *Minerals* 10, 1104.
- Skierszkan, E.K., Dockrey, J.W., Helsen, J., Findlater, L.-L., Bataille, C.P., de Laplante, G., McBeth, J.M., Mayer, K.U., Beckie, R.D., 2021. Persistence of uranium in old and cold subpermafrost groundwater indicated by linking ^{234}U - ^{235}U - ^{238}U , groundwater ages, and hydrogeochemistry. *ACS Earth Space Chem* 5, 3474–3487.
- Smedley, P.L., Nicolli, H.B., Macdonald, D.M.J., Barros, A.J., Tullio, J.O., 2002. Hydrogeochemistry of arsenic and other inorganic constituents in groundwaters from La Pampa, Argentina. *Appl. Geochem.* 17, 259–284. [https://doi.org/10.1016/S0883-2927\(01\)00082-8](https://doi.org/10.1016/S0883-2927(01)00082-8).
- Smedley, P.L., Zhang, M., Zhang, G., Luo, Z., 2003. Mobilisation of arsenic and other trace elements in fluvio-lacustrine aquifers of the Huhhot Basin, Inner Mongolia. *Appl. Geochem.* 18, 1453–1477. [https://doi.org/10.1016/S0883-2927\(03\)00062-3](https://doi.org/10.1016/S0883-2927(03)00062-3).
- Smedley, P.L., Kinniburgh, D.G., Macdonald, D.M.J., Nicolli, H.B., Barros, A.J., Tullio, J. O., Pearce, J.M., Alonso, M.S., 2005. Arsenic associations in sediments from the loess aquifer of La Pampa, Argentina. *Appl. Geochem.* 20, 989–1016. <https://doi.org/10.1016/j.apgeochem.2004.10.005>.
- Smedley, P.L., Bearcock, J.M., Fordyce, F.M., Everett, P.A., Chenery, S., Ellen, R., 2017. *Stream-water Geochemical Atlas of the Clyde Basin (Open Report)*, OR/16/015. British Geological Survey, Keyworth.
- Smith, B., 2000. The distribution of natural radioelements in ground waters and post-Cretaceous sediments from the southern Mediterranean margin. In: Hutchins, M.G., Powell, J.H., Talbot, D., Trick, J.K., Gedeon, R., Amro, H., Kilani, S., Constantinou, G., Afrodissis, S., Constantinou, C., Panayides, I., Xenophontos, C., Malpas, J. (Eds.), Presented at the Third International International Conference on the Geology of the Eastern Mediterranean, Ministry of Agriculture, Nicosia, Cyprus, p. 355.
- Smith, B., Powell, J., Gedeon, R., Amro, H., 1996. Groundwater Pollution by Natural Radionuclides: an Evaluation of Natural and Mining Contamination Associated with Phosphorite (Jordan). Presented at the Second IMM Conference on Minerals, Metals and the Environment, Prague.
- Smith, S.C., Douglas, M., Moore, D.A., Kukkadapu, R.K., Arey, B.W., 2009. Uranium extraction from laboratory-synthesized, uranium-doped hydrous ferric oxides. *Environ. Sci. Technol.* 43, 2341–2347. <https://doi.org/10.1021/es802621t>.
- Smrzka, D., Zwicker, J., Bach, W., Feng, D., Himmler, T., Chen, D., Peckmann, J., 2019. The behavior of trace elements in seawater, sedimentary pore water, and their incorporation into carbonate minerals: a review. *Facies* 65, 1–47.
- Snow, D.D., Spalding, R.F., 1994. Uranium isotopes in the Platte River drainage basin of the North American high plains region. *Appl. Geochem.* 9, 271–278. [https://doi.org/10.1016/0883-2927\(94\)90037-X](https://doi.org/10.1016/0883-2927(94)90037-X).

- Soltis, J.A., McBriarty, M.E., Qafoku, O., Kerisit, S.N., Nakouzi, E., De Yoreo, J.J., Ilton, E.S., 2019. Can mineral growth by oriented attachment lead to incorporation of uranium(VI) into the structure of goethite? *Environ.-Sci. Nano* 6, 3000–3009. <https://doi.org/10.1039/C9EN00779B>.
- Sørensen, H., 1992. Agpaitic nepheline syenites: a potential source of rare elements. *Appl. Geochem.* 7, 417–427. [https://doi.org/10.1016/0883-2927\(92\)90003-L](https://doi.org/10.1016/0883-2927(92)90003-L).
- Srinivasan, R., Pandit, S., Karunakara, N., Salim, D., Kumara K. S., Kumar, M., Khatel, G., Ramkumar, K., 2021. High uranium concentration in groundwater used for drinking in parts of eastern Karnataka, India. *Curr. Sci.* 121.
- Staines, A., McDermott, R., Sayers, G., Boyle, E., Johnson, H., Boran, G., Keogh, B., Kelly, P., 2004. Uranium in drinking water - human health effects. *Epidemiology* 15, S110.
- Stalder, E., Blanc, A., Haldimann, M., Dudler, V., 2012. Occurrence of uranium in Swiss drinking water. *Chemosphere* 86, 672–679. <https://doi.org/10.1016/j.chemosphere.2011.11.022>.
- Steiner, G., Geissler, B., Haneklaus, N., 2020. Making uranium recovery from phosphates great again? *Environ. Sci. Technol.* 54, 1287–1289. <https://doi.org/10.1021/acs.est.9b07859>.
- Stetten, L., Seder-Colomina, M., Le Pape, P., Ikogou, M., Zeyen, N., Thouvenot, A., Julien, A., Alcalde, G., Julien, A., Alcalde, G., 2018. Geochemical control on the reduction of U(VI) to mononuclear U(IV) species in lacustrine sediments. *Geochim. Cosmochim. Acta* 222, 171–186.
- Stewart, B.D., Neiss, J., Fendorf, S., 2007. Quantifying constraints imposed by calcium and iron on bacterial reduction of uranium(VI). *J. Environ. Qual.* 36, 363–372.
- Stirling, C.H., Andersen, M.B., Potter, E.-K., Halliday, A.N., 2007. Low-temperature isotopic fractionation of uranium. *Earth Planet. Sci. Lett.* 264, 208–225. <https://doi.org/10.1016/j.epsl.2007.09.019>.
- Stirling, C.H., Andersen, M.B., Warthmann, R., Halliday, A.N., 2015. Isotope fractionation of ²³⁸U and ²³⁵U during biologically-mediated uranium reduction. *Geochim. Cosmochim. Acta* 163, 200–218. <https://doi.org/10.1016/j.gca.2015.03.017>.
- Stockmann, M., Fritsch, K., Bok, F., Fernandes, M.M., Baeyens, B., Stuedtner, R., Müller, K., Nebelung, C., Brendler, V., Stumpf, T., Schmeide, K., 2022. New insights into U(VI) sorption onto montmorillonite from batch sorption and spectroscopic studies at increased ionic strength. *Sci. Tot. Environ.* 806, 150653 <https://doi.org/10.1016/j.scitotenv.2021.150653>.
- Stoliker, D.L., Campbell, K.M., Fox, P.M., Singer, D.M., Kaviani, N., Carey, M., Peck, N.E., Bargar, J.R., Kent, D.B., Davis, J.A., 2013. Evaluating chemical extraction techniques for the determination of uranium oxidation state in reduced aquifer sediments. *Environ. Sci. Technol.* 47, 9225–9232. <https://doi.org/10.1021/es401450v>.
- Stubbs, J.E., Veblen, L.A., Elbert, D.C., Zachara, J.M., Davis, J.A., Veblen, D.R., 2009. Newly recognized hosts for uranium in the Hanford Site vadose zone. *Geochim. Cosmochim. Acta* 73, 1563–1576. <https://doi.org/10.1016/j.gca.2008.12.004>.
- Stucker, V., Ranville, J., Newman, M., Peacock, A., Cho, J., Hatfield, K., 2011. Evaluation and application of anion exchange resins to measure groundwater uranium flux at a former uranium mill site. *Water Res* 45, 4866–4876. <https://doi.org/10.1016/j.watres.2011.06.030>.
- Sturchio, N.C., Antonio, M.R., Soderholm, L., Sutton, S.R., Brannon, J.C., 1998. Tetravalent uranium in calcite. *Science* 281, 971. <https://doi.org/10.1126/science.281.5379.971>.
- Stylo, M., Alessi, D.S., Shao, P.P., Lezama-Pacheco, J.S., Bargar, J.R., Bernier-Latmani, R., 2013. Biogeochemical controls on the product of microbial U (VI) reduction. *Environmental science & technology* 47, 12351–12358.
- Stylo, M., Neubert, N., Wang, Y., Monga, N., Romaniello, S.J., Weyer, S., Bernier-Latmani, R., 2015. Uranium isotopes fingerprint biotic reduction. *Proc. Natl. Acad. Sci. USA* 112, 5619–5624. <https://doi.org/10.1073/pnas.1421841112>.
- Sugiura, Y., Suyama, T., Tachi, Y., 2020. Development of JAEA Sorption Database (JAEA-SDB): Update of Sorption/QA Data in FY 2019. Japanese Atomic Energy Agency, Ibaraki-ken.
- Sun, Q., Aguila, B., Perman, J., Ivanov, Aleksandr, Bryantsev, V., Earl, L., Abney, C., Wojtas, L., Ma, S., Ivanov, Alexander, 2018. Bio-inspired nano-traps for uranium extraction from seawater and recovery from nuclear waste. *Nature Communications* 9. <https://doi.org/10.1038/s41467-018-04032-y>.
- Sun, Y., Amelung, W., Wu, B., Haneklaus, S., Maekawa, M., Lücke, A., Schnug, E., Bol, R., 2020. 'Co-evolution' of uranium concentration and oxygen stable isotope in phosphate rocks. *Applied geochemistry* 114, 104476.
- Sun, L., Liu, J., Li, L., Zhen, D., Dai, Z., Tang, S., Zhu, B., Chen, L., Chen, H., Gong, M., Tang, Z., Hu, Y., 2022. Advances of biosensors for UO₂²⁺ detecting based on specific DNzyme. *Inorg. Chem. Commun.* 138, 109234 <https://doi.org/10.1016/j.inoche.2022.109234>.
- Sutherland, D.S., 1991. Radon in Northamptonshire, England: geochemical investigations of some Jurassic sedimentary rocks. *Environ. Geochem. Health* 13, 143–145.
- Suzuki, Y., Kelly, S.D., Kemner, K.M., Banfield, J.F., 2002. Nanometre-size products of uranium bioreduction. *Nature* 419. <https://doi.org/10.1038/419134a>, 134–134.
- Suzuki, D., Saito-Kokubu, Y., Sakurai, S., Lee, C., Magara, M., Iguchi, K., Kimura, T., 2010. A new method for isotope ratio measurement of uranium in trace amount by thermal ionization mass spectrometry: the continuous heating method. *Int. J. Mass Spectrom.* 294, 23–27. <https://doi.org/10.1016/j.ijms.2010.04.007>.
- Swarzenski, P.W., Baskaran, M., 2006. Uranium distribution in the coastal waters and pore waters of Tampa Bay, Florida. *Mar. Chem.* 102, 252–266. <https://doi.org/10.1016/j.marchem.2006.06.016>.
- Swarzenski, P., Campbell, P., Porcelli, D., McKee, B., 2004. The estuarine chemistry and isotope systematics of ²³⁴U and ²³⁸U in the Amazon and Fly Rivers. *Cont. Shelf Res.* 24, 2357–2372. <https://doi.org/10.1016/j.csr.2004.07.025>.
- Sylwester, E.R., Hudson, E.A., Allen, P.G., 2000. The structure of uranium(VI) sorption complexes on silica, alumina, and montmorillonite. *Geochim. Cosmochim. Acta* 64, 2431–2438. [https://doi.org/10.1016/S0016-7037\(00\)00376-8](https://doi.org/10.1016/S0016-7037(00)00376-8).
- Szenknect, S., Mesbah, A., Descostes, M., Maihatchi-Ahamed, A., Bonato, L., Massonnet, M., Ziouane, Y., Vors, E., Vercouter, T., Clavier, N., 2020. Uranium removal from mining water using Cu substituted hydroxyapatite. *Journal of hazardous materials* 392, 122501.
- Taha, M.H., El-Maadawy, M.M., Hussein, A.E.M., Youssef, W.M., 2018. Uranium sorption from commercial phosphoric acid using kaolinite and metakaolinite. *J. Radioanal. Nucl. Chem.* 317, 685–699. <https://doi.org/10.1007/s10967-018-5951-9>.
- Tamborini, G., Betti, M., Forcina, V., Hiernaut, T., Giovannone, B., Koch, L., 1998. Application of secondary ion mass spectrometry to the identification of single particles of uranium and their isotopic measurement. *Spectrochim. Acta B* 53, 1289–1302. [https://doi.org/10.1016/S0584-8547\(98\)00121-9](https://doi.org/10.1016/S0584-8547(98)00121-9).
- Tan, W., Lu, S., Liu, F., Feng, X., He, J., Koopal, L.K., 2008. Determination of the point-of-zero charge of manganese oxides with different methods including an improved salt titration method. *Soil Sci* 173, 277–286.
- Tanimizu, M., Sugiyama, N., Ponzevera, E., Bayon, G., 2013. Determination of ultra-low ²³⁶U/²³⁸U isotope ratios by tandem quadrupole ICP-MS/MS. *J. Anal. At. Spectrom.* 28, 1372–1376. <https://doi.org/10.1039/C3JA50145K>.
- Tarafder, P.K., Ghosh, P.K., Chakrapani, G., 2015. Field method for the rapid determination of traces of uranium in rocks, soil and stream sediments by fluorescence measurement. *J. Radioanal. Nucl. Chem.* 306, 357–363. <https://doi.org/10.1007/s10967-015-4104-7>.
- Taylor, S.R., McLennan, S.M., 1985. *The Continental Crust: its Composition and Evolution*. Blackwell Scientific, Oxford.
- Tessier, A., Campbell, P.G.C., Bisson, M., 1979. Sequential extraction procedure for the speciation of particulate trace metals. *Anal. Chem.* 51, 844–851. <https://doi.org/10.1021/ac50043a017>.
- The Royal Society, 2001. *The Health Hazards of Depleted Uranium Munitions. Part I*. The Royal Society.
- The Royal Society, 2002. *The Health Hazards of Depleted Uranium Munitions. Part II*. The Royal Society, London.
- Thiyva, C., Chidambaram, S., Thilagavathi, R., Napolian, M., A, V.S., 2014. Evaluation of drinking water quality index (DWQI) and its seasonal variations in hard rock aquifers of Madurai district, Tamilnadu. *Int. J. Adv. Geosci.* 2, 48–52. <https://doi.org/10.14419/ijag.v2i2.2294>.
- Thomson, B.M., Smith, C.L., Busch, R.D., Siegel, M.D., Baldwin, C., 2003. Removal of metals and radionuclides using apatite and other natural sorbents. *Journal of Environmental Engineering* 129, 492–499.
- Tillman, F.D., Beisner, K.R., Anderson, J.R., Unema, J.A., 2021. An assessment of uranium in groundwater in the Grand Canyon region. *Sci. Rep-UK* 11, 22157. <https://doi.org/10.1038/s41598-021-01621-8>.
- Timofeev, A., Migdisov, A.A., Williams-Jones, A.E., Roback, R., Nelson, A.T., Xu, H., 2018. Uranium transport in acidic brines under reducing conditions. *Nature communications* 9, 1–7.
- Tippling, E., 1998. Humic ion-binding model VI: an improved description of the interactions of protons and metal ions with humic substances. *Aquat. Geochem.* 4, 3–47.
- Tippling, E., Lofts, S., Sonke, J.E., 2011. Humic Ion-Binding Model VII: a revised parameterisation of cation-binding by humic substances. *Environ. Chem.* 8, 225–235.
- Toner, J., Catling, D., Sletten, R., 2017. The geochemistry of don juan pond: evidence for a deep groundwater flow system in wright valley, Antarctica. *Earth Planet. Sci. Lett.* 474, 190–197.
- Tonkin, J.W., Balistrieri, L.S., Murray, J.W., 2004. Modeling sorption of divalent metal cations on hydrous manganese oxide using the diffuse double layer model. *Appl. Geochem.* 19, 29–53.
- Tourmassat, C., Tinnacher, R.M., Grangeon, S., Davis, J.A., 2018. Modeling uranium(VI) adsorption onto montmorillonite under varying carbonate concentrations: a surface complexation model accounting for the spillover effect on surface potential. *Geochim. Cosmochim. Acta* 220, 291–308. <https://doi.org/10.1016/j.gca.2017.09.049>.
- Town, R.M., Van Leeuwen, H.P., Duval, J.F., 2019. Rigorous physicochemical framework for metal ion binding by aqueous nanoparticulate humic substances: implications for speciation modeling by the NICA-Donnan and WHAM codes. *Environ. Sci. Technol.* 53, 8516–8532.
- Tran, E., Zavrín, M., Kersting, A.B., Klein-BenDavid, O., Teutsch, N., Weisbrod, N., 2021. Colloid-facilitated transport of ²³⁸Pu, ²³³U and ¹³⁷Cs through fractured chalk: laboratory experiments, modelling, and implications for nuclear waste disposal. *Sci. Tot. Environ.* 757, 143818.
- Trivedi, P., Axe, L., 1999. A comparison of strontium sorption to hydrous aluminum, iron, and manganese oxides. *J. Colloid. Interf. Sci.* 218, 554–563.
- Tsarev, S., Collins, R.N., Ilton, E.S., Fahy, A., Waite, T.D., 2017. The short-term reduction of uranium by nanoscale zero-valent iron (nZVI): role of oxide shell, reduction mechanism and the formation of U(V)-carbonate phases. *Environ. Sci. Nano* 4, 1304–1313. <https://doi.org/10.1039/C7EN00024C>.
- Tulsidas, H., Gabriel, S., Kiegiel, K., Haneklaus, N., 2019. Uranium resources in EU phosphate rock imports. *Resour. Policy* 61, 151–156.
- Turner, G.D., Zachara, J.M., McKinley, J.P., Smith, S.C., 1996. Surface-charge properties and UO₂²⁺ adsorption of a subsurface smectite. *Geochim. Cosmochim. Acta* 60, 3399.
- Ukalska-Jaruga, A., Bejger, R., Debaene, G., Smreczak, B., 2021. Characterization of soil organic matter individual fractions (fulvic acids, humic acids, and humins) by spectroscopic and electrochemical techniques in agricultural soils. *Agronomy* 11, 1067.

- Ulrich, S., Gillow, J., Roberts, S., Byer, G., Sueker, J., Farris, K., 2019. Hydrogeochemical and mineralogical factors influencing uranium in background area groundwater wells: grants, New Mexico. *J. Hydrol. Reg. Stud.* 26, 100636 <https://doi.org/10.1016/j.ejrh.2019.100636>.
- Um, W., Serne, R.J., Brown, C.F., Last, G.V., 2007. U(VI) adsorption on aquifer sediments at the Hanford Site. *J. Contam. Hydrol.* 93, 255–269. <https://doi.org/10.1016/j.jconhyd.2007.03.002>.
- Um, W., Wang, Z., Serne, R.J., Williams, B.D., Brown, C.F., Dodge, C.J., Francis, A.J., 2009. Uranium phases in contaminated sediments below Hanford's U tank farm. *Environ. Sci. Technol.* 43, 4280–4286. <https://doi.org/10.1021/es900203r>.
- Van de Weerd, H., Van Riemsdijk, W., Leijnse, A., 2002. Modeling transport of a mixture of natural organic molecules: effects of dynamic competitive sorption from particle to aquifer scale. *Water Resour. Res.* 38, 33–1.
- van der Lee, J., Lomenech, C., 2004. Towards a common thermodynamic database for speciation models. *Radiochim. Acta* 92, 811–818.
- van Gerwen, M., Alpert, N., Lieberman-Cribbin, W., Cooke, P., Ziadkhanpour, K., Liu, B., Genden, E., 2020. Association between uranium exposure and thyroid health: a national health and nutrition examination survey analysis and ecological study. *Int. J. Environ. Res. Pub. He.* 17 <https://doi.org/10.3390/ijerph17030712>.
- Van Riemsdijk, W.H., Koopal, L.K., Kinniburgh, D.G., Benedetti, M.F., Weng, L., 2006. Modeling the interactions between humics, ions, and mineral surfaces. *Environ. Sci. Technol.* 40, 7473–7480.
- van Veelen, A., Copping, R., Law, G.T.W., Smith, A.J., Bargar, J.R., Rogers, J., Shuh, D. K., Wogelius, R.A., 2012. Uranium uptake onto Magnox sludge minerals studied using EXAFS. *Min. Mag.* 76, 3095–3104. <https://doi.org/10.1180/minmag.2012.076.8.24>.
- Vandenhove, H., Gil-García, C., Rigol, A., Vidal, M., 2009. New best estimates for radionuclide solid-liquid distribution coefficients in soils. Part 2. Naturally occurring radionuclides. *J. Environ. Radioactiv.* 100, 697–703. <https://doi.org/10.1016/j.jenvrad.2009.03.014>.
- Velasco, C.A., Brearley, A.J., Gonzalez-Estrella, J., Ali, A.-M.S., Meza, M.I., Cabaniss, S. E., Thomson, B.M., Forbes, T.Z., Lezama Pacheco, J.S., Cerrato, J.M., 2021. From adsorption to precipitation of U(VI): what is the role of pH and natural organic matter? *Environ. Sci. Technol.* 55, 16246–16256.
- Vengosh, A., Coyte, R.M., Podgorski, J., Johnson, T.M., 2022. A critical review on the occurrence and distribution of the uranium- and thorium-decay nuclides and their effect on the quality of groundwater. *Science of The Total Environment* 808, 151914. <https://doi.org/10.1016/j.scitotenv.2021.151914>.
- Vercouter, T., Reiller, P.E., Ansoborlo, E., Février, L., Gilbin, R., Lomenech, C., Philippini, V., 2015. A modelling exercise on the importance of ternary alkaline earth carbonate species of uranium (VI) in the inorganic speciation of natural waters. *Applied Geochemistry* 55, 192–198.
- Vettese, G.F., Morris, K., Natrajan, L.S., Shaw, S., Vitova, T., Galanzew, J., Jones, D.L., Lloyd, J.R., 2020. Multiple lines of evidence identify U(V) as a key intermediate during U(VI) reduction by *Shewanella oneidensis* MR1. *Environ. Sci. Technol.* 54, 2268–2276. <https://doi.org/10.1021/acs.est.9b05285>.
- Višňák, J., Sobek, L., Hoth, N., 2018. Spectroscopic Experimental and Theoretical Study of uranyl(VI) in an Aqueous System - Molecular Modelling Meets Environmental Protection arXiv preprint arXiv:1811.10456 1811.10456.
- Waite, T.D., Davis, J.A., Payne, T.E., Waychunas, G.A., Xu, N., 1994. Uranium(VI) adsorption to ferrihydrite: application of a surface complexation model. *Geochim. Cosmochim. Acta* 58, 5465–5478.
- Wang, Z., Zachara, J.M., Yantasee, W., Gassman, P.L., Liu, C.X., Joly, A.G., 2004. Cryogenic laser induced fluorescence characterization of U(VI) in Hanford vadose zone pore waters. *Environ. Sci. Technol.* 38, 5591.
- Wang, Z., Lee, S.-W., Catalano, J.G., Lezama-Pacheco, J.S., Bargar, J.R., Tebo, B.M., Giammar, D.E., 2013a. Adsorption of uranium(VI) to manganese oxides: X-ray absorption spectroscopy and surface complexation modeling. *Environ. Sci. Technol.* 47, 850–858. <https://doi.org/10.1021/es304454g>.
- Wang, Z., Lee, S.-W., Kapoor, P., Tebo, B.M., Giammar, D.E., 2013b. Uraninite oxidation and dissolution induced by manganese oxide: a redox reaction between two insoluble minerals. *Geochim. Cosmochim. Acta* 100, 24–40. <https://doi.org/10.1016/j.gca.2012.09.053>.
- Wang, X., Johnson, T.M., Lundstrom, C.C., 2015. Low temperature equilibrium isotope fractionation and isotope exchange kinetics between U(IV) and U(VI). *Geochim. Cosmochim. Acta* 158, 262–275.
- Wang, G., Um, W., Wang, Z., Reinoso-Maset, E., Washton, N.M., Mueller, K.T., Perdrial, N., O'Day, P.A., Chorover, J., 2017. Uranium release from acidic weathered Hanford sediments: single-pass flow-through and column experiments. *Environ. Sci. Technol.* 51, 11011–11019. <https://doi.org/10.1021/acs.est.7b03475>.
- Wang, X., Shi, Z., Kinniburgh, D.G., Zhao, L., Ni, S., Wang, R., Hou, Y., Cheng, K., Zhu, B., 2019. Effect of thermodynamic database selection on the estimated aqueous uranium speciation. *J. Geochem. Explor.* 204, 33–42. <https://doi.org/10.1016/j.gexplo.2019.05.001>.
- Wang, J., Zhou, W., Shi, Y., Li, Y., Xian, D., Guo, N., Liu, C., 2022. Uranium sorption on oxyhydroxide minerals by surface complexation and precipitation. *Chinese Chem. Lett.* 33 (7), 3461–3467. <https://doi.org/10.1016/j.ccl.2022.01.019>.
- Warner, R., Meadows, J., Sojda, S., Price, V., Temples, T., Arai, Y., Fleisher, C., Crawford, B., Stone, P., 2011. Mineralogic investigation into occurrence of high uranium well waters in upstate South Carolina, USA. *Appl. Geochem.* 26, 777–788. <https://doi.org/10.1016/j.apgeochem.2011.01.035>.
- Warr, L.N., 2021. IMA–CNMNC approved mineral symbols. *Min. Mag.* 85, 291–320. <https://doi.org/10.1180/mgm.2021.43>.
- Wathen, J.B., 1987. The effect of uranium siting in two-mica granites on uranium concentrations and radon activity in ground water. In: Graves, B. (Ed.), *Radon, Radium, and Other Radioactivity in Ground Water*, National Water Well Association. CRC Press, Chelsea, Michigan.
- Wazne, M., Korfiatis, G.P., Meng, X., 2003. Carbonate effects on hexavalent uranium adsorption by iron oxyhydroxide. *Environ. Sci. Technol.* 37, 3619.
- Weibel, R., Friis, H., 2004. Opaque minerals as keys for distinguishing oxidising and reducing diagenetic conditions in the Lower Triassic Bunter Sandstone, North German Basin. *Sediment. Geol.* 169, 129–149. <https://doi.org/10.1016/j.sedgeo.2004.05.004>.
- Weir, E., 2004. Uranium in drinking water, naturally. *Can. Med. Assoc. J.* 170, 951–952. <https://doi.org/10.1503/cmaj.1040214>.
- Welch, A.H., Lico, M.S., 1998. Factors controlling As and U in shallow ground water, southern Carson Desert, Nevada. *Appl. Geochem.* 13, 521–539. [https://doi.org/10.1016/S0883-2927\(97\)00083-8](https://doi.org/10.1016/S0883-2927(97)00083-8).
- Weller, M., Light, M., Gelbrich, T., 2000. Structure of uranium(VI) oxide dihydrate, $UO_2 \cdot 2H_2O$; synthetic meta-schoepite $(UO_2)_4O(OH)_6 \cdot 5H_2O$. *Acta Crystallograph. B-Stru.* 56, 577–583. <https://doi.org/10.1107/S0108768199016559>.
- Wellmer, F.-W., Scholz, R.W., 2017. Peak minerals: what can we learn from the history of mineral economics and the cases of gold and phosphorus? *Mineral Economics* 30, 73–93. <https://doi.org/10.1007/s13563-016-0094-3>.
- Weng, L., Van Riemsdijk, W.H., Koopal, L.K., Hiemstra, T., 2006a. Ligand and Charge Distribution (LCD) model for the description of fulvic acid adsorption to goethite. *J. Colloid. Interf. Sci.* 302, 442–457.
- Weng, L., Van Riemsdijk, W.H., Koopal, L.K., Hiemstra, T., 2006b. Adsorption of humic substances on goethite: comparison between humic acids and fulvic acids. *Environ. Sci. Technol.* 40, 7494–7500.
- Weng, L., Van Riemsdijk, W.H., Hiemstra, T., 2007. Adsorption of humic acids onto goethite: effects of molar mass, pH and ionic strength. *J. Colloid. Interf. Sci.* 314, 107–118.
- Weng, L., Van Riemsdijk, W.H., Hiemstra, T., 2008a. Cu^{2+} and Ca^{2+} adsorption to goethite in the presence of fulvic acids. *Geochim. Cosmochim. Acta* 72, 5857–5870.
- Weng, L., Van Riemsdijk, W.H., Hiemstra, T., 2008b. Humic nanoparticles at the oxide–water interface: interactions with phosphate ion adsorption. *Environ. Sci. Technol.* 42, 8747–8752.
- Weng, L., Van Riemsdijk, W.H., Hiemstra, T., 2009. Effects of fulvic and humic acids on arsenate adsorption to goethite: experiments and modeling. *Environ. Sci. Technol.* 43, 7198–7204.
- Weng, L., Van Riemsdijk, W.H., Hiemstra, T., 2012. Factors controlling phosphate interaction with iron oxides. *J. Environ. Qual.* 41, 628–635.
- Wenrich, K.J., Sutphin, H.B., 1989. Lithotectonic Setting Necessary for Formation of a Uranium-Rich, Solution-Collapse Breccia-Pipe Province, Grand Canyon Region, Arizona, Open-File Report 89-0173. United States Geological Survey, Denver. <https://doi.org/10.3133/ofr89173>.
- Wersin, P., Hochella, M.F., Persson, P., Redden, G., Leckie, J.O., Harris, D.W., 1994. Interaction between aqueous uranium(VI) and sulfide minerals: spectroscopic evidence for sorption and reduction. *Geochim. Cosmochim. Acta* 58, 2829–2843. [https://doi.org/10.1016/0016-7037\(94\)90117-1](https://doi.org/10.1016/0016-7037(94)90117-1).
- Weyer, S., Anbar, A., Gerdes, A., Gordon, G., Algeo, T., Boyle, E., 2008. Natural fractionation of $^{238}U/^{235}U$. *Geochim. Cosmochim. Acta* 72, 345–359.
- WHO, 1993. Guidelines for Drinking-Water Quality: Volume 1: Recommendations, second ed. World Health Organization, Geneva.
- WHO, 2017. Guidelines for Drinking-Water Quality, fourth ed. incorporating First Addendum. World Health Organization, Geneva.
- Williams, K.H., Long, P.E., Davis, J.A., Wilkins, M.J., N'Guessan, A.L., Steefel, C.I., Yang, L., Newcomer, D., Spang, F.A., Kerkhof, L.J., McGuinness, L., Dayvault, R., Lovley, D.R., 2011. Acetate availability and its influence on sustainable bioremediation of uranium-contaminated groundwater. *Geomicrobiol. J.* 28, 519–539. <https://doi.org/10.1080/01490451.2010.520074>.
- Windom, H., Niencheski, F., 2003. Biogeochemical processes in a freshwater–seawater mixing zone in permeable sediments along the coast of Southern Brazil. *Mar. Chem.* 83, 121–130. [https://doi.org/10.1016/S0304-4203\(03\)00106-3](https://doi.org/10.1016/S0304-4203(03)00106-3).
- Winstanley, E.H., Morris, K., Abrahamsen-Mills, L.G., Blackham, R., Shaw, S., 2019. U(VI) sorption during ferrihydrite formation: underpinning radioactive effluent treatment. *J. Hazard Mater.* 366, 98–104. <https://doi.org/10.1016/j.jhazmat.2018.11.077>.
- WoldeGabriel, G., Boukhalfa, H., Ware, S.D., Cheshire, M., Reimus, P., Heikoku, J., Conradson, S.D., Batuk, O., Havrilla, G., House, B., Simmons, A., Clay, J., Basu, A., Christensen, J.N., Brown, S.T., DePaolo, D.J., 2014. Characterization of cores from an *in-situ* recovery mined uranium deposit in Wyoming: implications for post-mining restoration. *Chem. Geol.* 390, 32–45. <https://doi.org/10.1016/j.chemgeo.2014.10.009>.
- Wu, Y., Wang, Y., Xie, X., 2014. Occurrence, behavior and distribution of high levels of uranium in shallow groundwater at Datong basin, northern China. *Sci. Tot. Environ.* 472, 809–817. <https://doi.org/10.1016/j.scitotenv.2013.11.109>.
- Wu, W., Priest, C., Zhou, J., Peng, C., Liu, H., Jiang, D., 2016. Solvation of the $Ca_2UO_2(CO_3)_3$ complex in seawater from classical molecular dynamics. *J. Phys. Chem. B* 120, 7227–7233.
- Wu, X., Huang, Q., Mao, Y., Wang, Xiangxue, Wang, Y., Hu, Q., Wang, H., Wang, Xiangke, 2019. Sensors for determination of uranium: a review. *TrAC-Trend Anal. Chem.* 118, 89–111. <https://doi.org/10.1016/j.trac.2019.04.026>.
- Wu, X., Yin, Q., Huang, Q., Mao, Y., Hu, Q., Wang, H., 2020. Rational designing an azo colorimetric sensor with high selectivity and sensitivity for uranium environmental monitoring. *Anal. Chim. Acta* 1140, 153–167.
- Xiao, C., Hassanzadeh Fard, Z., Sarma, D., Song, T.-B., Xu, C., Kanatzidis, M.G., 2017. Highly efficient separation of trivalent minor actinides by a layered metal sulfide ($KInSn_2S_6$) from acidic radioactive waste. *J. Am. Chem. Soc.* 139, 16494–16497. <https://doi.org/10.1021/jacs.7b10464>.

- Xiong, J., Koopal, L.K., Tan, W., Fang, L., Wang, M., Zhao, W., Liu, F., Zhang, J., Weng, L., 2013. Lead binding to soil fulvic and humic acids: NICA-Donnan modeling and XAFS spectroscopy. *Environ. Sci. Technol.* 47, 11634–11642.
- Xoubi, N., 2015. Evaluation of uranium concentration in soil samples of Central Jordan. *Minerals* 5. <https://doi.org/10.3390/min5020133>.
- Xu, J., Zhu, S.-Y., Luo, T.-Y., Zhou, W., Li, Y.-L., 2015. Uranium mineralization and its radioactive decay-induced carbonization in a black shale-hosted polymetallic sulfide ore layer, southwest China. *Econ. Geol.* 110, 1643–1652.
- Yakshin, V.V., Krokhin, M.N., 2011. Determination of small amounts of uranium by redox potentiometric titration. *Radiochemistry* 53, 327–331. <https://doi.org/10.1134/S1066362211030179>.
- Yamazaki, I.M., Geraldo, L.P., 2003. Uranium content in phosphate fertilizers commercially produced in Brazil. *Appl. Radiat. Isotopes* 59, 133–136. [https://doi.org/10.1016/S0969-8043\(03\)00159-3](https://doi.org/10.1016/S0969-8043(03)00159-3).
- Yanase, N., Nightingale, T., Payne, T., Duerden, P., 1991. Uranium distribution in mineral phases of rock by sequential extraction procedure. *Radiochim. Acta* 52–53, 387. <https://doi.org/10.1524/ract.1991.5253.2.387>.
- Yanase, N., Payne, T.E., Sekine, K., 1995. Groundwater geochemistry in the Koongarra ore deposit, Australia (I): implications for uranium migration. *Geochem. J.* 29, 1–29. <https://doi.org/10.2343/geochemj.29.1>.
- Yang, Y., Saiers, J.E., Barnett, M.O., 2013. Impact of interactions between natural organic matter and metal oxides on the desorption kinetics of uranium from heterogeneous colloidal suspensions. *Environ. Sci. Technol.* 47, 2661–2669. <https://doi.org/10.1021/es304013r>.
- Ye, Y., Al-Khaleedi, N., Barker, L., Darwish, M.S., El Naggari, A.M., El-Yahyaoui, A., Hussein, A., Hussein, E.-S., Shang, D., Taha, M., 2019. Uranium Resources in China's Phosphate Rocks—Identifying Low-Hanging Fruits. Presented at the IOP Conference Series: Earth and Environmental Science. IOP Publishing, 052033.
- Zachara, J.M., Long, P.E., Bargar, J., Davis, J.A., Fox, P., Fredrickson, J.K., Freshley, M. D., Konopka, A.E., Liu, C., McKinley, J.P., Rockhold, M.L., Williams, K.H., Yabusaki, S.B., 2013. Persistence of uranium groundwater plumes: contrasting mechanisms at two DOE sites in the groundwater–river interaction zone. *J. Contam. Hydrol.* 147, 45–72. <https://doi.org/10.1016/j.jconhyd.2013.02.001>.
- Zamora, M.L., Tracy, B.L., Zielinski, J.M., Meyerhof, D.P., Moss, M.A., 1998. Chronic ingestion of uranium in drinking water: a study of kidney bioeffects in humans. *Toxicol. Sci.* 43, 68–77. <https://doi.org/10.1093/toxsci/43.1.68>.
- Zamora, M.L.L., Zielinski, J.M., Moodie, G.B., Falcomer, R.A.F., Hunt, W.C., Capello, K., 2009. Uranium in drinking water: renal effects of long-term ingestion by an Aboriginal community. *Arch. Environ. Occup. H.* 64, 228–241. <https://doi.org/10.1080/19338240903241267>.
- Zeng, H., Singh, A., Basak, S., Ulrich, K.-U., Sahu, M., Biswas, P., Catalano, J.G., Giammar, D.E., 2009. Nanoscale size effects on uranium(VI) adsorption to hematite. *Environ. Sci. Technol.* 43, 1373–1378. <https://doi.org/10.1021/es802334e>.
- Zhang, C., Liu, X., Tinnacher, R.M., Tournassat, C., 2018. Mechanistic understanding of uranyl ion complexation on montmorillonite edges: a combined first-principles molecular dynamics–surface complexation modeling approach. *Environ. Sci. Technol.* 52, 8501–8509. <https://doi.org/10.1021/acs.est.8b02504>.
- Zhang, B., Wang, X., Zhou, J., Han, Z., Liu, W., Liu, Q., Wang, W., Li, R., Zhang, Baoyun, Dou, B., 2020. Regional geochemical survey of concealed sandstone-type uranium deposits using fine-grained soil and groundwater in the Erlan basin, north-east China. *J. Geochem. Explor.* 216, 106573. <https://doi.org/10.1016/j.gexplo.2020.106573>.
- Zhang, G., Lu, P., Zhang, Y., Tu, K., Zhu, C., 2020. SupPhreeqc: a program for generating customized PHREEQC thermodynamic datasets from SUPCRTBL and extending calculations to elevated pressures and temperatures. *Comput. Geosci.* 143, 104560.
- Zhang, Y., Fein, J.B., Li, Y., Yu, Q., Zu, B., Zheng, C., 2021. U(VI) adsorption to Fe₃O₄ nanoparticles coated with lignite humic acid: experimental measurements and surface complexation modeling. *Colloid Surface A* 614, 126150.
- Zhao, D., Wang, X., Yang, S., Guo, Z., Sheng, G., 2012. Impact of water quality parameters on the sorption of U(VI) onto hematite. *J. Environ. Radioactiv.* 103, 20–29. <https://doi.org/10.1016/j.jenvrad.2011.08.010>.
- Zhao, J., Cornett, R.J., Chakrabarti, C.L., 2020. Assessing the uranium DGT-available fraction in model solutions. *J. Hazard Mater.* 384, 121134. <https://doi.org/10.1016/j.jhazmat.2019.121134>.
- Zhao, X., Liu, W., Cai, Z., Fu, J., Duan, J., Zhao, D., Bozack, M., Feng, Y., 2020. Reductive immobilization of uranium by stabilized zero-valent iron nanoparticles: effects of stabilizers, water chemistry and long-term stability. *Colloid Surface A* 604, 125315. <https://doi.org/10.1016/j.colsurfa.2020.125315>.
- Zhao, T., Wu, H., Sun, J., Wen, X., Zhang, J., Zeng, W., Shen, H., Hu, Z., Huang, P., 2022. Immobilization of uranium tailings by phosphoric acid-based geopolymer with optimization of machine learning. *Journal of Radioanalytical and Nuclear Chemistry* 331, 4047–4054.
- Zhao, W.-W., Li, L.-H., Liao, J.-Z., Liang, R.-P., Song, A.-M., Zhang, F.-D., Ke, H., Qiu, J.-D., 2022. Regenerable and stable biomimetic hydroxyl-modified metal-organic frameworks for targeted uranium capture. *Chem. Eng. J.* 433, 133787.
- Zhiwei, N., Qiaohui, F., Wenhua, W., Junzheng, X., Lei, C., Wangsuo, W., 2009. Effect of pH, ionic strength and humic acid on the sorption of uranium(VI) to attapulgite. *Appl. Radiat. Isotopes* 67, 1582–1590. <https://doi.org/10.1016/j.apradiso.2009.03.113>.
- Zhou, P., Gu, B., 2005. Extraction of oxidized and reduced forms of uranium from contaminated soils: effects of carbonate concentration and pH. *Environ. Sci. Technol.* 39, 4435–4440. <https://doi.org/10.1021/es0483443>.
- Zhou, Z., Zhou, Y., Liang, X., Luo, J., Liu, S., Ma, J., 2022. Electrochemical sensor for uranium monitoring in natural water based on poly Nile blue modified glassy carbon electrode. *J. Solid State Electr.* 1139–1149. <https://doi.org/10.1007/s10008-021-05102-w>.
- Zhuang, K., Ma, E., Lovley, D.R., Mahadevan, R., 2012. The design of long-term effective uranium bioremediation strategy using a community metabolic model. *Biotechnol. Bioeng.* 109, 2475–2483. <https://doi.org/10.1002/bit.24528>.
- Zielinski, R.A., Bloch, S., Walker, T.R., 1983. The mobility and distribution of heavy metals during the formation of first cycle red beds. *Econ. Geol.* 78, 1574–1589.
- Zielinski, R.A., Asher-Bolinder, S., Meier, A.L., Johnson, C.A., Szabo, B.J., 1997. Natural or fertilizer-derived uranium in irrigation drainage: a case study in southeastern Colorado. *U.S.A. Appl. Geochem.* 12, 9–21. [https://doi.org/10.1016/S0883-2927\(96\)00050-9](https://doi.org/10.1016/S0883-2927(96)00050-9).
- Zielinski, R., Simmons, K., Orem, W., 2000. Use of 234U and 238U isotopes to identify fertilizer-derived uranium in the Florida Everglades. *Appl. Geochem.* 15, 369–383.
- Zielinski, R.A., Orem, W.H., Simmons, K.R., Bohlen, P.J., 2006. Fertilizer-derived uranium and sulfur in rangeland soil and runoff: a case study in Central Florida. *Water Air Soil Poll* 176, 163–183. <https://doi.org/10.1007/s11270-006-9156-4>.
- Zsigrai, J., Nguyen, T.C., Berlizov, A., 2015. Gamma-spectrometric determination of 232U in uranium-bearing materials. *Nuclear Instruments and Methods in Physics Research Section B: Beam Interactions with Materials and Atoms* 359, 137–144. <https://doi.org/10.1016/j.nimb.2015.07.047>.